# Investigating Pharmacological Inhibition of the NLRP3 Inflammasome Acutely and Chronically Post Hypoxia in a Moderate Model of Hypoxic-Ischaemic Encephalopathy

**Thesis Submitted for the Degree of**

**Doctor of Philosophy, Physiology**

**2025**

**Aisling Leavy**

Supervised by
Assoc. Prof. Eva Jiménez-Mateos

Discipline of Physiology, School of Medicine

# Declaration and Statement of Plagiarism

I declare that this thesis has not been submitted as an exercise for a degree at this or any other university and it is entirely my own work. The unpublished and/or published work of others has been duly acknowledged in the text wherever included.

Prof. Eva Jimenez-Mateos was involved in study design, analysis, and interpretation of data. Research assistants Sophia Hjelseth and Jessica Kingston aided in various *in vivo* and molecular experiments and generated the PCR data presented in Results Chapter 2. Student Aidan Pepper designed the Novel Object Location Standardisation Equation used throughout the thesis and analysed the Novel Object Location videos in Results Chapter 1. Students Jacqui Ryall, Anupa Paulose, Grace Craig, Clodagh Grady, Joy Igbinosun, Hannah Sweeney, Alice Berturi, Lauryn Doherty and Caoimhe Massey aided in various experiments during their respective projects.

I agree to deposit this thesis in the University's open access institutional repository or allow Trinity College Library to do so on my behalf, subject to Irish Copyright Legislation and Trinity College Library conditions of use and acknowledgement. I consent to the examiner retaining a copy of the thesis beyond the examining period, should they so wish (EU GDPR May 2018).

Signed: 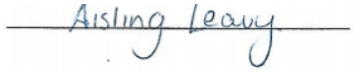

Date: 13th February 2025

# Summary

Neonatal Encephalopathy (NE) describes syndromes of “disturbed neurological function” during the neonatal period induced by a range of aetiologies and is the leading cause of death and disability in neonates worldwide. The most common aetiology is hypoxic-ischaemic encephalopathy (HIE), which accounts for 29% of NE cases and has an incidence of 1 to 3 in 1000 live births in developed countries. HIE is the most common cause of neonatal seizures, and the co-occurrence of HIE and neonatal seizures is strongly associated with poorer neurological outcomes. Diagnostic modalities and treatment strategies are suboptimal at best and rely upon an incredibly narrow therapeutic window of 6 hours post-injury to have any protective effects, highlighting a significant unmet clinical need. The involvement of neuroinflammation and microglia in HIE pathology has been demonstrated in preclinical and human studies, which is significant given their intrinsic role in neurodevelopment. Even in moderate models of HIE, microglia populations in the hippocampus are significantly elevated. Thanks to these advances, anti-inflammatory treatment strategies have garnered promising results in attenuating acute injury and managing chronic neuroinflammation. One pathway which has emerged is the NLRP3 inflammasome, responsible for IL-1β release by microglia, which is elevated post-HIE, and targeting activating receptors, such as P2X7R, has been neuroprotective. Therefore, this thesis aims to characterise microglia in the hippocampus using phenotypes and activation markers, followed by NOD-like Receptor Family Pyrin Domain containing 3 (NLRP3) inflammasome inhibition studies using MCC950 to understand how neuroinflammation in the hippocampus is impacted by inflammasome inhibition.

To do this, global hypoxia was induced at Postnatal Day 7 and microglia in the hippocampus were analysed at 72 hours and 5 weeks post-hypoxia. This found that microglia

populations were elevated at both timepoints and expressed higher proportions of pro-inflammatory microglia and fewer homeostatic microglia. Furthermore, neonatal reflex development was negatively impacted by hypoxia, as were hippocampal behaviours later in life such as anxiety and spatial memory.

To understand the role of inflammasome signalling in these deficits, mice were treated with MCC950 immediately post-hypoxia. Proinflammatory microglia were significantly reduced acutely but not chronically, and homeostatic microglia were increased at the chronic stage. Neonatal reflexes were only partially attenuated, 5 weeks later, spatial memory and anxiety were significantly improved. Accompanying gene and protein expression studies were performed, which attenuated expression of pro-inflammatory markers, while inducing persistent upregulation of the classical complement pathway acutely and chronically.

Next, a different approach was adopted whereby MCC950 was administered twice daily from PND21 to PND26 to see whether an anti-inflammatory approach is still neuroprotective far past the traditional treatment window. Proinflammatory microglia were significantly reduced at 5 weeks post-hypoxia, although proportions of homeostatic microglia were practically unchanged. MCC950 attenuated behavioural deficits, having a particularly beneficial effect on anxiety compared to spatial memory.

Overall, the results of this thesis provide compelling evidence that a significant and chronic immune and microglial response is induced by a moderate model of global hypoxia. Inhibiting the NLRP3 inflammasome after and 2 weeks post-hypoxia provides promising neuroprotective effects, opening potential avenues for future research into anti-inflammatory treatment approaches for HIE.

# Acknowledgements

First and foremost, I would like to thank my supervisor, Prof. Eva Jimenez-Mateos. It is no exaggeration to say that I would not have made it here without your support, and I could not have asked for a better mentor to guide me. At every step of the way you have gone above and beyond, always treating me with respect, kindness and patience. I am excited to see all the amazing work the Jimenez lab will do in the years to come.

Next, I would like to thank current and former members of the Jimenez lab. Thank you to the real boss, Jessie Kingston, who contributed to the PCR experiments in Results Chapter 2 and provided both scientific and moral support along the way. I'd also like to thank former research assistant Sophia Hjelseth for her contributions to this thesis, particularly to the molecular experiments in Results Chapter 2. Thank you to the undergraduate and master's students who contributed to this thesis. Finally, to Ronan and Harry for being sound out. I wish you all the absolute best in the future, I know you will do great things!

Thank you to past and present members of the Department of Physiology, particularly Dr Carol Murray, Mr Aidan Kelly, Mr Lucas O'Dowd, Mr Quentin Comerford and Ms Christine Monahan. A special shout out to my officemates in the Watts Building for providing endless chats and boosting my confidence by telling me how great I am at baking.

Thank you to the staff in Production in the Comparative Medicine Unit for facilitating the *in vivo* work conducted for this thesis, to Dr David Loane for kindly allowing me to use his behaviour apparatus for the behaviour testing, and to Dr Janeen Laabei for training me up on the Anymaze software.

Thank you to Dr Gavin McManus for his training and assistance on the Confocal Microscope in the TBSI Imaging and Microscopy Centre.

Thank you to my partner Glenn, you honestly deserve a medal for the patience, care and compassion you have shown me throughout this whole PhD. You have been there from the very start and had my back through every curveball and crisis, and I'm grateful to have you in my life.

To my friends, thank you for listening to me talk about mice way more than a normal person should, and for being there when shit has hit the fan, personally and professionally. The past 4 ½ years have brought difficulties that I could not have imagined when I started in September 2020, so I'm forever grateful for you all. A special shout out to my two surrogate sisters Jessica O'Neill and Francesca Matra, who know way too much for me to ever let them out of my life.

To my family, my parents Des and Paula and my sisters Ciara and Aoife. No matter how insurmountable a problem may seem, I know that I always have Mum and Dad to keep me steady, and Ciara and Aoife to keep me humble. Everything I am, I owe to you all. To my extended family, my Grandad Des, aunties, uncles and cousins, thank you for listening to my ramblings about mice, microscopes and God knows what else, for believing in me and cheering me on every step of the way.

# Table of Contents

# List of Figures

# List of Tables

# Abbreviations

**A**

| | |
|---|---|
| Aβ | Amyloid-Beta |
| ACOGP-AAP | American College of Obstetrics, Gynaecology and Pediatrics |
| AD | Alzheimer's Disease |
| ADHD | Attention Deficit Hyperactivity Disorder |
| ADO-A1R | Adenosine A1 Receptor |
| ADP | Adenosine Diphosphate |
| aEEG | Amplitude Electroencephalopgrahy |
| AMPARs | AMPA-type Ionotropic Glutamate Receptors |
| ANOVA | Analysis of Variance |
| ANSER | Algorithm for Neonatal Seizure Recognition |
| AP1 | Activator Protein 1 |
| APGAR | Appearance, Pulse, Grimace, Activity, Respiration |
| APP/PS1 | Amyloid Precursor Protein/Presenilin 1 |
| ASC | Apoptosis-associated Speck-like Protein |
| Atg5 | Autophagy Protein 5 |
| ATP | Adenosine Triphosphate |

**B**

| | |
|---|---|
| BBB | Blood Brain Barrier |
| BSA | Bovine Serum Albumin |

**C**

| | |
|---|---|
| C1q | Complement Protein 1q |
| C1qa | Complement Protein 1qa |
| C1qR1 | Complement Protein 1 Receptor 1 |
| C3 | Complement Protein 3 |
| C3a | Complement Protein 3a |
| C5a | Complement Protein 5a |
| C5b | Complement Protein 5b |
| C9 | Complement Protein 9 |
| Ca1 | Cornu Ammonis 1 |

| | |
|---|---|
| Ca3 | Cornu Ammonis 3 |
| $Ca^{2+}$ | Calcium |
| CAPS | Cryopyrin-Associated Periodic Syndrome |
| CARD | Caspase Recruitment Domain |
| CCL2 | Chemokine Ligand 2 |
| CCL3 | Chemokine Ligand 3 |
| CCL5 | Chemokine Ligand 5 |
| CCL7 | Chemokine Ligand 7 |
| CD36 | Cluster of Differentiation 36 |
| CD39 | Cluster of Differentiation 39 |
| CD68 | Cluster of Differentiation 68 |
| CD73 | Cluster of Differentiation 73 |
| CD86 | Cluster of Differentiation 86 |
| CD206 | Cluster of Differentiation 206 |
| cDNA | Complementary DNA |
| cEEG | Conventional Electroencephalography |
| $Cl^-$ | Chloride |
| CND | Candesartan Cilexetil |
| CNS | Central Nervous System |
| $CO_2$ | Carbon Dioxide |
| CR3 | Complement Receptor 3 |
| CX3CR1 | CXC3 Motif Chemokine Receptor 1 (Fractalkine) |
| CXCL1 | Chemokine Ligand 1 |
| CXCL9 | Chemokine Ligand 9 |
| CXCL10 | Chemokine Ligand 10 |
| CXCL11 | Chemokine Ligand 11 |
| CXCR3 | CXC3 Motif Chemokine Receptor 3 |

**D**

| | |
|---|---|
| DAMPs | Damage Associated Molecular Patterns |
| DAPI | 4',6-diamidino-2-phenylindole |
| $dH_2O$ | Distilled Water |

| | |
|---|---|
| DNA | Deoxyribonucleic Acid |
| **E** | |
| E10 | Embryonic Day 10 |
| EAE | Experimental Autoimmune Encephalomyelitis |
| EEG | Electroencephalography |
| ELISA | Enzyme-linked Immunosorbent Assay |
| EPO | Erythropoietin |
| EPOR | Erythropoietin Receptor |
| **G** | |
| GABA | Gamma Aminobutyric Acid |
| GABA-A | Gamma Aminobutyric Acid Type A |
| $GABA_A$-R | Gamma Aminobutyric Acid Type A Receptor |
| GABA-R | Gamma Aminobutyric Acid Receptor |
| GSDMD | Gasdermin D |
| GSDMD-NT | N-terminal Domain of Gasdermin D |
| **H** | |
| HIE | Hypoxic-Ischaemic Encephalopathy |
| HIF | Hypoxia-Inducible Factor |
| HRP | Horseradish Peroxidase |
| **I** | |
| IBA1 | Ionised Calcium Binding Adaptor Molecule 1 |
| ICH | Intracerebral Haemorrhage |
| IF | Immunofluorescence |
| IFNγ | Interferon Gamma |
| IL-1α | Interleukin 1 alpha |
| IL-1β | Interleukin 1 beta |
| IL-1R | Interleukin 1 Receptor |
| IL-1Ra | Interleukin 1 Receptor A |
| IL-6 | Interleukin 6 |
| IL-8 | Interleukin 8 |
| IL-10 | Interleukin 10 |

| | |
|---|---|
| IL-18 | Interleukin 18 |
| IL-33 | Interleukin 33 |
| IP | Intraperitoneal |
| **K** | |
| $K^+$ | Potassium |
| **L** | |
| LDB | Light Dark Box |
| LPS | Lipopolysaccharide |
| LRR | Leucine Rich Repeats |
| **M** | |
| MAC | Membrane Attack Complex |
| MBP | Myelin Basic Protein |
| MBT | Marble Burying Test |
| MCP1 | Monocyte Chemoattractant Protein 1 |
| MIP1α | Macrophage Inflammatory Protein 1 Alpha |
| MIP1β | Macrophage Inflammatory Protein 1 Beta |
| MIP2 | Macrophage Inflammatory Protein 2 |
| MRI | Magnetic Resonance Imaging |
| mRNA | Mature RNA |
| MS | Multiple Sclerosis |
| MT | Melatonin |
| mTNFα | Membrane-bound TNFα |
| Myd-88 | Myeloid Differentiation Primary Response 88 |
| **N** | |
| $N_2$ | Nitrogen |
| $Na^+$ | Sodium |
| NE | Neonatal Encephalopathy |
| NEK7 | NIMA-related Kinase 7 |
| NF-κB | Nuclear Factor kappa-light-chain-enhancer of activated B cells |
| NLR | NOD-like Receptor |
| NLRP3 | NLR family pyrin domain containing 3 |

| | |
|---|---|
| NMDARs | N-methyl-D-aspartate Receptor |
| NO | Nitrous Oxide |
| NOD | Nucleotide binding domain leucine rich repeat protein |
| NOL | Novel Object Location |

**O**

| | |
|---|---|
| $O_2$ | Oxygen |
| OCD | Obsessive Compulsive Disorder |
| OF | Open Field |
| OPC | Oligodendrocyte Progenitor Cells |

**P**

| | |
|---|---|
| P2RY12 | Purinergic Receptor P2Y12 |
| P2X7R | P2X Purinoreceptor 7 |
| PAMPs | Pathogen Associated Molecular Patterns |
| PBS | Phosphate Buffered Saline |
| PD | Parkinson's Disease |
| PFA | Paraformaldehyde |
| PhB | Phenobarbital |
| PLP | Myelin Proteolipid Protein |
| PND | Postnatal Day |
| PPARγ | Peroxisome Proliferator-Activated Receptor Gamma |
| PRR | Pattern Recognition Receptor |
| PSD-95 | Postsynaptic Density Protein 95 |
| PYD | Pyrin Domain |

**Q**

| | |
|---|---|
| qPCR | Quantitative PCR |

**R**

| | |
|---|---|
| RNA | Ribonucleic Acid |
| ROS | Reactive Oxygen Species |

**S**

| | |
|---|---|
| SAH | Subarachnoid Haemorrhage |
| SDA | Seizure Detection Algorithm |

| | |
|---|---|
| SEM | Standard Error of the Mean |
| sTNFα | Soluble TNFα |
| **T** | |
| TBI | Traumatic Brain Injury |
| TGN | Trans-Golgi Network |
| TH | Therapeutic Hypothermia |
| TLR | Toll-Like Receptor |
| TLR2 | Toll-Like Receptor 2 |
| TLR4 | Toll-Like Receptor 4 |
| TMB | Tetramethylbenzidine |
| TNFα | Tumour Necrosis Factor Alpha |
| TNFR1 | Tumour Necrosis Factor Receptor 1 |
| TNFR2 | Tumour Necrosis Factor Receptor 2 |
| **W** | |
| WHO | World Health Organisation |

# Chapter 1: Introduction

## 1.1. Neonatal Encephalopathy

Neonatal Encephalopathy (NE) is defined as a “syndrome of disturbed neurologic function in the earliest days of life in an infant born at or beyond 35 weeks of gestation, manifested by a subnormal level of consciousness or seizures, and often accompanied by difficulty with initiating and maintaining respiration and depression of tone and reflexes'' (American College of Obstetricians and Gynaecologists, 2014). NE is caused by several antenatal and perinatal factors, including hypoxia/ischaemia, perinatal infections, placental abnormalities, and metabolic disorders (Aslam et. al., 2019; McIntyre et. al., 2021). The most common aetiology of NE is hypoxic-ischaemic encephalopathy, which accounts for approximately 29% of NE cases (Molloy & Bearer., 2018). For this reason, hypoxia/ischaemia is the preferred aetiology of NE to examine in preclinical studies.

### 1.1.1. Hypoxic-Ischaemic Encephalopathy Incidence

Hypoxic-Ischaemic Encephalopathy (HIE) describes NE resulting from an anoxic or ischaemic brain injury, where blood flow and/or oxygen supply to the brain is compromised (Molloy & Bearer., 2018). HIE is highly correlative with economic regions, with an incidence of 1 to 3 in 1000 live births reported in developed countries (Shipley et. al., 2021; Cornet et. al., 2023), and up to 20 in 1000 births in developing countries (Badawi et. al., 1998: Kukka et. al., 2022). Seizures are the most common neurological sign of HIE, and over 50% of affected neonates develop seizures, even while receiving treatment for HIE (Boylan et. al., 2015).

### 1.1.2. Aetiology and Pathophysiology of HIE

HIE is often referred to as birth asphyxia, and the terms are sometimes used interchangeably. HIE is initiated either peripartum or intrapartum, often by a sentinel hypoxic or ischaemic event, such as severe abruptio placentae or a ruptured uterus (Aslam et. al., 2019). A state of

persistent hypoxia leads to hypercapnia (build-up of $CO_2$ in the blood), resulting in metabolic acidosis. During hypoxia, lower $O_2$ levels reduce the $O_2$ partial pressure in the blood, compromising $O_2$ transportation and metabolism, and blood flow to organs. HIE intracellular cascades can be separated into phases: the primary energy failure, a latent phase, a secondary energy failure and a tertiary energy failure (Figure 1.1). The primary energy failure, which is the acute phase post-injury, is characterised by mitochondrial disruption and reduced ATP production, resulting in depletion of ATP pools and disruption of cell machinery such as the $Na^+/K^+$ ATPase pump (Brillault et. al., 2008). The subsequent membrane depolarisation causes the release of neurotransmitters, such as glutamate, into the synaptic cleft (Tan et. al., 1996; Gunn & Gunn., 1997), where they interact with AMPARs and NMDARs post-synaptically resulting in an increase of intracellular calcium. This is followed by the release of secondary messengers, such as nitrous oxide (NO) and reactive oxygen species (ROS), and subsequent neuronal cell death and damage (Rocha-Ferreira & Hristova., 2016; Kleuskens et. al., 2021). The presence of hyperexcitability and neuronal death or damage thus induces a significant neuroinflammatory response to combat the worsening of damage and clear cell debris. During the latent phase there is a recovery of sorts, as cerebral blood flow and/or oxygenation is restored and ATP pools are replenished. This is followed by a secondary energy failure starting several hours and lasting up to days post-HIE, characterised by further neuronal death, depletion of ATP pools, excitotoxicity and continued neuroinflammation (Liu & McCullough., 2013; Rocha-Ferreira & Hristova., 2016; Samaiya et. al., 2021). The extent of the damage seen in the secondary energy failure is determined by the severity of the primary energy failure. Finally, the tertiary phase is the resultant chronic brain injury which can last for years post-HIE. Here, we see chronic neuroinflammation, astrogliosis and tissue repair (Kleuskens et. al., 2021).

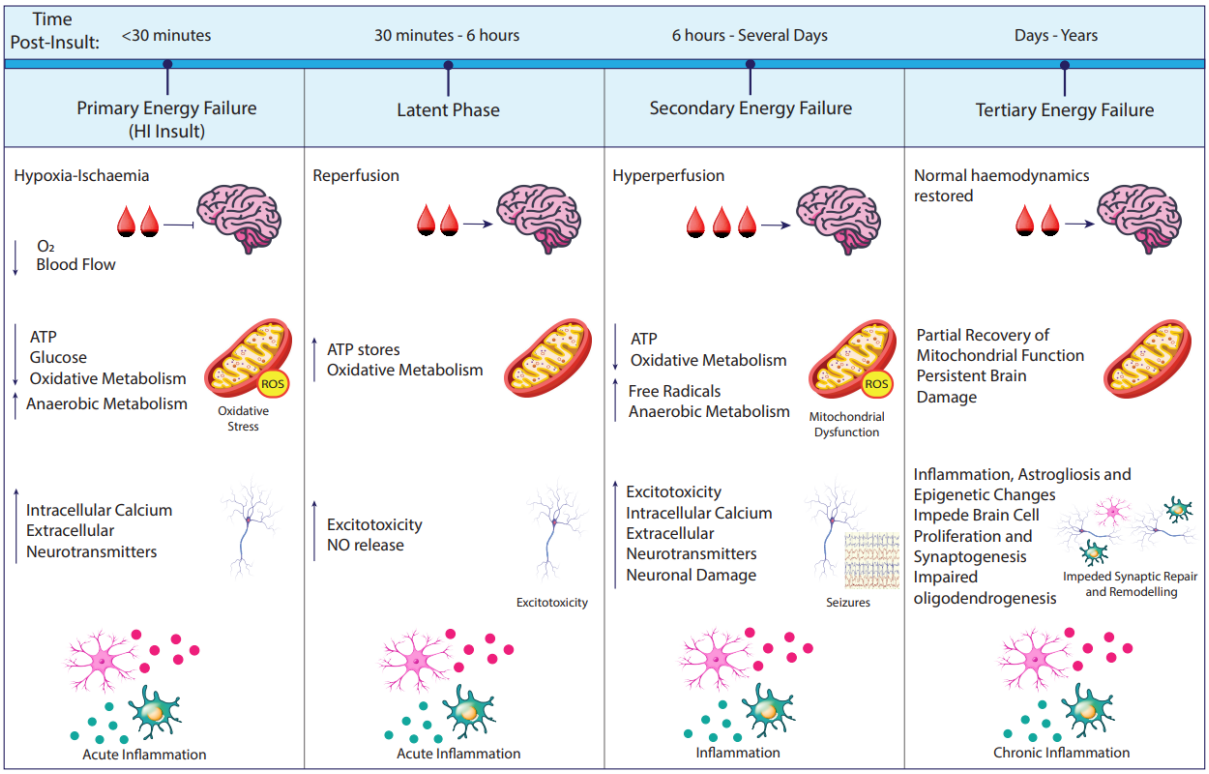


***Figure 1.1. Summary of Energy Failure Phases post-HIE. (A)*** *A hypoxic and/or ischaemic insult causes reduced oxygen and/or reduced blood flow for up to 30 minutes, inducing a primary energy failure. ATP and glucose stores are depleted, leading to increased anaerobic metabolism and oxidative stress in mitochondria, accompanied by elevated intracellular* $Ca^{2+}$ *and extracellular neurotransmitter concentrations in neurons. A significant inflammatory response is induced.* ***(B)*** *Upon reperfusion and/or re-introduction of oxygen, there is a latent phase of normal metabolism for up to 6 hours post-injury, regarded as the therapeutic window to prevent further damage. Mitochondria resume oxidative metabolism, restoring ATP pools. Neurons remain under excitotoxic stress, thus releasing nitrous oxide. The inflammatory response remains active to clear damage and debris from the primary energy failure.* ***(C)*** *The secondary energy failure lasts for several days post-injury. The severity of damage in this stage depends on the severity of the primary energy failure. Mitochondrial dysfunction resumes, once again depleting ATP stores and reverting to anaerobic metabolism. Neuronal excitotoxicity persists, causing seizures, neuronal damage, and neuronal death in severe HIE. A strong inflammatory response persists throughout.* ***(D)*** *The tertiary energy failure describes damage persisting years after the original insult. Normal haemodynamics are restored, although other functions remain affected. In mild/moderate injury, mitochondria recover full functionality, although regardless of injury severity, there is persistent brain damage. Brain cell proliferation, synaptogenesis and synaptic remodelling are impaired by chronic inflammation, astrogliosis and epigenetic changes. Oligodendrogenesis is impacted, causing long-term white matter damage. Chronic inflammation has been extensively characterised in both animal and human studies, regardless of injury severity, with widespread consequences.*

Hypoxia and ischaemia affect all organs, but the brain is especially vulnerable (Hankins et. al., 2002; Bhatti & Kumar., 2014; Iribarren et. al., 2022). The high $O_2$ demand of the central nervous system (CNS) makes it more susceptible to hypoxic/ischaemic insults. Within the brain, the hippocampus is especially prone to elevated immunoreactivity and damage due to the higher density of microglia and inflammatory receptors (Williamson & Bilbo., 2013). The hippocampus is an incredibly plastic region, central to learning and memory and neurogenesis throughout life (Balschun et. al., 2004; Bhattacharyya et. al., 2008; Williamson et. al., 2011). Immune signalling and microglia mediate and support these functions, requiring a basal level of neuroimmune signalling in the hippocampus i.e. cytokine receptor expression (Williamson & Bilbo., 2013). Moreover, immune molecules are integral to guiding neurodevelopment, governing synaptogenesis (Tremblay & Majewska., 2011), synaptic pruning (Schafer et. al., 2012; Weinhard et. al., 2018) and neural migration (Addison et. al., 2000; Imitola et. al., 2004). Microglia and cytokine signalling are associated with neonatal seizure activity post-HIE, and long-term neurodevelopmental complications arising from early-life inflammation (Cunningham & De Souza, 1993; Williamson & Bilbo., 2013; Shaker et. al., 2021).

### 1.1.3. HIE and Neonatal Seizures

HIE is the aetiology of NE most likely to present with neonatal seizures (Aslam et. al., 2019), and is the most common aetiology overall, causing 38-46% of neonatal seizures (Weeke et. al., 2015; Glass et. al., 2016). Neonatal seizures are the most common neurological emergency in neonates, significantly associated with mortality and neurological disability in surviving infants (Pembegul Yildiz et. al., 2020). They are regarded as transient electrographic changes in the brain because of excessive, abnormal, or synchronous neurologic function, presenting with or without clinical signs in the first 28 days of life for a full-term neonate, or before 44 weeks gestational age for a preterm neonate (Pellegrin et. al., 2019). The brain is most

susceptible to seizures during the neonatal period due to factors including immature GABAergic inhibition (Briggs & Galanopoulou., 2011) and altered glutamatergic receptor configuration (Rakhade & Jensen., 2009; Katsarou et. al., 2018), some of which are sexually dimorphic (Giorgi et. al., 2014). Immature GABAergic neurotransmission results in depolarisation instead of hyperpolarisation of neurons and altered glutamate receptor configurations cause a higher influx of $Ca^{2+}$, thus reducing the seizure threshold (Rakhade & Jensen., 2009). Neonatal seizures can be either electro-clinical, presenting with both clinical signs and electroencephalographic (EEG) abnormalities, or electrographic only, which present as EEG abnormalities with no clinical signs, making them challenging to detect reliably in a clinical setting (Pressler et. al., 2021). Neonatal seizures are associated with poor long-term clinical outcomes, with studies reporting higher incidence of neurodevelopmental conditions such as epilepsy, cerebral palsy, intellectual disability, and autism (Ronen et. al., 2007; Yildiz et. al., 2012; Tadic et. al., 2018; Pembegul Yildiz et. al., 2020).

### 1.1.4. Diagnosis of HIE

Timely and accurate diagnosis of neonatal brain injury is crucial to initiate appropriate care and optimise outcomes. HIE treatment is dependent upon early intervention: the gold standard treatment for HIE, therapeutic hypothermia (TH), must be initiated up to 6 hours post-HIE to have any neuroprotective effects (Thoresen et. al., 2013; Yildiz et. al., 2017). The American Colleges of Obstetrics, Gynaecology and Paediatrics (ACOGP-AAP) task force define HIE as a retrospective diagnosis; clinicians initially provide a diagnosis of NE which may be reassigned as HIE after revising the case for factors such as foetal difficulty during labour, clinical or imaging signs of acute neurological abnormalities, APGAR scores, resuscitation at birth, metabolic acidosis, and exclusion of differential diagnoses (Executive Summary, 2014; Molloy et. al., 2023). A neonate with HIE usually presents with foetal umbilical artery

acidaemia, indicated by a blood pH below 7.0, an APGAR score below 3 at 1- and 5-minutes post-birth for severe injury or a score between 3-5 for more moderate injury (described in Table 1.1), abnormal EEG results indicating seizure activity, and abnormal neurological signs, such as hypotonia (Executive Summary., 2014).

| | Parameter | Score of 0 | Score of 1 | Score of 2 |
|---|---|---|---|---|
| **A** | Appearance (skin tone/complexion) | Blue or Pale all over | Blue at extremities, body normal (acrocyanosis) | No cyanosis, body and extremities normal |
| **P** | Pulse rate | Absent | <100 | >100 |
| **G** | Grimace (Reflex Irritability) | No response to stimulation | Grimace/feeble cry when stimulated | Cry or pull away when stimulated |
| **A** | Activity (muscle tone) | None | Some Flexion | Flexed arms and legs that resist extension |
| **R** | Respiration | Absent | Weak, irregular gasping | Strong, lusty cry. |

***Table 1.1. APGAR Scoring.*** *Five parameters assess health of a neonate after birth/ resuscitation on a 10-point scale. A score >7 is normal, <3-5 indicates possible encephalopathy.*

Magnetic resonance imaging (MRI) can assess the severity of brain damage and potentially predict outcomes on neonates as young as 5 days old (Miller et. al., 2005; Thayyil et. al., 2010; Machie et. al., 2021). In a patient with NE, a typical pattern of injury emerges involving the thalami with the associated posterior limb of the internal capsule, and, in severe cases, the brain stem. Severe cases also exhibit damage in the most metabolically active regions of the brain, such as the hippocampus (Chao et. al., 2006; Izbudak & Grant, 2011). Cortical white matter injury is more common in neonates with moderate or prolonged hypoxia (Volpe & Pasternak, 1977; Izbudak & Grant, 2011). Mild HIE causes more subtle injury patterns, which are easily missed by MRI. Machie (et. al., 2021) showed how to identify obscure injury patterns in mild HIE using high frequency MRI and Weeke scores. The Weeke score is a more detailed evaluation which examines both magnetic resonance spectroscopy and diffusion-weighted imaging, assessing each MRI component separately, e.g. the basal ganglia and the thalamus

are evaluated separately, with bilateral injury receiving a higher severity score than unilateral injury in each component (Weeke et. al., 2018). This could assess the neuroprotective effects of TH or other candidate therapies in the future (Machie et. al., 2021).

Amplitude-integrated EEG (aEEG) has been used to assess neonatal seizures and predict outcomes post-HIE for decades and is still widely used. aEEG is a trend measure of background EEG activity, more suited to long-term monitoring of electro-cortical activity. aEEG recordings in the first six hours post-birth are a robust predictor of neurological outcomes (Spitzmiller et. al., 2007; Meder et. al., 2022). Continuous aEEG bedside recordings in the days post-birth can also track the recovery of normal background activity and establishment of the sleep-wake cycle (Osredkar et. al., 2005; Van Laerhoven et. al., 2013). Delayed establishment of the sleep-wake cycle and circadian rhythm associated sleep problems are associated with HIE (Tian et. al., 2021), providing an additional prognostic tool for neurodevelopmental outcomes (Meder et. al., 2022). Continuous aEEG is also favoured by clinical staff as it can be applied and interpreted at the bedside by neonatal unit staff to inform patient care. Conventional EEG (cEEG) is regarded as the most reliable and accurate method to confirm a neonatal seizure (duPont-Thibodeau et. al., 2017; Pellegrin et. al., 2019), although the ambiguous presentation of neonatal seizures can still lead to misdiagnosis. cEEG is more specialised, requiring more expertise to record and interpret than aEEG, which may not always be feasible (Nagarajan & Ghosh., 2016). This has led to the development of seizure detection algorithms (SDAs). The Algorithm for Neonatal Seizure Recognition (ANSeR), intended for use with cEEG, assessed 264 babies born between the gestational age of 36 to 44 weeks in a multi-centre randomised control trial (Pavel et. al., 2020). The ANSeR algorithm accurately identified more seizure hours in afflicted neonates than with cEEG alone, but there was no difference in the number of seizures detected between the algorithm and cEEG monitoring by clinicians (Pavel et. al.,

2020). A secondary analysis of ANSeR using cEEG recordings for term infants before, during and after TH highlighted that seizure activity after cessation of active cooling correlated with worse outcomes. This analysis therefore affirmed the importance of continuous monitoring even after cooling for predicting long-term neurological outcomes (Pavel et. al., 2024).

Biochemical biomarkers, such as blood lactate levels, umbilical cord blood pH and arterial blood gas, also indicate the presence or severity of HIE. In the initial hours post-injury, neonates with HIE have higher blood lactate levels, although there is no difference between those with moderate or severe injury (Heljic et. al., 2018; Michniewicz et. al., 2020). However, higher blood lactate between 4- and 24-hours post-HIE were associated with more severe injury and poorer outcomes (Shah., 2004; Boerger et. al., 2024). Arterial blood gas and umbilical cord blood pH are routinely investigated by clinicians as they are objective and complementary measurements, given that hypercapnia causes blood pH to become acidic (acidaemia) (White et. al., 2010; Ahmadpour-Kacho et. al., 2015). They can also be predictive of outcomes: Lau (et. al., 2023) found that infants with APGAR scores under 7 and a blood pH 6.9 - 7.0 had a 4.3% chance of developing adverse outcomes, but this rose to 30% for infants in the same APGAR score range with a blood pH < 6.9.

### 1.1.5. Clinical Outcomes of HIE

HIE is the leading cause of death in neonates, accounting for 23% of infant mortality worldwide (Millar et. al., 2017). In 2017, birth asphyxia and birth trauma caused 4.35 deaths per 1000 live births globally according to the World Health Organisation (WHO). In surviving neonates, HIE is a leading cause of acquired brain injury and life-long neurological impairments (Kurinczuk et. al., 2010; Black et. al., 2010; Rocha-Ferreira & Hristova., 2016). The co-occurrence of HIE and neonatal seizures is more strongly associated with long-term

neurological deficits (Pembegul Yildiz et. al., 2020). TH significantly improves mortality in moderate to severe cases of HIE, although approximately 40% of surviving infants develop adverse neurological outcomes (Jacobs et. al., 2013). Clinical outcomes include cerebral palsy, intellectual disability, autism, ADHD, and epilepsy (Lou., 1996; Tadic et. al., 2018; Pembegul Yildiz et. al., 2020). There is a growing body of evidence to suggest that even infants with mild HIE are also at risk of adverse outcomes (Conway et. al., 2018; Machie et. al., 2021).

### 1.2. Treatment of HIE and Neonatal Seizures.

HIE and Neonatal Seizures are both potentially life-altering conditions with limited therapeutic options and suboptimal clinical outcomes. These options are a mixture of pharmacological and non-pharmacological methods. The most appropriate treatment is dependent on the aetiology of HIE and presence of seizure activity. As discussed previously, diagnostic methods for identifying and assessing severity for both HIE and neonatal seizures leave much to be desired with regards to their sensitivity and specificity.

#### 1.2.1. Non-Pharmacological Treatment - Therapeutic Hypothermia

The gold-standard treatment strategy for HIE is TH. During TH, the core body temperature of the neonate is reduced to 33-34°C, inducing a mild state of hypothermia, which is maintained for a maximum of 72 hours (Aker et. al., 2019). This is achieved through either full body cooling or head cooling. A major limitation of TH is that it must be initiated within 6 hours of the originating insult for it to have any therapeutic effect (Thoresen et. al., 2013; Laptook et. al., 2017). This is challenging when the originating insult or sentinel event is not always easily identifiable. The mechanisms by which TH elicits its neuroprotective effects are complex, but in principle, TH slows the exacerbation of damage (i.e. secondary injury) which occurred in the acute timeframe following the original insult (primary injury). In targeting this toxicity, this

dampens the overproduction of ROS, neurotransmitters, inflammatory markers, and apoptosis (González-Ibarra et. al., 2011). While TH effectively attenuates damage in the infant brain after moderate HIE (Sinha et. al., 2018), it does not come without complications. The rewarming process is fraught with risk and must be done gradually, usually by raising the infant's core temperature by 0.5°C every 1 or 2 hours over a period of 6 to 12 hours (Lemyre & Chau., 2018). Some infants experience seizures or a worsening of clinical encephalopathy during rewarming, and in these instances, infants are returned to hypothermic temperatures for 24 hours before rewarming is resumed (Kendall et. al., 2012). Other potential complications include bradycardia, hypotension, thrombocytopenia, and subcutaneous fat necrosis, potentially leading to hypercalcemia (Boutaybi et. al., 2014; Karcioglu et. al., 2018; Rodd et. al., 2021). A meta-analysis of 29 randomised controlled trials from high-income and low-income healthcare settings found that TH reduced the incidence of neurological disability and cerebral palsy, although did not affect neonatal mortality. TH treatment also did not reduce seizure incidence in the neonates or the incidence of childhood epilepsy later in life (Mathew et. al., 2022).

TH is also the gold standard non-pharmacological treatment strategy for neonatal seizures, but with far-from-optimal results, and is often only employed when seizures co-occur with NE or HIE. TH reduces the duration of seizures, but not the number of events (Low et. al., 2012; Boylan et. al., 2015). While TH provides modest neuroprotection in the acute stages post-HIE and/or neonatal seizure, its prevention of long-term neurological outcomes associated with HIE and seizures is more limited (Shankaran et. al., 2012).

### 1.2.2. Pharmacological Treatment - Anti Seizure Medications

Pharmacological treatment is used for HIE when seizures also occur (Glass., 2014). The WHO recommend the gamma-amino butyric acid receptor A ($GABA_A$-R) agonist Phenobarbital (PhB) as the first-line pharmacological drug to treat HIE-induced neonatal seizures, followed by phenytoin and fosphenytoin (Glass et. al., 2012). Despite being the first-line treatment, only 50% of infants respond positively to PhB treatment, and the remaining 50% experience either no change or exacerbated seizures (Painter et. al., 1999; Slaughter et. al., 2013; Donovan et. al., 2016; Spagnoli et. al., 2016). Phenytoin is the second line treatment, and while it is similarly efficacious to PhB, phenytoin treatment is more complicated due to adverse effects, including the requirement for frequent blood monitoring to prevent toxicity (Slaughter et. al., 2013).

PhB is a positive allosteric modulator of the $GABA_A$-R. In the neonatal brain, $GABA_A$-R activation leads to depolarisation of immature neurons via $Cl^-$ efflux, promoting hyperexcitability (Ben-Ari et. al., 2007). Neonates exhibit increased intra- and inter-individual variability in pharmacokinetic properties for a range of drugs, including PhB (Marsot et. al., 2014), due to rapid developmental changes (Sami et. al., 2021). PhB pharmacokinetics is also affected by other pathophysiological consequences of a disease state, such as HIE, altered drug elimination capacities either by renal or hepatic impairment, altered haemodynamics or decreased cardiac output (Pokorna et. al., 2015; Smits et. al., 2020). Another factor implicated in PhB pharmacokinetic variability is TH. Hypothermia often delays the clearance of drugs, resulting in increased plasma concentrations and longer half-lives, as demonstrated in studies of chlorzoxazone, fentanyl, gentamicin, theophylline and morphine (Koren et. al., 1985; 1987; Bansinath et. al., 1988; Tortorici et. al., 2006; 2007). Studies of PhB pharmacokinetics post-TH have had mixed results; Fillippi (et. al., 2011) showed that PhB clearance is delayed in a study

of hypothermic newborns versus normothermic newborns, while Shellhaas (et. al., 2013) found no significant changes in PhB clearance during TH treatment. Pokorna and colleagues (2019) found that both asphyxia severity and TH treatment were important pharmacokinetic covariables, suggesting that the variability in PhB clearance is a more complex interplay of factors rather than solely caused by TH.

Several harmful and persisting consequences of PhB treatment during the neonatal period have been recorded. As early as 1978 it was found that perinatal treatment with PhB reduces brain weight (Diaz & Schain, 1978), and by 1989 researchers had found PhB treatment to reduce pyramidal and granule cells in the hippocampus (Pick & Yanai, 1985), and Purkinje and granule cells in the cerebellum (Yanai et. al., 1989). Introducing anticonvulsants to the developing brain can hinder vital functions such as synaptogenesis, neurogenesis, and synaptic plasticity (Bittigau et. al., 2002; Forcelli et. al., 2011; 2012; Ahmad et. al., 2018). PhB treatment in the neonatal period is also associated with long-term neurodevelopmental consequences and non-improvement of outcomes post-HIE (Quinlan et. al., 2018). Clinical studies support this, showing that children treated with PhB as neonates perform significantly poorer in cognitive and motor function tests at 12 to 24 months of age compared to same-age untreated infants (Maitre et. al., 2013; Ghosh et. al., 2019; Liu et. al., 2020).

### 1.2.3. Clinical Trials for HIE

#### 1.2.3.1. Melatonin

Melatonin (MT) is an indoleamine endogenously produced in the pineal gland, best known for its regulation of circadian rhythm. It is also a potent scavenger of free radicals (a by-product of oxidative stress), easily crosses the blood-brain barrier (BBB), and its receptors are widely distributed throughout the brain, including on microglia (Calvo et. al., 2013). Preclinical

studies have shown that MT is neuroprotective, both as a single therapy and as an adjuvant with TH, improving neuronal viability, infarct volumes and long-term neurological outcomes (Carloni et. al., 2008; Alonso-Alconada et. al., 2013; Robertson et. al., 2013a; Hu et. al., 2017). Pilot studies in human neonates comparing MT and TH treatment to TH alone show that MT and TH treatment increased survival post-HIE (Aly et. al., 2015; Ahmad et. al., 2018) and reduced neurological disabilities detected at 6 months (Aly et. al., 2015) and 18 months of age versus TH alone (Jerez-Calero et. al., 2020). The MELPRO study is the first Phase III trial for MT as an adjuvant with TH for moderate to severe HIE (NCT 03806816), assessing acute and chronic outcomes up to 24 months of age.

#### 1.2.3.2. Erythropoietin

Erythropoietin (EPO) is a glycoprotein produced in the liver, which is expressed, along with its receptor (EPO-R) by many cell types in the brain. EPO is required for normal brain development, and is involved in inflammation inhibition, upregulating expression of anti-apoptotic genes, reducing oxygen free radicals and decreasing caspase activation (Robertson et. al., 2013b). EPO is also involved in neurogenesis, angiogenesis, inflammation and promoting white matter development (Shingo et. al., 2001; Gonzalez et. al., 2013). Activation of Hypoxia-inducible factor (HIF) by hypoxia or pro-inflammatory cytokines stimulate increased expression of EPO and EPO-Rs (Zhao et. al., 2013). EPO can downregulate elevated pro-inflammatory cytokines through negative feedback loops to prevent an uncontrolled continuation of the inflammatory response (Villa et. al., 2003; Brines & Cerami., 2013). At the site of injury, neurons express EPO-Rs, which is followed by astrocytic release of EPO (Spandou et. al., 2004). EPO treatment was proposed to upregulate EPO-Rs post-HIE, enhancing tissue protection and erythropoiesis (Teramo et. al., 2018). Preclinical studies demonstrated the neuroprotective effects of exogenous EPO treatment on HIE-induced brain damage (Juul.,

2004; Traudt et. al., 2013; Pang et. al., 2020). In animal models, higher doses of EPO were associated with both histological and functional attenuations post-HIE, although combining EPO with TH provided no additional neuroprotection (Statler et. al., 2007; van der Kooij et. al., 2008; Wassink et. al., 2020; 2021). Clinical trials for EPO monotherapy conducted in clinical settings where TH was unavailable (Zhu et. al., 2009; Malla et. al., 2017) found that EPO was neuroprotective after acute treatment. Clinical trials for EPO and TH combined therapy have had mixed results. The Phase II NEATO trial (NCT 01913340) showed limited attenuation of neurodevelopmental outcomes at 9 and 12 months of age (Wu et. al., 2016; Massaro et. al., 2018). Similarly, the Phase III HEAL trial (NCT 02811263) and the Phase III PAEAN trial (NCT 03079167) found that EPO had no impact on survival or neurodevelopmental outcomes and was associated with a heightened risk of serious adverse events (Wu et. al., 2022; Juul et. al., 2023).

#### 1.2.3.3. Complement Inhibitor RLS-0071

Recently, studies have highlighted the complement pathway as participatory in the neuroprotective effects of TH. Shah (et. al., 2021) found that, when TH treatment reduced the size of brain infarctions, it also decreased systemic serum levels of C1q and C5a, downregulated mitochondrial C1q expression and decreased microglial and neuronal depositions of C3 and C9. Based on these findings, Kumar (et. al., 2021) utilised a complement C1 inhibitor, the peptide inhibitor RLS-0071 (ReAlta Life Sciences, USA), as an adjuvant with TH in a rat model of HIE. RLS-0071 and TH reduced infarct size, attenuated neuronal death, reduced C1q protein levels and improved long-term brain growth and neurocognitive outcomes versus TH alone (Kumar et. al., 2021). Phase II clinical trials are underway to evaluate RLS-0071 as an adjuvant with TH in severe HIE (NCT05778188).

## 1.3. Experimental Models of HIE

Preclinical models have been used extensively to study NE and neonatal seizures. As mentioned before, HIE is the most widely studied aetiology of NE. Preclinical studies of HIE rely upon *in vivo* models to further probe the pathophysiology of HIE and neonatal seizures under a variety of conditions. The species used include higher mammals such as sheep, pigs or monkeys, and rodents, rats and mice. HIE *in vivo* models can be further divided into two loose categories: hypoxia-ischaemia models and hypoxia-only models.

### 1.3.1. Modelling HIE in Higher Mammals

Preclinical studies of HIE in higher mammals, such as sheep, pigs, or monkeys, are far less common than those conducted using rodents, primarily due to high costs.

Very few studies of HIE have been conducted in non-human primates. The first model of birth asphyxia was published in 1979 (Fahn et al., 1979), inducing asphyxia in term monkey foetuses by covering their heads with a rubber sac and clamping the umbilical cord. 12 minutes of asphyxia was required to produce neuropathological injury, and monkeys resuscitated after 20 minutes of asphyxia had extremely high mortality. The damage exhibited in this model was primarily found in the brain stem. Fahn (et. al., 1979) also designed a partial ischaemia model whereby pregnant females were made hypotensive during their third trimester. Foetal blood $O_2$ saturation was reduced to 10% for 5 hours, inducing profound acidaemia. At birth, these monkeys displayed postural abnormalities associated with brain damage and convulsions (Fahn et. al., 1979). A model of white matter injury in baboons was also devised, whereby baboons were delivered prematurely by hysterotomy and treated in an intensive care setting (Inder et. al., 2004). Half of these baboons exhibited white matter injury, although further behavioural testing was not undertaken.

Piglets are considered a translatable model, as they display similar neuropathological patterns post-HIE to humans (Johnston., 1998), and a piglet at birth is developmentally comparable to a full-term infant. Both hypoxia-ischaemia and hypoxia-only models of HIE have been developed in piglets. Piglet models of hypoxia-ischaemia are performed by transiently occluding the carotid arteries (Kerenyi et. al., 2012) or the airways (Martin et. al., 1997) to induce ischaemia, and inducing hypoxia by reducing the $O_2$ concentration during this period (Martin et. al., 1997: Kerenyi et. al., 2012; Alonso-Alconada et. al., 2015). In hypoxia-only models of HIE, piglets are anaesthetised, intubated and kept on cardiac and EEG monitoring throughout. The $O_2$ concentration is reduced to 6% at the beginning of hypoxia, lasting for an average of 45 minutes if piglets do not experience cardiac arrest. $O_2$ concentration is transiently increased when piglets are severely bradycardic or hypotensive and reduced back down to 6% upon recovery (Thoresen et. al., 1996). A limitation of the hypoxia-only models is that the piglet heart is more sensitive to hypoxic injury than the brain, so cardiac monitoring and transient cessation of hypoxia are crucial to their survival for further study (LaRosa et. al., 2017).

Sheep are more developmentally advanced than humans at birth, so foetal sheep are studied at 0.85 gestation (~125 – 130 days, term = 145) to model HIE at full-term, and at 0.65-0.75 gestation (~95 – 108 days) to model HIE in premature infants (Dobbing & Sands., 1979). HIE is induced in foetal sheep by umbilical cord occlusion, cerebral ischaemia or asphyxia. During umbilical cord occlusion, the umbilical cord is partially occluded for 1 minute every 3 minutes over the course of 2 hours (Clapp et. al., 1988) or for more severe models, 2 minutes of every 5 minutes for 2 hours (De Haan et. al., 1997). In cerebral ischaemia models, bilateral carotid occlusion for 10 to 20 minutes induces selective neuronal necrosis, and 30 to 40 minutes induces epileptiform activity and robust neuronal damage in the striatum, parasagittal cortex,

and hippocampus (Williams et. al., 1990; 1992). In asphyxia models, asphyxia repeated every 5 hours induces injury almost exclusively to the striatum, whereas asphyxia repeated every 5 minutes causes extensive diffuse damage to the cortex, thalamus, and cerebellum in 40% of animals, and selective neuronal necrosis in these regions for the remaining 60% (Gunn et. al., 1992; Richardson & Bocking., 1998; Dalitz et. al., 2003).

### 1.3.2. Rodent Models of Hypoxia-Ischaemia

The most widely used rodent model of hypoxia-ischaemia is the Rice-Vanucci model, first defined by Rice et. al., in 1981. In the original protocol, performed on a P7 rat pup, the right carotid artery is ligated surgically, inducing ischaemia, and 4 to 8 hours following surgery, the pup is placed in a hypoxia chamber at 8% $O_2$ for three and a half hours, inducing hypoxia. The pathology observed replicates anatomical damage patterns seen in human neonates, including grey matter injury in the hippocampus, the cortex, the basal ganglia, and the thalamus (Rice et. al., 1981; Vanucci et. al., 1999), and white matter lesions, the severity of which correlates with the duration of hypoxia (Liu et. al., 2002; Drobyshevsky et. al., 2005; 2007). The Rice-Vanucci model causes decreased cerebral blood flow (Vannucci et. al., 1988), decreased cerebral glucose uptake (Vannucci et. al., 1989), brain acidosis (Yager et. al., 1991) and a heightened inflammatory response, both acutely and chronically (Bona et. al., 1999). This model has been widely used to study severe HIE for decades, although it is associated with high variability in infarct size and symptomatology. Researchers have tried to address this by modifying the original model, producing slightly different phenotypes but consistent overall hallmarks, such as seizures, memory impairment and hyperactivity (Shimomura & Ohta 1988; Jensen et. al., 1995; Laroia et. al., 1997; Mortola & Naso., 1998; Caputa et. al., 2005).

### 1.3.3. Rodent Hypoxia-only Models

The first rodent hypoxia-only model of HIE was described by Jensen et. al., (1991). This model induces acute seizures by global hypoxia in P10 rats, exposing them to 3-4% $O_2$. Hypoxia-only models were developed to mimic mild to moderate HIE following perinatal asphyxia. Few hypoxia-only models exist, most of which are permutations of the original Jensen model. The model used in this study is a hypoxia-only model of HIE, based on the Jensen model and developed by Rodriguez-Alvarez (et. al., 2015). C57BL6/J P7 mice are exposed to 5% $O_2$ for fifteen minutes to induce global hypoxia, modelling moderate hypoxia in a full-term neonate (Rodriguez-Alvarez et. al., 2015). The pathological features in hypoxia-only models are more subtle than those seen in hypoxia-ischaemia models, with histological damage detected by silver staining and no differences in cell death markers (Boss et. al., 2005; Rodriguez-Alvarez et. al., 2015). Several studies have recorded altered levels of neurotransmitters (Gunn & Gunn., 1997; Millar et. al., 2017), a lower seizure threshold later in life and a heightened neuroinflammatory response (Rakhade et. al., 2011; Sun et. al., 2012; Cleary et. al., 2013; Rodriguez-Alvarez et. al., 2015; Quinlan et. al., 2018). Further evidence to support its translatability was demonstrated by the response to PhB treatment during acute seizures. 50% of P7 pups do not respond to PhB treatment for acute seizures post-HIE, which reflects the response rate reported in human patients (Rodriguez-Alvarez et. al., 2015; Quinlan et. al., 2018). Longer-term studies with this model demonstrate that mice developed lower seizure thresholds, memory impairments and anxiety-like behaviours, which echo neurological conditions such as intellectual disability and epilepsy which patients are much more likely to develop post-HIE (Mikati et. al., 2005; Talos et. al., 2012; Rodriguez-Alvarez et. al., 2015; Quinlan et. al., 2018). The similarities between the mouse model and the human condition are summarised in Table 1.2. below.

| | Mouse Model | Human Neonates |
|---|---|---|
| **Acute Response** | Clinical/Electrographic Seizures | Clinical/Electrographic Seizures |
| | 56% response to Phenobarbital | 50% response to Phenobarbital |
| **Chronic Response** | Lower seizure threshold | Epilepsy |
| | Memory impairment | Cognitive disabilities |
| | Anxiety-like behaviour | Cerebral palsy |

***Table 1.2.*** *Summary of the major acute and chronic features of the global hypoxia mouse model, relating them to the hallmarks of the acute and chronic response to moderate neonatal hypoxia in humans. This summary demonstrates the translatability of this model, which had many similarities to the human condition, more so than several other models (Forcelli et. al., 2011; Chapman et. al., 2012; Maitre et. al., 2013; Rodriguez-Alvarez et. al., 2015; Ahearne et. al., 2016; Low et. al., 2016; Sun et. al., 2016; Pisani et. al., 2018; Quinlan et. al., 2018).*

## 1.4. Neuroinflammation

### 1.4.1. Inflammation

The inflammatory response is integral to the body's defences against disease and injury. Temporally, the inflammatory response has an acute phase and a chronic phase. The acute phase is characterised by the recruitment of immune cells to the site of injury, triggering the expansion of the immune response by releasing pro-inflammatory mediators such as interleukin 1β (IL-1β) (Aderem & Ulevitch., 2000; Chen et. al., 2017; Kim et. al., 2019). In normal tissue repair, this response subsides within a few hours or days; however, in some instances, this immune response can persist for longer and become chronic (Zhou et. al., 2016; Chen et. al., 2017). Chronic inflammation is associated with diseases such as arthritis, diabetes, and neurological conditions (Lintermans et. al., 2014; Chen et. al., 2017).

### 1.4.2. Inflammation in the CNS

Neuroinflammation – inflammation in the CNS – is inextricably linked to the pathology of many neurological diseases such as Alzheimer's Disease (AD), Parkinson's Disease (PD), Multiple Sclerosis (MS), epilepsy, and HIE (Linker et. al., 2002; Vezzani & Baram, 2007; Green & Nolan., 2014; Ng et. al., 2018; Tan et. al., 2020). This response is mediated by resident glial cells (microglia and astrocytes) and peripheral immune cells, which release cytokines, chemokines, ROS and secondary messengers, such as NO or prostaglandins (Dunn et. al., 2006; Norden et. al., 2016). The functions of microglia go far beyond mediating the response to injury and disease: for instance, microglia and pro-inflammatory cytokines play a central role in mediating early brain development (Schafer & Stevens., 2013; Salter & Beggs., 2014). During the neuroinflammatory response, usually initiated by infection or injury, features such as elevated pro-inflammatory mediator signalling, recruitment of microglia, astrogliosis, blood-brain barrier (BBB) permeability and resultant peripheral immune cell infiltration emerge (Werner & Englehard., 2007; Liesz et. al., 2009; 2011; Michael et. al., 2016), all of which are associated with neurological diseases.

### 1.4.3. The Inflammasome in Neuroinflammation

Pattern recognition receptors (PRRs) are a family of either transmembrane or cytosolic receptors that recognise pro-inflammatory stimuli, such as Pathogen-Associated Molecular Patterns (PAMPs) or Damage-Associated Molecular Patterns (DAMPs) and are integral to the innate immune response. Transmembrane PRRs include toll-like receptors (TLRs), while cytosolic receptors include the nucleotide-binding domain (NOD) – Leucine-Rich repeats (LRR) – containing receptors (NLRs) (Becker & O'Neill., 2007). Activation of PRRs by PAMPs and DAMPs triggers a signalling cascade which causes cytosolic PRRs, such as NLRs, to form a multimeric protein complex called the inflammasome (Yang et. al., 2019). The inflammasome

is then responsible for the activation and release of pro-inflammatory cytokines, such as IL-1β (Martinon et. al., 2002; Agostini et. al., 2004). Microglia release IL-1β both as a regulator of neurodevelopment and in response to pro-inflammatory stimuli (Del Rey et. al., 2013; Krumm et. al., 2014).

### 1.4.4. NLRP3 Inflammasome Formation

NLR family Pyrin Domain Containing 3 (NLRP3) is a 118kDa cytosolic PRR protein expressed mainly by microglia in the CNS. The C-terminal consists of a leucine-rich repeat (LRR) domain, the centre is comprised of an ATP-ase containing NACHT, to facilitate oligomerisation, and the N-terminal is a Pyrine (PYD) domain to recruit proteins for inflammasome formation (Kelley et. al., 2019). As with other inflammasomes, the NLRP3 inflammasome complex consists of a sensor, an adaptor, and an effector: NLRP3 is the sensor, apoptotic-associated speck protein (ASC) is the adaptor, and caspase-1 is the effector (Duncan et. al., 2007; Lu et. al., 2014; Schmidt et. al., 2016; Boucher et. al., 2018). The two stages of NLRP3 inflammasome formation are priming and activation (Figure 1.2). During priming, TLR or IL-1 Receptor (IL-1R) ligand-mediated signalling upregulates transcription of NLRP3 and pro-inflammatory cytokines via proteins such as myeloid differentiation primary response protein (MyD-88), the activator protein 1 (AP-1) and nuclear factor kappa-light-chain-enhancer of activated B cells (NF-κB) (Takeuchi & Akira., 2010; Yang et. al., 2020). Priming also governs post-translational modifications of NLRP3, namely ubiquitination and phosphorylation, which regulate NLRP3 activation (Yang et. al., 2017). The activation step is initiated by a secondary stimulus. NLRP3 is activated by a diverse range of stimuli, such as particulate matter, extracellular ATP, toxins, and pathogens (Figure 1.2). It has been suggested that, rather than NLRP3 recognising and binding all signals, it instead senses a common cellular event caused by all stimuli, such as disassembly of the trans-Golgi network (TGN) (Chen & Chen., 2018; Kelley et. al., 2019). Upon

activation, NIMA-related kinase 7 (NEK-7) binds to NLRP3 to modulate NLRP3 inflammasome assembly. The NACHT-domain is first activated, then the PYD domain recruits the adaptor molecule ASC to form a filamentous complex called the ASC pyroptosome (Figure 1.2). The caspase recruitment domain (CARD) of ASC binds to pro-caspase-1, which is converted into active caspase-1 via proximity-induced autoproteolysis (Lu et. al., 2014: Malik & Kanneganti., 2017). Caspase-1 cleaves the inactive pro-IL-1β and pro-IL-18 into the active IL-1β and IL-18 respectively, which are released to engage in neuroinflammatory signalling. Caspase-1 also cleaves and activates the membrane pore-forming gasdermin D (GSDMD), a protein involved in pyroptosis. The N-terminal domain of GSDMD (GSDMD-NT) shows high affinity for plasma membrane lipids, so upon cleavage GSDMD-NT oligomerises to form pores in the cell membrane, resulting in pyroptosis and the release of inflammatory cytokines IL-1β and IL-18 (Figure 1.2) (Ding et. al., 2016; Evavold et. al., 2018). Within the brain, all neural cell types express NLRP3, however it is preferentially expressed by microglia (Chiarini et. al., 2020; Pike et. al., 2021). While NLRP3 inflammasome signalling is best known for its role in pathological signalling, it also has a use in homeostatic functions. Indeed, young mice express basal levels of NLRP3 inflammasome signalling in neurogenic niches of the ventral hippocampus and basal amygdala to upkeep conditioning-induced synaptic plasticity and memory consolidation (Komleva et. al., 2021).

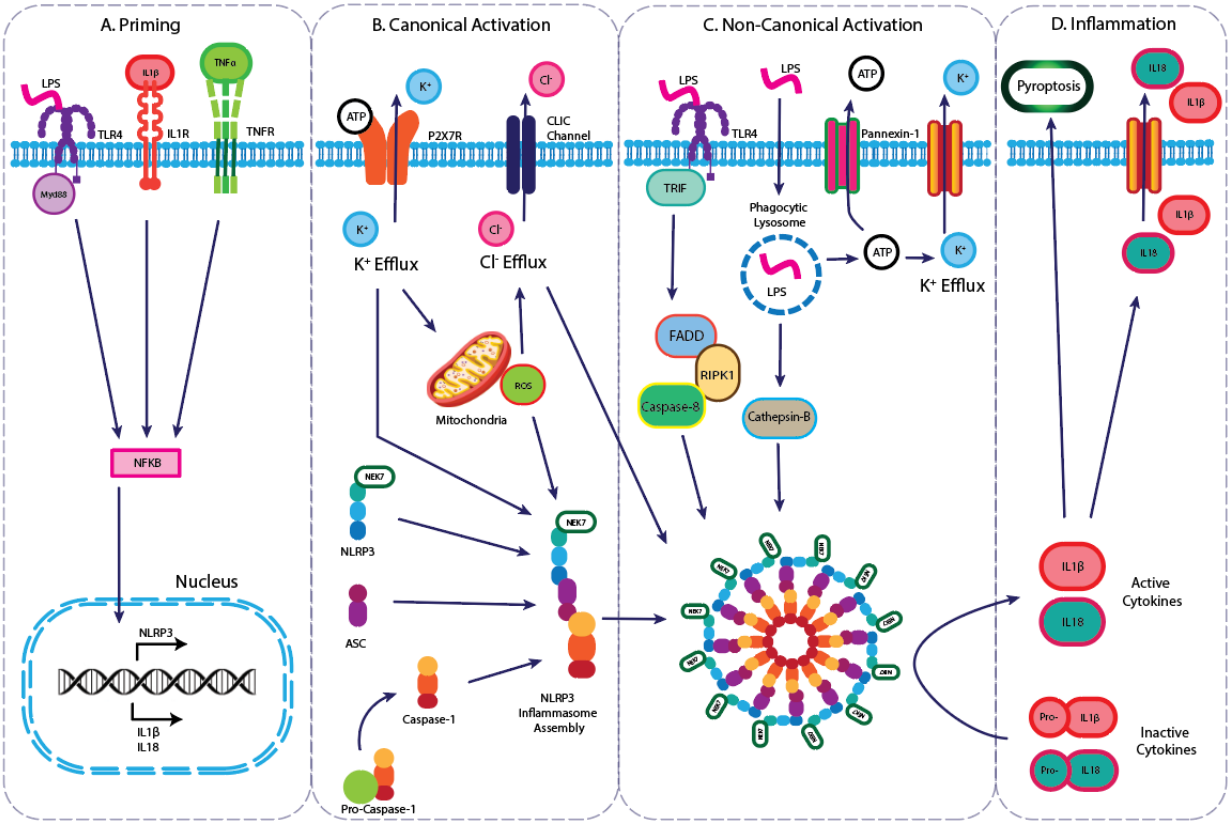


***Figure 1.2. NLRP3 Inflammasome Pathways Summary.*** *(A) NLRP3 Inflammasome formation is primed by PRR or cytokine receptor activation, leading to upregulated transcription of inflammasome related genes. (B) Priming is followed by either canonical or non-canonical activation. Canonical activation is triggered by DAMP receptors, such as P2X7R, or from mitochondrial production of ROS and the resultant $Cl^-$ efflux from the cell. Pro-caspase-1 is cleaved to release active Caspase-1. NLRP3, ASC and Caspase-1 join to form the inflammasome. (C) Non-canonical activation is triggered by PAMP receptors such as TLR4, phagocytosis of PAMPs or by ATP efflux via pannexin-1 and the resultant $K^+$ efflux. (D) The inactive pro-IL-1ϐ and pro-IL-18 are cleaved by caspase-1 in the inflammasome to release the active cytokines IL-1ϐ and IL-18. These cytokines are transported to the cell membrane and released via GSDMD pores. In some cases, pyroptosis of the cell may also occur.*

NLRP3 inflammasome activity in microglia has been linked to several neurological disorders, including Alzheimer's disease (McManus et. al., 2025), traumatic brain injury (Wallisch et. al., 2017), and Parkinson's disease (Lee et. al., 2019). In HIE, inflammasome priming signals such as IL-1β and TNF-α are upregulated. Furthermore, expression of P2X7R, a canonical activator of the NLRP3 inflammasome (Di Virgilio et. al., 2020), is upregulated post-hypoxia in a mouse model (Rodriguez-Alvarez et. al., 2017; Smith et. al., 2023). NLRP3 inflammasome is also

activated by mitochondrial dysfunction and ROS production, both of which are elevated during the primary and secondary energy failure (Rousset et. al., 2012; Stepanova et. al., 2019). These results all support findings that NLRP3 activation is elevated post-HIE (Chen et. al., 2018; Li et. al., 2021a).

Further research is needed to understand the role of the NLRP3 inflammasome in HIE, as when HIE was induced in NLRP3-knockout mice, they displayed more severe brain injury and increased microglial activation compared to wild-type mice, whereas ASC-knockout was neuroprotective post-HIE (Ystgaard et. al., 2019). This contrasts with studies where pharmacological inhibition of NLRP3 activation and formation post-HIE is neuroprotective (Lv et. al., 2020; Luo et. al., 2021; Chen et. al., 2023). This highlights how much there is yet to learn about the functional role and consequences of the NLRP3 inflammasome and its individual components during the neonatal period and post-HIE.

### 1.4.5. Treatment Observations from Preclinical Studies

The hypothesis that neuroinflammation plays a role in long-lasting outcomes following HIE and neonatal seizures is firmly supported by both clinical and preclinical studies. This allows researchers to identify potential therapeutic targets for an anti-inflammatory treatment approach with the potential to provide greater and more reliable success than conventional treatment methods. Current research in HIE treatment is focused on administering an anti-inflammatory drug as an adjuvant therapy alongside TH to improve on the modest neuroprotection provided by TH treatment (Chevin et. al., 2018).

Whether an anti-inflammatory drug could ameliorate or inhibit the pathophysiology of HIE was examined on the hypoxia-only mouse model (Quinlan et. al., 2019). The small molecule drug was the sartan molecule candesartan cilexetil (CND), an angiotensin II receptor Type 1

antagonist currently used to treat high blood pressure and heart failure. CND is in Phase II clinical trials as an acute treatment for traumatic brain injury in adults aged 18-65 (NCT05826912). CND regulates the neuroinflammatory response in microglia through inhibition of TLR4, and in neurons by activation of the anti-inflammatory neuronal receptor peroxisome proliferator-activated receptor gamma (PPARγ) (Saavedra., 2016; Qie et. al., 2020). Following hypoxia, neuronal damage was attenuated, and these mice experienced reduced anxiety, less memory dysfunction and reduced incidence of later-life epilepsy compared to mice not treated with CND (Quinlan et. al., 2019). Furthermore, CND caused no adverse effects in control mice.

The emerging role of the NLRP3 inflammasome in microglia-mediated neuroinflammation has suggested the value of NLRP3 inflammasome inhibition as a therapeutic avenue for a range of neurological disorders, including HIE. One such inhibitor is MCC950, also known as CRID3, a sulfonylurea compound which potently and selectively inhibits the assembly of the NLRP3 inflammasome by binding to the NACHT domain of NLRP3 (Coll et. al., 2015; Coll et. al., 2019). Preclinical studies have found that NLRP3 inflammasome inhibition with MCC950 is neuroprotective in models of Alzheimer's Disease (AD), traumatic brain injury (TBI), intracerebral haemorrhage (ICH), spinal cord injury (SCI), experimental autoimmune encephalomyelitis (EAE) and HIE (Coll et. al., 2015: Dempsey et. al., 2017; Ren et. al., 2017; Ismael et. al., 2018; Jiao et. al., 2020; Lv et. al., 2020). MCC950 was investigated in clinical trials for rheumatoid arthritis; however, indications of hepatotoxicity in participants resulted in the cessation of the study at Phase II (Mangan et. al., 2018). Further studies have been called for to understand the source of this hepatotoxicity, as this was not observed in preclinical models (Li et. al., 2022).

## 1.5. Microglia

Microglia, astrocytes, and oligodendrocytes are the three types of glial cells resident in the brain which create and support an optimal environment for healthy neuronal function. This thesis focuses on microglia, which are known as the permanent resident immune cells of the CNS, although this is only one of their many roles. Microglia are heavily involved in guiding and supporting neurodevelopment, and times of highest microglial activity coincide with times of rapid and active neurodevelopment, such as the perinatal period (Schafer et. al., 2012; Weinhard et. al., 2018; Logiacco et. al., 2021).

N. Achúcarro and P. Del Río-Hortega first described microglia in 1919, releasing a series of three publications recording the diverse range of microglial morphologies they encountered, from homeostatic to ameboid (Río-Hortega., 1919; Sierra et. al., 2019). The M1/M2 classification, where M1 microglia are pro-inflammatory and M2 microglia are homeostatic, was later devised to classify microglia phenotypes; however, this system is outdated as it does not reflect the multifunctional and multi-phenotypic nature of microglia (Paolicelli et. al., 2022). Diz-Chaves (et. al., 2012) extends on the M1/M2 classification by proposing five morphology types, each with a distinct functional role. Type I, II and III microglia, traditionally M2 microglia, are morphologically consistent with homeostatic microglia. Type IV and V microglia, traditionally M1 microglia, are morphologically consistent with pro-inflammatory microglia. Homeostatic microglia have small cell bodies, long and ramified processes and are highly motile. They also express cell-surface markers associated with supporting neuronal function and maintenance, such as P2RY12, CX3CR1 or CD206 (Sipe et. al., 2016; Hellström Erkenstam et. al., 2016; Tsuda., 2017). In the neonatal period they are highly active and essential to neuronal maturation through synaptic and dendritic pruning (Mitchell-Robinson

et. al., 2015). When an insult occurs in the brain, microglia become pro-inflammatory, resembling macrophages more closely – their cell bodies become enlarged, their processes retract and become less ramified and they express cell surface markers associated with the inflammatory response, such as CD36, CD68 or CD86 (Cho et. al., 2006; Wakselman et. al., 2008; Hellström Erkenstam et. al., 2016; Hendrickx et. al., 2017). These cells engage in phagocytosis, chemokine and cytokine release, and antigen presentation.

### 1.5.1. Microglia and Neurodevelopment

Unlike the rest of the cell types in the CNS that originate in the ectoderm, microglia originate in the yolk sac from primitive macrophages and invade the CNS between embryonic day (E) 8.5 – 17.5 in mice, or 4.5 - 5.5 gestational weeks in humans (Andjelkovic et. al., 1998; Ginhoux et. al., 2010; Stremmel et. al., 2018). This occurs in parallel with the birth of primitive neurons, prior to astrocytogenesis or oligodendrogenesis (Frost & Schafer., 2016). Within the brain environment they develop from early microglia (E10 to E14 in mice), to pre-microglia (E15 to postnatal day (PND) 9 in mice), finally reaching maturity as adult microglia from PND28 in mice (Matcovitch-Natan et. al., 2016). Development through these three stages is characterised by changes in gene expression, morphology and functional profile of the cells (Alliot et. al., 1999; De et. al., 2018; Spittau et. al., 2020). Early microglia express genes associated with cell cycling and chromatin remodelling, such as Dab2, Mcm5, Dnmt1 and Lyz2 (Matcovitch-Natan et. al., 2016). The transition from early to pre-microglia is marked by the downregulation of cell differentiation genes and upregulation of synaptic pruning genes – an important function of pre-microglia – such as Crybb1 and Cxcr2 (Paolicelli et. al., 2011; Matcovitch-Natan et. al., 2016). Finally, adult microglia transition towards the expression of traditional homeostatic genes and cytokine signalling, and the maintenance of this homeostatic profile is dependent on the transcription factor MAFB (Matcovitch-Natan et. al., 2016; Jurga et. al., 2020).

This maturation progresses in synchrony with wider brain development, allowing microglia to coordinate both neuronal and immune responses temporally to maintain homeostasis (Matcovitch-Natan et. al., 2016). Microglia regulate both neuronal numbers and early neuronal circuit formation by localising to several neurogenic niches, such as the neocortex or the subventricular zone to regulate neurogenesis (Barry-Carroll & Gomez-Nicola., 2024). The early neonatal stage is when synaptic connections are formed in the rodent brain – these connections are initially overproduced, with half of these connections pruned (Chechik et. al., 1998) in a neuronal activity-dependent manner (Wake et. al., 2009; Schafer et. al., 2012). The complement pathway is an important molecular determinant in synaptic pruning (Wilton et. al., 2023). Schafer (et. al., 2012) suggested that this is mediated specifically by complement receptor 3 (CR3), expressed by microglia, and complement protein C3, localised to synaptically enriched regions, and Weinhard (et. al., 2018) further demonstrated that trogocytosis, or selective partial phagocytosis, by microglia is also mediated by this C3-CR3 interaction.

Microglia communicate with oligodendrocytes and astrocytes to maintain homeostasis and guide development. In myelination, microglia support oligodendrocyte progenitor cells (OPCs) and oligodendrocytes (Hagemeyer et. al., 2017; Wlodarczyk et. al., 2018). In the developing white matter, microglia form clusters and secrete TNF-α, IL-1β, IL-6 and IFN-γ to promote oligodendrocyte development and synthesis of proteins for myelin formation, such as myelin basic protein (MBP) and myelin proteolipid protein (PLP) (Althaus et. al., 2008; Shigemoto-Mogami et. al., 2014). Microglia-astrocyte communication is also important to neuronal development, as astrocytes release IL-33 to promote microglial engagement in synaptic pruning and neuronal maturation (Vainchtein et. al., 2018). Microglia in the adult brain can also induce the polarisation of astrocytes into a pro-inflammatory, neurotoxic phenotype, known as the A1 reactive phenotype, by releasing IL-1α, TNF-α and C1q (Liddelow et. al.,

2017). In turn, A1 astrocytes can activate pro-inflammatory microglia by releasing IL-1β, TNF-α and IL-6 (Li et. al., 2015). The interplay between microglia and astrocytes, and how these impact on BBB dysfunction in the hippocampus, is shown in Figure 1.3.

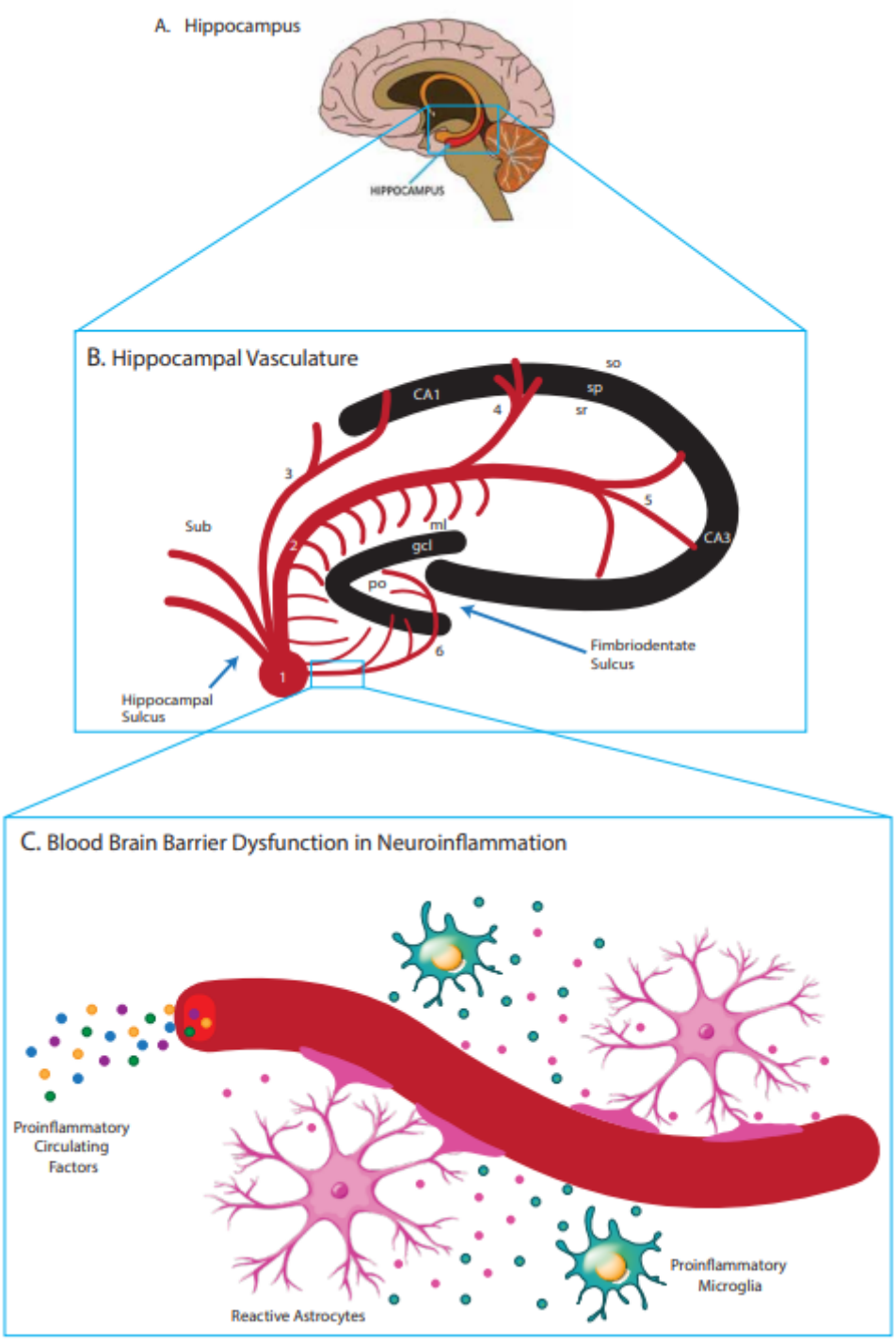


***Figure 1.3. The interplay between astrocytes and microglia and its impact on BBB dysfunction in neuroinflammation. (A)*** *The hippocampus is located deep within the medial temporal lobe of the human brain.* ***(B)*** *Schematic diagram showing the pattern of transverse hippocampal vessels. 1: The*

*main blood vessels of the hippocampus give off the internal transverse hippocampal veins (ITHVs) and the external transverse hippocampal vein (ETHVs); 2: The internal transverse hippocampal artery (ITHA) enters the CS by the hippocampal sulcus; 3: The branches directly generating from the main blood vessels to supply the CA1; 4/5: the branches of ITHV respectively supplying CA2 and CA3; 6: ETHV entering the dentate gyrus by penetrating the fimbriodentate sulcus. In CA: so – stratum oriens; sp – stratum pyramidale; sr – stratum radiatum. In dentate gyrus: ml – molecular layer; po – polymorph layer; gcl – granule cell layer.* ***(C)*** *During neuroinflammation, reactive astrocytes and proinflammatory microglia release pro-inflammatory signals which lead to BBB dysfunction and the infiltration of proinflammatory circulating factors into the hippocampus.*

Microglia express purinergic receptors to sense ATP release by neurons, with both neuromodulatory and neuroimmune functions. Microglia can inhibit neuronal activity via the P2Y12 purinergic receptor (P2RY12), mainly found on homeostatic microglia (Badimon et. al., 2020; Beamer et. al., 2021). P2RY12 is activated by ATP and inhibits glutamatergic neurotransmission during hyperexcitability, and P2RY12 depletion in adult mice is associated with higher seizure severity (Badimon et. al., 2020). A key factor in this inhibition is the neuronal co-transmitter ATP, which is converted to ADP by microglial CD39 and CD73. This ADP then binds to neuronal Adenosine A1 Receptor (ADO-A1R) to inhibit neuronal activity (Castellano et. al., 2016; Lanser et. al., 2017). During inflammation, microglial expression of P2RY12 is diminished as they adopt a more pro-inflammatory phenotype (Koizumi et. al., 2013). Another purinergic receptor expressed by microglia is P2X Purinoreceptor 7 (P2X7R), which is stimulated by ATP during neuroinflammation to activate the inflammasome, leading to the release of IL-1β (Figure 1.1) (Kahlenberg & Dubyak., 2004; Thornton et. al., 2006; Keyel., 2014). Active IL-1β release is also mediated by P2X7R pores (Ferrari et. al., 2006; Monif et. al., 2016). Inhibition and knockout of P2X7R has provided neuroprotective effects post-hypoxia, namely by downregulating release of IL-1β (Rodriguez-Alvarez et. al., 2017; Smith et. al., 2023).

### 1.5.2. Microglia and HIE

Microglia activation in the brain is a central hallmark of the neuroinflammatory response post-HIE (Bona et. al., 1999; Cowell et. al., 2003; Quinlan et. al., 2019; Mallard et. al., 2019). Microglia are also thought to contribute to excitotoxic injury post-hypoxia (Mallard et. al., 2019), particularly by their association with neuronal morphological alterations in vulnerable structures, such as the hippocampus (Takemiya et. al., 2017). Many studies show that microglial aggregation and activation occurs regardless of HIE injury severity in both hypoxia-ischaemia and hypoxia-only models (Del Bigio & Becker., 1994; McRae et. al., 1995; Bona et. al., 1999; Liu & McCollough., 2013; Serdar et. al., 2019). Comparing mild and severe injury post-HIE using the Rice-Vanucci model found that increased microglial populations were recruited to the infarct site and present throughout the brain, regardless of injury severity, and attributed the differences in pro-inflammatory cell populations between the mild and severely injured mice to invading peripheral immune cells (Min et. al., 2020). Initial studies using the hypoxia-only model in this thesis showed that microglia numbers in the hippocampus are significantly higher 72 hours post-hypoxia compared to same age controls (Quinlan et. al., 2019).

The morphological differences in microglia and their physiological consequences post-HIE have yet to be fully explored, particularly in the chronic stages. Serdar (et. al., 2019) explored microglial phenotypes acutely in a rat model of inflammation sensitised HIE. Microglia were key drivers of the neuroinflammatory response with primarily pro-inflammatory phenotypes in the first 24 hours post-HIE (Serdar et. al., 2019). Previous studies in this model have found increased numbers of microglia in the hippocampus at 72 hours post-hypoxia, and effectively targeted neuroinflammatory signalling using a broad-spectrum anti-inflammatory compound and inhibition of P2X7R, an activator of the NLRP3 inflammasome (Rodriguez-Alvarez et. al.,

2017; Quinlan et. al., 2019; Smith et. al., 2023). This both reduced the acute inflammatory response and provided more positive neurodevelopmental outcomes chronically (Quinlan et. al., 2019; Smith et. al., 2023). Molecular studies of inflammatory marker expression support findings of increased microglial pro-inflammatory activation at both acute and chronic timepoints post-HIE (Lalancette-Hébert et. al., 2007; 2017; Stridh et. al., 2011).

### 1.5.3. Cytokines and Chemokines in Microglia Post-HIE

Cytokines and chemokines are released by microglia in response to neonatal HIE, amplifying inflammatory cascades and recruiting resident and peripheral immune cells to the site of injury. This inflammatory response is a double-edged sword; while it is intended to repair and protect the brain from further damage, strong associations have emerged between worsened neurological outcomes following HIE and elevated pro-inflammatory cytokines, particularly IL-1β, TNF-α and IL-6 (Jenkins et. al., 2012; Aly et. al., 2015; Orrock et. al., 2016; Numis et. al., 2019).

IL-1β is released from microglia by several pathways, including the NLRP3 inflammasome as a regulator of neurodevelopment and in response to pro-inflammatory stimuli, while also expressing IL-1Rs. IL-1β-IL-1R signal transduction is cell-type specific, regardless of the intracellular signalling cascade (Cohen., 2014). For a pro-inflammatory response to be invoked, only 2-3% of IL-1Rs need to be occupied, indicating that low levels of IL-1β can produce a strong immune response (Dinarello., 1996). IL-1R activation stimulate pro-inflammatory microglia to release more IL-1β, creating a positive feedback loop (Vezzani & Viviani., 2015). Further, in LPS-induced inflammation in neonatal rats, IL-1R antagonist (IL-1Ra) treatment attenuated long-term neurobehavioural outcomes and dopaminergic neuronal injury in adulthood by dampening this positive feedback loop (Pang et. al., 2015). Numerous

studies have shown strong correlations between increased IL-1β expression and worsened outcomes in HIE in both animal and human studies (Chalak et. al., 2014; Orrock et. al., 2015; Rocha-Ferreira & Hristova., 2016; Massaro et. al., 2020).

TNF-α is a member of the type-2 transmembrane protein family, expressed in a full-length membrane-bound form (mTNF-α) which is cleaved to release soluble TNF-α (sTNF-α). There are two main TNF-α receptors, TNFR1 (p55), preferred by sTNF-α and TNFR2 (p75), preferred by mTNF-α (Grell et. al., 1995; 1998; Schäfers et. al., 2008). Like IL-1β, TNF-α release has both neuroprotective and neuroinflammatory functions. TNF-α is strongly associated with neuroinflammatory disorders such as Alzheimer's Disease (AD) (Dempsey et. al., 2017), Multiple Sclerosis (MS) (Coll et. al., 2015), ischaemia (Xue et. al., 2022), epilepsy (Chen et. al., 2021) and HIE (Rocha-Ferreira & Hristova., 2016; Zareen et. al., 2020). TNF-α also contributes to apoptotic cell death in oligodendrocytes (Hovelmeyer et. al., 2005), and serum TNF-α levels positively correlate with mortality and abnormal neuroimaging findings in neonates with HIE (O'Hare et. al., 2017; Massaro et. al., 2020)

Jenkins (et. al., 2012) conducted a study on how cytokine levels in infants post-HIE are impacted by TH. Neonates treated with TH had significantly higher serum levels of IL-6, IL-8, IL-10 and monocyte chemoattractant protein 1 (MCP1) compared to normothermic infants post-HIE. Additionally, in those infants who died and those who survived with more severe neurodevelopmental outcomes at 12 months of age; there were higher levels of IL-6 and MCP1 within 9 hours post-birth, followed by lower levels of macrophage inflammatory protein 1α (MIP1α) between 60- and 70-hours post-birth (Jenkins et. al., 2012).

Rodent models of HIE have found upregulated expression of alpha-chemokines, such as MIP2, and beta-chemokines such as MIP1α, MIP1β and CCL5, and lymphocyte markers expressed at

the infarct site (Bona et. al., 1999; Jenkins et. al., 2012). Other chemokines upregulated post-HIE are CCL2, CCL3 and CCL7, to recruit monocytes from bone marrow, CXCL1, to recruit monocytes to inflamed tissue (Shi & Pamer., 2011) and CXCL10 (Jaworska et. al., 2017; Teo et. al., 2023), which is involved in natural killer cell migration to sites of cerebral ischaemia and exacerbation of blood brain barrier injury (Zhang et. al., 2014).

## 1.6. The Hippocampus

The hippocampus is a region of the brain best known for its role in learning, memory and spatial navigation, and forms part of the limbic system (Bird & Burgess., 2008; Miller et. al., 2014).

### 1.6.1. Hippocampal Structure and Function.

Located under the cerebral cortex in primates, the hippocampus is divided into two regions: the cornu ammonis (CA), divided further into three sub-regions (CA1-CA3), and the dentate gyrus (DG). The CA is comprised of three layers across the three CA subregions: the *stratum oriens* (SO) the *stratum pyramidale* (SP) and the *stratum radiale* (SR). Animal and human studies have shown that the hippocampal subregions each serve their own distinct functions: the CA3 is specialised to perform pattern completion, the DG is involved in pattern separation and the CA1 is linked to representation of special and temporal sequences over repeated exposure (Gilbert et. al., 2001; Bakker et. al., 2008; Nakashiba et. al., 2008). The subfields also have different retention functions; memories supported by the CA3 and the DG form rapidly, sometimes from just one exposure, whereas the CA1 requires repeated exposures for memory formation (Nakashiba et. al., 2008). Hippocampal function is also divided along the longitudinal axis. Dorsal hippocampal structures are preferentially involved in processing spatial information and memories, and has outputs connected to the anterior cingulate

cortex, the mammillary nuclei and the anterior thalamus. The ventral hippocampus preferentially mediates the stress response, and its outputs connect to the olfactory system, the prefrontal cortex, the amygdala and the hypothalamus (Moser et. al., 1993; 1998; Fanselow & Dong., 2010; Strange et. al., 2014; Bienkowski et.al., 2018).

### 1.6.2. Microglia and Neurodevelopment in the Hippocampus

As mentioned previously, the hippocampus presents with a high density of microglia, and that the density varies between subregions. Microglia are pivotal to guiding hippocampal development in early life, and to supporting neuroplasticity and memory formation throughout adulthood (Borst et. al., 2022).

In the human brain, the structure of the hippocampus is mostly established by 18 to 20 weeks of gestation, although the dorsal and ventral areas continue to differentiate well into childhood (Gotgay et. al., 2006). In rodents, hippocampal development is protracted over the embryonic and postnatal stages, characterised by distinct waves of cellular proliferation and migration (Bayer et. al., 1980; Kim et. al., 2015). Microglia first invade the rodent hippocampus at E14, and hippocampal microglia density increases rapidly after birth, reaching its peak at PND15 (Kim et. al., 2015). In the early stages of circuit maturation microglia release factors such as brain-derived neurotrophic factor (BDNF), nerve growth factor and IL-10 to induce the formation of both excitatory and inhibitory synapses (Liao et. al., 2008; Lim et. al., 2013) and spinal filopodia in hippocampal neurons (Weinhard et. al., 2018). Microglia also regulate neuronal numbers and engulf apoptotic cells, the numbers of which peak at PND4 (Eyo et. al., 2016). This function is intrinsically tied to their role in neurogenesis, as disruption in microglial clearance of apoptotic cells directly disrupts hippocampal neurogenesis (Diaz-Aparicio et. al., 2020). In adulthood, microglia play a constitutive role in synaptic plasticity, remodelling of neuronal circuits and regulation of neuronal activity (Wake et. al., 2013). Microglia are also

essential to learning and memory processes, as demonstrated by the deleterious effects of loss-of-function mutations or deletions in microglia on hippocampal long-term potentiation (Roumier., 2004; 2008; Maggi et. al., 2011; Rogers et. al., 2011), as reviewed by Paolicelli (et. al., 2014). This is supported by murine studies where microglial deficiencies such as CX3CR1-KO, BDNF deletion or microglial depletion resulted in impaired performance in motor learning, fear conditioning, Morris Water Maze and Novel Object Recognition Test (Maggi et. al., 2011; Rogers et. al., 2011; Parkhurst et. al., 2013).

#### 1.6.3. The Hippocampus in HIE

The hippocampus is particularly vulnerable to damage following a hypoxic or ischaemic insult (Bird & Burgess., 2008). The CA1 and the CA3 areas, connected through the Schaffer collaterals, respond differently to hypoxic or ischaemic conditions (Kirino et. al., 2000). CA1 pyramidal neurons are amongst the most vulnerable, demonstrated repeatedly in the literature in both animal and human studies (Almli et. al., 2000; McClendon et. al., 2019). Even a moderate model of neonatal hypoxia induced long-lasting morphological changes to the pyramidal neurons of the SO in the CA1, which corresponded behaviourally with a lower seizure threshold and impaired spatial memory consolidation (Quinlan et. al., 2019). In addition to these findings, González-Fuentes and colleagues (2021) found that perinatal HIE in humans reduces the density of hippocampal GABAergic interneurons, particularly in the DG, which could have major implications for the long-term balance of excitatory/inhibitory neurotransmission.

## 1.7. Hypothesis and Aims

HIE is a leading cause of death and disability in neonates, and the lack of effective treatments available in clinical settings represents a significant unmet clinical need. Research in both

animal models and human patients has shown the intrinsic role played by neuroinflammation in HIE pathophysiology. One example is the strong association between IL-1β and brain damage post-HIE, and the correlation between increased IL-1β signalling and poorer neurodevelopmental outcomes. Anti-inflammatory treatment studies in preclinical models and clinical trials brings potential for novel therapeutic targets, although more work is needed to understand the wider implications of anti-inflammatory treatment with respect to microglial function and neurodevelopment. Some studies have also posited the merits of anti-inflammatory treatments administered past the traditional therapeutic window. One such study found that treatment with a P2X7R antagonist administered 24 hours post-hypoxia for a course of 7 days was profoundly neuroprotective (Smith et. al., 2023), and a review by Chakkarpani and colleagues (2021) proposed EPO as a neurorestorative treatment when administered during the tertiary energy failure. Therefore, this study aims to characterise the neuroprotective effects of MCC950 treatment during the tertiary energy failure post-hypoxia.

The hypothesis of this study is that more microglia will express pro-inflammatory phenotypes in the hippocampus both acutely and chronically post-hypoxia, and this will correspond with behavioural deficits in neonatal reflexes and adult behaviour tests. When MCC950 is administered immediately post-hypoxia, this will dampen the immune response, reduce the prevalence of pro-inflammatory microglia and rescue any behavioural deficits caused by hypoxia. MCC950 treatment from PND21 to PND26 will also reduce the prevalence of pro-inflammatory microglia and attenuate behavioural deficits, although this effect may not be as profound as this treatment will be administered far beyond the traditional therapeutic window.

The aims of this thesis are as follows:

1. Characterise microglia in the hippocampus acutely and chronically post-hypoxia, using morphological analyses and activity markers to understand how hypoxia affects the prevalence of pro-inflammatory microglia.
2. Investigate the consequences of hypoxia on neonatal reflexes and behaviours related to the hippocampus.
3. Treat mice with MCC950 immediately post-hypoxia and investigate how this affects microglia, the neuroinflammatory response and behavioural test performance.
4. Treat mice with MCC950 from PND21 to PND26 to investigate how this affects microglia and behavioural test performance.

# Chapter 2: Methods

## 2.1. Animal Housing and Husbandry

All procedures were performed in accordance with the guidelines of the European Communities Council Directives (86/609/EU and 2010/63/EU) and were reviewed and approved by the Research Ethics Committee of Trinity College Dublin (TCD) under license from the Health Products Regulatory Authority, Ireland (AE19136/P140). Neonatal litters of C57Bl/6 mice [weight, 3 - 5g; age, postnatal day 6.5-7.5 (PND7)] were bred using breeding trios of one male and two females procured from the Comparative Medicine Unit in TCD. Mice had access to food and water *ad libitum* and were kept in a barrier-controlled environment with their dams on a 12hr light-dark standard cycle. Mice were housed in GM500 cages with 2-3cm of bedding, nesting and a red tube for enrichment. Mice were weaned at PND21 and separated by sex, unless separation led to singly housed animals. Sex was determined by visual inspection, agreed upon by two experimenters. Experiments were performed in the morning during the light cycle, and each experimental group was handled by the same experimenter.

## 2.2. Mouse Model of Neonatal Hypoxia

Hypoxia in mouse pups was carried out as previously described (Rodriguez-Alvarez et. al., 2015, Quinlan et. al., 2019). PND7 pups were selected and placed in either a control or hypoxia chamber, with each litter split between hypoxia and control [litter size, 4-10 mice; controls per litter, 1-5 mice; hypoxia mice per litter, 1-7 mice]. Those in the hypoxia chamber were exposed to a premixed gas containing 5% $O_2$ / 95% $N_2$ for 15 minutes to induce global hypoxia, while the control pups were in a chamber containing room air for this period. Throughout hypoxia, the chambers were kept in an incubator to maintain the temperature and humidity at 34°C and 80% humidity (Figure 2.1), and $O_2$ concentration and temperature were monitored throughout. $O_2$ concentration was reduced gradually to reach 5%, and gas flow was adjusted

throughout hypoxia to maintain a consistent 5% $O_2$ concentration throughout hypoxia. An extra opening in the hypoxia chamber wall prevented a build-up of pressure. $CO_2$ concentrations were not monitored, nor were they controlled for. All animals were observed during the 15-minute hypoxia period and assessed for behavioural or clinical seizures every 5 minutes using a modified Morrison's Scale, detailed in Table 2.1 (Morrison et. al., 1996; Quinlan et. al., 2019). Upon cessation of hypoxia, pups were kept in the incubator for continued monitoring and Morrison score assessment every 5 minutes until they were returned to their mother in the home cage, usually for 10 to 15 minutes post-hypoxia.

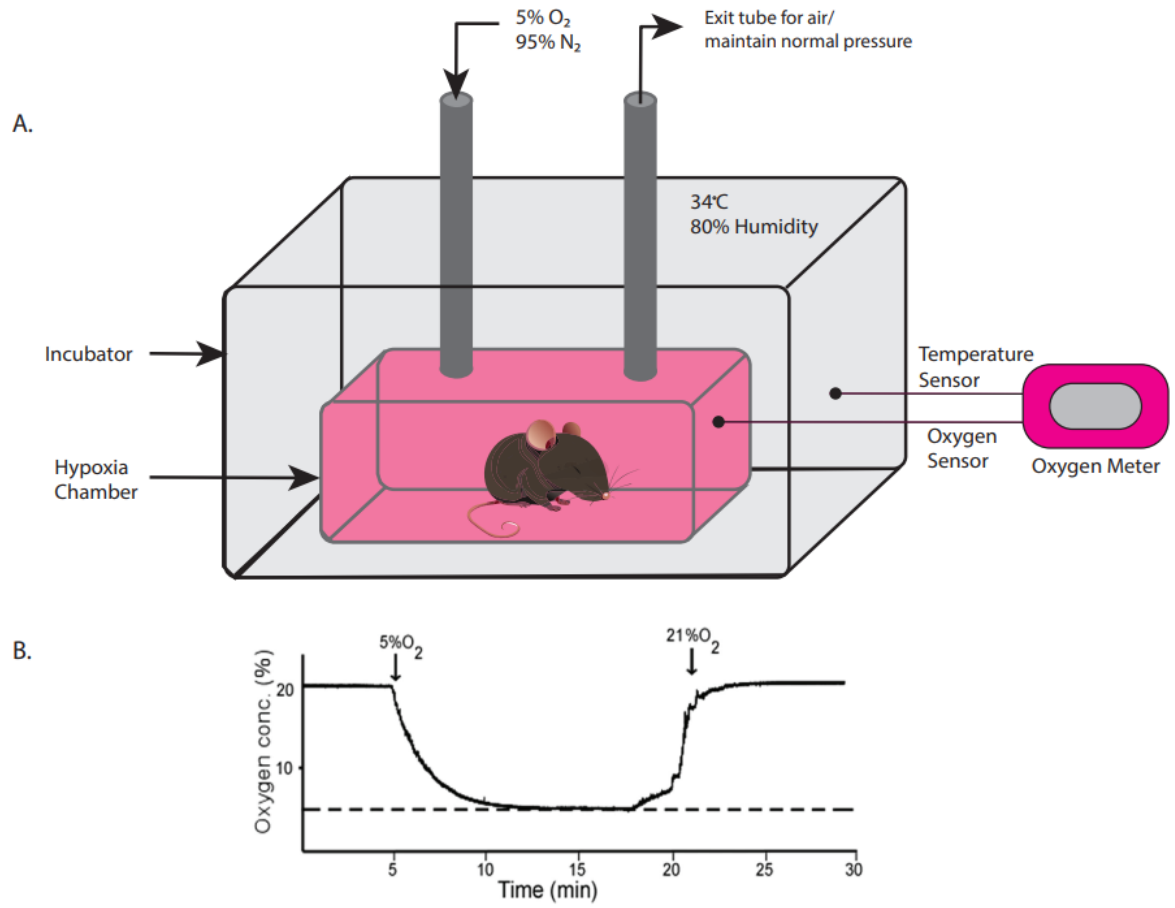


***Figure 2.1. Hypoxia Experiment Apparatus.*** *(A) PND7 mouse pups were exposed to 5% $O_2$ for 15 minutes as previously described (Rodriguez-Alvarez et. al., 2015; Quinlan et. al., 2018). $O_2$ levels and temperature were monitored throughout. (B) Trace of $O_2$ concentrations throughout hypoxia showing the gradual lowering of $O_2$ concentration to 5%, and the gradual reintroduction of 21% $O_2$ concentrations.*

| SCORE | BEHAVIOUR |
|---|---|
| **0** | Normal Behaviour |
| **1A** | Immobility/Motionless |
| **1B** | Immobility and myoclonic jerks (spasms/shivers) |
| **2** | Rigid/ loss of posture |
| **3** | Circling, swimming, pedalling, tail extension |
| **4** | Spasms, forelimb tonic-clonic |
| **5** | Score 4 repeatedly |

***Table 2.1. Modified 5-point Morrison Scale****. Used to Quantify Hypoxia-induced seizures, as described in the literature (Rodriguez-Alvarez et. al., 2015; Quinlan et. al., 2018).*

Pups were monitored closely in the 5 days post-hypoxia using rodent pup wellbeing scoresheets approved for use under this license (Morton., 2000; European Communities Directive 2010/63/EU). Scoresheets monitored daily weight gain, assessed for maternal care by the quality of the nesting, and checked other features such as stomach fullness of each pup, breathing patterns, gait, and posture. The scoring system is outlined in Table 2.2 below.

| Category | Parameter | 0 | 1 | 2 | 3 |
|---|---|---|---|---|---|
| **Appearance** | Bodyweight gain per day (% of P7 weight) | 20+% | 15-19% | 10-14% | 0-9% |
| **Body Function** | Drinking and eating | | Full Stomach | Empty Stomach | |
| | Breathing | | Slow/calm breathing | Fast breathing | Difficulty Breathing |
| | Locomotion/posture | | Normal gait/posture | Slightly abnormal gait/posture | Markedly Abnormal gait/posture |
| **Other Indicators** | Nesting/ Maternal Care | Nest greater than body height | 50% torn, but not nest | Partially torn, 50-90% intact | Nestlet 90% intact |

***Table 2.2. Scoring system for all features observed for neonatal wellbeing assessments.*** *Scores assigned to each parameter, ranging from 0 to 3, were added up to give the wellbeing score for that day. A score of 0-5 required no further action. A score of 6-9 required twice daily checks. A score of 10+ once or 6-9 more than 3 days in a row required consultation with the DV and euthanasia if required.*

## 2.3. *In vivo* Drug Administration

### 2.3.1. PND 7 MCC950 treatment

For the experiments described in Results Chapter 2 of this thesis, hypoxia mice were selected from each litter to be treated with MCC950 immediately post-hypoxia [Hypoxia mice, 1-6 mice; Vehicle-treated, 1-3 mice; MCC-treated, 1-3 mice]. Previous studies in various models have shown that MCC950 effectively crosses the BBB (Coll et. al., 2015; Dempsey et. al., 2017; Lv et. al., 2020). This timepoint was chosen as this reflects the current clinical approach, where treatment is administered as soon as possible post-HIE (Laptook et. al., 2017; Quinlan et. al., 2019). Given the short half-life (3.27 hours) and an oral bioavailability of 68%, mice received a dose of $10mg.kg^{-1}$ MCC950 (Cat. No. 5.38120.0001, Merck Millipore, USA) dissolved in sterile saline solution in a maximum of 100µl by intraperitoneal (IP) injection (Coll et. al., 2015; Luo et. al., 2019). All other mice were administered an IP injection of 100µl sterile saline vehicle solution. Therefore, the three treatment groups were Normoxia-Vehicle (n=42), Hypoxia-Vehicle (n=38) and Hypoxia-MCC950 (n=43). Following their injections, mice were returned to the incubator to recover from hypoxia as normal.

### 2.3.2. PND 21-25 treatment

For the experiments conducted for Results Chapter 3 of this thesis, hypoxia mice from each litter were selected to receive a longer treatment regimen of MCC950 from PND21 to PND25 [Hypoxia mice, 3-7 mice; Vehicle-treated, 1-4 mice; MCC-treated, 2-3 mice]. Several factors contributed to the rationale behind this timeframe. Firstly, at PND21 these mice had been weaned from their home cage, therefore this eliminates the possibility of causing stress to the mother and other litters living in the same cage pre-weaning. The course of injections was ceased at PND25 to allow mice to recover from the stress of injections before proceeding to

adult behaviour tests at PND28, thus minimising the possibility of stress confounding behavioural test performance. Most treatment studies for HIE, both clinical and preclinical, administer protective agents very shortly post-HIE, during the latent phase. It has been suggested that targeting the long-lasting neuroinflammatory response post-HIE may provide significant neuroprotective and neurorestorative effects (Covey et. al., 2011; Fleiss & Gressens., 2012). Chakkarapani and colleagues (2021) argued that EPO treatment could provide tertiary neuroprotection by curbing the delayed rise in IL-1β and attenuating leukocyte infiltration (Wu et. al., 2015). Stem cell therapy, using either human umbilical cord blood mononuclear cells (hUCB cells) or mesenchymal stromal cells (MSCs), was also discussed, as both cell types decreased markers of inflammation and expression of proliferating inflammatory cells in preclinical studies post-HIE (van Velthoven et. al., 2010; Nabetani et. al., 2018).

MCC950 was administered by IP injection twice daily for five consecutive days at a dose of 10mg.kg$^{-1}$ MCC950 dissolved in sterile saline in a maximum of 100µl injection, a dosage used previously in the literature (Dempsey et. al., 2017; Ren et. al., 2018; He et. al., 2019). All other mice were given 100µl sterile saline vehicle solution at all injection times. Therefore, the three treatment groups were Normoxia-Vehicle (n=9), Hypoxia-Vehicle (n=11) and Hypoxia-MCC950 (n=11). Doses were administered at 8am and 4pm by Dr. Jimenez using a 25G needle, ensuring to alternate between the left and right IP injection sites to minimise risks of adverse effects. Following each injection, mice were returned to their cages immediately.

### 2.4. Neonatal Reflexes

Neonatal reflexes were assessed using a battery of reflex tests at 24- and 72-hours post-hypoxia in 54 mice for Chapter 1 and 80 mice for Chapter 2. Prior to testing, mice were scored

on their rodent pup wellbeing scoresheet. All reflex tests were carried out as previously described (Feather-Schussler & Ferguson., 2016) (Figure 2.2).

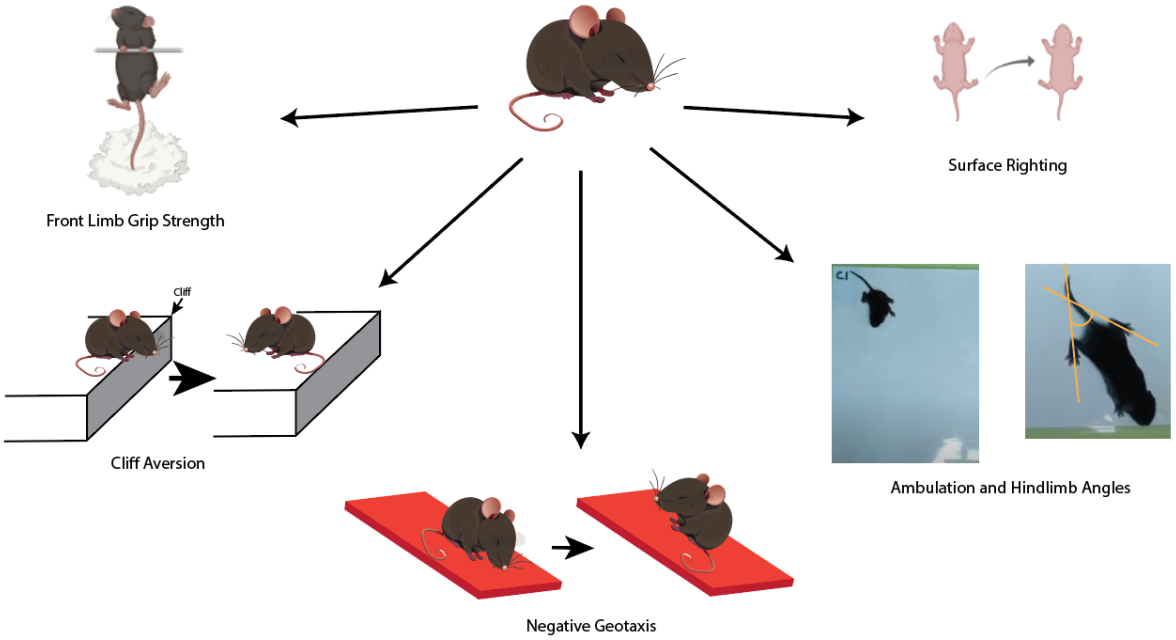


***Figure 2.2. Overview of Neonatal Reflex Testing.*** *All tests were carried out at PND8 and PND10 according to protocols previously published (Feather-Schussler & Ferguson., 2016).*

### 2.4.1. Front Limb Grip Strength Test

This test, to assess forelimb grip strength, is ideally conducted by two experimenters. One experimenter introduces the pup to a wire and allows them to grip it with their front paws. Once gripped with both paws, the experimenter lets go of the pup, so it is now suspended from the wire by its front paws. The second experimenter, equipped with a stopwatch, records how long until the pup lets go of the wire, as seen in the literature (Liu et. al., 2013; Feather-Schussler & Ferguson., 2016). Longer suspension times indicate superior grip strength.

### 2.4.2. Cliff Aversion Test

The cliff aversion test assesses strength, coordination, vestibular responses and labyrinth reflexes (Heyser., 2003; Bouslama et. al., 2007; Feather-Schussler & Ferguson, 2016). To set up

the cliff aversion test, a flat, elevated surface with straight ledges within an enclosed space was prepared. The mother was allowed to wander around the top of the surface for two minutes so the smell of the dam could help guide pups away from the ledge. Each pup was then placed on the edge of the surface with their front paws and head over the edge and timed until they moved away from the edge (Figure 2.2). Pups with a stronger cliff aversion reflex will take less time to complete this task. Exclusion criteria are pups that did not move from their starting position for 30 seconds and litters with more than 50% of pups refused to run the test. High refusal rates were recorded due to these exclusion criteria, particularly at 24 hours post-hypoxia. Due to inter-litter variability, the times recorded for each pup was normalised by litter, expressing their time with respect to the average of their control littermates.

| COHORT | TIMEPOINT | CONTROL | HYPOXIA | HYPOXIA MCC |
|---|---|---|---|---|
| **CHAPTER 1** | 24hr | 13/32 | 19/32 | |
| | 72hr | 13/29 | 14/26 | |
| **CHAPTER 2** | 24hr | 9/17 | 11/17 | 11/19 |
| | 72hr | 8/15 | 10/15 | 10/17 |

***Table 2.3. Refusals for Cliff Aversion Test.*** *Shown are the numbers of refusals out of the total number of animals in each cohort for Chapters 1 and 2 at 24- and 72-hours post-hypoxia.*

2.4.3. Negative Geotaxis

This test relies on the negative geotaxis reflex, which develops in mice between PND3 to PND15 (Heyser., 2003) to assess the integration of motor coordination and vestibular responses to gravity (Sanches et. al., 2012; Wang et. al., 2013). Each mouse was tested once, where they were placed on a slope facing downwards, and in a successful test they should reposition themselves to be facing upwards (Figure 2.2). The time it took to turn 180° and face up the slope was recorded, and a shorter test time indicated a stronger negative geotaxis

response. If a pup refused to move for 30 seconds, or if they turned a small bit and did not move again for 30 seconds, they were recorded as a refusal. Litters with more than 50% of pups marked as refusals were also excluded. High refusal rates were recorded due to these exclusion criteria. Due to inter-litter variability, the times recorded for each pup was normalised by litter, expressing their time with respect to the average of their control littermates.

| COHORT | TIMEPOINT | CONTROL | HYPOXIA | HYPOXIA MCC |
|---|---|---|---|---|
| **CHAPTER 1** | 24hr | 24/32 | 19/28 | |
| | 72hr | 20/29 | 19/26 | |
| **CHAPTER 2** | 24hr | 9/17 | 10/17 | 12/19 |
| | 72hr | 5/15 | 5/15 | 10/17 |

***Table 2.4. Refusals for Negative Geotaxis Test.*** *Shown are the numbers of refusals out of the total number of animals in each cohort for Chapters 1 and 2 at 24- and 72-hours post-hypoxia.*

2.4.4. Ambulation Test and Hindlimb Angles

Mice were placed on a flat surface and filmed walking within the boundaries of their assigned region for three minutes, and the videos were watched to assess walking patterns for each pup. The protocol was adapted from that described in rats by Balasubramaniam (et. al., 2006). Ambulation testing places particular emphasis on assessing the symmetry of movement. Symmetric movement is the smooth transition between steps, where the hind paw meets the front paw in a synchronistic manner with an even rhythm between steps. Asymmetric movement is characterised by more erratic paw placement and less fluid movement between steps (Feather-Schussler & Ferguson., 2016). This study assesses ambulation at PND8 and PND10, during which pups transition from crawling to walking, allowing for the development of normal motor function to be assessed (Williams & Scott., 1954). The scoring system outlined in Table 2.5 is adapted from the literature (Feather-Schussler & Ferguson 2016).

| SCORE | CHARACTERISTICS |
|---|---|
| **0** | No Movement |
| **0.5** | Lots of turning, encouragement needed, little to no straight-line crawling |
| **1** | Straight-line crawling with asymmetrical limb movement |
| **1.5** | Crawling with Asymmetrical limb movement interspersed with symmetrical limb movement |
| **2** | Slow crawling with symmetric limb movement |
| **2.5** | Fast crawling with symmetric limb movement |
| **3** | Walking |

***Table 2.5. Modified Ambulation Scoring scale.*** *This scale expands on the 3-point scale used by Feather-Schussler & Ferguson (2016). The characteristics associated with each score are also described.*

2.4.5. Surface Righting

In this surface righting test, mice were placed on their backs and held by their paws for five seconds, released, and a second experimenter recorded the time taken for them to assume a standing position. This test was performed as a measure of subcortical maturation (Wang et. al., 2013). Unlike the negative geotaxis test, there were no refusals for this test.

## 2.5. Adult Behaviour Tests

To investigate how neonatal hypoxia impacted cognition, memory and neurodevelopmental outcomes later in life, behavioural testing was performed three weeks after hypoxia, between PND28 and PND35. Prior to testing, mice were habituated in the testing room for 45 minutes. The lid of their home cage was replaced with one holding a water bottle to ensure mice continued to have access to water *ad libitum* throughout long days of testing. A white noise machine was switched on at the beginning of habituation to keep noise levels consistently at 45 decibels throughout testing. Lighting was also kept consistently at 35 lux throughout the

room so environmental conditions would not affect performance. All tests were recorded using the Anymaze software (Stoelting Company, Europe). The battery of behaviour tests assessed is illustrated in Figure 2.3, consisting of the Light-Dark Box Test, the Open Field Test, the Novel Object Location Test and the Marble Burying Test.

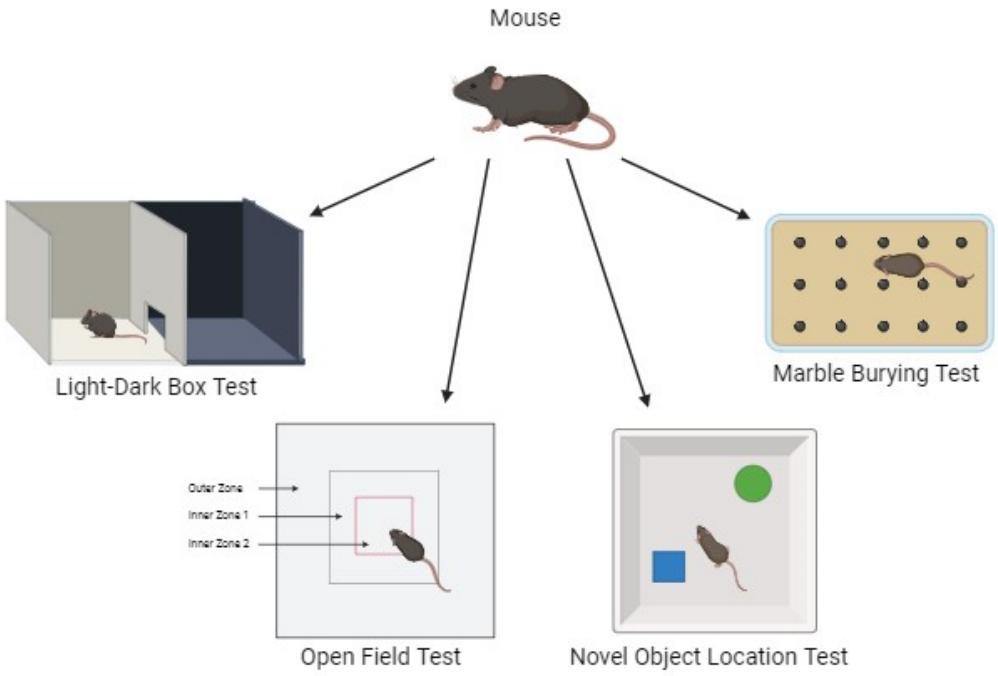


***Figure 2.3. Battery of Adult Behaviour Tests.*** *All tests were carried out between PND28 and PND35 according to the literature.*

2.5.1. Light Dark Box Test

The light-dark box test protocol was adapted from the literature (Quinlan et. al., 2019) and conducted on 14 mice in Chapter 1, 59 mice in Chapter 2 and 32 mice in Chapter 3. In summary, mice walked around the light-dark testing apparatus for 10 minutes, with the light box and the dark box measuring 20 x 40cm each and connected by a small opening in the middle (Figure 2.3). Anymaze traced the movement of the mouse to provide an in-depth analysis of each mouse's movement in both the light and dark regions. The main parameter

analysed was the latency for each mouse to enter the dark box after being placed in the light box at the beginning of testing (Rodriguez-Alvarez et. al., 2015; Quinlan et. al., 2019).

### 2.5.2. Open Field and Novel Object Location Test

The Novel Object Location Test protocol was adapted from the literature (Quinlan et. al., 2018) to test 14 mice in Chapter 1, 28 mice in Chapter 2 and 32 mice in Chapter 3. To summarise, the entire testing regimen was conducted over two days; the first day was comprised of training, and the second day was the test itself. After habituation, the first stage of training allowed mice to become familiar with the arena without objects over two 10-minute sessions. The first session was recorded as the Open Field test, conducted as described previously with minor adaptations in a 40 x 40cm arena (Quinlan et. al., 2019). Anymaze traced the movement of the mouse for parameters such as speed, distance travelled, and freezing episodes. The second stage of training was familiarisation with the objects in the same 40 x 40cm arena. Each mouse spent three 10-minute-long sessions with the test objects in set locations (Figure 2.3). After familiarisation, mice were returned to their home cage until the next day. On the second day, objects 1 and 2 were placed in the arena, except Object 2 was moved to a different quadrant of the arena (Figure 2.3). Each mouse was tested once for 10 minutes to allow them to interact with the new configuration. All videos were analysed manually to record the time spent by each mouse interacting with both objects for the familiarisation and testing periods. The time spent with Object 2 was expressed as a percentage for both the familiarisation sessions and the test session, calculated as follows:

$$\left(\frac{Object\ 2}{Object\ 1 + Object\ 2}\right) * 100$$

The time each animal spent with the novel object location was normalised using the average percentage of time spent with Object 2 during the three familiarisation sessions to account for object preferences. The formula devised for this normalisation step is as follows:

$$\left(\frac{50}{Familiarisation\ average\ \%\ time\ with\ Object\ 2}\right) * (NOL\ \%\ time\ with\ Object\ 2)$$

This formula produces the standardised time spent with the Novel Object Location during the testing period, and this was used for comparisons and statistical analysis. Animals were excluded if the time spent with both objects during the test period was less than 20 seconds.

### 2.5.3. Marble Burying Test

The marble-burying test protocol was adapted from the literature (Angoa-Pérez et. al., 2013) to test 14 mice in Chapter 1. This test is designed to assess repetitive or compulsive burying tendencies associated with autism or obsessive-compulsive disorder (Angoa-Pérez et. al., 2013; Deacon., 2006). The marble burying test was conducted in GM500 cages (W x D x H; 391 x 199 x 160mm) filled with a 5cm thick layer of bedding, with 12 marbles placed in a 4 by 3 configuration (Figure 2.3) and covered by a flat Perspex screen to allow for testing to be filmed. The testing period for each mouse lasted 30 minutes, after which they were returned to their home cage. Each testing cage was analysed manually to identify marbles which were not buried, marbles that were buried <1cm, 1-3cm, and >3cm under the surface of the bedding.

## 2.6. Immunofluorescence staining for Microglia.

### 2.6.1. Intracardial perfusion

Mice were killed by overdose of pentobarbital (200mg/ml, Table 2.8) by IP injection 72 hours (PND10) and 5 weeks post-hypoxia (PND42) (Table 2.7). An incision from the mid abdomen to

the level of the forelimbs exposed the abdominal cavity and the ribcage. The right atrium of the heart was punctured, and the mice were transcardially perfused through the left ventricle with 1x phosphate buffered saline (PBS) followed by 4% paraformaldehyde (PFA). Brains were removed and post-fixed in 4% PFA for 24 hours followed by a 30% sucrose solution. Brains were embedded in 4% agar and cut at 50µm using a Vibratome (VT1000). Once cut, slices were suspended in an anti-freezing solution (30% sucrose, 30% ethylene glycol and 15% glycerol in phosphate buffer solution, Table 2.8) in 24-well plates and stored at -20°C.

### 2.6.2. Immunofluorescence for Iba1 and P2RY12/Iba1

Immunofluorescence was performed as described previously by Quinlan (et. al., 2019). Slices of mouse brain tissue taken from the level of the medial hippocampal region were removed from the freezer and suspended in PBS in a 24-well plate. Slices were washed with 1x PBS three times for 5 minutes, before being suspended in 3% Triton-X in PBS for 20 minutes, to permeabilise the tissue. Following this, slices were incubated in 0.1M glycine for 30 minutes, washed in PBS, and blocked with 10% BSA/0.3% Triton in 1x PBS solution for 1 hour (Table 2.8). The primary antibodies: Rabbit anti-Iba1 (1:500, Table 2.9) and Rat anti-P2RY12 (1:100, Table 2.9) were added after the block and left 18-72hrs at 4°C. Then, slices were washed and incubated in secondary antibody for 2 hours in the dark: donkey anti-rat Alexafluor-594 (1:500, Table 2.9), goat anti-rabbit Alexafluor-488 (1:500, Table 2.9). Then, slices were washed and mounted onto glass slides with Fluoroshield with DAPI (Table 2.8) for visualisation of nuclei. In double staining, primary and secondary antibodies were incubated in sequence.

### 2.6.3. CD68/Iba1 Immunofluorescence

The staining protocol for the CD68/Iba1 stain was conducted as previously described (Guillot-Sestier et. al., 2021) on all cohorts detailed in Table 2.7. Briefly, slices were first submerged in

40% methanol/60% $dH_2O$ for 5 minutes, followed by 0.04% pepsin in PBS for 20 minutes (Table 2.8). Slices were washed, permeabilised with 0.3% Triton in PBS, washed again and blocked in 10% BSA/0.3% Triton in PBS. Primary antibodies were incubated sequentially: Rat Anti-CD68 (1:500, Table 2.9) for 72 hours at 4°C, then Rabbit Anti-Iba1 (1:500, Table 2.9) overnight. After washing, slices were incubated in the dark with the secondary antibodies for two hours: donkey anti-rat Alexafluor-594 (1:500, Table 2.9); goat anti-rabbit Alexafluor-488 (1:500, Table 2.9). Slices were mounted with Fluoroshield with DAPI (Table 2.8) to visualise nuclei.

| CHEMICALS | CATALOG CODE | MANUFACTURER | COUNTRY |
|---|---|---|---|
| **SODIUM PENTOBARBITAL** | Dolethal | Vetoquinol | UK |
| **PHOSPHATE BUFFER SALINE (PBS)** | BP2944 | Fisher Bioreagents/ Thermofisher Scientific | USA |
| **PARAFORMALDEHYDE** | P6148 | Sigma-Aldrich, Merck | USA |
| **AGAR** | A1296 | Sigma-Aldrich, Merck | USA |
| **SUCROSE** | S0389 | Sigma-Aldrich, Merck | USA |
| **ETHYLENE GLYCOL** | 324558 | Sigma-Aldrich, Merck | USA |
| **GLYCEROL** | G5516 | Merck | USA |
| **PHOSPHATE BUFFER SOLUTION** | P3619 | Sigma-Aldrich, Merck | USA |
| **TRITON-X** | 9400 | Calbiochem, Merck | USA |
| **GLYCINE** | 1504 | JT Baker | USA |
| **BOVINE SERUM ALBUMIN (BSA)** | A9418 | Sigma-Aldrich, Merck | USA |
| **FLUOROSHIELD WITH DAPI** | F6057 | Sigma-Aldrich, Merck | USA |
| **METHANOL** | 34860 | Sigma-Aldrich, Merck | USA |
| **PEPSIN** | P7012 | Sigma-Aldrich, Merck | USA |

***Table 2.6. Product Information for Chemicals used in Immunofluorescence staining.***

| ANTIBODIES | HOST | CATALOG CODE | MANUFACTURER | COUNTRY |
|---|---|---|---|---|
| **ANTI-IBA1** | Rabbit | 019-19741 | Fujifilm WAKO | Japan |
| **ANTI-P2RY12** | Rat | 848004 | Biolegend | USA |
| **ANTI-CD68** | Rat | 14-0681-82 | Invitrogen/ Thermofisher Scientific | USA |
| **ANTI-RABBIT ALEXAFLUOR-488** | Donkey | A31627 | Invitrogen/ Thermofisher Scientific | USA |
| **ANTI-RAT ALEXAFLUOR-594** | Donkey | A21209 | Invitrogen/ Thermofisher Scientific | USA |

***Table 2.7. Product information for antibodies used in Immunofluorescence staining.***

2.6.4. Imaging

For the cell density and morphological analyses of $Iba1^+$ cells in Chapter 1, images were taken at 20x magnification of the dentate gyrus, Ca1 and Ca3 regions of the hippocampus using the Leica SP8 scanning confocal microscope. At each region, a z-stack was taken at 1µm intervals, and a z-projection of this z-stack was used for subsequent analyses. For the double staining with CD68/Iba1 and P2RY12/Iba1, images were instead taken at 40x magnification for more accurate identification of double-labelled cells. As before, the Ca1, the dentate gyrus and the Ca3 were imaged with the Leica SP8 scanning confocal microscope. At each region, a z-stack was taken at 0.4µm intervals, and from this, a z-projection was created for analysis. The hippocampus taken, either left or right, from each slice had no bearing on the results of the analysis as this is a global model which affects both hippocampi equally. Only one hippocampus from each slice was imaged, chosen for better staining quality or structural integrity.

## 2.7. Microglia Analysis

The images generated from the IF staining were analysed manually to determine the number of positively stained cells and to categorise these cells based on their morphological features.

### 2.7.1. Number of Iba1$^+$ Cells

To determine the number of microglia in the hippocampus, Iba1$^+$ cells in each region were counted manually. All images represented a region 581.25µm x 581.25µm in size. To account for variability seen in the total number of cells identified in the cell type and number of branch categorisations, the average of these three counts was taken as the final number of Iba1$^+$ cells in each region. Whole hippocampus results were compiled by adding these final aggregate results obtained for the three regions of the hippocampus. The sum of these aggregates was taken as the whole hippocampus because these images took a large enough field of view for most of the hippocampus to be represented in these counts. For a cell to be counted, the whole cell must be visible within the frame; therefore, cells which were missing some or all their ramifications or soma area were excluded.

### 2.7.2. Number of Branches

This analysis was conducted using the same set of 20x images analysed in Methods Section 2.7.1, using the same exclusion criteria. Each microglial cell was assigned to one of three groups based on the number of ramifications emitting from their cell body: 0-1 branches, 2-3 branches and 4+ branches. The 0-1 branch groups and the 2-3 branch groups were considered to account for active, phagocytic, or primed microglia, and the 4+ branch group constituted the inactive microglia phenotypes. Each image was counted twice for the three groups manually, and the average of these two counts was used in the statistical analysis for these groups.

### 2.7.3. Microglia Cell Types

To categorise cells by type, each microglial cell was assigned to one of five types based on their physical characteristics (Diz-Chaves et. al., 2012). Type I cells have small cell bodies with

few cell processes, characteristic of primitive microglia at 72 hours post-hypoxia and primed microglia at 5 weeks post-hypoxia. Type II microglia have small cell bodies with 4 short processes, while Type III microglia are hypertrophic with highly ramified processes. Both Types II and III would be considered homeostatic microglia. Type IV and Type V microglia both active, immunoreactive microglia; Type IV cells have large cell somas and retracted processes, and Type V cells are ameboid and macrophage-like due to their increased phagocytic activity. This analysis was guided by sample images provided (Diz-Chaves et. al., 2012) and those chosen from each experimental group at both timepoints for all three Chapters. Each image was counted twice, and the average of the two counts was used in the statistical analysis, using the same exclusion criteria as detailed in 2.7.1 to eliminate partially visible cells. Results were represented as a percentage of the total number of $Iba1^+$ cells from that image. Whole hippocampus results were represented by an average of the three regions. This morphological analysis was conducted on the 20x images used in Methods Section 7.1 and 7.2, and on 40x images of double stained tissue for CD68/Iba1 for all three Chapter cohorts.

### 2.7.4. Double Staining Analysis

Two double staining experiments were performed on each cohort for this thesis: a CD68/Iba1 double stain and a P2RY12/Iba1 double stain, both of which are described in Methods Sections 6.3 and 6.4 and imaged as detailed in Methods Section 6.5. 40x images represent an area 291.1µm x 291.1µm in size. Sample images of double stained cells were selected from each experimental group at both timepoints from all three Chapters to guide the identification process. Each region was counted manually, marking the number of $Iba1^+$ cells and the number of double stained cells. In images with DAPI added, only $DAPI^+$ cells were counted for analysis. As in previous counts, only cells which were fully visible within the frame of each

image were counted. For analysis, the amount of double stained cells was expressed as a percentage of the total Iba1$^{+}$ cells present. When representing the full hippocampus, the average result for the three regions was taken to represent how many double stained cells are to be found on average in a region taken at 40x magnification throughout the hippocampus. This is because the 40x images represent much smaller areas of the whole structure than the 40x images, therefore, these counts could not be pooled as they did not represent the full hippocampus.

## 2.8. Protein Quantification by ELISA

### 2.8.1. Sample Preparation

Samples for analysis by ELISA were prepared as previously described (Quinlan et. al., 2019). Briefly, mice were deeply anaesthetised by IP injection of pentobarbital, and transcardially perfused with PBS. Brains were removed and hippocampi were isolated. One hippocampus was taken for protein studies, placed in 75µl of Lysis buffer and kept on ice. The other was placed in a dry Eppendorf tube and stored at -80°C for gene expression studies.

### 2.8.2. Protein Assay

A protein assay was conducted so ELISA concentrations could be quantified with respect to total protein for each sample. A modified Lowry Assay was conducted according to manufacturer's instructions for the microplate assay protocol. Briefly, 4mg/ml BSA was used to make the standard curve, a 7-point 1:2 serial dilution. Each point on the curve was added to a 96-well microplate in triplicate, along with a lysis buffer blank, 5µl per well. Samples were diluted 1:4 in lysis buffer for supernatants and 1:10 for pellets, and 5µl of these dilutions were added in triplicate. Next, reagent A' was made by adding 20µl of Reagent S to every 1000µl of Reagent A. 25µl of Reagent A' was then added to all wells containing standards, blanks and

samples, followed by 200µl of Reagent B. The plate was left to incubate for 15 minutes and read immediately at 750nm.

### 2.8.3. ELISA

ELISAs were used to quantify protein concentrations of the markers listed in Table 2.8 according to manufacturer's instructions, which followed the premise of a sandwich ELISA in a 96-well plate. Briefly, wells were coated with the capture antibody, followed by a blocking step to eliminate non-specific binding. In kits with pre-coated plates, these steps were not necessary. The standard curve was made as instructed, usually entailing a 7-point 1:2 serial dilution. The most common concentration range was 15.6-1000ng/ml, usually for cytokines. Each dilution and a blank were added to the plate in triplicate. Protein samples were diluted 3:100 and added in triplicate to the plate along with a negative control, which was lysis buffer diluted 3:100 in the sample diluent provided. Samples, standards and blanks were incubated at room temperature according to the protocol. Samples were then decanted, and the plate was washed before incubation with the biotinylated detection antibody. Following this and a further wash step, the plate was incubated with Streptavidin-HRP. A final wash step was followed by addition of the substrate tetra-methyl-benzidine (TMB) for 10-20 minutes. This reaction was stopped by addition of stop solution and read immediately using a spectrophotometer (wavelengths in Table 2.8).

| MARKER | ABSORBANCE (NM) | CAT. CODE | MANUFACTURER | COUNTRY |
|---|---|---|---|---|
| **IL1B** | 450 & 540 | DY401 | R&D Systems, Bio-techne | USA |
| **IL6** | 450 & 540 | DY406 | R&D Systems, Bio-techne | USA |
| **P2RY12** | 450 | MOEB1050 | AssayGenie | Ireland |
| **IL18** | 450 | MOFI00929 | AssayGenie | Ireland |
| **CXCR3** | 450 | MOFI00760 | AssayGenie | Ireland |
| **C1QR1** | 450 | MCD930 | R&D Systems, Bio-techne | USA |
| **C3** | 450 | MOES00893 | Assaygenie | Ireland |
| **C5A** | 450 & 540 | DY2150 | R&D Systems, Bio-techne | USA |

***Table 2.8. Product information for ELISA kits used.***

| REAGENTS | CAT. CODE | MANUFACTURER | COUNTRY |
|---|---|---|---|
| **PENTOBARBITAL** | Dolethal | Vetoquinol | UK |
| **PBS** | BP2944 | Fisher Bioreagents/ Thermofisher Scientific | USA |
| **PROTEASE INHIBITOR COCKTAIL (LYSIS BUFFER)** | cOmplete Ultra Tablets, EDTA Free, 5892791001 | Roche, Merck | USA |
| **DC PROTEIN ASSAY** | 500-0116 | Bio-rad | USA |
| **BSA** | A9418 | Sigma-Aldrich, Merck | USA |
| **TMB** | T0440 | Sigma-Aldrich, Merck | USA |

***Table 2.9. Product information for reagents used in Protein Assay and ELISA studies.***

## 2.9. Gene Expression Analysis by qPCR

### 2.9.1. RNA Extraction

Hippocampi were isolated as described in Section 8.1, placed in a dry Eppendorf tube, and stored at -80°C until required. RNA was extracted using Trizol as described previously (Jimenez-Mateos et. al., 2015) by Sophia Hjelseth and Jessie Kingston. To summarise, each hippocampus was homogenised in 800µl Trizol, then centrifuged (12,000g, 10 minutes, 4°C). The clear supernatant was transferred to a new tube, and 200µl chloroform was added. This

mixture was shaken vigorously and left for 3 minutes. Tubes were centrifuged (13,000rpm, 15 minutes, 4°C) to complete phase separation into an aqueous phase an organic phase, and a small interphase. The aqueous phase was transferred to a fresh Eppendorf, 450µl isopropanol was added and this was incubated at -20°C overnight. The next day, the tube was centrifuged (13,000rpm, 15 minutes, 4°C). The supernatant was removed, and the pellet was washed by adding 75% ethanol, mixing briefly and centrifugation (12,000g, 5 minutes, 4°C). Ethanol was removed and the tube was left open to air-dry the pellet. The dry pellet was dissolved in 25µl $dH_2O$ and incubated at 55-60°C for 10 minutes. Finally, each sample was measured on the nanodrop. RNA concentration was calculated automatically and recorded, and a 260/280 value of 1.8 or higher was considered uncontaminated. Then, RNA was stored at -80°C.

2.9.2. cDNA Synthesis

cDNA was synthesised from generated RNA using the Reverse Transcription Kit following manufacturer's instructions by Sophia Hjelseth and Jessie Kingston (Table 2.17). cDNA 2x master mix was prepared as in Table 2.12. In a 0.5ml PCR tube, 500ng of total RNA was added to 10µl of 2x master mix and made up to the total reaction volume of 20µl with $dH_2O$. Tubes were centrifuged briefly then placed in a thermocycler for cDNA synthesis (Table 2.13). cDNA samples are then stored at -20°C.

| CDNA MASTER MIX INGREDIENTS | VOLUME PER REACTION |
|---|---|
| **10X RT BUFFER** | 2µl |
| **10X RT RANDOM PRIMERS** | 2µl |
| **25X DNTP MIX (100µM)** | 0.8µl |
| **RNASE INHIBITOR** | 1µl |
| **MS REVERSE TRANSCRIPTASE** | 1µl |
| **NUCLEASE FREE $H_2O$** | 3.2µl |
| **TOTAL** | **10µl** |

***Table 2.10. cDNA 2x Master Mix instructions to make one reaction.***

| THERMOCYCLER TEMPERATURE | TIME (MINS) |
|---|---|
| **25°C** | 10 |
| **37°C** | 120 |
| **85°C** | 5 |
| **4°C** | ∞ |

***Table 2.11. cDNA Thermocycler Protocol.***

2.9.3. qPCR studies

qPCR was conducted as previously described (Quinlan et. al., 2018) to analyse for *Il1β*, *Il6*, *Tnfα* and *C1qa*, with *β-Actin* used as the housekeeping gene, information detailed in Table 2.14. Briefly, Taqman master mix was prepared according to the instructions in Table 2.15, making up 9µl for each reaction. 9µl of master mix per well was added to a 96-well PCR plate, and to this 1µl of cDNA template was added, making a total reaction volume of 10µl. Each sample was run in triplicates. Once filled, the 96-well plate was covered with a plastic film and run on the thermocycler using the protocol outlined in Table 2.16. Results were subsequently analysed using the ΔΔCt Method. Firstly, for each mouse, the average CT value was found for that marker and for actin. The ΔCT was calculated by taking the average actin CT from the average marker CT. e.g. For mouse X, average Actin CT = 25 and average IL1b CT = 28. ΔCT is 28-25=3

From this, the ΔΔCT was calculated using the C1 sample from each litter. The ΔCT for this first control animal was taken from the ΔCT for all animals in that litter. e.g. The ΔCT for the C1 mouse in Mouse X's litter is 4. ΔΔCT for mouse X is 4-3=1

Finally, these ΔΔCT values are used to calculate fold change. Fold change is $2^{-\Delta\Delta CT}$ for each animal. This means that all C1 animals have a Fold change of 1 ($2^{-0} = 1$). e.g. ΔΔCT of mouse X is 1. Therefore, the fold change is $2^{-1} = 0.5$.

The ranges of CT values obtained for all markers are shown in Table 2.X, and the mean and standard deviation for Actin are shown in Table 2.X.

| QPCR GENES | ASSAY ID |
|---|---|
| ***Actin*** | - |
| ***Il1β*** | Mm00434228_m1 |
| ***Il6*** | Mm00446190_m1 |
| ***Tnfα*** | Mm00443258_m1 |
| ***C1qa*** | Mm07295529_m1 |

***Table 2.12. Primer Details****. Assay Identification codes are given for the housekeeping gene, Actin beta, and the four genes assessed in the qPCR study (Invitrogen, Thermofisher, USA).*

| QPCR MASTER MIX INGREDIENTS | VOLUME PER REACTION (µL) |
|---|---|
| **2XMM TAQMAN** | 5 |
| **$DH_2O$** | 3.5 |
| **PRIMER** | 0.5 |
| **TOTAL** | 9 |

***Table 2.13. qPCR Master Mix instructions to make one reaction.***

| CYCLE | TARGET TEMPERATURE | TIME (MINS) | TEMPERATURE TRANSITION RATE |
|---|---|---|---|
| **PRE-INCUBATION** | 95°C | 15 | 20 |
| **AMPLIFICATION (40 CYCLES)** | 95°C | 15 | 20 |
| | 55°C | 20 | 20 |
| | 72°C | 40 | 20 |
| **MELTING CURVE** | 95°C | 0 | 0 |
| | 65°C | 15 | 20 |
| | 95 | . | 0.1 |
| **COOLING** | 40°C | 30 | 20 |

***Table 2.14. qPCR Thermocycler Protocol.*** *Comparative CT-Fast Protocol chosen from the thermocycler (Step One Real-Time PCR System, Applied Biosystems, ThermoFisher, USA).*

| REAGENT | CATALOG CODE | MANUFACTURER | COUNTRY |
|---|---|---|---|
| **TRIZOL (TRI REAGENT)** | T9424 | Sigma Aldrich, Merck | USA |
| **CHLOROFORM** | 1.02431 | Sigma Aldrich, Merck | USA |
| **ISOPROPANOL** | BP2618 | Fisher Scientific | USA |
| **ETHANOL** | 02851 | Sigma Aldrich, Merck | USA |
| **CDNA REVERSE TRANSCRIPTION KIT** | 4374966 | Applied Biosystems | USA |
| **RNASE INHIBITOR** | N808119-C | Applied Biosystems | USA |
| **TAQMAN FAST UNIVERSAL PCR MASTERMIX (2X)** | 4352042 | Applied Biosystems | USA |

***Table 2.15. Product Details for reagents and kits used in Gene Expression Studies.***

| MARKER | | 3HR | 72HR | 5WK |
|---|---|---|---|---|
| **ACTIN** | Min | 15.84709 | 17.08264 | 18.8332235 |
| | Max | 35.99171 | 28.761 | 36.9584937 |
| **IL1B** | Min | 32.16374 | | 33.0518977 |
| | Max | 36.85108 | | 37.946405 |
| **IL6** | Min | 31.13389 | | |
| | Max | 34.89904 | | |
| **TNFA** | Min | 28.77269 | 30.87557 | 32.1203284 |
| | Max | 38.19844 | 39.66315 | 36.4463866 |
| **C1QA** | Min | 22.3585 | 22.68532 | 23.0960574 |
| | Max | 32.86204 | 24.67643 | 33.4611251 |

***Table 2.16. Minimum and Maximum CT values for each marker at 3hr, 72hr and 5wks post-hypoxia.***

| ACTIN | 3HR | 72HR | 5WK |
|---|---|---|---|
| **MEAN** | 20.84723201 | 19.44953173 | 23.20001 |
| **STANDARD DEVIATION** | 5.436407179 | 2.257014026 | 4.278798 |

***Table 2.17. Mean and standard deviation for Actin CT values at 3 hours, 72 hours and 5 weeks post-hypoxia.***

## 2.10. Data Analysis

All data are presented as the mean ± the standard error of the mean (SEM). In all Results Chapters (1-3), statistical analyses were carried out in Prism (V10) software. For Results Chapter 1-3, all pairwise comparisons were conducted using Student's unpaired, one-tailed t-tests, with $p<0.05$ considered significant.

In Results Chapter 2 and 3, the Shapiro-Wilk test was first applied to all data to determine whether the data was parametric or non-parametric. Group comparisons with equal variances between three groups were conducted using one-way ANOVA with Tukey's post-hoc testing. For non-normally distributed groups the non-parametric Kruskal-Wallis's rank sum test was used.

In Results Chapters 1, 2 and 3, some test results showed inter-litter variability. Therefore, results for these tests were normalised by litter before statistical analysis could be performed. This was done by calculating the average of the control group for each litter and dividing each animal by the average of their control littermates, therefore expressing its result relative to the control results for their litter. These values were then analysed using the appropriate statistical test and graphed for visualisation.

Unless specified in the results, all graphs represent both male and female animals. This is because there was little to no sexual dimorphism identified in these results, consistent with previously published literature for this model (Rodriguez-Alvarez et. al., 2015; Quinlan et. al., 2019).

# Chapter 3: Results Chapter 1

## 3.1. Introduction

Microglia are dynamic and multifunctional cells, key to both neurodevelopment and the neuroinflammatory response (Cunningham et. al., 2013; Matcovitch-Natan et. al., 2016). An inflammatory insult during the perinatal period shifts the focus of microglia towards resolving the injury, disturbing neurodevelopment (Bilbo & Schwartz., 2012; Delpech et. al., 2016). This is evidenced by increased numbers of pro-inflammatory microglia seen acutely post-HIE and increased levels of pro-inflammatory signals in the brain (Del Bigio & Becker., 1994; Bona et. al., 1999; Liu & McCullough., 2013; Quinlan et. al., 2019; Serdar et. al., 2019). Current evidence has linked early-life neuroinflammation to long-term adverse neurological outcomes and persistent neuroinflammation later in life (Williamson et. al., 2011; Bilbo & Schwartz., 2012; Cardoso et. al., 2015; Bilbo et. al., 2018), and the few studies which have studied this in models and patients with HIE have supported the long-term consequences of this neuroinflammatory response, regardless of injury severity (Bona et. al., 1999; Winerdal et. al., 2012; Akula et. al., 2023).

### **3.1.1.** Microglia in Neurodevelopment

Homeostatic microglia are highly ramified and motile, allowing them to survey their surroundings and provide support where needed. This is important during times of active neurodevelopment, such as the perinatal period, as microglia are responsible for shaping neural circuits and morphology via synaptic pruning (Tremblay & Majewska., 2011; Schafer et. al., 2012; Paolicelli et. al., 2022). Synaptic pruning is a finely balanced process, and any disturbance to this process i.e., an inflammatory insult, can potentially lead to long-term changes, with both over- and under-pruning are associated with neurodevelopmental disorders (Glausier & Lewis., 2013; Tang et. al., 2014; Neniskyte & Gross., 2017).

### **3.1.2.** Microglia in HIE

HIE induces a significant acute neuroinflammatory response, with potent pro-inflammatory mediators such as IL-1β and TNF-α upregulated in both human patients and preclinical models (Hellström Erkenstam et. al., 2016; Orrock et. al., 2016; Quinlan et. al., 2018). Microglia respond to the CNS insult, migrating to the site of injury in the case of an ischaemic event and adopting a pro-inflammatory phenotype (Hellström Erkenstam et. al., 2016). Several studies have shown that microglia populations are increased acutely post-HIE in both human and preclinical studies, and that the hippocampus is particularly vulnerable to this due to its high concentration of inflammatory receptors and resident microglia (Lawson et. al., 1990; Bona et. al., 1999; Quinlan et. al., 2019; Tan et. al., 2020). Furthermore, some studies have found that neuroinflammation may persist for weeks, even months, after the HIE has been resolved. In rat models of severe HIE, elevated microglia populations were found in the brain 5 weeks post-HIE (Bona et. al., 1999) and neuroinflammatory markers were elevated up to 3 months post-HIE (Winerdal et. al., 2012).

### **3.1.3.** Neuroinflammation and comorbidities post-HIE.

The introductory chapter of this thesis presented ample evidence of the long-term neurological comorbidities associated with HIE identified in both human longitudinal studies and preclinical models. Many of the studies, particularly the preclinical studies, focus on severe HIE, which is associated with more serious long-term neurological outcomes. Recently, a growing body of research has shown that these are also present in moderate, and even mild, HIE, in both human and animal studies (Rakhade et. al., 2011; Rodriguez-Alvarez et. al., 2015; Pisani & Spagnoli., 2016; Ahearne et. al., 2016; Akula et. al., 2023), presenting more often as neurodevelopmental disorders such as learning difficulties, epilepsy or ADHD (Mikati et. al., 2005; Talos et. al., 2012; Park et. al., 2023). Previous work has focused on the acute stages of

injury, when the process of neurodevelopment is disrupted by the injury response, but it is now clear from the literature that the chronic stage post-injury is also deserving of attention (Winerdal et. al., 2012; Akula et. al., 2023).

### 3.1.4. Hypothesis and Aims

We hypothesise that microglia will be more abundant in the hippocampus at both acute and chronic timepoints post-hypoxia, with higher proportions adopting more pro-inflammatory phenotypes compared to controls. We also expect to see deficits in both neonatal reflexes and adult behaviour in the hypoxia cohort compared to controls, particularly in the memory-based tasks during adult behaviour due to the involvement of the hippocampus and its vulnerability post-HIE.

The aims of this study are:

1. Investigate how hypoxia affects the development of acute neurological reflexes and chronic behavioural outcomes of mice post-hypoxia.
2. Characterise microglia populations in the hippocampus 72 hours and 5 weeks post-hypoxia, looking at microglia numbers and categorising microglia by morphology.
3. Compliment the morphological analysis using markers for homeostatic and pro-inflammatory microglia to further understand how hypoxia affects microglia function.

## 3.2. Methods

Mice were prepared for hypoxia as described previously and sacrificed at the specified timepoints detailed in Figure 3.1. Wellbeing score performance presented in Table 3.2.

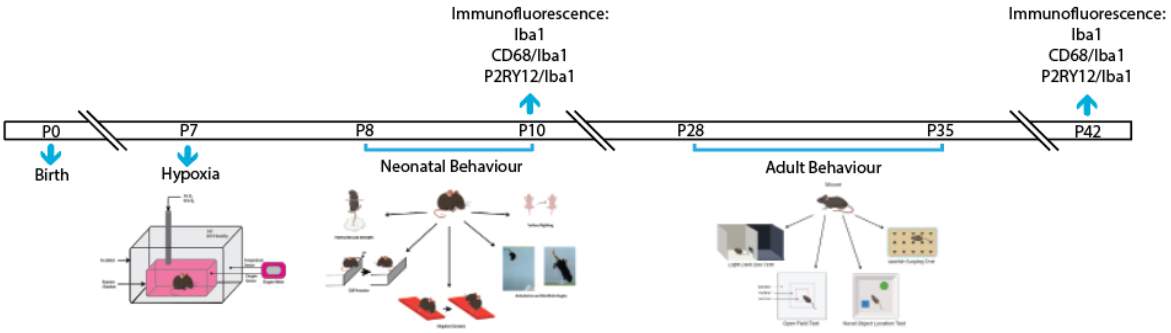


***Figure 3.1. Timeline showing the points at which different molecular and behavioural studies were conducted.***

### 3.2.1. Immunofluorescence Staining

Immunofluorescence staining was conducted as described previously (Quinlan et. al., 2019). For microglia counting and morphological analyses, slices of brain tissue were incubated overnight at 4°C with Anti-Iba1 (1:500), followed by Alexafluor 488 goat anti-rabbit (1:500). Phagocytic microglia were visualised with a modified IF protocol as described in Methods Chapter 2, Section 2.6.3 (Guillot-Sestier et. al., 2021). Briefly, slices were incubated in 40% Methanol followed by 0.04% pepsin to facilitate antigen retrieval. Following further permeabilization with 0.3% Triton and blocking with 10% BSA, slices were incubated with Anti-CD68 (1:500) for 72 hours followed by Anti-Iba1 (1:500) overnight. Secondary antibodies Alexafluor 594 Donkey anti-Rat (1:500) and Alexafluor 488 goat anti-rabbit (1:500), were incubated sequentially for 2 hours in the dark. To stain for homeostatic microglia, the IF protocol described in Methods Chapter 2, Section 2.6.2 was followed. Slices were incubated in Anti-P2RY12 (1:100), followed by Anti-Iba1 (1:500). Secondary antibodies were Alexafluor 594 Donkey anti-Rat (1:500) and Alexafluor 488 goat anti-rabbit (1:500). Z-stack images for

each region on all slices were generated with the Leica SP8 scanning confocal microscope (TBSI Imaging and Microscopy Centre). Images were taken at 20x, at steps of 1µm along the z-plain, for the initial morphological analyses in Results Chapter 1, Section 3.3.3. Images were taken at 40x for the CD68/Iba1 and P2RY12/Iba1 double staining, with steps of 0.4µm.

| EXPERIMENT | TIME POST-HX | NO. CONTROL | NO. HYPOXIA |
|---|---|---|---|
| **Iba1$^+$ Cell counting** | 72hrs | 7 | 5 |
| | 5wks | 6 | 6 |
| **Morphology Analysis** | 72hrs | 7 | 5 |
| | 5wks | 6 | 6 |
| **CD68/Iba1** | 72hrs | 5 | 6 |
| | 5wks | 7 | 5 |
| **P2RY12/Iba1** | 72hrs | 8 | 6 |
| | 5wks | 7 | 5 |

***Table 3.1. Experimental cohorts for immunofluorescence studies in Results Chapter 1.***

### **3.2.2.** Cell Counting

Z-stack images were converted to Z-projections in Image J, which was counted manually. Each image was counted twice, and the average was taken as the final count. Two morphological analyses were conducted; the first grouped cells on the number of ramifications emitting from the cell soma; the second grouped cells by morphological features as described previously (Diz-Chaves et. al., 2012). Both methods are described in finer detail in Methods Chapter 2, Section 2.7.

### **3.2.3.** Neonatal Behaviour

As described in Methods Chapter 2, Section 2.4, neonatal reflexes were analysed using a battery of tests adapted from Feather-Schussler & Ferguson (2016). This battery is comprised of the ambulation test and hindlimb angles, negative geotaxis test, cliff aversion test, surface

righting test and front limb grip strength test. For the negative geotaxis and the cliff aversion tests, a refusal was counted as any mouse which did not begin to move or turn over 90° away from their original position within the first 30 seconds of testing.

### **3.2.4.** Adult Behaviour

The adult behaviour tests selected for these experiments were the Open Field Test, the Light-Dark Box test, the Marble Burying Test and the Novel Object Location Test. The protocols for these tests are described fully in Methods Chapter 2, Section 2.5.1, 2.5.2 and 2.5.3.

| PARAMETER | SCORING | P8 | | P9 | | P10 | |
|---|---|---|---|---|---|---|---|
| | | Control | Hypoxia | Control | Hypoxia | Control | Hypoxia |
| **WEIGHT GAIN** | 0-9% | 1 | 4 | 0 | 0 | 0 | 0 |
| | 10-14% | 14 | 12 | 1 | 2 | 0 | 0 |
| | 15-19% | 13 | 11 | 2 | 4 | 0 | 1 |
| | 20%+ | 4 | 1 | 29 | 21 | 29 | 25 |
| **DRINKING/ EATING** | Empty stomach | 4 | 6 | 5 | 5 | 14 | 15 |
| | Full Stomach | 28 | 22 | 27 | 22 | 15 | 11 |
| **BREATHING** | Difficulty | 0 | 0 | 1 | 0 | 0 | 0 |
| | Fast | 0 | 2 | 0 | 0 | 0 | 0 |
| | Slow/calm | 32 | 26 | 31 | 27 | 29 | 26 |
| **GAIT/ POSTURE** | Markedly Abnormal | 0 | 0 | 0 | 0 | 0 | 0 |
| | Slightly Abnormal | 0 | 19 | 1 | 22 | 0 | 21 |
| | Normal | 32 | 9 | 31 | 5 | 29 | 5 |
| **NESTING/ MATERNAL CARE** | Nestlet 90% intact | 0 | 0 | 0 | 0 | 0 | 0 |
| | Partially torn mostly intact | 0 | 0 | 0 | 0 | 0 | 0 |
| | 50% torn but not nest | 10 | 7 | 8 | 6 | 7 | 7 |
| | Greater than body height | 22 | 21 | 24 | 21 | 22 | 19 |
| **TOTAL NO. MICE** | | 32 | 28 | 32 | 27 | 29 | 26 |

***Table 3.2. Breakdown of pups in the Chapter 1 cohort to receive each score in their wellbeing sheets at PND8, PND9 and PND10, separated by control and hypoxia.***

## 3.3. Results

### 3.3.1. Hypoxia Mice Perform Worse in Both Neonatal Wellbeing Assessments and Neonatal Reflex Testing

Mice were monitored closely during and post-hypoxia to assess how hypoxia affected acute neurological and overall development. As previously published, Morrison scores were recorded to characterise seizure development during global hypoxia (Rodriguez-Alvarez et. al., 2015; Quinlan et. al., 2018). Neonatal wellbeing scoresheets assessed pup health and maternal care allowing for control and hypoxia pups to be compared. Parallel to these wellbeing checks, a battery of neonatal reflex tests was conducted to assess whether global hypoxia caused acute neurological deficits.

#### 3.3.1.1. Mice Exposed to Global Hypoxia at P7 Develop Seizures During Hypoxia.

All pups were monitored and scored throughout hypoxia and directly afterwards on a modified Morrison Scores Scale (Morrison., 1996; Quinlan et. al., 2018), which measured both the presence of seizure activity and seizure severity based on clinical symptoms, such as myoclonic jerks or rigidity (Methods Section Table 2.1 for detailed breakdown). All control mice received scores of 0 throughout, indicating normal behaviour, so their scores were not recorded for analysis. All pups exposed to hypoxia developed seizures, varying in severity (Figure 3.2). As expected, Morrison Scores worsened as hypoxia progressed but began to recover as soon as normoxia was re-established. Pups were returned to their cage as soon as all pups in their respective litter received a score of 1b or lower, which varied from litter to litter but never exceeded 15 minutes.

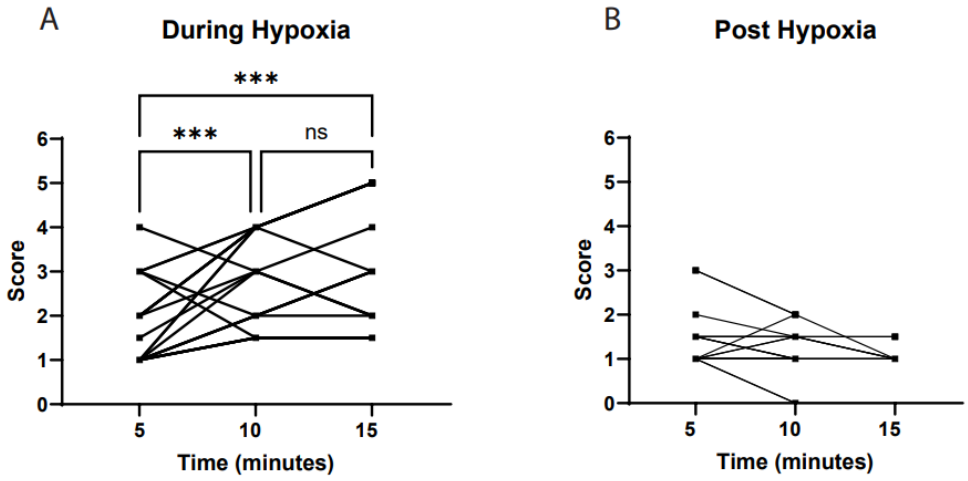


***Figure 3.2. Morrison Scores Show worsening seizures as hypoxia progresses and a quick recovery post-hypoxia. (A)*** *Morrison Scores recorded 5, 10 and 15 minutes into the hypoxia period. Only hypoxia pups were scored (n=23). One-way ANOVA with Tukey's Post-Hoc test, p<0.0001.* ***(B)*** *Morrison Scores recorded 5, 10 and 15 minutes after hypoxia cessation. Pups were returned to their dam once all pups from their litter received a score of 1b or less, which varied between litters.*

**3.3.1.2.** Hypoxia Mice Receive Higher Neonatal Wellbeing Scores, Indicating Poorer Overall Health, and Gain Weight Slower Over Time.

Neonatal wellbeing scoresheets were important for assessing pup health and maternal care, with higher scores representing mice with poorer overall health (Methods Section Table 2.2 for detailed breakdown). Hypoxia pups consistently receive higher wellbeing scores than controls at all timepoints post-hypoxia, indicating that hypoxia pups are in poorer overall health compared to controls (Figure 3.3). Weight gain was normalised by litter, and as previously described (Rodriguez-Alvarez et al., 2015) the hypoxia-exposed mice gained less weight over time than their control littermates (Figure 3.3).

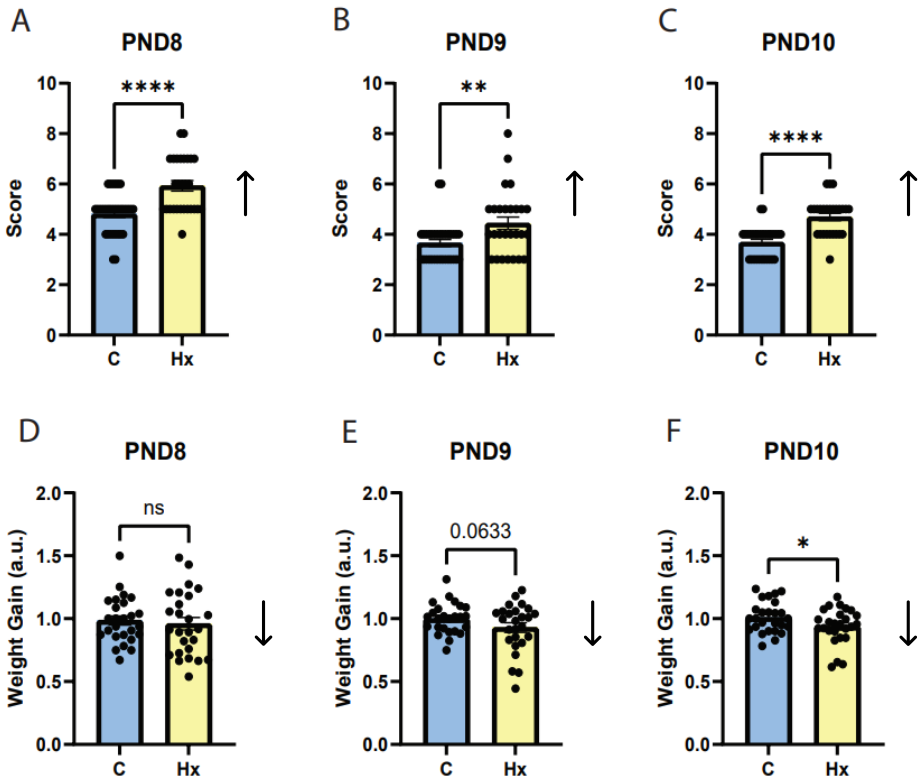


***Figure 3.3. Mice have poorer overall health and gain weight slower post-hypoxia compared to controls. (A)*** *Wellbeing scores for each mouse at PND8 (C n=32, Hx n=28). PND8 C v Hx p<0.0001.* ***(B)*** *Wellbeing scores at PND9 (C n=32, Hx n=27). PND9 C v Hx p=0.0027.* ***(C)*** *Wellbeing scores at PND10 (C n=29, Hx n=26). PND10 C v Hx p<0.0001.* ***(D)*** *Weight gained by pups 24hrs post-hx. Weight gain expressed as a percentage of PND7 weight was normalised by litter with respect to the average of the controls. No differences in weight gain found between control and hypoxia. N=26 per group, PND8 C v Hx p=0.3359.* ***(E)*** *Weight gained 48hrs post-hx normalised by litter. A trend towards slower weight gain in hypoxia pups versus control is seen. C n=25, Hx n=26, PND9 C v Hx p=0.0633.* ***(F)*** *Weight gain 72hr post-hx normalised by litter. Hypoxia pups gain significantly less weight than control littermates. N=26 per group, PND10 C v Hx p=0.0324. All unpaired, one-tailed t-test, a-priori hypothesis indicated by arrow, p < 0.05.*

### 3.3.1.3. Hypoxia Causes no Changes to Surface Righting Reflex.

Reflex testing in human infants is routinely used to identify those at risk of developing neurodevelopmental disabilities (Romeo et. al., 2016; Novak et. al., 2017). Therefore, neonatal reflexes were assessed in this mouse model of hypoxia using a battery of tests adapted from Feather-Schussler & Ferguson (2016) at 24- and 72-hours post-hypoxia, a critical period for neurodevelopment (Heyser et. al., 2003; Castelanho-Carlos et. al., 2010).

Surface righting measures the core strength and coordination required for a pup to right themselves from supine to standing (Figure 3.4.A), a reflex which usually develops around PND5 (Heyser et. al., 2003). At both 24 hours and 72 hours post-hypoxia, no differences were observed between groups (Figure 3.4.B-D).

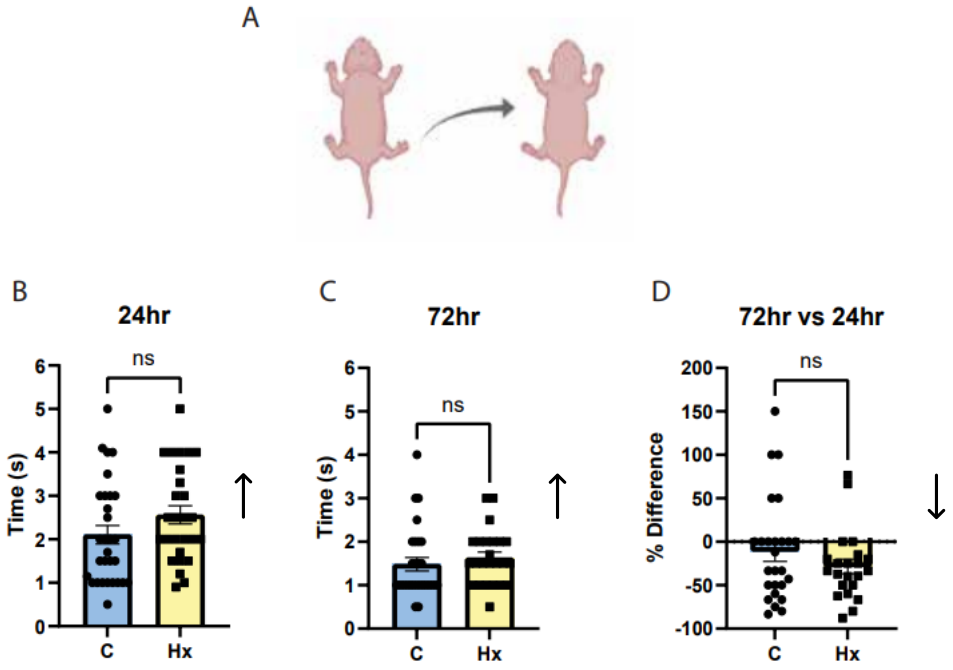


***Figure 3.4. No Differences in Surface Righting Response post-hypoxia. (A)*** *Surface Righting Test Illustration.* ***(B)*** *Time taken to complete test 24hrs post-hx, with no trends emerging. C n=30, Hx n=27, 24hr C v Hx p=0. 0679.* ***(C)*** *At 72hrs post-hx there are no significant differences between groups. C n=28, Hx n=24, 72hrs C v Hx p=0.2329.* ***(D)*** *Difference in time between 24-and 72-hrs post-hx. No significant trends emerge. C n=26, Hx n=22, Difference C v Hx p=0.1230. Unpaired, one-tailed t-test, with arrows to indicate direction of a-priori hypothesis, $p < 0.05$.*

**3.3.1.4.** Hypoxia Mice Have Poorer Front Limb Grip Strength at 24hrs post-hypoxia and Recover this Deficit by 72 hours post-hypoxia.

Front-limb grip strength was designed to measure grip force and strength in the forelimbs (Sun et. al., 2015; Xu et. al., 2016). To account for inter-litter variability, the time taken for each animal to complete the test was normalised by litter. At 24 hours post-hypoxia, the hypoxia cohort performed significantly worse than their control littermates, but this difference was no

longer found at 72 hours post-hypoxia (Figure 3.5.B-C). This was reflected in the relative difference over time, where hypoxia mice had a significantly better improvement over time to same-age controls (Figure 3.5.D).

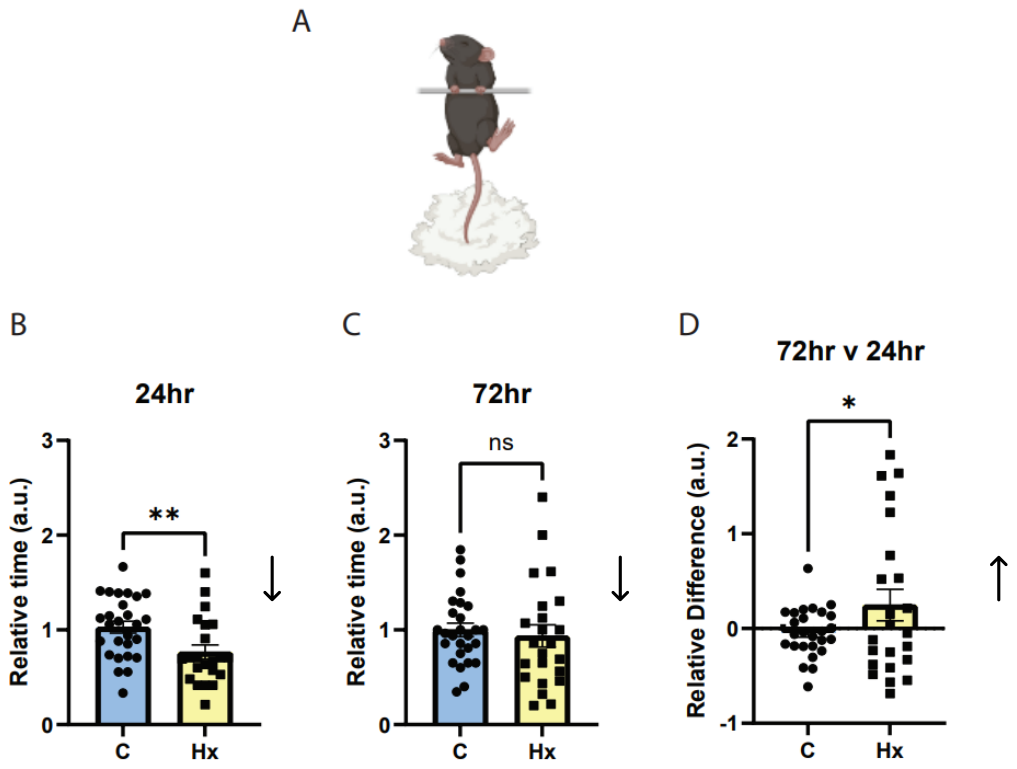


***Figure 3.5. Hypoxia mice perform worse relative to their same age control littermates at 24 hours post-hypoxia, but not at 72 hours post-hypoxia. (A)*** *Forelimb Grip Strength Test Illustration.* ***(B)*** *Grip Strength Time recorded 24hrs post-hx and normalised by litter. Hypoxia mice had significantly worse relative times to their same age controls. C n=27, Hx n=22, 24hr C v Hx p=0.0044.* ***(C)*** *Grip Strength Time recorded 72hrs post-hx normalised by litter. There is no longer any difference between control and hypoxia littermates. C n=27, Hx n=23, 72hr C v Hx p=0.3168.* ***(D)*** *Relative difference between the normalised times at 24 and 72hrs. Hypoxia mice had a significantly higher relative difference over time than controls. C n=26, Hx n=23, Difference C v Hx p=0.0432. Unpaired, one-tailed t-test, with arrows to indicate direction of a-priori hypothesis, $p < 0.05$.*

**3.3.1.5.** Hypoxia Mice Have a Weaker Cliff Aversion Response than Controls at 24 hours post-hypoxia Which Recovers by 72 hours post-hypoxia.

The Cliff Aversion Test was designed to assess a pup's response to vestibular cues and labyrinth reflexes. This test assesses the ability of each mouse to sense that their head and front paws

are over a cliff, and a successful response is removing themselves from the edge (Figure 3.6.A). There was a high refusal rate, particularly at 24 hours post-hypoxia. To control for inter-litter variability, the time taken for each mouse to complete the test was normalised by litters, with each mouse's time expressed with respect to the average of their control littermates. Due to the high refusal rate, only a small number of mice were eligible for the difference over time comparison. At 24 hours post-hypoxia, the relative time taken for hypoxia mice to perform the test was higher than their control counterparts, indicating a weaker reflex response (Figure 3.6.B). At 72 hours however, there is no significant difference between the groups, indicating a similar reflex response between control and hypoxia mice (Figure 3.6.C). When the relative difference between 24- and 72-hours is assessed, there is no significant difference between control and hypoxia mice (Figure 3.6.D).

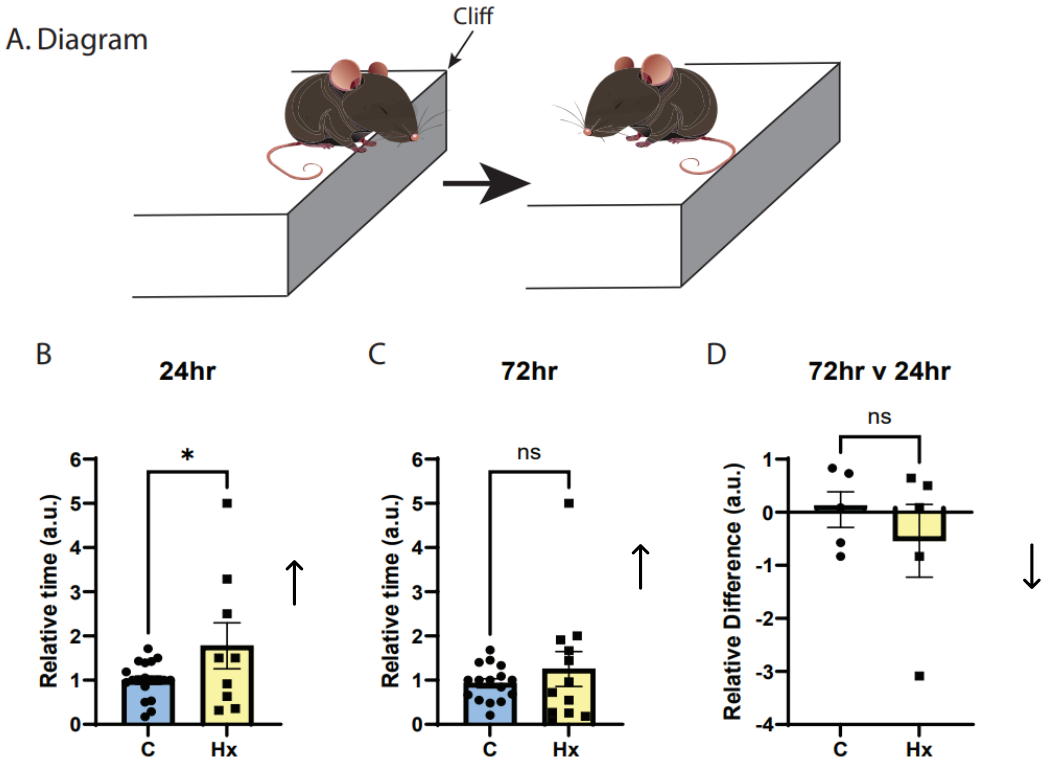


***Figure 3.6. The Cliff Aversion Reflex develops more slowly in Hypoxia pups, but this difference disappears by 72 hours post-hypoxia. (A)*** *Cliff Aversion Test Illustration.* ***(B)*** *Time taken to move away from cliff, normalised by litter, at 24hrs post-hx. Hypoxia pups have a significantly higher relative time to control littermates. C n=19, Hx n=9, 24hr C v Hx p=0.0245.* ***(C)*** *Graph shows the relative times to*

*conduct the test at 72hrs post-hx. No differences were found between groups. C n=16, Hx n=12, 72hr C v Hx p=0.1891.* ***(D)*** *Relative difference between the normalised 24- and 72-hour times. No significant differences were found, although the sample size for this was reduced due to the high refusal rate. C n=5, Hx n=5, Difference C v Hx p=0.2326. Unpaired, one-tailed t-test, with arrows to indicate direction of a-priori hypothesis, p < 0.05.*

**3.3.1.6.** Hypoxia Mice Display Deficits in Ambulation Test and Hindlimb Angles at 24 hours and 72 hours post-hypoxia.

During the ambulation test, pups walked around an arena for 3 minutes to assess their locomotion and hindlimb angles, as seen in sample images in Figure 3.7.A. Their locomotion was scored based on movement patterns such as limb placement symmetry, excessive turning and their transition from crawling to walking using the 6-point scale in Methods Table 2.6. At 24 hours post-hypoxia, there were no significant differences between groups (Figure 3.7.B). At 72 hours post-hypoxia, the hypoxia pups had significantly worse ambulation scores than controls, reflecting a slower development of the walking reflex (Figure 3.7.C), with less than half of the hypoxia mice are capable of symmetric limb movement, while almost all control pups are moving symmetrically, with some already walking. This is further supported by the higher improvement in score over time in control versus hypoxia mice (Figure 3.7.D).

Hindlimb angles complemented the ambulation scores by assessing limb placement and posture during straight line movement (Figure 3.7.E). At both 24 hours and 72 hours post-hypoxia, hypoxia mice have a significantly wider relative hindlimb angle than their control counterparts when their hindlimb angles are normalised with respect to control littermates (Figure 3.7.F-G). This wider relative stance is consistent with the higher proportion of hypoxia mice seen crawling at both timepoints, which is partly characterised by a wider stance than that required for walking. When the relative difference in hindlimb angles over time is assessed, no differences were observed between groups (Figure 3.7.H).

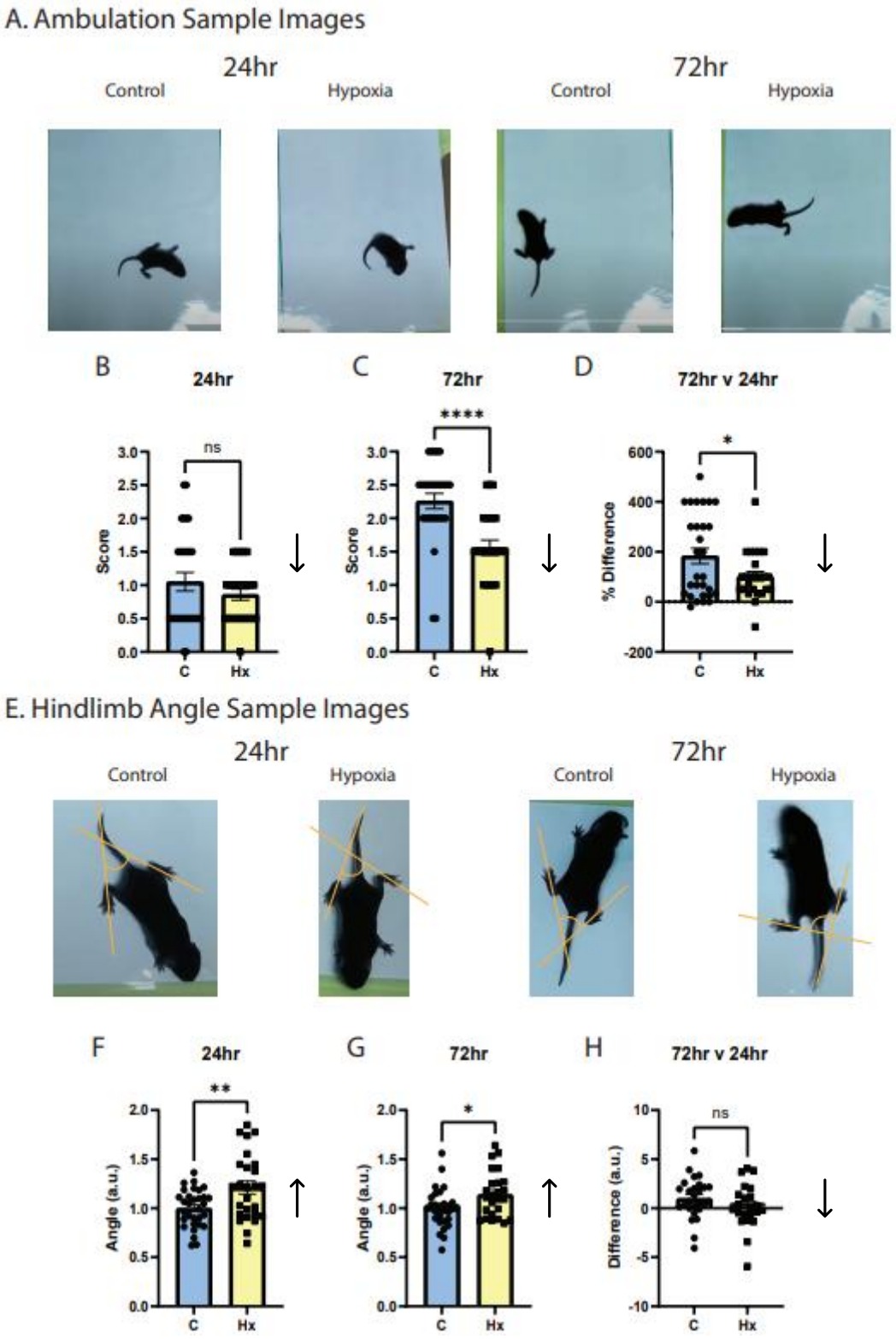


***Figure 3.7. Ambulation scores and Hindlimb Angles at 24- and 72-hours post-hypoxia. (A)*** *Samples Images of Ambulation. Ambulation scores were assigned on a modified 6-point scale (Feather-Schussler & Ferguson., 2016). 0– no movement; 0.5– very little movement, only turning, needs encouragement; 1– slow crawling in straight lines, asymmetrical limb movement; 1.5– crawling in straight lines, mixture of symmetrical and asymmetrical limb movement; 2– slow crawling with*

*symmetrical limb movement; 2.5– fast crawling with symmetrical limb movement; 3– walking.* ***(B)*** *Ambulation scores 24hrs post-hx, which showed no significant difference. C n=29, Hx n=25, 24hr C v Hx p=0.1309.* ***(C)*** *Ambulation scores 72hr post hx; hypoxia pups perform significantly worse to controls. C n=29, Hx n=25, 72hr C v Hx p<0.0001.* ***(D)*** *Difference in score over time, whereby controls have a significantly better improvement in ambulation over time versus hypoxia pups. C n=29, Hx n=25, Difference C v Hx p=0.0188.* ***(E)*** *Sample Hindlimb Angle Images with guidelines drawn.* ***(F)*** *Hindlimb angle 24hrs post-hx normalised by litter. Hypoxia mice have significantly wider relative hindlimb angles compared to controls. C n=31, Hx n=26, 24hr C v Hx p=0.0023.* ***(G)*** *Normalised hindlimb angles at 72hrs post-hx remained significantly wider than control littermates. C n=29, H n=25, 72hr C v Hx p=0.0105.* ***(H)*** *Relative difference between the normalised 24 and 72hr angles. While there is a trend towards poorer improvement over time in the hypoxia cohort, this does not reach significance. C n=27, Hx n=22, Difference C v Hx p=0.1007. All tests are one-tailed, unpaired t-tests with arrows to indicate the a-priori hypothesis, $p < 0.05$.*

#### 3.3.1.7. Hypoxia Mice have a Poorer Negative Geotaxis Response 72 hours post-hypoxia.

The Negative Geotaxis test evaluates the negative geotaxis reflex, a response to vestibular and proprioceptive cues which indicate that the mouse's head is below its body, causing the mouse to correct itself so that its head is above its body (Xu et. al., 2016). During this test, the mouse is placed on an angled surface facing downwards and should correct itself to face upwards (Figure 3.8.A). Due to inter-litter variability, the time taken for each mouse to complete the test was normalised by litter. There was a high refusal rate in this test, particularly at 24 hours post-hypoxia. At 24 hours post hypoxia, there is no significant difference between control and hypoxia groups (Figure 3.8.B), and at 72 hours post-hypoxia, the hypoxia group take significantly longer to complete the test relative to controls (Figure 3.8.C). No significant differences are seen in the relative difference over time (Figure 3.8.D).

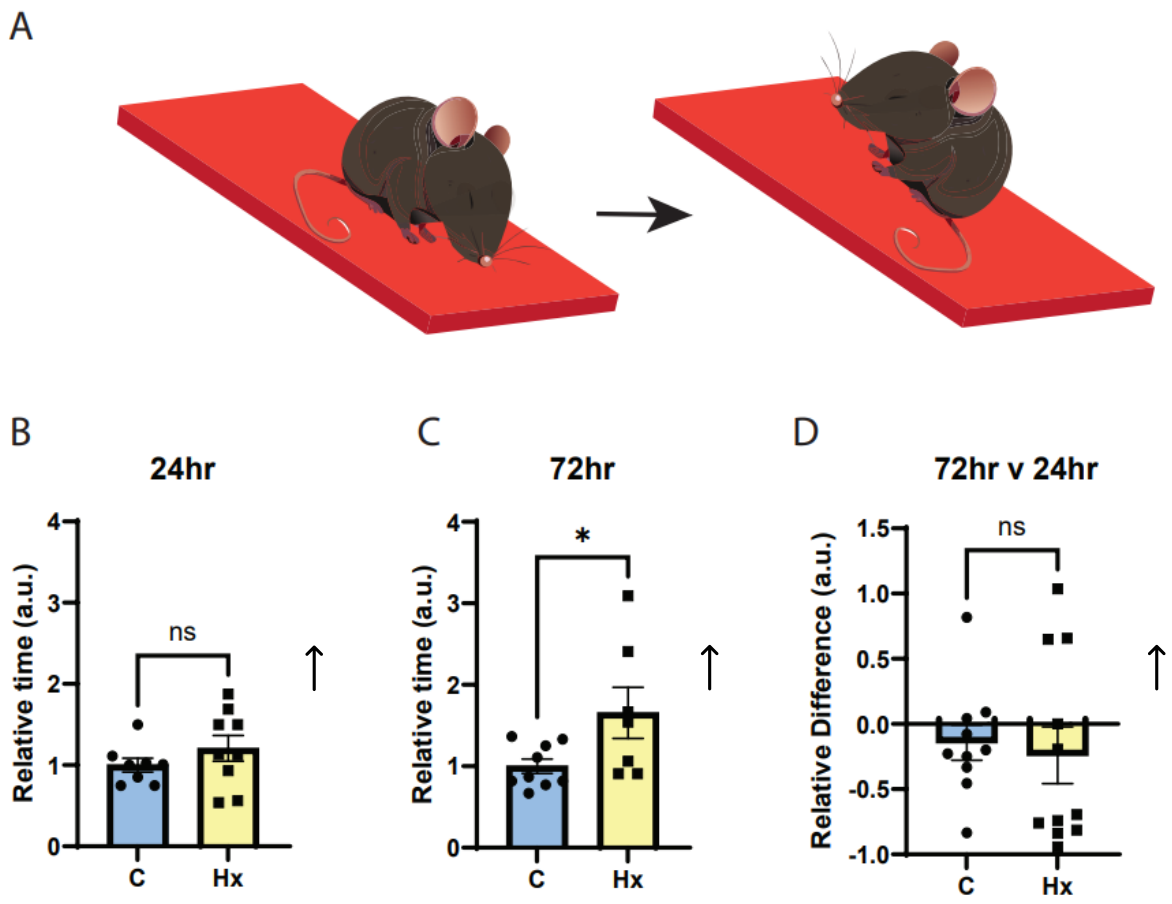


***Figure 3.8. Negative Geotaxis Reflex Develops More Slowly Post-Hypoxia. (A)*** *Negative Geotaxis Test Illustration, showing start position (left) and intended end position (right)* ***(B)*** *Time taken for test at 24hrs, normalised by litter, showing no difference. C n=8, Hx n=9, 24hr C v Hx p=0.144.* ***(C)*** *Time taken for test at 72hrs, normalised by litter. Hypoxia mice take significantly longer relative to control littermates. C n=9, Hx n=7, 72hr C v Hx p=0.0205.* ***(D)*** *Relative Difference between 24 and 72hour normalised times, showing no significance. C n=10, Hx n=11, Difference C v Hx p=0.3579. All tests are unpaired, one-tailed t-tests with arrows indicating the a-priori hypothesis, $p < 0.05$.*

### 3.3.2. Hypoxia Promotes Anxiety, Poorer Spatial Memory, and Compulsive Behaviours Later in Life.

Long-term neurobehavioural changes have been characterised before in this model (Rodriguez-Alvarez et. al., 2015; 2017; Quinlan et. al., 2018), consistently showing that global hypoxia affects behaviour later in life. The Open Field (OF) test was conducted to measure motor function, ensuring that any differences between groups in other behaviour tests are

resulting from behavioural changes rather than mobility deficits, measuring average speed and the number of line crossings for each animal. In both parameters, no significant differences were found between hypoxia and control groups (Figure 3.9.B).

The Light Dark Box (LDB) Test is used to assess anxiety behaviours in mice. Previous work in this model has observed increased anxiety post-hypoxia (Rodriguez-Alvarez et. al., 2015; Quinlan et. al., 2018; 2019), supported by the results of this study, which found that hypoxia mice take longer to enter the dark box than their control counterparts (Figure 3.9.D).

The Novel Object Location (NOL) test is a task which assesses spatial memory, a function governed by the dorsal Ca1 of the hippocampus (Geiller et. al., 2023). The time spent with the novel object location during the test period was normalised for each animal to account for object preferences using the formula detailed in Methods Section 2.5.2. Hypoxia mice performed significantly poorer in the NOL task relative to controls, demonstrating the detrimental effects of hypoxia on spatial memory (Figure 3.9.F).

The Marble Burying Test (MBT) assesses compulsive and repetitive behaviours, like those seen in autism or obsessive-compulsive disorder (OCD) (Dixit et. al., 2020). When the entire cohort is compared, there is no significant difference, although when separated by sex, hypoxia males bury significantly more marbles than male controls (Figure 3.9.H).

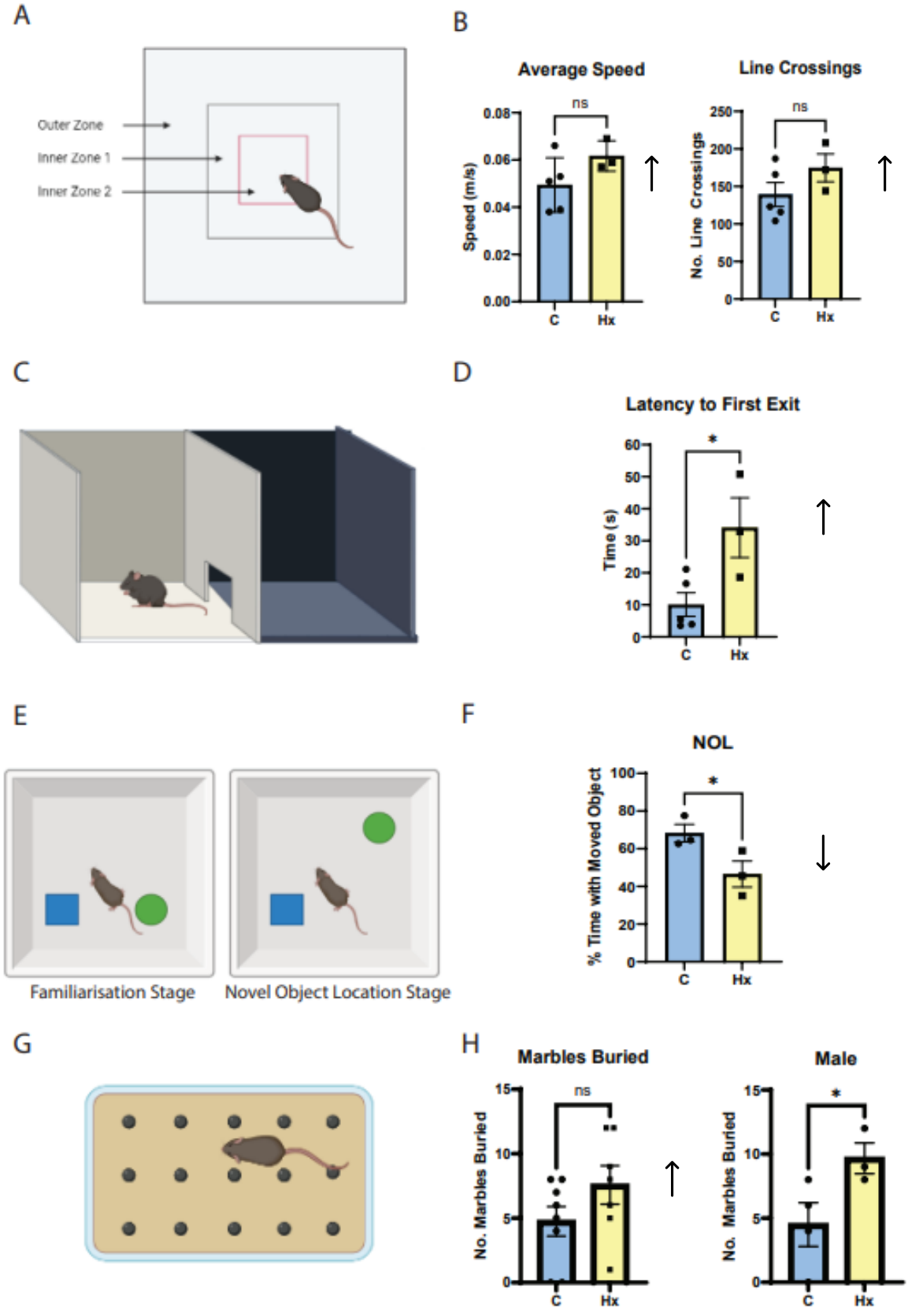


***Figure 3.9. A battery of behaviour tests shows behavioural differences between control and hypoxia mice. (A)*** *Illustration of the OF test apparatus.* ***(B)*** *No significant differences were found between*

*control and hypoxia in their average speed or the number of line crossings during the OF test. C n=5, Hx n=3, Average Speed C v Hx p=0.1473, Line Crossings C v Hx p=0.2078.* ***(C)*** *Illustration of the LDB apparatus.* ***(D)*** *Time taken for each mouse to exit the Light Box after being placed in the arena. Hypoxia mice take significantly longer to enter the dark box compared to controls. C n=5, Hx n=3, Latency C v Hx p=0.0285.* ***(E)*** *Illustration of the NOL apparatus. For the familiarisation stage (left), objects are in set positions, and for the NOL stage (right), one object is moved.* ***(F)*** *Standardised time spent with the moved object during the NOL stage. Hypoxia mice spend less time interacting with the moved object relative to controls, indicating that they do not remember the object was moved. C n=3, Hx n=3, NOL C v Hx p=0.0297.* ***(G)*** *Illustration shows the MBT apparatus.* ***(H)*** *Number of marbles buried for all mice (left) and for males only (right). There are no significant differences between control and hypoxia mice in the number of marbles buried; however, when only males are analysed, hypoxia males bury significantly more marbles than male controls. C n=8, Hx n=7, Marbles Buried C v Hx p=0.1524. C n=4, Hx n=3, Males only C v Hx p=0.0354. All tests are unpaired, one-tailed t-tests with arrows indicating the a-priori hypothesis, $p < 0.05$.*

### 3.3.3. Iba1$^+$ cells are more abundant in the hippocampus, with higher proportions of pro-inflammatory morphologies post-hypoxia both acutely and chronically.

Preliminary data in this model suggests changes in microglial populations acutely post-hypoxia (Quinlan et. al., 2019). The next stage of this study will examine how the neuroinflammatory response is altered post-hypoxia, with respect to microglia function and phenotype, and whether the neuroinflammatory response persists chronically post-hypoxia, as seen before in the literature (Bona et. al., 1999). The timepoint selected to represent the chronic stage post-hypoxia, 5 weeks post-injury at PND42, is equivalent to late adolescence in humans (Semple et. al., 2013).

The number of Iba1$^+$ cells in the hippocampus at 72 hours and 5 weeks post-hypoxia was counted and Iba1$^+$ cells were categorised by morphology using two different classification systems to investigate whether microglia present with different phenotypes post-hypoxia.

**3.3.3.1.** Increased numbers of Iba1$^{+}$ cells are seen in the hippocampus at 72 hours and 5 weeks post-hypoxia.

Previous work from the Jimenez laboratory has found that microglia populations are significantly increased at 72 hours post-hypoxia (Quinlan et. al., 2019). Here, we evaluated if microglia numbers remain elevated chronically post-hypoxia, as seen before in a rat model of severe HIE (Bona et. al., 1999), or if they recover.

It is evident that, at 72 hours post-hypoxia, there is a significantly higher number of Iba1$^{+}$ cells in hypoxia mice versus controls in the hippocampus (Figure 3.10.C). When Iba1$^{+}$ cells are counted 5 weeks post-hypoxia, there are significantly more Iba1$^{+}$ cells in the hippocampus overall post-hypoxia versus same-age controls, with most of this difference attributed to the dentate gyrus (Figure 3.10.D). These results corroborate what has been seen in the literature previously (Quinlan et. al., 2018; Bona et. al., 1999), and warrant a more detailed morphological analysis.

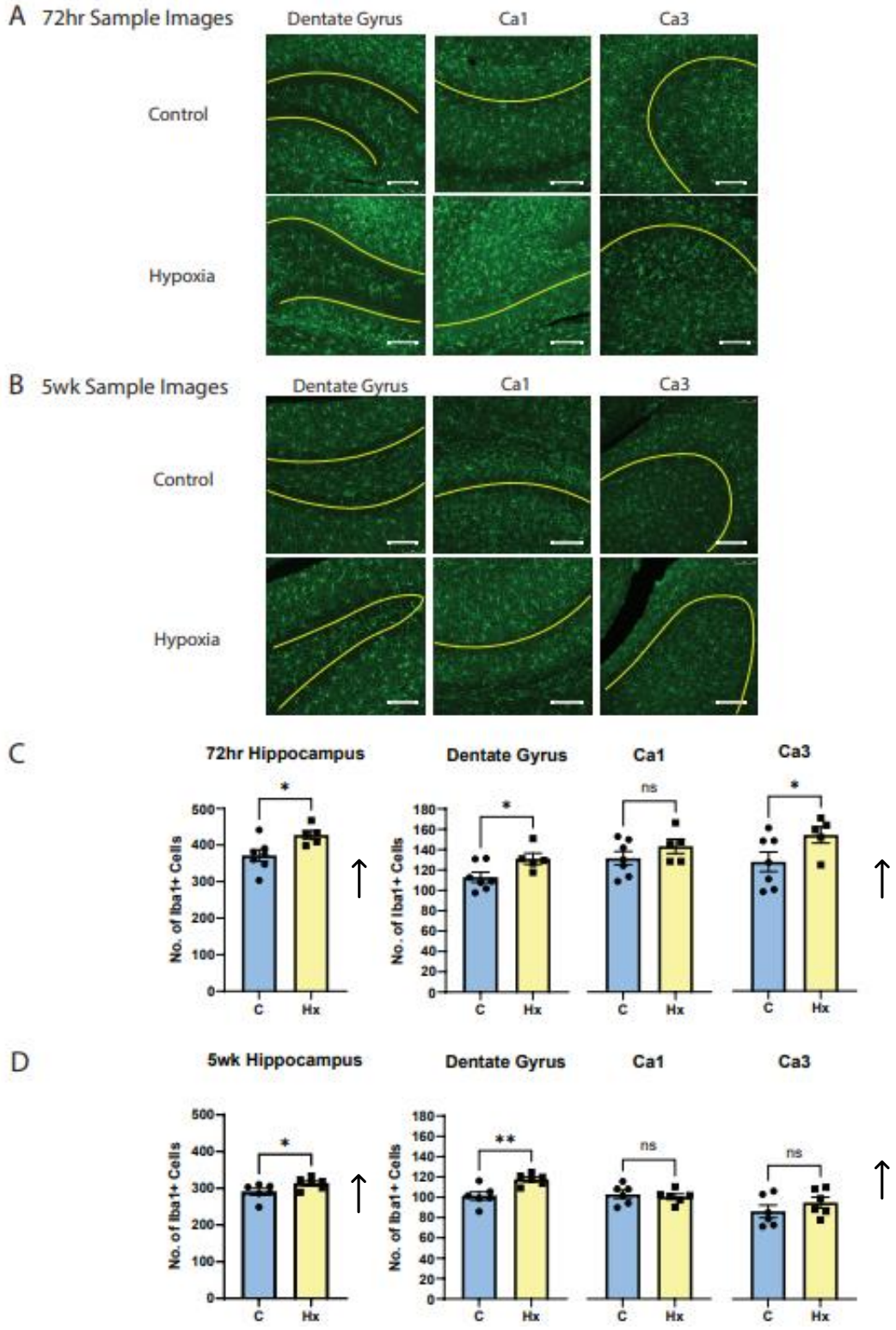


***Figure 3.10. Higher numbers of Iba1⁺ cells are found in the hippocampus at 72 hours and 5 weeks post-hypoxia. (A)*** *Sample images of each hippocampal region in control and hypoxia mice 72hr post-hx. Scale bar 100µm.* ***(B)*** *Sample images of each hippocampal region in control and hypoxia mice 5wk post-hx. Scale bar 100µm.* ***(C)*** *Number of Iba1⁺ cells in each region 72hrs post-hx. The sum of the Iba1⁺ cells in the three regions is the hippocampus (left). In all regions but the Ca1, there are significantly*

*more Iba1$^+$ cells in hypoxia mice versus controls. C n=7, Hx n=5, Hipp C v Hx p=0.013; DG C v Hx p=0.0183; Ca1 C v Hx p=0.1312; Ca3 C v Hx p=0.0374.* ***(D)*** *Iba1$^+$ cell counts by region 5wks post-hx. There are significantly more Iba1$^+$ cells in hypoxia mice relative to controls in the dentate gyrus and the hippocampus. N=6 per group, Hipp C v Hx p=0.0365; DG C v Hx p=0.0026; Ca1 C v Hx p=0.315; Ca3 C v Hx p=0.154. All tests are unpaired, one-tailed t-tests, arrows shown to indicate a-priori hypothesis, p < 0.05.*

**3.3.3.2.** Categorising Iba1$^+$ cells based on number of ramifications shows that there is a reduction in more ramified, homeostatic-like microglia at both 72 hours and 5 weeks post-hypoxia.

The first morphological analysis of microglia categorised cells based on the number of ramifications, or branches, emitting from the cell soma, assigning each cell to one of three groups: those with 0-1 branches, those with 2-3 branches and those with 4 or more branches, based on the premise that microglia with fewer branches are primed or pro-inflammatory, and that those with 4+ branches are more homeostatic-like. For each image, the number of cells in each morphology group was represented as a percentage of the total Iba1$^+$ counted. Sample images for each morphology group were selected to guide the analysis (Figure 3.11.A; Figure 3.12.A). In the 72-hour cohort, the Ca1 showed trends towards a higher percentage of 0-1 branch cells in hypoxia mice relative to controls (Figure 3.11.B). There were no significant differences between control and hypoxia groups in the percentage of 2-3 branch Iba1$^+$ cells (Figure 3.11.C). There were significantly lower percentages of 4+ branch Iba1$^+$ cells in hypoxia mice compared to controls in the Ca1 region and the hippocampus, and the Ca3 trended towards a reduced percentage of 4+ branch Iba1$^+$ cells in hypoxia mice (Figure 3.11.D).

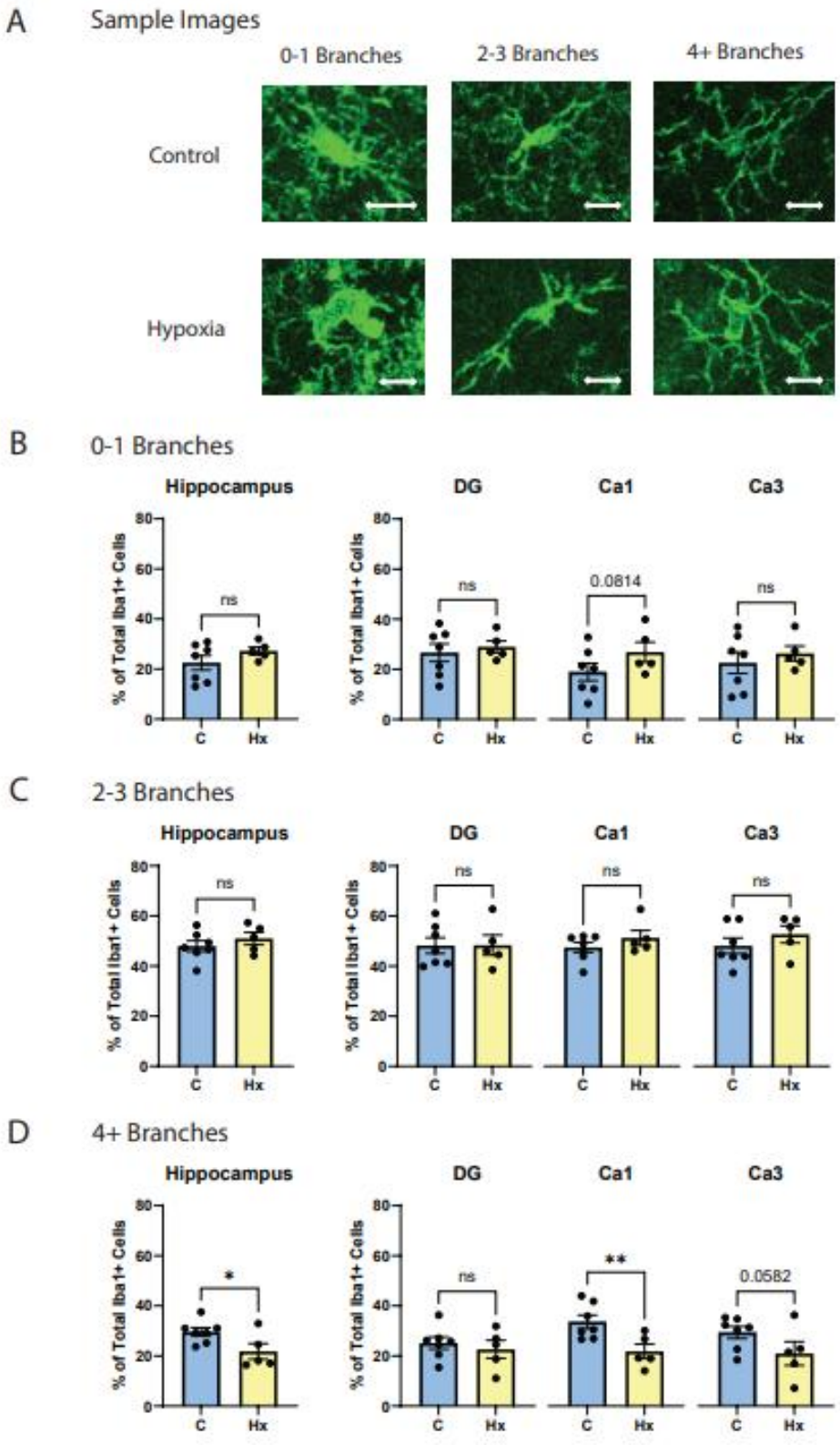


***Figure 3.11. There are differences in the proportions of morphology types of Iba1⁺ cells identified in the hippocampus at 72 hours post-hypoxia. (A)*** *Sample images of each morphology type found in control and hypoxia hippocampi were used to guide the analysis. Scale bars 10µm.* ***(B)*** *Percentage of Iba1⁺ cells with a 0-1 branch morphology in each region and in the full hippocampus. While no*

*significant differences were found, there is a trend towards more 0-1 branch cells in the Ca1 post-hypoxia versus controls. C n=7, Hx n=5, Hipp C v Hx p=0.1124, DG C v Hx p=0.3142, Ca1 C v Hx p=0.0814, Ca3 C v Hx p=0.2591.* ***(C)*** *Percentage of Iba1$^+$ cells with 2-3 branches. No significant differences were found. C n=7, Hx n=5, Hipp C v Hx p=0.1902, DG C v Hx p=0.4889, Ca1 C v Hx p=0.1466, Ca3 C v Hx p=0.1744.* ***(D)*** *Percentage of Iba1$^+$ cells with 4 or more branches. All regions except for the DG had lower percentages of 4+ branch cells post-hypoxia mice relative to controls. C n=7, Hx n=5, Hipp C v Hx p=0.0204, DG C v Hx p=0.2823, Ca1 C v Hx p=0.0072, Ca3 C v Hx p=0.0582.*

As with the 72-hour analysis, sample images to represent each morphology type at 5 weeks post-hypoxia guided the analysis (Figure 3.12.A). No significant differences in the percentage of 0-1 branch microglia were identified in any region of the hippocampus between control and hypoxia (Figure 3.12.B). There were trends towards higher percentages of 2-3 branch Iba1$^+$ cells in hypoxia mice versus controls in all regions except for the dentate gyrus (Figure 3.12.C). The 4+ branch group saw a significantly lower percentage of 4+ branch Iba1$^+$ cells in hypoxia animals relative to same-age controls in the hippocampus and the Ca3, and a trend towards lower percentages in the Ca1 of hypoxia mice, and no differences in the dentate gyrus (Figure 3.12.D).

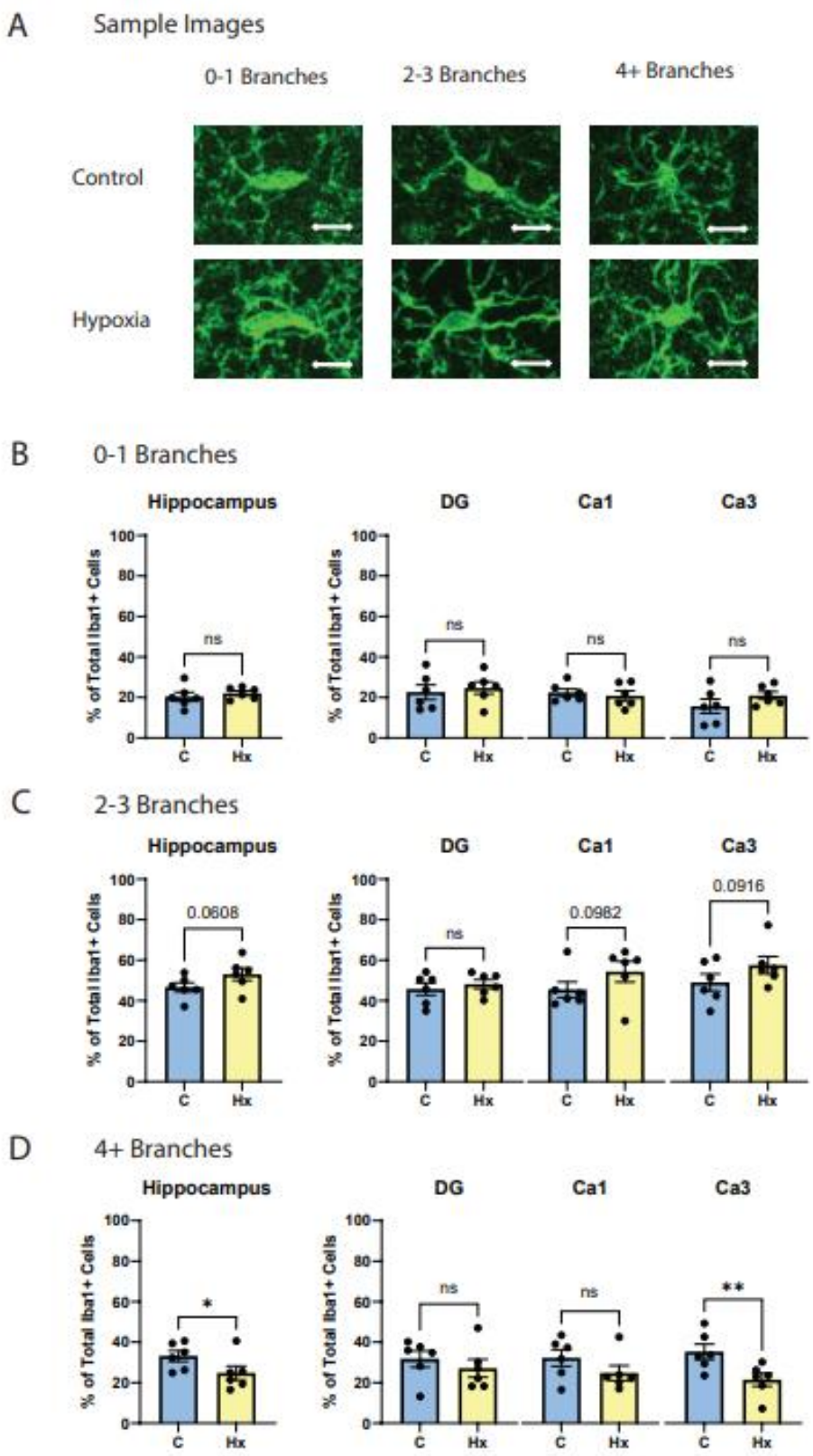


***Figure 3.12. There are differences in the proportions of morphology types of Iba1⁺ cells in the hippocampus 5 weeks post-hypoxia. (A)*** *Sample images of each morphology type found in control and hypoxia hippocampi were used to guide the analysis. Scale bars 10µm.* ***(B)*** *Percentage of Iba1⁺ cells with a 0-1 branch morphology in each region and in the hippocampus. No significant differences found.*

*N=6 per group, Hipp C v Hx p=0.2413, DG C v Hx p=0.3312, Ca1 C v Hx p=0.3128, Ca3 C v Hx p=0.1073.* ***(C)*** *Percentage of Iba1$^+$ cells with 2-3 branches. Trends towards lower numbers of 2-3 branch cells post-hypoxia emerge in all regions except the DG. N=6 per group, Hipp C v Hx p=0.0608, DG C v Hx p=0.2684, Ca1 C v Hx p=0.0982, Ca3 C v Hx p=0.0916.* ***(D)*** *Percentage of Iba1$^+$ cells with a 4+ branch morphology. The hippocampus and the Ca3 had lower percentages of 4+ branch cells in hypoxia mice relative to same-age controls. N=6 per group Hipp C v Hx p=0.0429, DG C v Hx p=0.2332, Ca1 C v Hx p=0.1034, Ca3 C v Hx p=0.0099.*

**3.3.3.3.** Type I–V method of categorising microglia finds higher percentages of Iba1$^+$ cells with proinflammatory morphologies at 72 hours and 5 weeks post-hypoxia.

This morphological analysis was based on the Type I-V method of categorising microglia published by Diz-Chaves (et. al., 2012), with each type representing a different functional state in microglia. Sample images of cells representing each group were selected to guide the analysis (72 hour (Figure 3.13.A); 5 weeks (Figure 3.14.A)). The number of cells belonging to each morphology type present in the hippocampal regions were expressed as a percentage of total Iba1$^+$ cell population.

At 72 hours post-hypoxia, higher proportions of Type V microglia and lower proportions of Type I microglia were found in hypoxia mice versus controls in the full hippocampus (Figure 3.13.B). There is a higher percentage of Type IV Iba1$^+$ cells in the dentate gyrus (Figure 3.13.C) and Type V cells in the Ca1 (Figure 3.13.D), and a lower percentage of Type I cells in the Ca3 post-hypoxia versus controls (Figure 3.13.E).

More differences between control and hypoxia microglia are seen at 5 weeks post-hypoxia. In the full hippocampus and the dentate gyrus, hypoxia mice have lower percentages of Type I Iba1$^+$ cells, and higher percentages of Type III, Type IV and Type V Iba1$^+$ cells versus controls (Figure 3.14.B). In the Ca1 and Ca3, there are lower percentages of Type I cells, and higher percentages of both Type III and Type IV cells post-hypoxia (Figure 3.14.C-E).

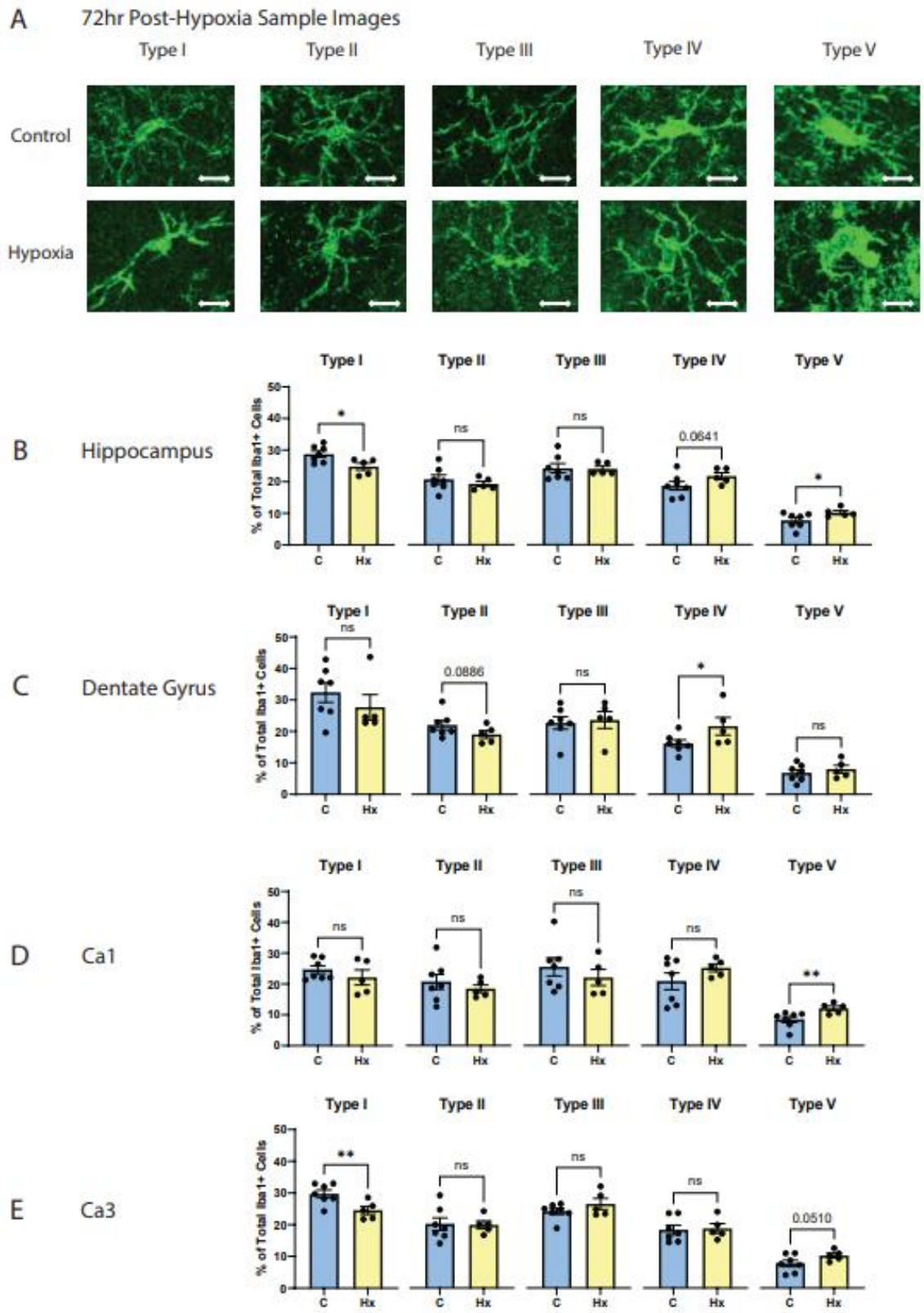


***Figure 3.13. Higher proportions of pro-inflammatory morphology types and lower proportions of primed and primitive microglia are found in hypoxia mice versus controls at 72 hours post-hypoxia.*** ***(A)*** *Sample images for each morphology type identified in control and hypoxia images. Scale bar 10µm.* ***(B)*** *Percentages of total Iba1⁺ cells for morphology type in the hippocampus. Hypoxia mice had lower*

*percentages of Type I cells and higher percentages of Type IV & V cells. C n=7, Hx n=5, Type I C v Hx p=0.0125; Type II C v Hx p=0.2323; Type III C v Hx p=0.4585; Type IV C v Hx p=0.0541; Type V C v Hx p=0.0332.* ***(C)*** *Percentage of each morphology type in the dentate gyrus. Hypoxia mice had higher percentages of Type IV cells, and trended towards lower percentages of Type II cells. Type I C v Hx p=0.1859; Type II C v Hx p=0.0886; Type III C v Hx p=0.388; Type IV C v Hx p=0.0351; Type V C v Hx p=0.2348.* ***(D)*** *Percentage of each morphology type in the Ca1. Hypoxia mice had higher percentages of Type V cells. Type I C v Hx p=0.1772; Type II C v Hx p=0.2446; Type III C v Hx p=0.2109; Type IV C v Hx p=0.116; Type V C v Hx p=0.0095.* ***(E) P****ercentage of each morphology type in the Ca3. Hypoxia mice had lower percentages of Type I cells, and trended towards higher percentages of Type V cells. Type I C v Hx p=0.0077; Type II C v Hx p=0.4674; Type III C v Hx p=0.1127; Type IV C v Hx p=0.4212; Type V C v Hx p=0.051.*

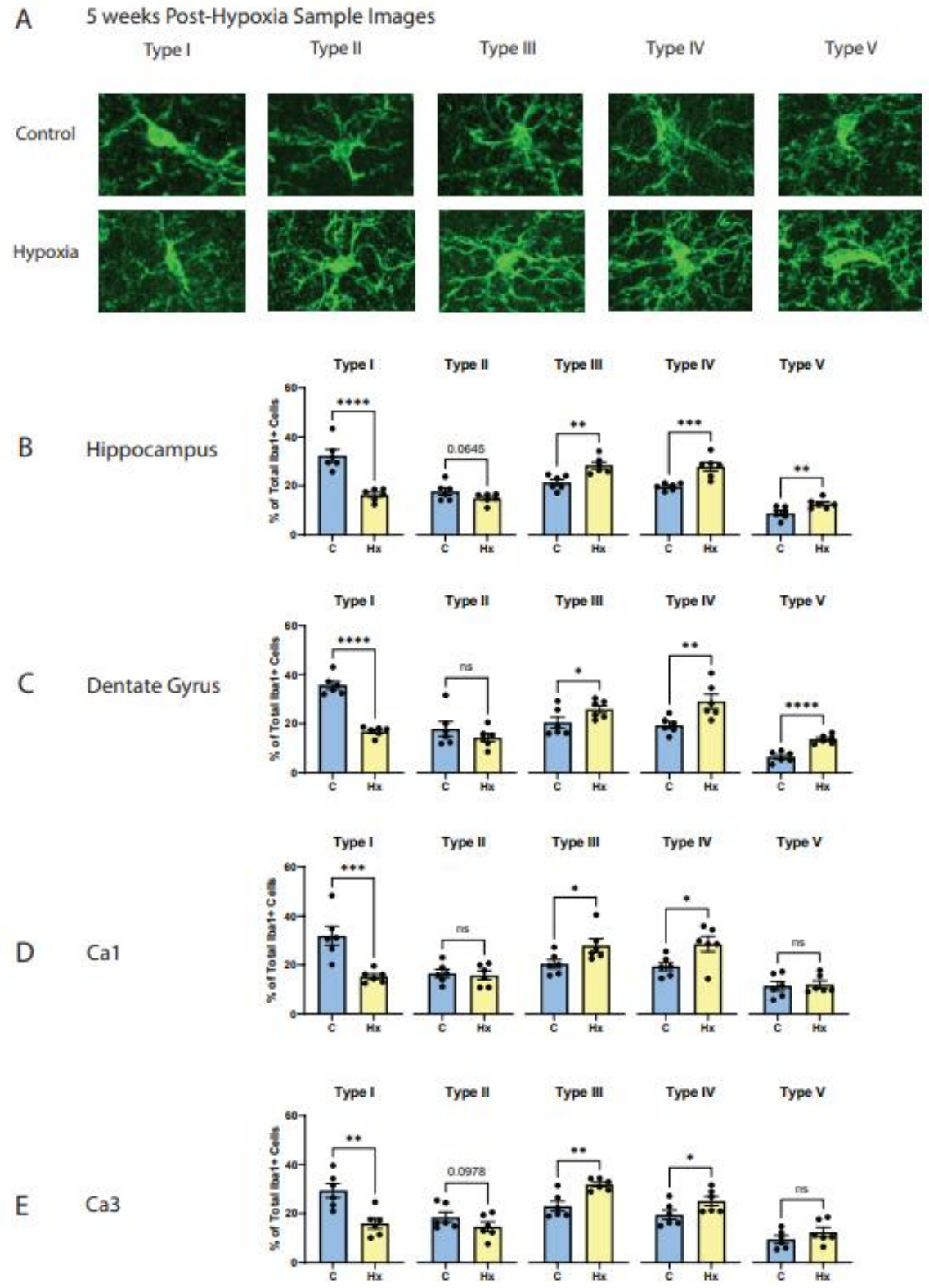


***Figure 3.14. Different morphological profile still persists 5 weeks post-hypoxia, with differences seen in all Types of Iba1⁺ cells in hypoxia mice relative to controls. (A)*** *Sample images for each morphology type from control and hypoxia images. Scale bar 10µm.* ***(B)*** *Percentage of each morphology type in the hippocampus. Hypoxia mice had lower percentages of Type I & II cells, higher percentages of Type III,*

*IV and V cells. N=6 per group, Type I C v Hx p<0.0001; Type II C v Hx p=0.0645; Type III C v Hx p=0.002; Type IV C v Hx p=0.0009; Type V C v Hx p=0.0095.* ***(C)*** *Percentages of morphology types in the dentate gyrus. Hypoxia mice had higher percentages of Type III, IV and V cells, and lower percentages of Type I cells. Type I C v Hx p<0.0001; Type II C v Hx p=0.1625; Type III C v Hx p=0.0391; Type IV C v Hx p=0.0065; Type V C v Hx p<0.0001.* ***(D)*** *Percentages of morphology types in the Ca1. Hypoxia mice had higher percentages of Type III and IV cells, and lower percentages of Type I cells. Type I C v Hx p=0.001; Type II C v Hx p=0.3847; Type III C v Hx p=0.0205; Type IV C v Hx p=0.0134; Type V C v Hx p=0.3953.* ***(E)*** *Percentages of morphology types in the Ca3. Hypoxia mice had lower percentages of Type I & II cells and higher percentages of Type III and IV cells. Type I C v Hx p=0.0019; Type II C v Hx p=0.0978; Type III C v Hx p=0.0014; Type IV C v Hx p=0.0339; Type V C v Hx p=0.1306.*

### 3.3.4. Double staining for CD68/Iba1 shows that there are higher percentages of $CD68^{+}Iba1^{+}$ cells at both 72 hours and 5 weeks post-hypoxia relative to same age controls, and these cells have active morphology types.

CD68 is a marker for phagocytic lysosomes, and this has been used previously in the literature to identify phagocytic or pro-inflammatory microglia (Guillot-Sestier et. al., 2021). A double stain with CD68 and Iba1 allowed for phagocytic microglia to be identified, counted and morphologically profiled according to the Type I-V method previously employed (Diz-Chaves et. al., 2012).

#### 3.3.4.1. Higher percentages of $CD68^{+}Iba1^{+}$ cells are present in the hippocampus at both 72 hours and 5 weeks post-hypoxia.

To quantify the prevalence of CD68 in $Iba1^{+}$ cells for comparison between control and hypoxia groups, $Iba1^{+}$ cells which were also positive for CD68 were expressed as a percentage of total $Iba1^{+}$ cells present. At both 72 hours and 5 weeks post-hypoxia, there was a significantly higher percentage of $CD68^{+}Iba1^{+}$ cells in hypoxia mice relative to same-age controls, indicating that there is elevated phagocytic activity in response to hypoxia which begins in the acute stages and persists long after the neonatal period (Figure 3.15).

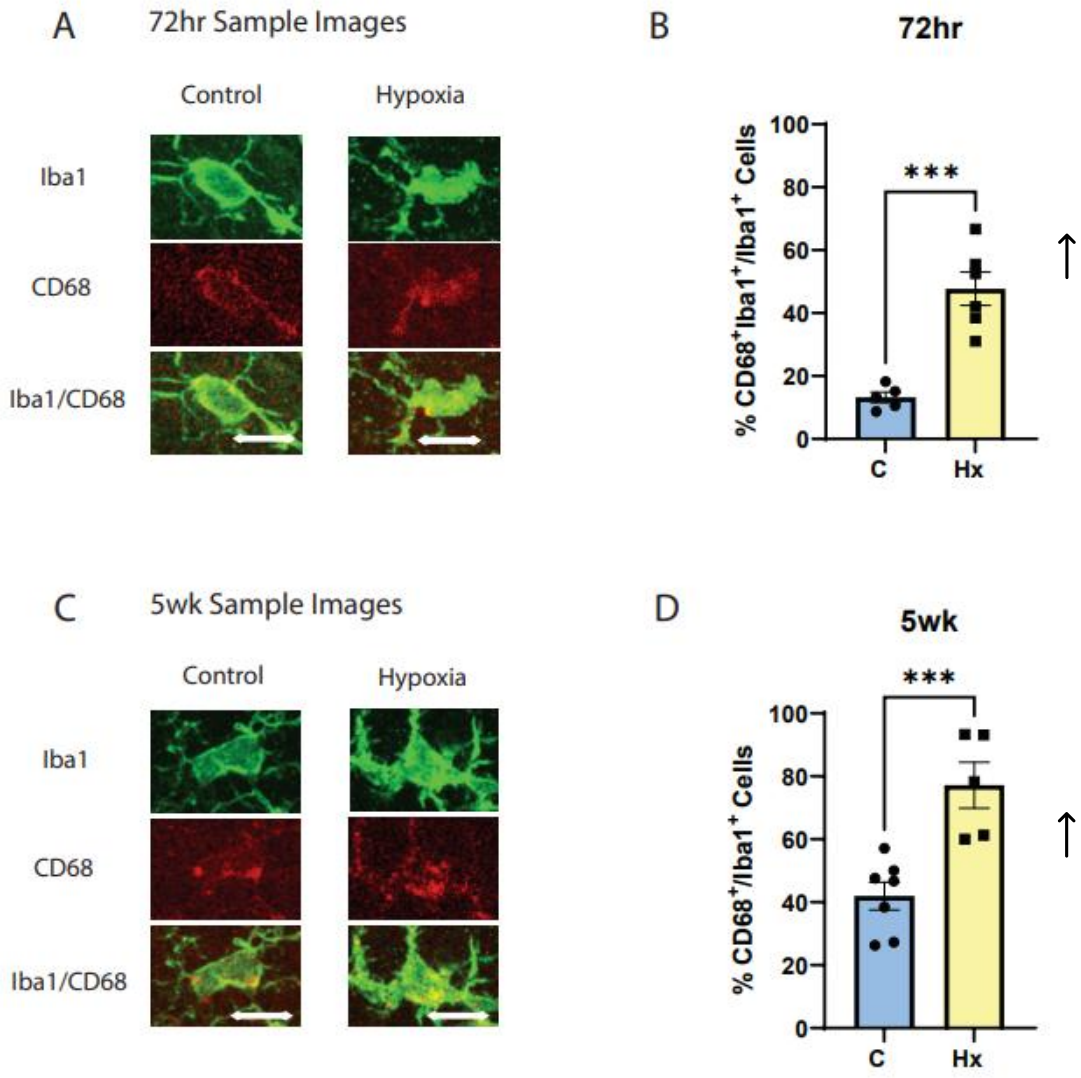


***Figure 3.15. Higher percentages of CD68⁺Iba1⁺ cells are identified at both 72hr and 5 weeks post-hypoxia. (A)*** *Sample images of CD68/Iba1 double labelled cells in control and hypoxia 72hrs post-hx. Scale bar 10µm.* ***(B)*** *Significantly higher percentage of Iba1⁺ cells in the hippocampus were CD68 positive at 72hrs post-hx versus controls. C n=5, Hx n=6, 72hr C v Hx p=0.0001.* ***(C)*** *Sample images of CD68/Iba1 double-labelled cells in control and hypoxia 5wks post-hx. Scale bar 10µm.* ***(D)*** *Significantly higher percentage of CD68⁺Iba1⁺ cells found in the hippocampus at 5wks post-hx versus controls. C n=7, Hx n=5, 5 weeks C v Hx p=0.0007. Unpaired, one-tailed t-tests, a-priori hypothesis indicated by arrows, $p < 0.05$.*

3.3.4.2. Using the Type I-V morphological analysis method shows that CD68⁺Iba1⁺ cells have pro-inflammatory morphologies at both timepoints.

After finding elevated CD68 expression at both acute and chronic timepoints, the Type I-V morphological analysis was carried out on these cells to ascertain whether any correlation

existed between CD68 expression and morphology type. A notable observation is that, upon completion of the morphological analysis, none of the samples contained $CD68^{+}Iba1^{+}$ cells with Type I, II or III morphologies at either time point. Therefore, the morphological analyses only show proportions of Type IV and Type V cells identified (Figure 3.16.B; Figure 3.17.B).

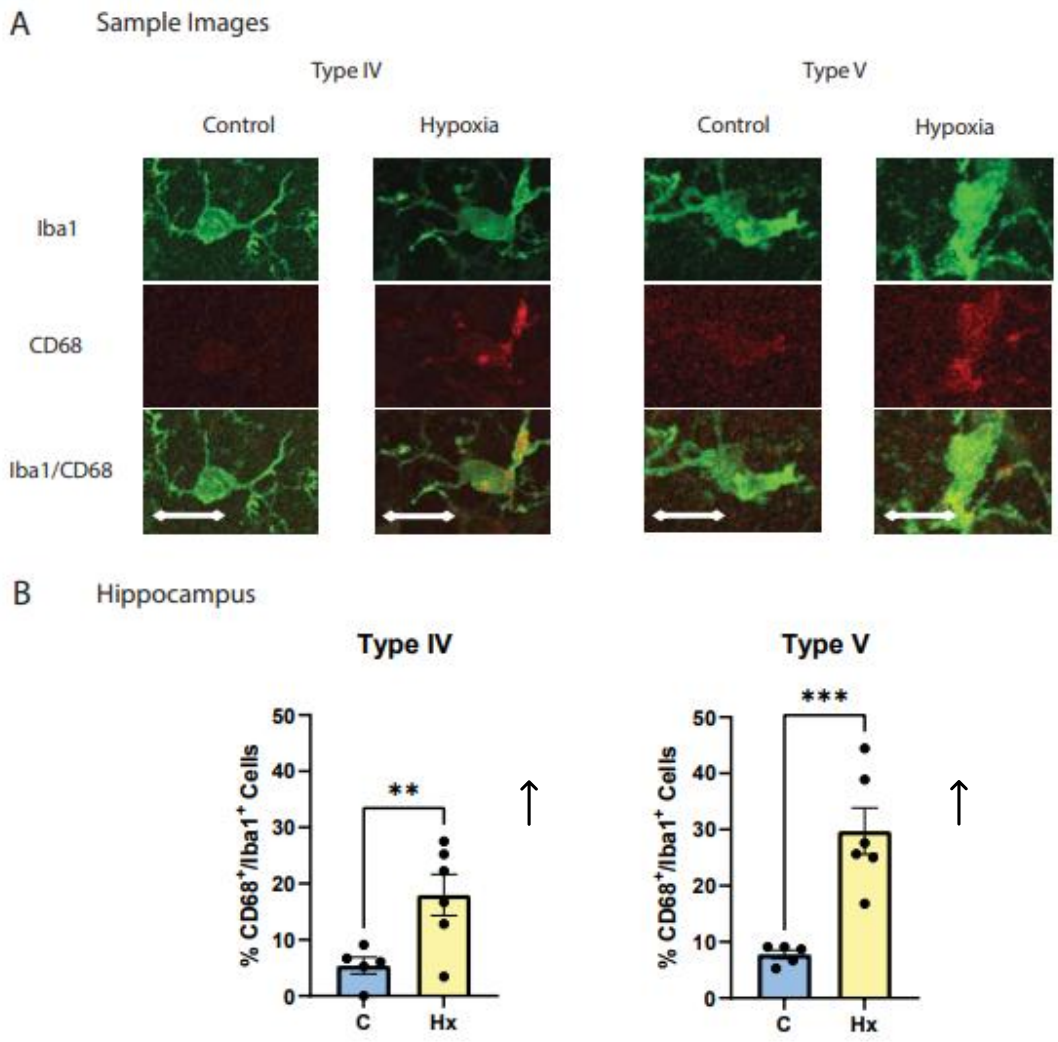


***Figure 3.16. Higher Percentages of $CD68^{+}Iba1^{+}$ Type IV and Type V cells found in the hippocampus 72 hours post-hypoxia. (A)*** *Samples Images of Type IV and Type V cells found in control and hypoxia images. Scale bar 10µm.* ***(B)*** *Hypoxia mice have higher percentages of CD68 cells with Type IV and Type V morphology compared to same age controls. C n=5, Hx n=6, Type IV C v Hx p=0.0081, Type V C v Hx p=0.0005. Unpaired, one-tailed t-tests, a-priori hypothesis indicated by arrows, $p < 0.05$.*

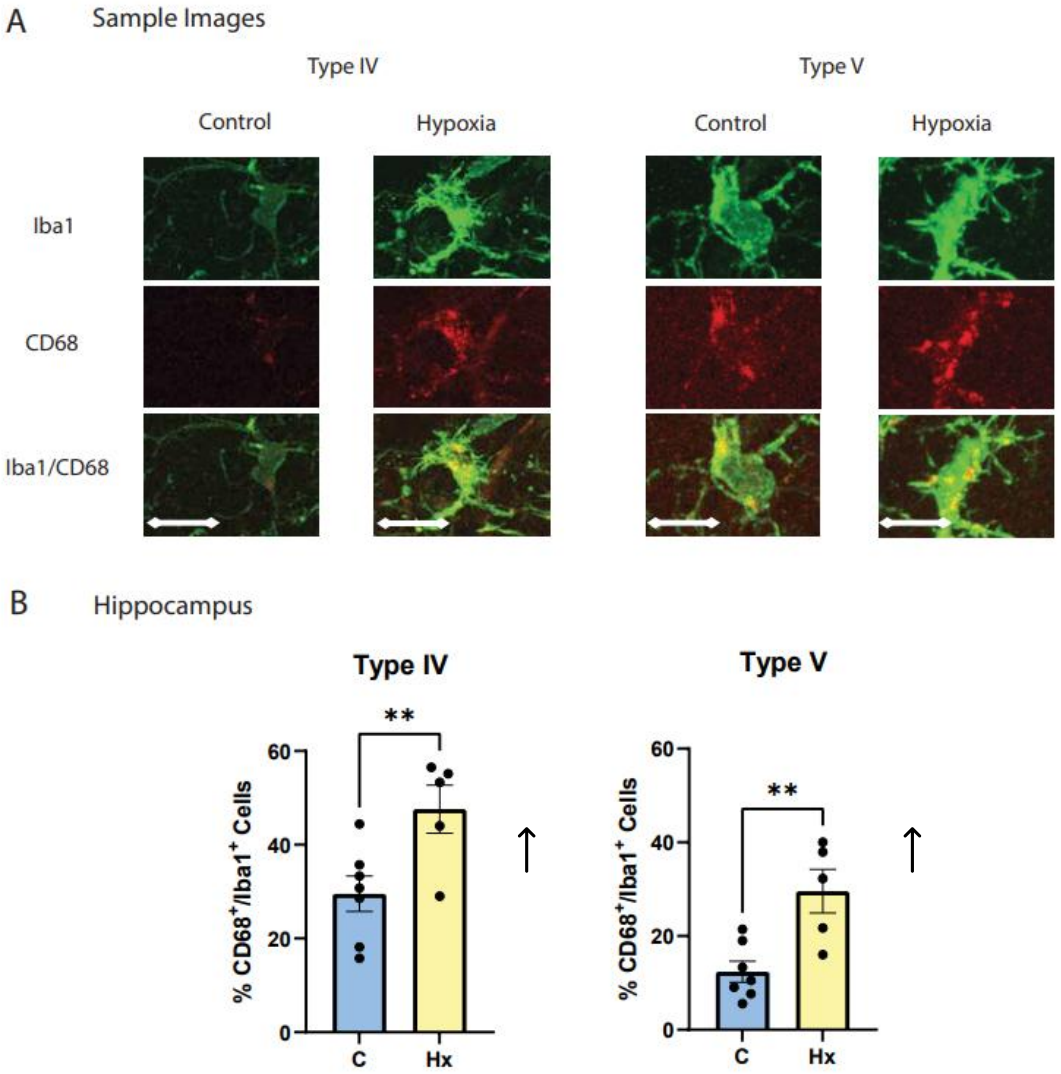


***Figure 3.17. Higher Percentages of CD68$^+$Iba1$^+$ Type IV and Type V cells found in the hippocampus 5 weeks post-hypoxia. (A)*** *Samples Images of Type IV and Type V cells found in control and hypoxia images.* ***(B)*** *Hypoxia mice express significantly more CD68$^+$Iba1$^+$ cells with Type IV and Type V morphologies than control littermates. C n=7, Hx n=5, Type IV C v Hx p=0.0078, Type V C v Hx p=0.0022. Unpaired, one-tailed t-tests, a-priori hypothesis indicated by arrows, p < 0.05.*

### 3.3.5. Lower Percentages of P2RY12$^+$Iba1$^+$ cells are present in the hippocampus both 72 hours and 5 weeks post-hypoxia.

P2RY12 was used as a marker for homeostatic microglia in the hippocampus for quantification (Gómez-Morillas et. al., 2021). To quantify the prevalence of P2RY12 in Iba1$^+$ cells, Iba1$^+$ cells which were also positive for P2RY12 were expressed as a percentage of total Iba1$^+$ cells. At both 72 hours and 5 weeks post-hypoxia, there was a significantly lower percentage of

P2RY12$^{+}$Iba1$^{+}$ cells in hypoxia mice relative to controls, indicating that, post-hypoxia, microglia in the hippocampus have reduced capability to respond to their extracellular environment and communicate with neurons which persists long after the neonatal period (Figure 3.18).

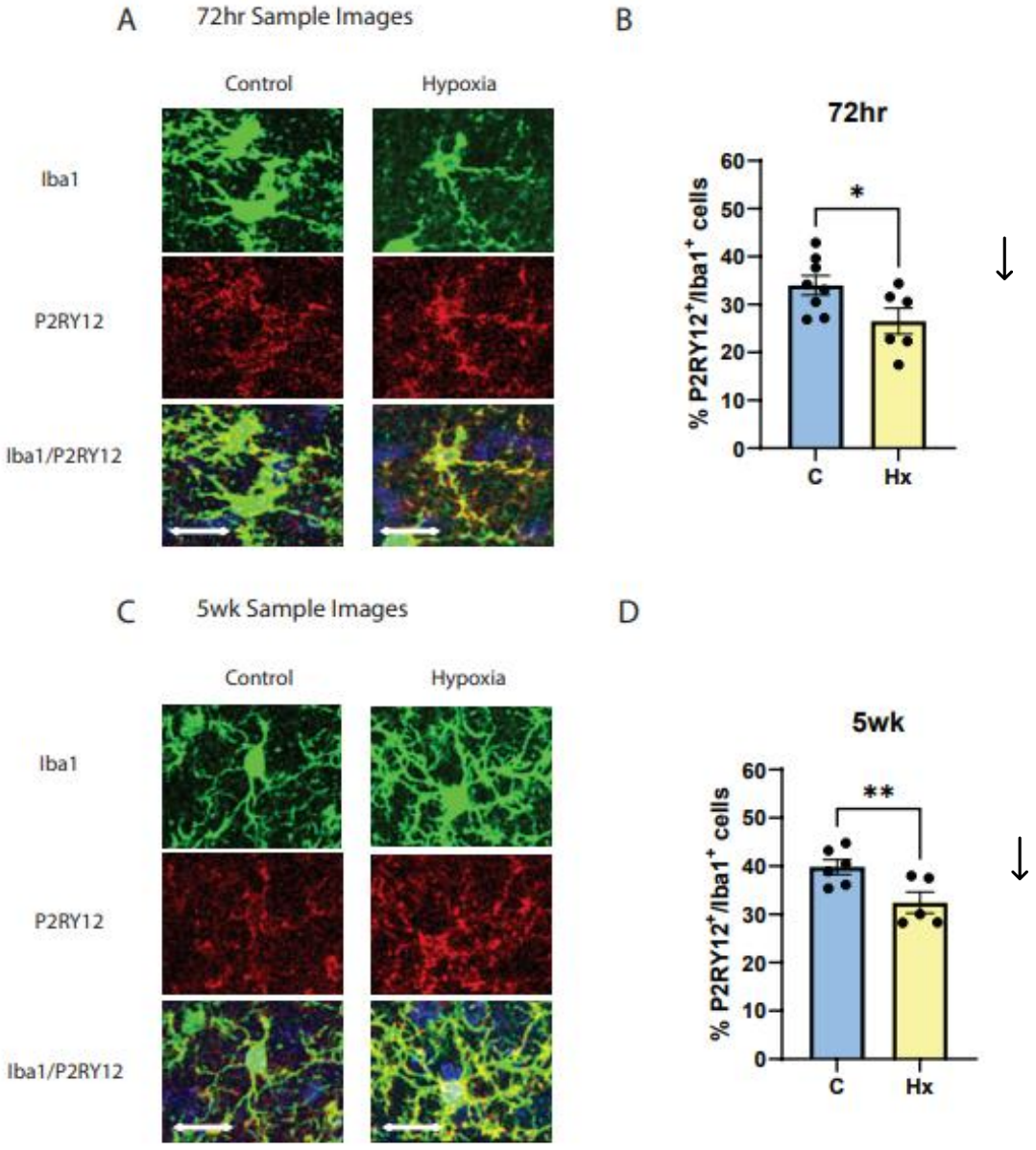


***Figure 3.18. Lower percentages of P2RY12$^{+}$Iba1$^{+}$ cells are found in the hippocampus at 72 hours and 5 weeks post-hypoxia. (A)*** *Sample images of P2RY12/Iba1 cells 72hrs post-hx.* ***(B)*** *Significantly lower percentage of Iba1$^{+}$ cells in the hippocampus were also P2RY12 positive at 72hrs post-hx relative to same-age controls. C n=8, Hx n=6, 72hr C v Hx p=0.0216.* ***(C)*** *Sample images of P2RY12/Iba1 cells 5wk post-hx.* ***(D)*** *Significantly lower percentages of P2RY12$^{+}$Iba1$^{+}$ cells found in the hippocampus at 5wk post-hx relative to same age controls. C n=6, Hx n=5, 5wk C v Hx p=0.0098. Unpaired, one-tailed t-tests, a-priori hypothesis indicated by arrows, $p < 0.05$.*

### 3.4. Discussion

Previous results have found increased numbers of microglia in the hippocampus acutely following moderate global hypoxia accompanied by chronic behavioural changes (Quinlan et. al., 2019). Therefore, this study expands on these observations to study microglia more closely acutely and chronically post-hypoxia, with accompanying neonatal reflex testing and adolescent behavioural assays. In this study, we showed that hypoxia causes slower development of neonatal reflexes, and long-lasting deficits in behaviours pertaining to spatial memory, anxiety and compulsive or repetitive behaviours. When microglia were studied, hypoxia induced a long-lasting elevation of microglial populations within the hippocampus which express much higher proportions of phagocytic microglia than same-age controls.

For the first time in this moderate model, neurodevelopmental differences were identified in the acute period post-hypoxia through neonatal reflex tests. Hypoxia negatively impacted general neonatal pup wellbeing and the development the vestibular response to gravity, proprioception, forelimb grip strength and the rostro-caudal gradient of limb movement. For some tests, this difference is no longer detected by 72 hours post-hypoxia, indicating a delay rather than a persistent deficit, for example in the forelimb grip strength and the cliff aversion. For others, there is little to no difference seen at 24 hours post-hypoxia, but a deficit emerges in hypoxia cohorts by 72 hours post-hypoxia, such as in the negative geotaxis. Although this battery of tests was designed for testing mice at PND8 and PND10 (Feather-Schussler & Ferguson., 2016), previous literature has questioned the suitability of the grip strength test in mice younger than PND10 (Heyser., 2003). Nevertheless, the full set of reflexes shows the detrimental consequences of hypoxia. Impaired neonatal reflex development has also been recorded in rodent models of severe HIE (Ten et. al., 2003; Lubics et. al., 2005; Sun et. al., 2015) and in humans via Denver score testing (Hallioglu et. al., 2001). Furthermore, studies in

humans have found that, even after TH treatment, MRI abnormalities in the neonatal stage correlate with poorer performance in developmental testing in infancy (Massaro et. al., 2015; Chalak et. al., 2018; Reiss et. al., 2020). Neonatal inflammation impairs the developmental programme of white matter and drives white matter injury (Favrais et. al., 2011; Holloway et. al., 2021), a finding corroborated by MRI studies of infants (Machie et. al., 2021), therefore supporting the translatability of our model in precipitating similar developmental delays in infancy as seen in humans.

The next stage of this study performed behaviour tests on mice at 5 weeks old, focusing on spatial memory, anxiety, and compulsivity. The NOL test assesses spatial memory, the LDB test measures anxiety and the MBT tests for compulsive or repetitive behaviours. As reported previously, spatial memory was negatively impacted by hypoxia (Rodriguez-Alvarez et. al., 2015; Quinlan et. al., 2019), consistent with a model of neonatal LPS exposure (Wang et. al., 2012). Studies with anxiety tests in rodents have observed that the behavioural manifestation of anxiety is governed by age. In younger mice, anxiety manifests as heightened curiosity to explore the “danger zone” i.e. the light region in this case (Wang et. al., 2012; Arrant et. al., 2013), whereas older mice exhibit a protective response causing them to hide in the “safe zone” i.e. the dark region (Hascoët., 1999; Arrant et. al., 2013). Consistent with the literature, hypoxia mice in this study were more curious to explore the light box, therefore displaying increased anxiety (Wang et, al., 2012; Rodriguez-Alvarez et. al., 2015). Testing for compulsive or repetitive behaviours using the MBT found that hypoxia males were the most prone to increased compulsivity or repetition. Spatial memory and anxiety are governed by the dorsal and ventral Ca1 of the hippocampus respectively (Bannerman et. al., 2014; Geiller et. al., 2023; Li et. al., 2024), while compulsive behaviours are directed by the cortico-basal ganglia-

thalamic pathway (Garner et. al., 2004; Garner., 2005), which is connected to the hippocampus via the amygdala and the striatum (Ciocchi et. al., 2015). There is evidence that hippocampal dysfunction can contribute to compulsive behaviours (Feduccia et. al., 2012; Ciocchi et. al., 2015), and it has been hypothesised that compulsive behaviours may be linked to addiction, a behaviour which involves memory and the hippocampus (Feduccia et. al., 2012; Kutlu & Gould., 2016; Figee et. al., 2016). The vulnerability of the hippocampus to inflammatory insults (Williamson & Bilbo., 2013) makes it imperative to study behaviours which reflect hippocampal function. The results of this thesis agree with human studies where even mild HIE can cause worse long-term behavioural outcomes and increase the risk of neurodevelopmental disorders (Ahearne et. al., 2016; Akula et. al., 2023).

Next, microglia activation in the hippocampus was characterised via a density assessment followed by morphological analyses. As mentioned above, microglia were more abundant in the hippocampus 72 hours post-hypoxia (Quinlan et. al., 2019). This study confirmed and expanded on these findings, as microglia were more abundant at 72 hours and 5 weeks post-hypoxia. This agrees with the literature, which has found a significant accumulation of microglia in the brain, regardless of HIE severity (Del Bigio & Becker., 1994; Liu & McCullough., 2013; Serdar et. al., 2019). Two morphological analyses were conducted, the first of which characterised microglia based on the number of branches emitting from their soma, and the second where microglia were classed into one of five morphology types, based on the work of Diz-Chaves and colleagues (2012). In the number of branches method, those with fewer branches were taken as mostly pro-inflammatory, and those with more than 4 branches were taken as mostly homeostatic. While this analysis did show that there were more homeostatic-like microglia in control groups than hypoxia, this method did not account for other features such as cell body size or branch complexity. Therefore, the Type I-V method was employed on

the same images to give a more detailed profile of the microglia present (Diz-Chaves et. al., 2012). A greater proportion of microglia from hypoxia pups had bigger bodies and shorter, less complex dendrites, a phenotype related to pro-inflammatory microglia, acutely and chronically post-hypoxia. These findings are supported by the literature describing chronic upregulation of pro-inflammatory markers in the brain post-HIE (Bona et. al., 1999; Lalancette-Hébert et. al., 2007; 2017; Stridh et. al., 2011; Winerdal et. al., 2012).

Microglia were further characterised via double staining with CD68 and P2RY12, which represented pro-inflammatory and homeostatic microglia respectively. Microglia expressing CD68 were more abundant at both acute and chronic time points, with these $CD68^{+}$ microglia also exhibiting Type IV and Type V pro-inflammatory phenotypes (Diz-Chaves et. al., 2012). These findings are corroborated by previous studies, as upregulation of CD68 as a marker for phagocytosis has been reported in severe models of HIE (Li et. al., 2017; Lv et. al., 2020). Furthermore, KEGG pathway analysis found that phagosome pathways are enriched in rodents post-HIE (Tao et. al., 2024), a finding supported by single cell RNA sequencing which identified a subset of highly reactive microglia whose expression is promoted following neonatal inflammation (Dufour et. al., 2025).

Fewer microglia expressed P2RY12 at acute and chronic timepoints post-hypoxia relative to same age controls, supporting the findings that there were fewer microglia with homeostatic phenotypes overall, particularly at 72 hours post-hypoxia. Downregulation of P2RY12 is associated with a functional shift towards more pro-inflammatory or phagocytic microglia (Koizumi et. al., 2013), as seen in a model of neonatal stroke (Rayasam et. al., 2020). Single cell RNA sequencing also found that developmentally associated microglia are impaired and downregulated by neonatal inflammation (Dufour et. al., 2025). The functional consequences

of P2RY12 downregulation are far-reaching, as this receptor is involved in functions such as microglial chemotaxis (Haynes et. al., 2006), maintenance of the microglial ramified morphology (Sipe et. al., 2016) and communication with neurons (Badimon et. al., 2020).

# Chapter 4: Results Chapter 2

## 4.1. Introduction

### 4.1.1. NLRP3 Inflammasome and Microglia

The NLRP3 inflammasome is a multimeric protein complex which activates and releases pro-inflammatory cytokines, such as IL-1β and IL-18, and can induce pyroptosis in response to PAMPs and DAMPs as part of the innate immune response (Martinon et. al., 2002; Agostini et. al., 2004; Becker & O'Neill., 2007; Yang et. al., 2019). Research has shown that the NLRP3 inflammasome is mainly expressed by microglia within the CNS (Gustin et. al., 2015). The inflammasome, and IL-1β release, have been implicated in a range of both acute and chronic neurological conditions, such as Alzheimer's disease (AD) (Dempsey et. al., 2017; McManus et. al., 2025), traumatic brain injury (TBI) (Wallisch et. al., 2017) and Parkinson's disease (Lee et. al., 2019).

### 4.1.2. NLRP3 Inflammasome and HIE

It comes as little surprise that the NLRP3 inflammasome has been implicated in the neuroinflammatory response following HIE, given its role in IL-1β activation and release (Chen et. al., 2018; Li et. al., 2021a). This has been found in both rat models and human studies; neonates suffering from HIE at birth had elevated peripheral blood levels of NLRP3, IL-1β, ASC, caspase-1 and GSDMD compared to controls, and that the levels of these markers were positively correlated with clinical HIE severity, measured by APGAR scores (Lv et. al., 2020). The importance of the NLRP3 inflammasome in driving IL-1β release by microglia is further evidenced by the upregulation of P2X7R in neonatal HIE (Rodriguez-Alvarez et. al., 2017; Smith et. al., 2023), which is a canonical activator of NLRP3 inflammasome assembly (see Introduction Figure 1.2). A study of HIE found that NLRP3-knockout mice have increased microglial activation and more severe brain injury compared to wild type mice, whereas in the same study, ASC-knockout was neuroprotective compared to wild-type mice (Ystgaard et. al.,

2019). This contrasts with studies which find pharmacological inhibition of NLRP3 inflammasome formation to be neuroprotective (Lv et. al., 2020; Luo et. al., 2021), highlighting the existing gap in knowledge regarding the complex interplay between inflammatory pathways in the aftermath of HIE.

#### 4.1.3. MCC950, a NLRP3 inhibitor.

A growing body of research has used various compounds to suppress different elements of the NLRP3 inflammasome in a range of disease models, including HIE, to understand how NLRP3 inflammasome suppression impacts on disease progression (Blevins et. al., 2022). MCC950, also known as CRID3, is a potent and selective inhibitor of NLRP3 inflammasome assembly, as demonstrated initially in severe experimental autoimmune encephalomyelitis (EAE), a disease model of multiple sclerosis (MS), and cryopyrin-associated periodic syndrome (CAPS) (Coll et. al., 2015). Since then, MCC950 has also been proven beneficial in preclinical models of neurological conditions such as AD (McManus et. al., 2025), TBI (Ismael et. al., 2018), intracerebral haemorrhage (ICH) (Ren et. al., 2018) and subarachnoid haemorrhage (SAH) (Luo et. al., 2019). All these conditions are characterised by a strong neuroimmune component to disease pathology, particularly with regards to IL-1β signalling, which is released by microglia via NLRP3 inflammasome signalling.

#### 4.1.4. Hypothesis and Aims

The hypothesis of this study is that administering MCC950 immediately post-hypoxia will dampen the neuroinflammatory response and lead to fewer pro-inflammatory microglia in the hippocampus. These attenuations will be reflected in behavioural attenuations in the developmental reflex testing and the adult behaviour assays.

The aims of this chapter are as follows:

1. To determine whether MCC950 treatment influences neonatal reflex development or adult behaviour testing performance post-hypoxia.
2. To characterise microglia using morphological analyses and microglial markers acutely and chronically post-hypoxia and MCC950 treatment.
3. Gene and protein expression studies to see how markers relating to microglia function and the neuroinflammatory response are affected by hypoxia and MCC950 treatment.

## 4.2. Methods

Mice were prepared for hypoxia as described previously and sacrificed at the specified timepoints in the flowchart below in Figure 4.1. Wellbeing scores documented in Table 4.2.

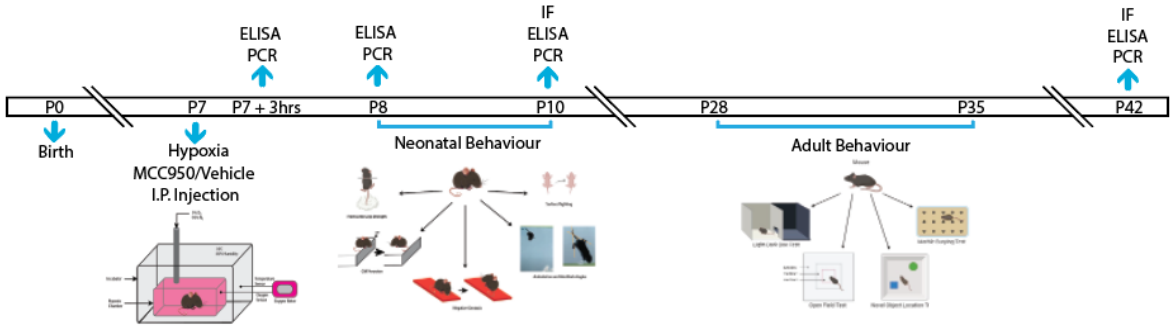


***Figure 4.1. Timeline of the molecular and behavioural studies conducted.***

### 4.2.1. Neonatal Behaviour

Neonatal Reflexes were analysed using a battery of tests adapted from Feather-Schussler & Ferguson (2016), detailed fully in Methods Chapter 2, Section 2.4. The tests used were the Ambulation test and hindlimb angles, negative geotaxis test, cliff aversion test, surface righting tests and front limb grip strength test. Due to inter-litter variability, animals were normalised by litter for the negative geotaxis test, the cliff aversion test, the grip strength test and the hindlimb angles.

### 4.2.2. Adult Behaviour

The Adult behaviour tests conducted were the Open Field test, the Light Dark Box test and the Novel Object Location test as detailed in the Methods Chapter 2, Section 2.5.

### 4.2.3. Immunofluorescence Staining and Imaging

Phagocytic microglia were visualised with the modified IF protocol described in Methods Chapter 2, Section 2.6.3 (Guillot-Sestier et. al., 2021), incubated with Anti-CD68 (1:500) and Anti-Iba1 (1:500), followed by the secondary antibodies Alexafluor 594 Donkey anti-Rat

(1:500) and Alexafluor 488 goat anti-rabbit (1:500). Homeostatic microglia were visualised as described previously in the literature and in Methods Chapter 2, Section 2.6.2 (Quinlan et. al., 2019) using Anti-P2RY12 (1:100), and Anti-Iba1 (1:500), followed by secondary antibodies Alexafluor 594 Donkey anti-Rat (1:500) and Alexafluor 488 goat anti-rabbit (1:500). Z-stacks for each region were imaged at 40x at 0.4µm intervals along the Z-plain using a Leica SP8 scanning confocal microscope (TBSI Imaging and Microscopy Centre).

| EXPERIMENT | TIME POST-HX | NO. C-VEH | NO. HX-VEH | NO. HX-MCC |
|---|---|---|---|---|
| **CD68/Iba1** | 72hrs | 5 | 4 | 6 |
| | 5wks | 4 | 5 | 3 |
| **P2RY12/Iba1** | 72hrs | 6 | 7 | 7 |
| | 5wks | 7 | 7 | 7 |

***Table 4.1. Experimental cohorts for immunofluorescence studies in Results Chapter 2.***

4.2.4. Cell Counting

Z-stack images were converted into a Z-projection in Image J for manual counting. Each image was counted twice, and the average was taken as the final count. The morphological analyses grouped cells by morphological features (Diz-Chaves et. al., 2012). This analysis is described more fully in Methods Chapter 2 Section 2.7.3, and the double staining analysis is described in Methods Chapter 2 Section 2.7.4.

4.2.5. Protein Assay and ELISA

Hippocampi were isolated at 3 hours, 24 hours, 72 hours and 5 weeks post-hypoxia for protein quantification with a modified Lowry assay, detailed in Methods Chapter 2, Section 2.8.2. ELISAs were used to measure the concentration of IL-1β, IL-6, P2RY12, CD68, IL-18, CXCR3, C1qR1, C3 and C5a in the hippocampus (manufacturer details for all kits in Table 2.10), as described in Methods Chapter 2, Section 2.8.3. Once the analyte concentration was

extrapolated from the generated standard curve, data was expressed as ng cytokine X per mg of total protein.

### 4.2.6. RNA Extraction, cDNA Synthesis and qPCR

Hippocampi were isolated at 3 hours, 24 hours, 72 hours and 5 weeks post-hypoxia for gene quantification by qPCR. RNA was first extracted using Trizol as described in Methods Chapter 2, Section 2.9.1, from which cDNA was synthesised (Methods Chapter 2, Section 2.9.2). This cDNA was used in qPCR to quantify transcription of the following genes: *Il1β, Il6, C1qa2, Tnfα,* with *Actin* used as the housekeeping gene (protocol described in Methods Chapter 2, Section 2.9.3; primer details in Table 2.14).

| PARAMETER | SCORING | P8 | | | P9 | | | P10 | | |
|---|---|---|---|---|---|---|---|---|---|---|
| | | C-Veh | Hx-Veh | Hx-MCC | C-Veh | Hx-Veh | Hx-MCC | C-Veh | Hx-Veh | Hx-MCC |
| **WEIGHT GAIN** | 0-9% | 6 | 3 | 2 | 0 | 0 | 0 | 0 | 0 | 0 |
| | 10-14% | 16 | 18 | 20 | 2 | 1 | 2 | 0 | 0 | 0 |
| | 15-19% | 8 | 7 | 10 | 7 | 6 | 6 | 1 | 1 | 3 |
| | 20%+ | 3 | 2 | 1 | 19 | 18 | 20 | 27 | 24 | 25 |
| **DRINKING/ EATING** | Empty stomach | 4 | 5 | 3 | 5 | 0 | 2 | 11 | 10 | 9 |
| | Full Stomach | 29 | 25 | 30 | 23 | 25 | 26 | 17 | 15 | 19 |
| **BREATHING** | Difficulty | 0 | 0 | 0 | 0 | 0 | 0 | 0 | 0 | 0 |
| | Fast | 0 | 0 | 0 | 0 | 0 | 0 | 0 | 0 | 0 |
| | Slow/calm | 33 | 30 | 33 | 28 | 25 | 28 | 28 | 25 | 28 |
| **GAIT/ POSTURE** | Markedly Abnormal | 0 | 0 | 0 | 0 | 0 | 0 | 0 | 0 | 0 |
| | Slightly Abnormal | 3 | 27 | 27 | 0 | 20 | 22 | 0 | 16 | 11 |
| | Normal | 30 | 3 | 6 | 28 | 5 | 6 | 28 | 9 | 17 |
| **NESTING/ MATERNAL CARE** | Nestlet 90% intact | 0 | 0 | 0 | 0 | 0 | 0 | 0 | 0 | 0 |
| | Partially torn mostly intact | 1 | 2 | 2 | 0 | 0 | 0 | 0 | 0 | 0 |
| | 50% torn but not nest | 13 | 11 | 15 | 11 | 9 | 13 | 9 | 8 | 12 |
| | Greater than body height | 19 | 17 | 16 | 17 | 16 | 15 | 19 | 17 | 16 |
| **TOTAL NO. MICE** | | 33 | 30 | 33 | 28 | 25 | 28 | 28 | 25 | 28 |

***Table 4.2. Breakdown of pups in each treatment group of the Chapter 2 cohort to receive each score in their wellbeing sheets at PND8, PND9 and PND10.***

## 4.3. Results

### 4.3.1. MCC950 Partially Attenuates Neonatal Reflex Deficits Caused by Hypoxia.

To evaluate the effects of MCC950 injection just after hypoxia, pups were randomly allocated to one of three groups: C-Veh (normoxia + vehicle), Hx-Veh (hypoxia + vehicle) and Hx-MCC (hypoxia + 10mg/kg MCC950). A battery of neonatal reflex tests was conducted to identify how MCC950 treatment affected the acute neurological deficits described in Chapter 1.

#### 4.3.1.1. Surface Righting Shows No Differences Between Groups.

Surface Righting measures core strength and coordination required to right a mouse to standing (Heyser et. al., 2003). There were no differences between control and hypoxia mice at any timepoint, nor was there a difference between Hx-Veh and Hx-MCC mice (Figure 4.2).

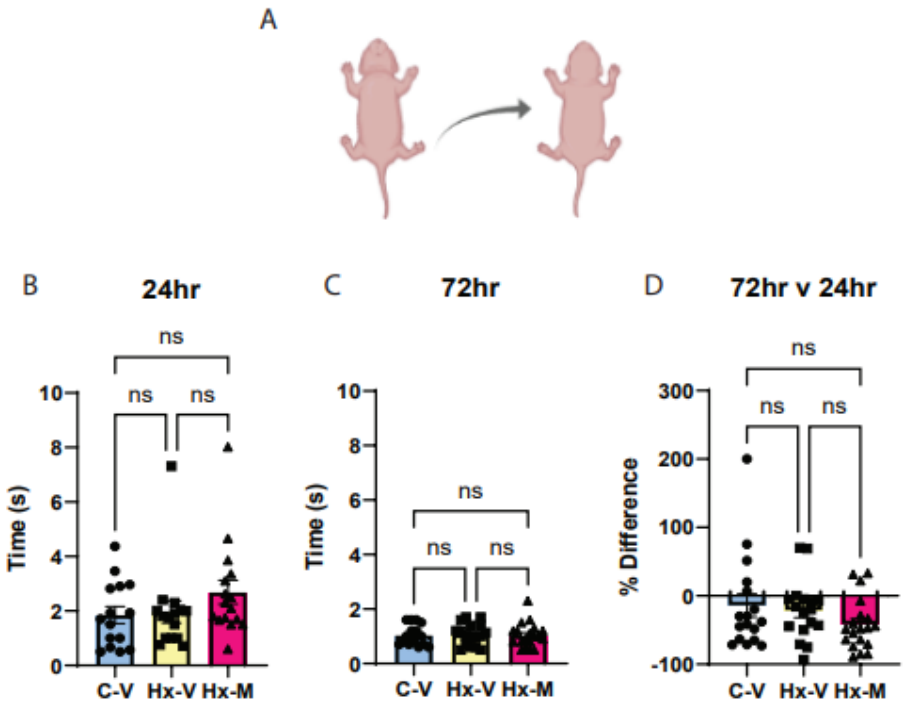


***Figure 4.2. No Differences in the Surface Righting Reflex Post-Hypoxia or Post-MCC950 treatment.*** ***(A)*** *Surface Righting Test Illustration.* ***(B)*** *Time taken to complete the test 24hrs post-hx, with no trends between groups. C-V n=15, Hx-V n=15, Hx-M n=16, 24hr C-V v Hx-V p=0.978, Hx-V v Hx-M p=0.3967, C-V v Hx-M p=0.2937.* ***(C)*** *At 72hrs post-hx there are no differences between groups. C-V n=17, Hx-V n=17, Hx-M n=19, 72hr C-V v Hx-V p=0.9662, Hx-V v Hx-M p=0.9674, C-V v Hx-M p<0.9999.* ***(D)*** *No trends between groups when the difference over time is compared. C-V n=17, Hx-V n=17, Hx-M n=19, 72hr vs*

*24hr C-V v Hx-V p=0.9175, Hx-V v Hx-M p=0.4681, C-V v Hx-M p=0.2591. All tests are one-way ANOVA with Tukey's post-hoc, P < 0.05.*

4.3.1.2. MCC950 Slightly Improves the Negative Geotaxis Response 24 hours post-hypoxia.

The negative geotaxis test assesses a pup's response to gravity when placed on a surface facing downwards (Xu et. al., 2016). To account for inter-litter variability, the time taken for each pup to complete the test was normalised by litter with respect to the average of their control littermates. At 24 hours post-hypoxia, Hx-Veh mice take twice as long as controls to complete the test (Figure 4.3.B). When the difference between 24- and 72-hour relative times are compared, no differences are seen (Figure 4.3.C).

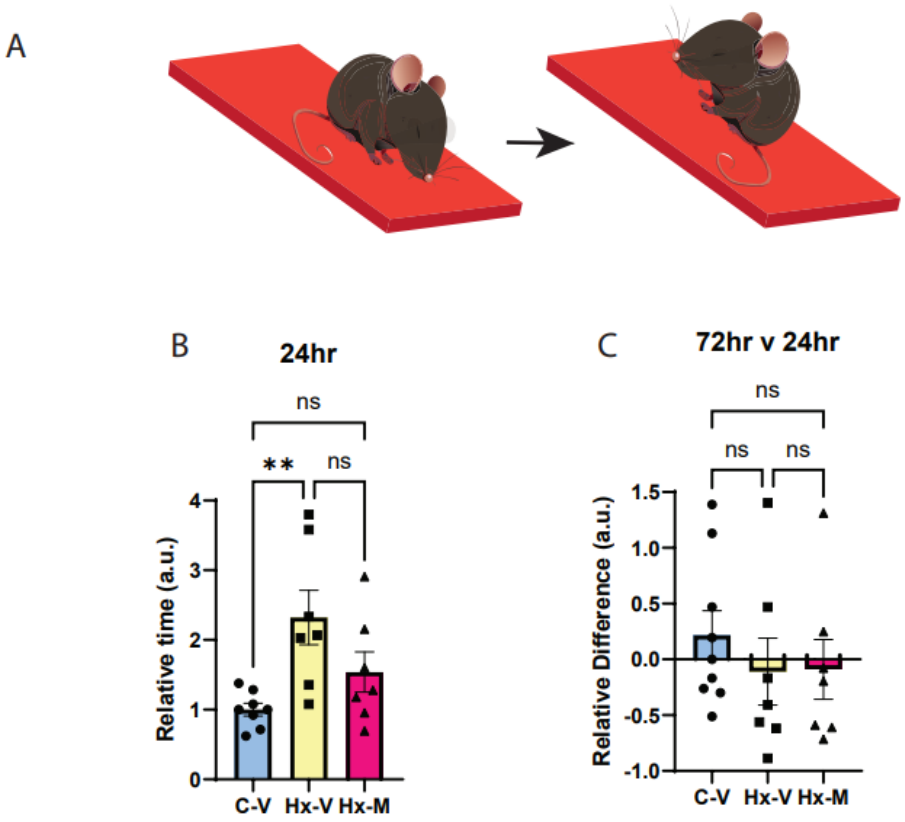


***Figure 4.3. Negative Geotaxis is slightly improved by MCC950 24 hours post-hypoxia. (A)*** *Illustration of negative geotaxis test.* ***(B)*** *Time taken to complete the test at 24hrs post-hx was normalised by litter. Hx-V take relatively longer than controls to complete the test, with no differences between Hx-V and Hx-M groups. C-V n=8, Hx-V n=7, Hx-M n=7, 24hr C-V v Hx-V p=0.0071, Hx-V v Hx-M p=0.1448, C-V v Hx-M p=0.3552.* ***(C)*** *No trends in the relative difference over time between any groups. C-V n=8, Hx-V*

*n=7, Hx-M n=7, 72hr v 24hr C-V v Hx-V p=0.5616, Hx-V v Hx-M p=0.9985, C-V v Hx-M p=0.5939. One-way ANOVA with Tukey's post-hoc, p < 0.05.*

#### 4.3.1.3. MCC950 Rescues Front Limb Grip Strength at 24 hours post-hypoxia.

Front-limb grip strength was designed to measure grip force and strength in the forelimbs (Sun et. al., 2015; Xu et. al., 2016). As in Chapter 1, the time taken for each mouse to complete the test was normalised by litter. At 24 hours post-hypoxia, the Hx-Veh cohort performed significantly worse relative to their C-Veh and Hx-MCC littermates (Figure 4.4.B). These differences are no longer found at 72 hours post-hypoxia (Figure 4.4.C). This is reflected in the difference over time, where the Hx-Veh mice have a significantly higher relative difference over time compared to C-Veh and Hx-MCC mice (Figure 4.4.D).

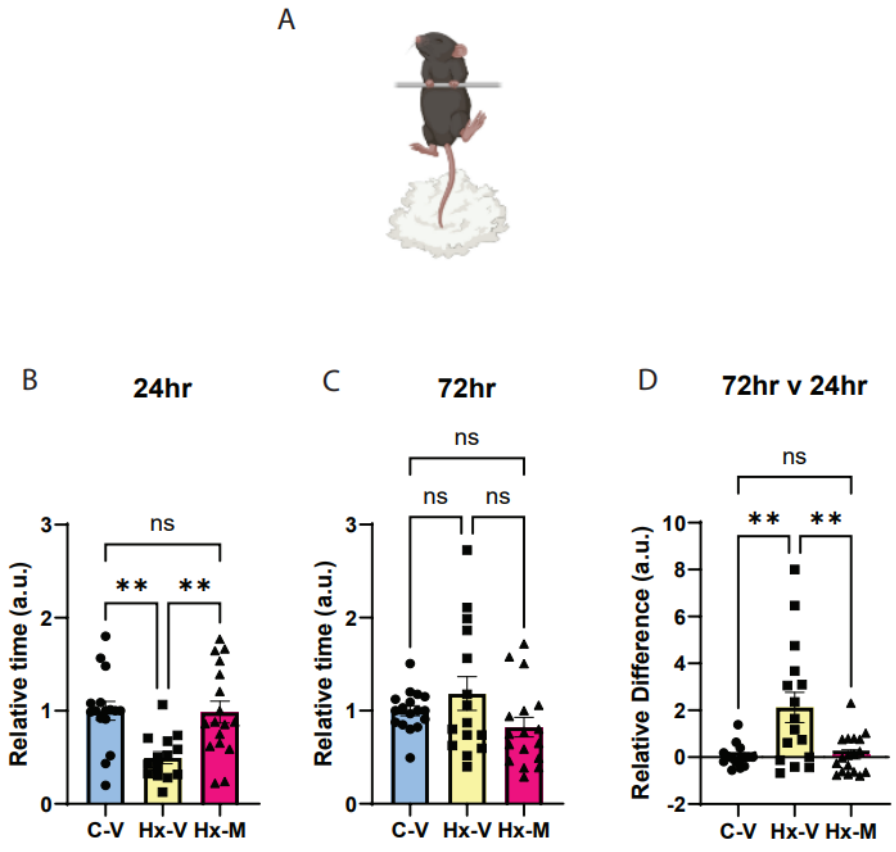


***Figure 4.4. HX-Veh mice have poorer front limb grip strength than C-Veh and Hx-MCC mice at 24 hours post-hypoxia. (A)*** *Forelimb Grip Strength Illustration.* ***(B)*** *Hx-V mice had significantly worse times than C-V and Hx-M pups 24hrs post-hx. C-V n=16, Hx-V n=14, Hx-M n=17. 24hr C-V v Hx-V p=0.0032, Hx-V v Hx-M p=0.0037, C-V v Hx-M p=0.9946.* ***(C)*** *There are no differences 72hrs post-hx. C-V n=17, Hx-*

*V n=15, Hx-M n=17. 72hr C-V v Hx-V p=0.5267, Hx-V v Hx-M p=0.0957, C-V v Hx-M p=0.5358.* ***(D)*** *Hx-V mice improved significantly better over time than C-V and Hx-M groups. C-V n=15, Hx-V n=16, Hx-M n=18. 72hr vs 24hr C-V v Hx-V p=0.0019, Hx-V v Hx-M p=0.0017, C-V v Hx-M p=0.991. One-way ANOVA with Tukey's post-hoc, p < 0.05.*

#### 4.3.1.4. MCC950 Rescues the Poorer Cliff Aversion Response 24 hours post-hypoxia.

The cliff aversion test challenges a pup's vestibular cues to recognise that their head and front paws are over a cliff, as well as proprioception, strength and coordination to manoeuvre themselves away from this danger. As before, there was a high refusal rate, particularly at 24 hours post-hypoxia. To account for inter-litter variability, each pup score was normalised by litter. While Hx-Veh pups took twice as long to turn from the cliff than C-Veh and Hx-MCC pups at 24 hours, this difference was no longer detected 72 hours post-hypoxia (Figure 4.5).

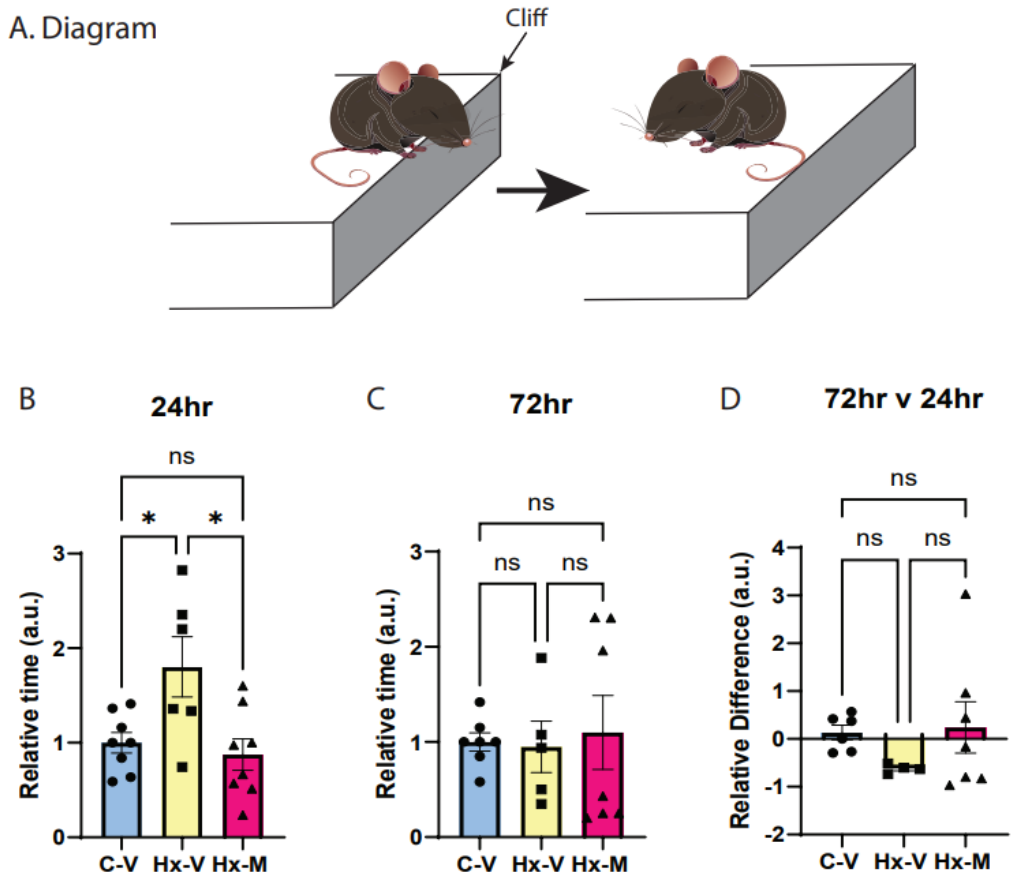


***Figure 4.5. The Cliff Aversion Reflex develops more slowly in Hx-Veh pups versus C-Veh and Hx-MCC mice. (A)*** *Cliff Aversion Test Illustration.* ***(B)*** *Time to complete the test at 24hrs was normalised by litter. Hx-V mice take significantly longer to perform this test than C-V and Hx-M littermates. C-V n=8, Hx-V*

*n=6, Hx-M n=8. 24hr C-V v Hx-V p=0.0276, Hx-V v Hx-M p=0.0108, C-V v Hx-M p=0.8842.* ***(C)*** *There are no differences in relative times 72hrs post-hx. C-V n=7, Hx-V n=5, Hx-M n=7. 72hr C-V v Hx-V p=0.9921, Hx-V v Hx-M p=0.9314, C-V v Hx-M p=0.9628.* ***(D)*** *Relative Difference between normalised times at 72- and 24-hrs post-hx. No differences are seen between any groups. C-V n=6, Hx-V n=4, Hx-M n=7. 72hr vs 24hr C-V v Hx-V p=0.2206, Hx-V v Hx-M p=0.8064, C-V v Hx-M p>0.9999. One-way ANOVA with Tukey's post-hoc, p < 0.05.*

#### 4.3.1.5. MCC950 Does Not Improve Overall Ambulation but provides some postural improvements.

The Ambulation test was conducted as previously described (Feather-Schussler & Ferguson., 2016), assessing locomotion using the modified 6-point ambulation scores (Methods Chapter Table 2.6). At 24 hours post-hypoxia, no trends emerge between groups in their ambulation scores; most animals, and all the Hx-Veh mice, have yet to develop symmetric limb movement (Figure 4.6.B). At 72 hours post-hypoxia, a trend emerges whereby control-vehicle mice have higher ambulation scores compared to both Hx-Veh and Hx-MCC mice (Figure 4.6.C). There are no significant differences between groups in their difference over time (Figure 4.6.D).

The hindlimb angles provided a complementary assessment of limb symmetry and posture during straight line movement, which was normalised by litter for analysis. At both 24 hours and 72 hours post-hypoxia, Hx-Veh mice have wider relative angles than Hx-MCC mice, although this is only significant 72 hours post-hypoxia (Figure 4.6.E-G).

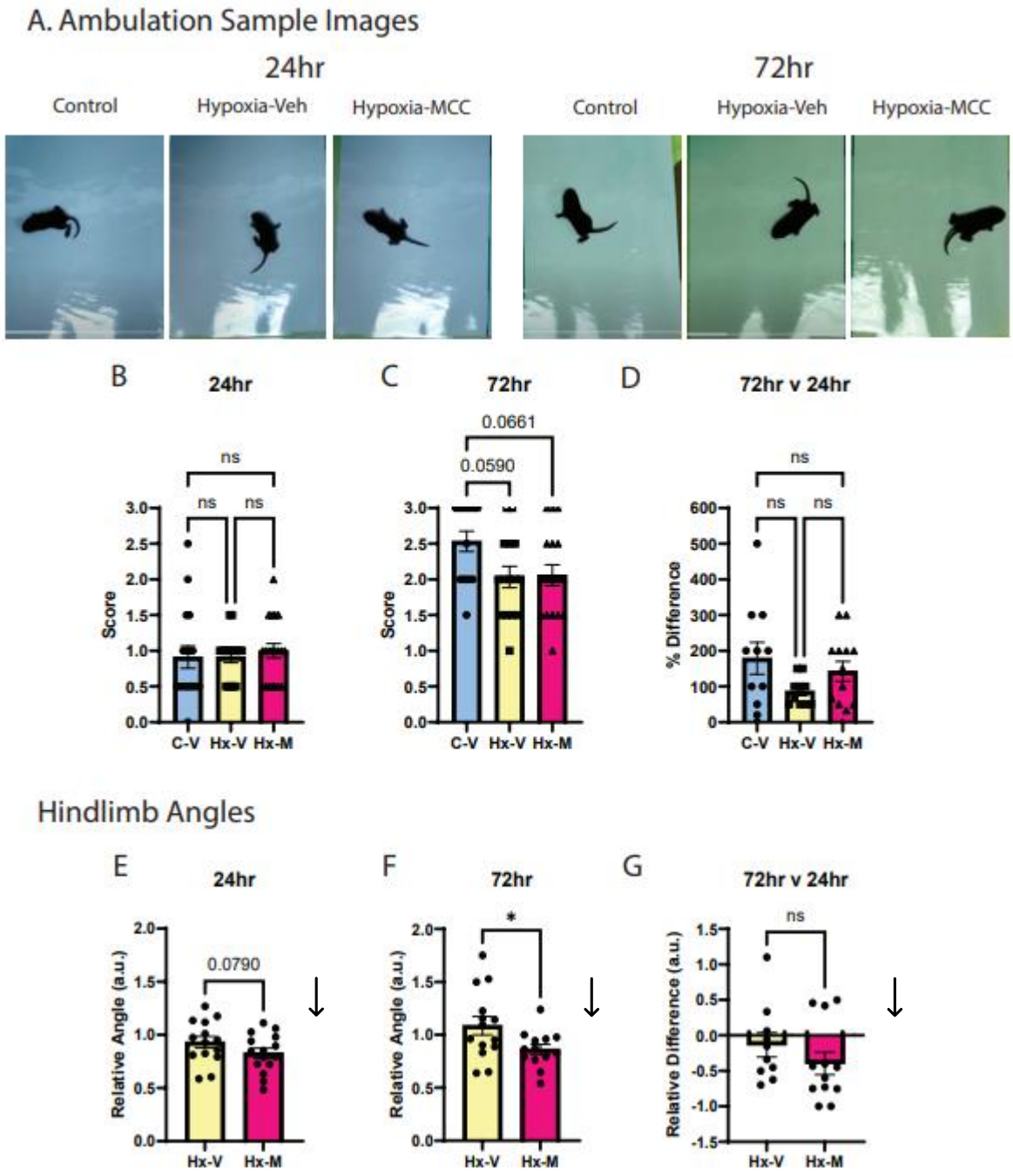


***Figure 4.6. Ambulation Scores and Hindlimb Angles at 24- and 72-hours post-hypoxia. (A)*** *Sample Images of Ambulation. Ambulation Scores: 0- no movement; 0.5- very little movement, only turning, needs encouragement; 1- slow crawling in straight lines, asymmetrical limb movement; 1.5– crawling in straight lines, mixture of asymmetric and symmetric limb movement; 2- slow crawling in straight lines with symmetric limb movement; 2.5- fast crawling with symmetric limb movement; 3- walking.* ***(B)*** *Ambulation Scores 24hrs post-hx, which show no significant differences between groups. C-V n=17, Hx-V n=17, Hx-M n=19. 24hr C-V v Hx-V p>0.9999, Hx-V v Hx-M p=0.8452, C-V v Hx-M p=0.8452.* ***(C)*** *At 72hrs post-hx, control pups trend towards higher ambulation scores than both Hx-V and Hx-M littermates. C-V n=15, Hx-V n=15, Hx-M n=17. 72hr C-V v Hx-V p=0.059, Hx-V v Hx-M p=0.9916, C-V v*

*Hx-M p=0.0661.* ***(D)*** *No trends in the difference in scores over time. C-V n=11, Hx-V n=10, Hx-M n=13. 72hr vs 24hr C-V v Hx-V p=0.1343, Hx-V v Hx-M p=0.4406, C-V v Hx-M p=0.6814. B-D One-way ANOVA with Tukey's post-hoc, p < 0.05.* ***(E)*** *Hindlimb Angles were recorded from ambulation videos and normalised by litter. At 24hrs post-hx, Hx-V mice trend towards wider hindlimb angles than Hx-M mice. Hx-V n=14, Hx-M n=15. 24hr Hx-V v Hx-M p=0.079.* ***(F)*** *Hx-M mice have significantly narrower hindlimb angles compared to Hx-V mice 72hrs post-hx. Hx-V n=14, Hx-M m=13, 72hr Hx-V v Hx-M p=0.0345.* ***(G)*** *No differences are seen in the relative difference over time between Hx-Veh and Hx-MCC mice. Hx-V n=10, Hx-M n=12, 72hr v 24hr p=0.9724. E-G unpaired, one-tailed t-tests with arrow indicating a-priori hypothesis, p < 0.05.*

### 4.3.2. MCC950 Rescues Behavioural Deficits in Anxiety and Spatial Memory.

Following the attenuations recorded in the neonatal reflex assessments after MCC950 treatment, mice underwent a battery of adult behaviour tests to assess the long-term neurological attenuations, if any, of acute MCC950 treatment immediately post-hypoxia.

The OF Test, as in Chapter 1, was used to assess motor function to make sure differences in other behaviour tests were not resulting from mobility deficits, comparing average speed and the number of line crossings between groups. In both parameters, no differences or trends emerged, consistent with our Chapter 1 findings (Figure 4.7.B).

The LDB Test is used to assess anxiety behaviours in mice (Li et. al., 2024). Previous work in this model has observed LDB behaviour consistent with increased anxiety (Rodriguez-Alvarez et. al., 2015; Quinlan et. al., 2018; 2019). Consistent with Chapter 1 findings and previous literature, Hx-Veh mice take significantly longer to enter the dark box compared to C-Veh and Hx-MCC mice (Figure 4.7.D), therefore MCC950 post-hypoxia attenuates the LDB response.

The NOL test assesses spatial memory, which is governed primarily by the dorsal Ca1 of the hippocampus (Bannerman et. al., 2014; Geiller et. al., 2023). The time spent with the novel object location during the test period was standardised for each animal using familiarisation

sessions to account for object preferences. Hx-Veh mice performed poorer in this test than Hx-MCC mice (Figure 4.7.F).

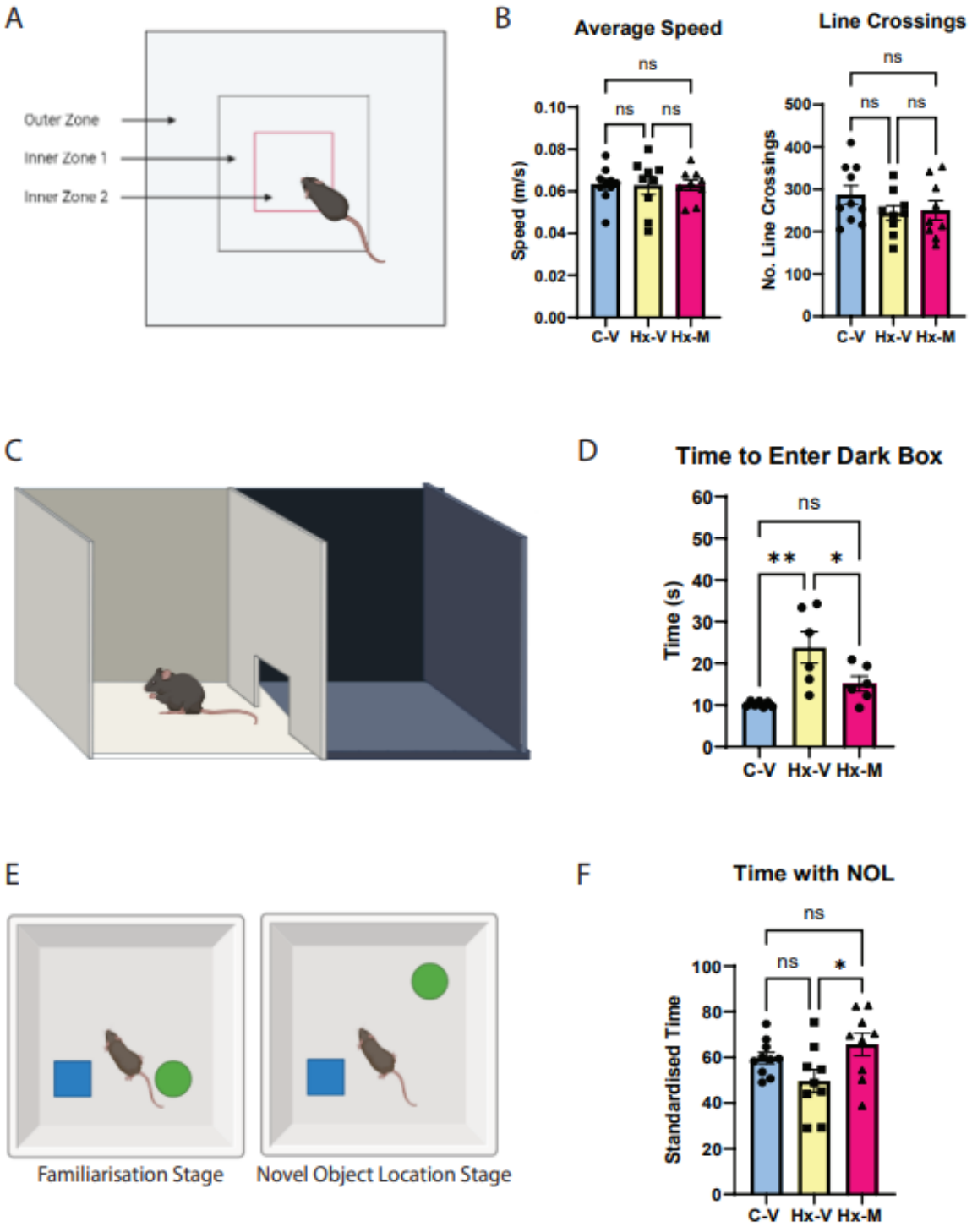


***Figure 4.7. MCC950 Treatment post-hypoxia causes some attenuations in adult behaviour compared to vehicle-treated hypoxia littermates. (A)*** *Illustration of the OF test apparatus.* ***(B)*** *No differences were found in the average speed (L) or the number of line crossings (R) between groups. N=12 per*

*group. Average Speed C-V v Hx-V p=0.9936, Hx-V v Hx-M p=0.8186, C-V v Hx-M p=0.8734. Line Crossings C-V v Hx-V p=0.2614, Hx-V v Hx-M p=0.905, C-V v Hx-M p=0.4789.* ***(C)*** *Illustration of the LDB apparatus.* ***(D)*** *Time taken for each animal to enter the dark box after being placed in the light box. Hx-V mice take significantly longer to enter the dark box versus C-V and Hx-M mice. C-V n=7, Hx-V n=6, Hx-M n=6. Time to Enter Dark Box C-V v Hx-V p=0.0016, Hx-V v Hx-M p=0.0464, C-V v Hx-M p=0.2962.* ***(E)*** *Illustration of the NOL apparatus. For the familiarisation stage (L), objects are in set positions, and for the NOL stage (R), one object is moved.* ***(F)*** *When the time spent with the moved object during the NOL stage is standardised, Hx-V mice spent less time with the moved object than the Hx-M group, indicating poorer memory in Hx-V mice. NOL C-V n=10, Hx-V n=9, Hx-M n=9. NOL C-V v Hx-V p=0.2259, Hx-V v Hx-M p=0.0373, C-V v Hx-M p=0.5855. One-way ANOVA with Tukey's post-hoc, $p < 0.05$.*

### 4.3.3. Double Staining for CD68/Iba1 show that MCC950 alters microglia at 72 hours post-hypoxia but has no effect at 5 weeks post-hypoxia.

CD68, the marker for phagocytic lysosomes, was used with Iba1 to identify, quantify and morphologically assess phagocytic or pro-inflammatory microglia in the hippocampus (Diz-Chaves et. al., 2012; Waller et. al., 2019). $CD68^{+}Iba1^{+}$ cells are expressed as a percentage of total $Iba1^{+}$ cells.

Quantification of $CD68^{+}Iba1^{+}$ cells was conducted as previously described. At 72 hours post-hypoxia, MCC950 treatment did not reduces the percentage of double positive cells in the hippocampus (Figure 4.8.B). At 5 weeks post-hypoxia, there is no difference between Hx-Veh and Hx-MCC mice, and both groups have significantly higher percentages than controls (Figure 4.8.D).

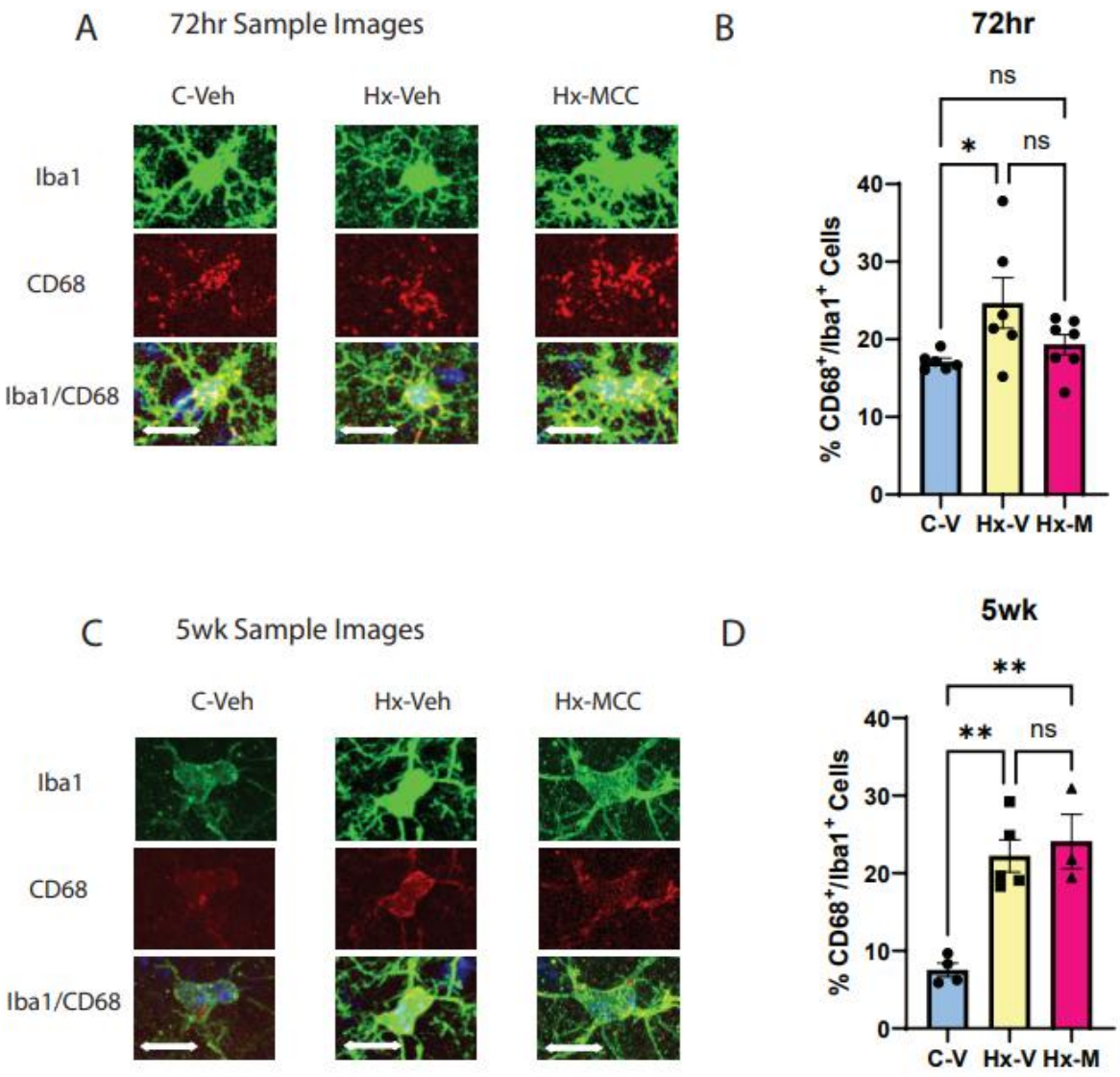


***Figure 4.8. MCC950 treatment does not attenuate CD68⁺Iba1⁺ cell prevalence at 72 hours or 5 weeks post-hypoxia. (A)*** *Sample Images of CD68/Iba1 double-labelled cells in C-V, Hx-V and Hx-M 72hrs post-hx. Scale bar 10µm.* ***(B)*** *Hx-V mice have significantly higher percentages of CD68⁺Iba1⁺ cells versus C-V, although no significance is found between Hx-V and Hx-M. C-V n=5, Hx-V n=4, Hx-M n=6. 72hr C-V v Hx-V p=0.025, Hx-V v Hx-M p=0.5223, C-V v Hx-M p=0.1123.* ***(C)*** *Sample Images of CD68/Iba1 double labelled cells in C-V, Hx-V and Hx-M 5wks post-hx. Scale bar 10µm.* ***(D)*** *Hx-V and Hx-M mice have significantly higher percentages of CD68⁺Iba1⁺ cells than C-V. C-V n=4, Hx-V n=5, Hx-M n=3. 5wks C-V v Hx-V p=0.0018, Hx-V v Hx-M p=0.835, C-V v Hx-M p=0.002. One-way ANOVA with Tukey's post-hoc, $p < 0.05$.*

#### 4.3.3.1. $CD68^+Iba1^+$ cells have pro-inflammatory phenotypes in all groups at both timepoints post-hypoxia.

$CD68^+Iba1^+$ cells were analysed for morphology as described previously (Diz-Chaves et. al., 2012). As observed in Chapter 1, no cells were found which were morphologically consistent with Type I, II or III cells at either time point, therefore only Types IV and V are analysed. As in Results Chapter 1, there were more $CD68^+Iba1^+$ cells in hypoxia versus controls, particularly in the Type V morphology groups. Hx-MCC mice had significantly more Type IV microglia and significantly less Type V microglia than both C-Veh and Hx-Veh mice at 72 hours post-hypoxia (Figure 4.9.B), but express Type IV and Type V $CD68^+Iba1^+$ microglia in virtually identical proportions as the Hx-Veh group at 5 weeks-post-hypoxia (Figure 4.10.B). These differences infer that acute MCC950 treatment alters pro-inflammatory microglial properties at 72 hours post-hypoxia, but this difference is no longer detected chronically.

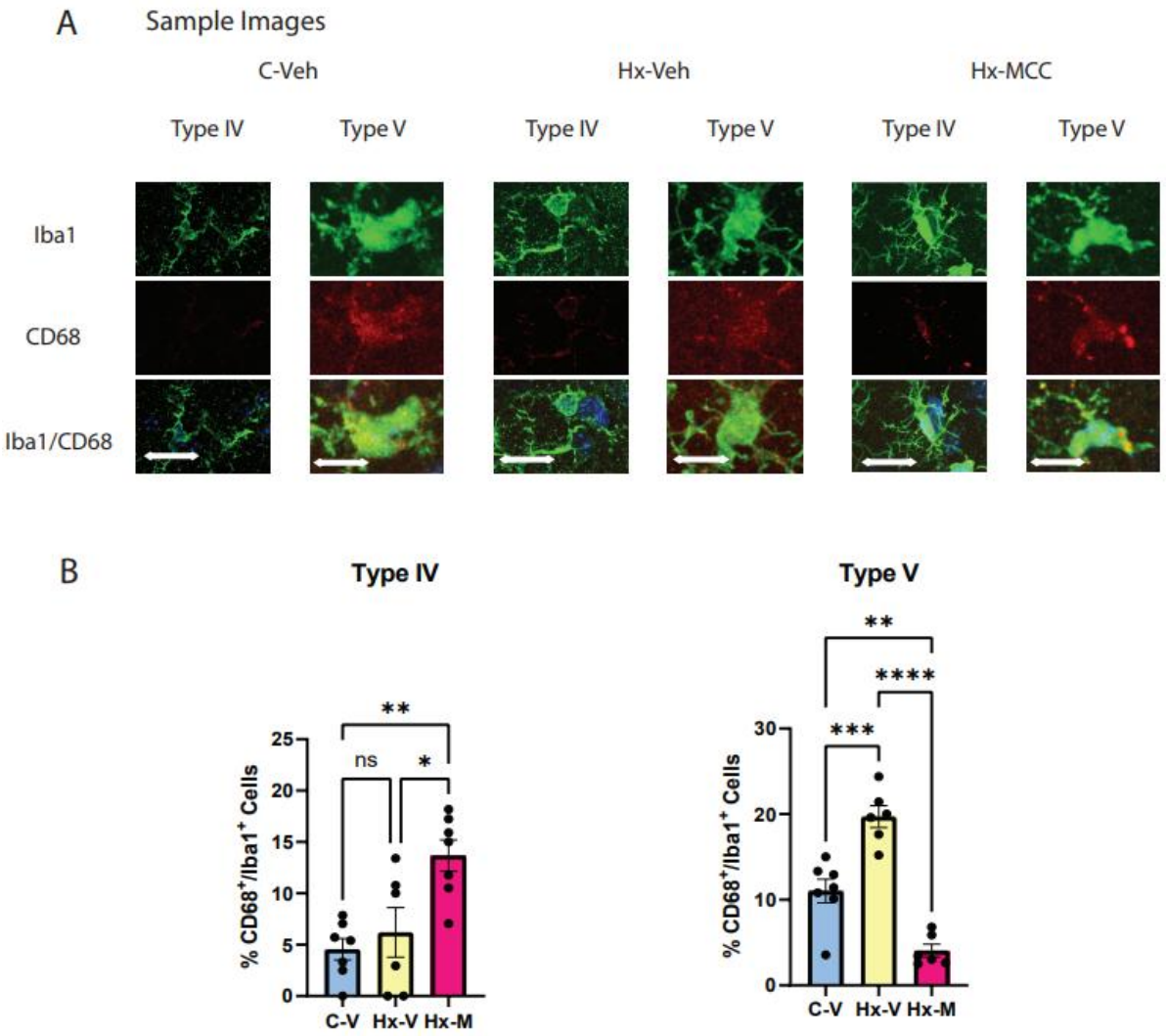


***Figure 4.9. MCC950 post-hypoxia gives a different profile of morphology types to both C-Veh and Hx-Veh Mice 72 hours post-hypoxia. (A)*** *Representative images of Type IV and Type V cells found in C-V, Hx-V and Hx-M. Scale bar 10µm.* ***(B)*** *Hx-M have significantly higher Type IV and significantly lower Type V cells than both C-V and Hx-V. C-V n=5, Hx-V n=4, Hx-M n=6. Type IV C-V v Hx-V p=0.9974, Hx-V v Hx-M p=0.0005, C-V v Hx-M p=0.0003. Type V C-V v Hx-V p=0.0077, Hx-V v Hx-M p<0.0001, C-V v Hx-M p=0.0094. One-way ANOVA with Tukey's post-hoc, p < 0.05.*

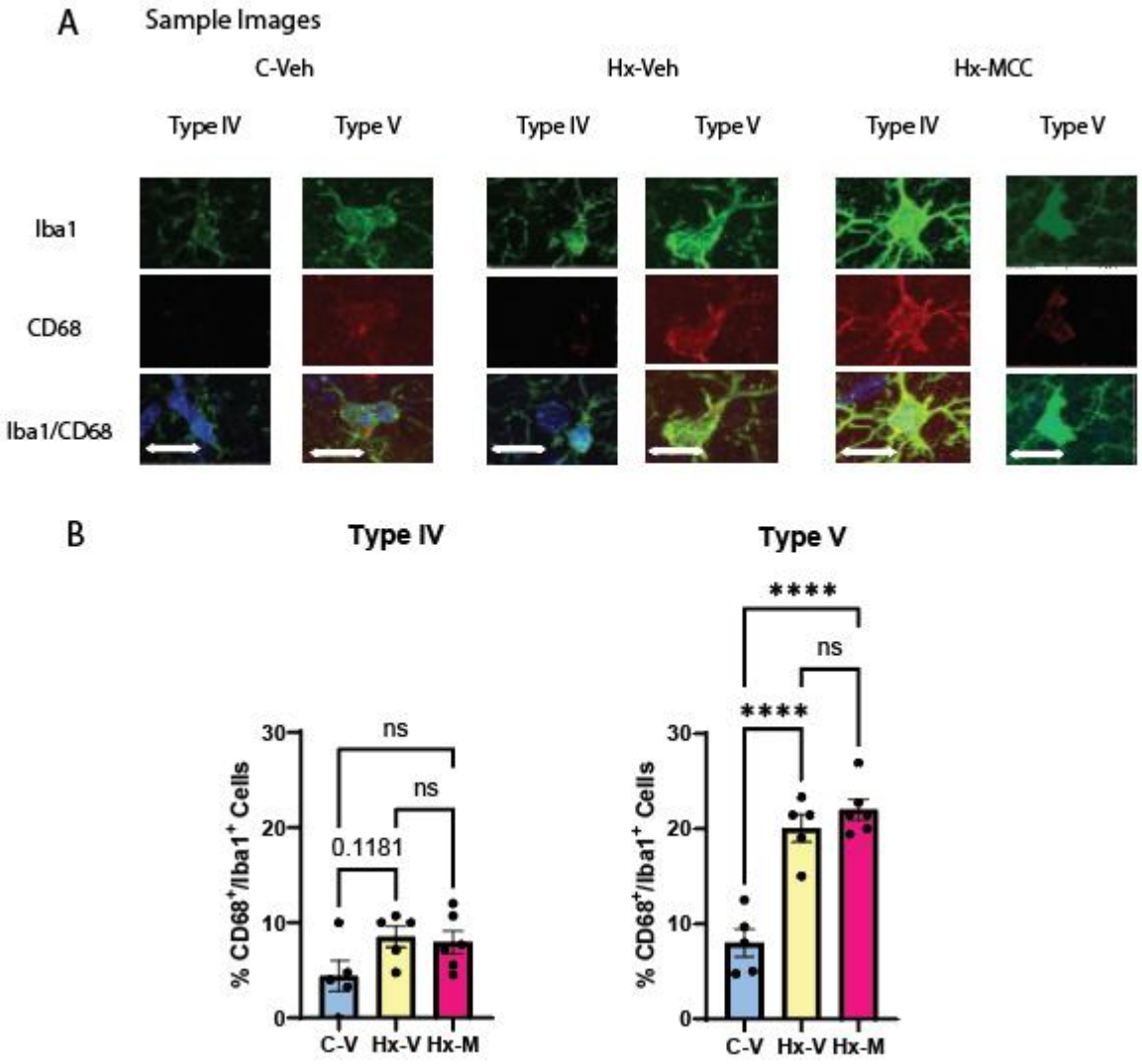


***Figure 4.10. MCC950 has no effect on morphology compared to Hx-Veh mice 5 weeks post-hypoxia.*** ***(A)*** *Representative images of Type IV and Type V cells found in C-V, Hx-V and Hx-M Images.* ***(B)*** *There is a trend towards higher Type IV cells in Hx-V mice vs C-V mice, and no significant differences between Hx-M and C-V or Hx-M. Hx-V and Hx-M mice have significantly more Type V cells than C-V mice. C-V n=4, Hx-V n=5, Hx-M n=3. Type IV C-V v Hx-V p=0.1181, Hx-V v Hx-M p=0.9464, C-V v Hx-M p=0.1699. Type V C-V v Hx-V p<0.0001, Hx-V v Hx-M p=0.5549, C-V v Hx-M p<0.0001. One-way ANOVA with Tukey's post-hoc, p < 0.05.*

### 4.3.4. MCC950 has no effect on the proportions of $P2RY12^{+}Iba1^{+}$ cells present in the hippocampus both acutely and chronically post-hypoxia

P2RY12 was used in this study as a marker for homeostatic microglia in the hippocampus for quantification (Rodríguez et. al., 2020; Gómes-Morrillas et. al., 2021). This is a purinergic receptor expressed on the cell surface of microglia which is activated by ATP to inhibit glutamatergic neurotransmission, and its expression is diminished on pro-inflammatory microglia (Koizumi et. al., 2013). Double staining with P2RY12 and Iba1 allowed for microglia to be identified and counted. $P2RY12^{+}Iba1^{+}$ cells were expressed as a percentage of total $Iba1^{+}$ cells present. $P2RY12^{+}Iba1^{+}$ cell quantification was conducted as previously described in Results Chapter 1 Section 3.4. At both 72 hours and 5 weeks post-hypoxia, there was a lower percentage of $P2RY12^{+}$ cells in the hippocampus post-hypoxia versus controls, with no differences seen between Hx-Veh and Hx-MCC mice (Figure 4.11).

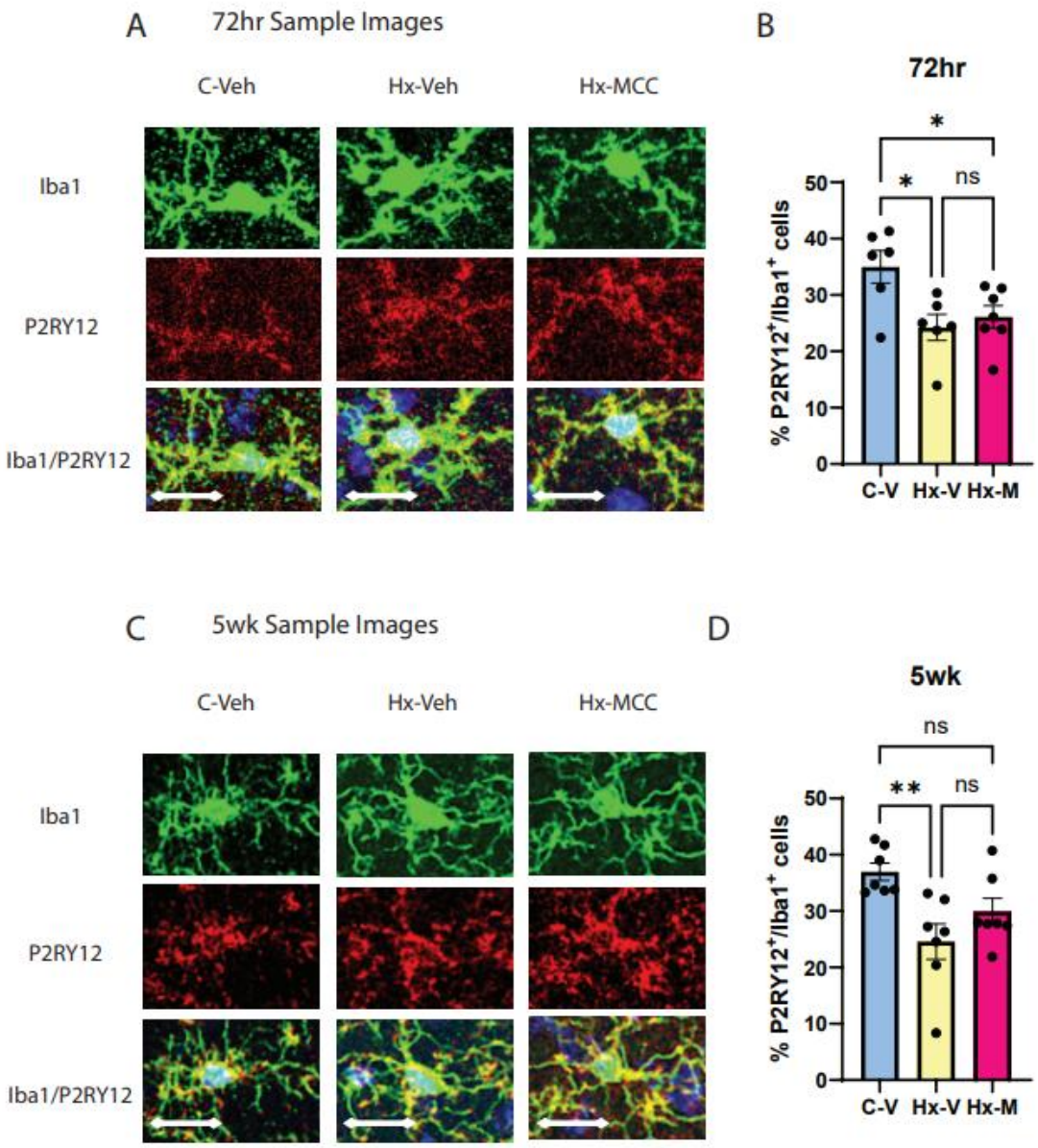


***Figure 4.11. P2RY12$^{+}$Iba1$^{+}$ cells are less abundant post-hypoxia relative to controls, with no differences found between Hx-Veh and Hx-MCC mice at either timepoint.*** *(A) Representative images of P2RY12$^{+}$Iba1$^{+}$ cells 72hrs post-hx. (B) C-V mice have a higher percentage of P2RY12$^{+}$Iba1$^{+}$ cells in the hippocampus than Hx-V and Hx-M mice 72hrs post-hx. C-V n=6, Hx-V n=7, Hx-M n=7. 72hr C-V vs Hx-V p=0.0175, Hx-V v Hx-M p=0.8409, C-V v Hx-M p=0.0425. (C) Representative images of P2RY12$^{+}$Iba1$^{+}$ cells 5wks post-hx. (D) Hx-V and Hx-M have lower percentages of P2RY12$^{+}$Iba1$^{+}$ cells than C-V mice 5wks post-hx. N=7 per group. 5wks C-V v Hx-V p=0.0057, Hx-V v Hx-M p=0.2989, C-V v Hx-M p=0.1294. One-way ANOVA with Tukey's post-hoc, $p < 0.05$.*

### 4.3.5. MCC950 Induces Changes in the Expression of Genes and Proteins Related to Neuroinflammation and Microglia.

To better understand the molecular mechanisms underlying the results in this Chapter so far, gene transcription and protein levels were analysed for a range of inflammatory markers.

#### 4.3.5.1. MCC950 treatment causes some differences in Gene and Protein Expression Related to the NLRP3 Inflammasome

The first set of markers tested were those associated with NLRP3 inflammasome expression and function in microglia, at 3 hours (Figure 4.12), 72 hours (Figure 4.13) and 5 weeks post-hypoxia (Figure 4.14). The time course was undertaken to gain a clearer picture of how these markers are expressed over time, and whether these are affected by MCC950 treatment immediately post-hypoxia. At 3 hours post-hypoxia, Hx-Veh mice display significantly higher IL-1β protein expression (Figure 4.12.B) than C-Veh and Hx-MCC mice. No differences are seen between groups in IL-6 mRNA or protein expression (Figure 4.12.C-D). TNF-α expression is lowest in C-Veh and highest in Hx-MCC mice (Figure 4.12.E). Hx-Veh mice trend towards higher IL-18 protein expression than C-Veh and Hx-MCC mice (Figure 4.12.F). At 72 hours post-hypoxia, no differences in expression are seen in IL-1β protein (Figure 4.13.A), IL-6 protein (Figure 4.13.B), and IL-18 protein (Figure 4.13.C) between any groups. At 5 weeks post-hypoxia, no differences are seen in IL-1β mRNA (Figure 4.14.A), IL-1β protein (Figure 4.14.B), IL-6 mRNA (Figure 4.14.C) and IL-6 protein expression (Figure 4.14.D). TNF-α mRNA expression is significantly higher than controls in both Hx-Veh and Hx-MCC, indicating some inflammatory response (Figure 4.14.E). No significant differences emerge when IL-18 protein expression is quantified (Figure 4.14.F)

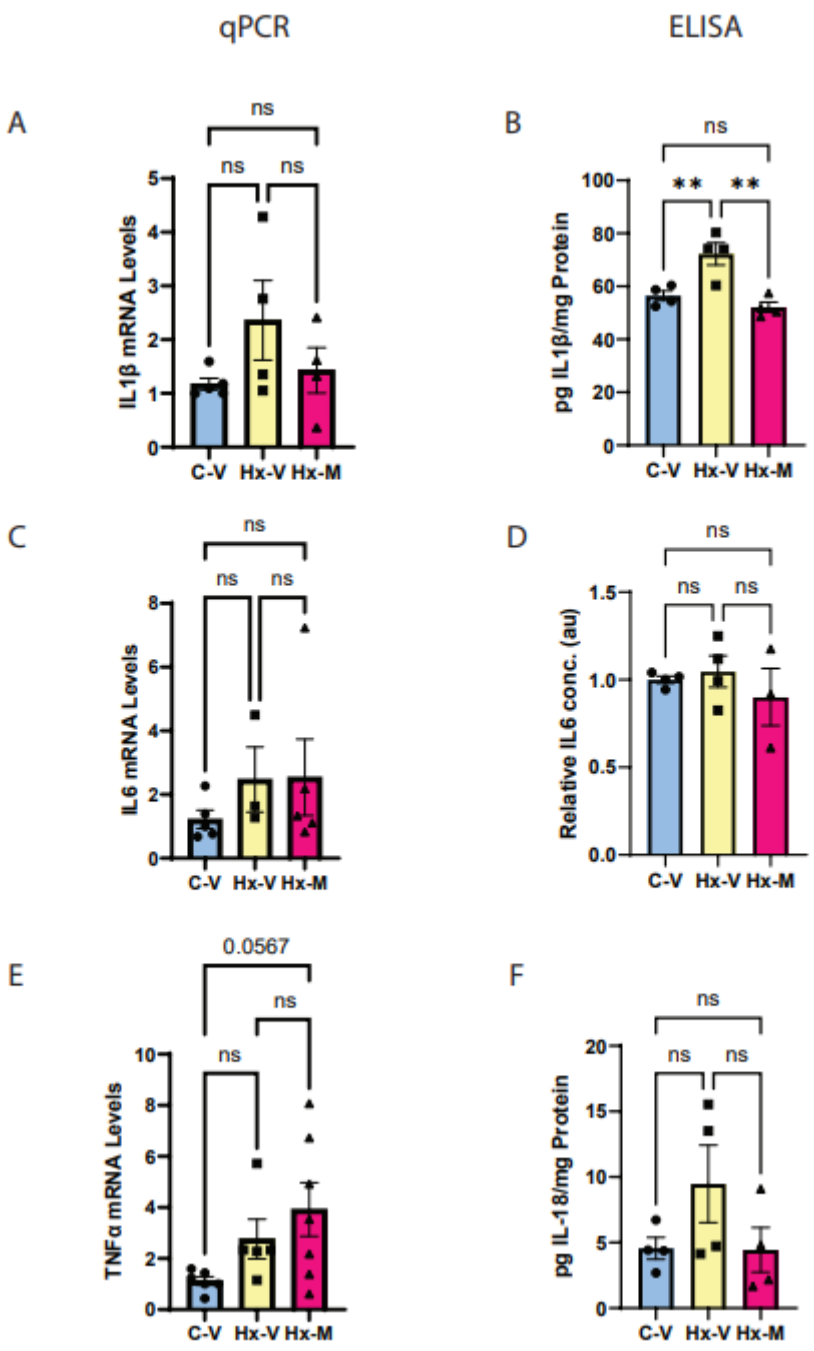


***Figure 4.12. Expression of NLRP3 inflammasome-related genes and proteins 3 hours post-hypoxia, identified by qPCR and ELISA respectively. (A)*** *Gene expression of IL-1β, expressed as mRNA fold change. No significant differences are found between groups. C-V n=5, Hx-V n=4, Hx-M n=4. IL-1β mRNA C-V vs Hx-V p=0.1981; Hx-V vs Hx-M p=0.383; C-V vs Hx-M p=0.9144.* ***(B)*** *Protein expression of IL-1β, expressed as pg IL-1β per mg protein. Hx-V has significantly higher IL-1β protein than C-V and Hx-M groups. N=4 per group. IL-1β protein C-V vs Hx-V p=0.0095; Hx-V vs Hx-M p=0.002; C-V vs Hx-M p=0.5521.* ***(C)*** *Gene expression of IL-6, expressed as mRNA fold change. No significant differences found. C-V n=5, Hx-V n=3, Hx-M n=5. IL-6 mRNA C-V vs Hx-V p=0.6557; Hx-V vs Hx-M p=0.9986; C-V vs Hx-M p=0.5404.* ***(D)*** *Protein expression of IL-6 normalised by litter and expressed as relative IL-6*

*concentration. No significant differences found. C-V n=4, Hx-V n=4, Hx-M n=3. IL-6 protein C-V vs Hx-V p=0.9302; Hx-V vs Hx-M p=0.567; C-V vs Hx-M p=0.7614.* ***(E)*** *Gene expression of TNF-α, expressed as mRNA fold change. Hx-M is trending towards significantly higher concentration than C-V. C-V n=6, Hx-V n=5, Hx-M n=7. TNF-α mRNA C-V vs Hx-V p=0.384; Hx-V vs Hx-M p=0.5913; C-V vs Hx-M p=0.0567.* ***(F)*** *Protein expression of IL-18, expressed as pg IL-18 per mg protein. No significant differences are found between groups. N=4 per group. IL-18 protein C-V vs Hx-V p=0.2492; Hx-V vs Hx-M p=0.2352; C-V vs Hx-M p=0.999. One-way ANOVA with Tukey's post-hoc, p < 0.05.*

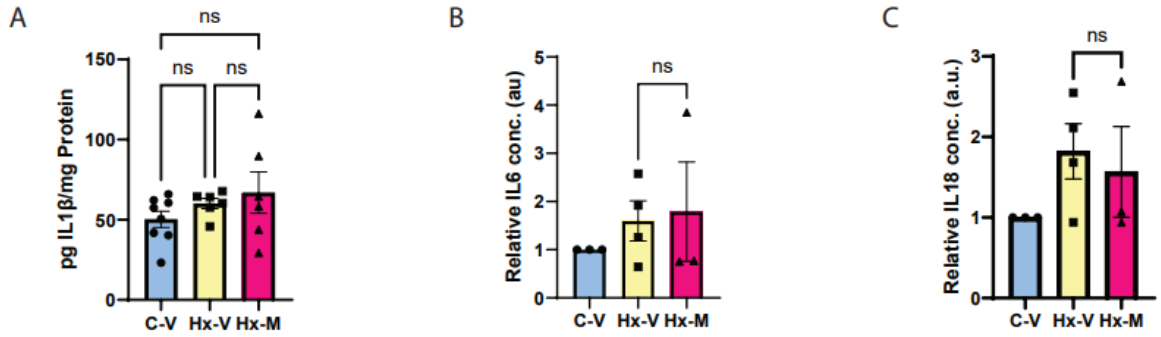


***Figure 4.13. Expression of NLRP3 inflammasome-related proteins 72 hours post-hypoxia, identified by ELISA.*** ***(A)*** *Protein expression of IL-1β, expressed as pg IL-1β per mg protein. No significant differences emerge. C-V n=8, Hx-V n=6, Hx-M n=6. IL-1β protein C-V vs Hx-V p=0.6404; Hx-V vs Hx-M p=0.8216; C-V vs Hx-M p=0.2919. One-way ANOVA with Tukey's post-hoc, p < 0.05.* ***(B)*** *Protein expression of IL-6 normalised by litter and expressed as relative IL-6 concentration. No significant differences found. C-V n=3, Hx-V n=4, Hx-M n=3. IL-6 protein Hx-V vs Hx-M p=0.4271.* ***(C)*** *Protein expression of IL-18 normalised by litter and expressed as relative IL-18 concentration. No significant differences found. C-V n=3, Hx-V n=4, Hx-M n=3. IL-18 protein Hx-V vs Hx-M p=0.3494. B-C Unpaired t-test, p< 0.05.*

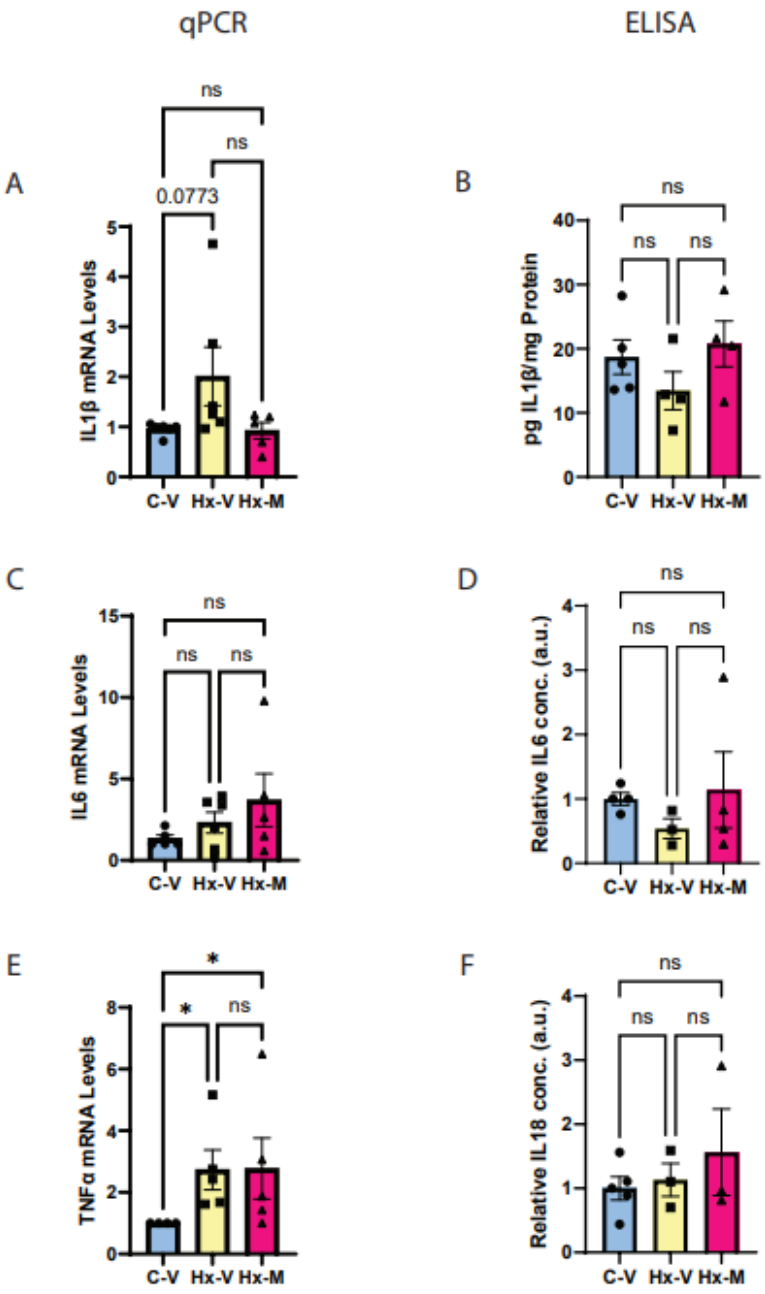


***Figure 4.14. Expression of NLRP3 inflammasome-related genes and proteins 5 weeks post-hypoxia, identified by qPCR and ELISA respectively. (A)*** *Gene expression of IL-1β, expressed as mRNA fold change. Hx-V trends towards higher IL-1β mRNA expression than C-V and Hx-M groups. C-V n=6, Hx-V n=6, Hx-M n=5. IL-1β mRNA C-V vs Hx-V p=0.0773; Hx-V vs Hx-M p=0.261; C-V vs Hx-M p>0.9999.* ***(B)*** *Protein expression of IL-1β, expressed as pg IL-1β/ mg protein. No significance found between groups. C-V n=5, Hx-V n=4, Hx-M n=4. IL-1β protein C-V vs Hx-V p=0.462; Hx-V vs Hx-M p=0.2794; C-V vs Hx-M p=0.881.* ***(C)*** *Gene expression of IL-6, expressed as mRNA fold change. No significant differences found. C-V n=5, Hx-V n=6, Hx-M n=5. IL-6 mRNA C-V vs Hx-V p=0.449; Hx-V vs Hx-M p=0.8149; C-V vs Hx-M p=0.4728.* ***(D)*** *Protein expression of IL-6 normalised by litter expressed as relative IL-6 concentration. No significant differences found between groups. C-V n=4, Hx-V n=3, Hx-M n=4. IL-6 protein C-V vs Hx-*

*V p=0.1605; Hx-V vs Hx-M p=0.7213; C-V vs Hx-M p=0.9925.* ***(E)*** *Gene expression of TNF-α, expressed as mRNA fold change. Both Hx-V and Hx-M express significantly more TNF-α than C-V. C-V n=4, Hx-V n=5, Hx-M n=5. TNF-α mRNA C-V vs Hx-V p=0.0256; Hx-V vs Hx-M p>0.9999; C-V vs Hx-M p=0.0473.* ***(F)*** *Protein expression of IL-18 normalised by litter expressed as relative IL-18 concentration. No significant differences found between groups. C-V n=5, Hx-V n=3, Hx-M n=3. IL-18 C-V vs Hx-V p=0.9625; Hx-V vs Hx-M p=0.7332; C-V vs Hx-M p=0.5293. A, D Kruskal-Wallis Test with Dunn's post-hoc, p < 0.05. B, C, E, F One-way ANOVA with Tukey's post-hoc, p < 0.05.*

#### 4.3.5.2. MCC950 Alters Expression of Proteins Related to Microglia Activation

The markers representing microglia activation were CXCR3 and P2RY12. CXCR3 is significantly upregulated in Hx-MCC mice versus C-Veh and Hx-Veh mice 24hrs post-hypoxia (Figure 4.15.A), although this is no longer seen 5wks post-hypoxia (Figure 4.15.B). P2RY12 expression is not significant at either timepoint (Figure 4.15.C-D).

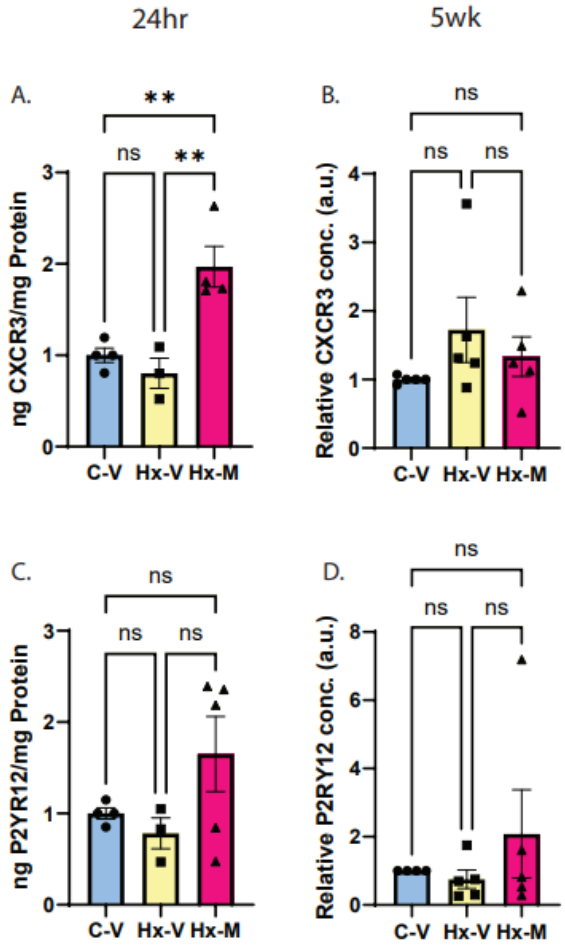


***Figure 4.15. Microglia markers measured by ELISA are differentially expressed post-hypoxia and MCC950 treatment at 24 hours and 5 weeks post-hypoxia. (A)*** *CXCR3 expression is represented as ng*

*CXCR3 per mg total protein. At 24hrs post-hx, CXCR3 expression is significantly higher in Hx-M than both C-V and Hx-V mice. C-V n=4, Hx-V n=3, Hx-M n=4. 24hr C-V v Hx-V p=0.7152; Hx-V v Hx-M p=0.0037; C-V v Hx-M p=0.0069.* ***(B)*** *CXCR3 concentrations were normalised by litter and represented as relative CXCR3 concentration. No significant differences found between groups. N=5 per group. 5wk C-V v Hx-V p=0.2823; Hx-V v Hx-M p=0.6741; C-V v Hx-M p=0.7443.* ***(C)*** *P2RY12 expression is represented as ng P2RY12 per mg total protein. No significant differences found between groups. C-V n=4, Hx-V n=3, Hx-M n=5. 24hr C-V v Hx-V p=0.8949; Hx-V v Hx-M p=0.1989; C-V v Hx-M p=0.3206.* ***(D)*** *P2RY12 expression 5wks post-hx is normalised by litter and represented as relative concentration. No significant differences between groups. C-V n=4, Hx-V n=5, Hx-M n=5. 5wk C-V v Hx-V p=0.9767; Hx-V v Hx-M p=0.4882; C-V v Hx-M p=0.648. One-way ANOVA with Tukey's post-hoc, $p < 0.05$.*

#### 4.3.5.3. MCC950 Significantly Upregulates the Complement Pathway and Classical Complement Initiation Both Acutely and Chronically Post-hypoxia.

This Chapter has shown that MCC950 does not modulate the phagocytic activity of microglia seen by using the broad marker CD68. Here, we evaluate if the complement pathway, which is a modulator of phagocytosis in synaptic pruning during development, is affected by MCC950. Complement has been implicated in HIE, as the neuroprotection offered by TH treatment has been at least partially attributed to the downregulation of complement pathway proteins such as C1q, C3, C5a and C9 (Shah et. al., 2021). Therefore, an inhibitor of complement protein C1, RLS-0071, is currently in Phase II clinical trials as an adjuvant therapy with TH for severe HIE (Kumar et. al., 2021). Classical pathway initiation, represented by C1qA mRNA fold change (Figure 4.16.A), was significantly upregulated post-hypoxia in both Hx-Veh and Hx-MCC mice 3 hours post-hypoxia, although this difference was no longer detected at 72 hours and 5 weeks post-hypoxia. Other elements of the classical pathway were analysed at 72 hours post-hypoxia – C1qR1 (Figure 4.16.B), C3 (Figure 4.16.C) and C5a (Figure 4.16.D). Expression of C1qR1 and C3 was higher in Hx-MCC mice compared to C-Veh and Hx-Veh mice.

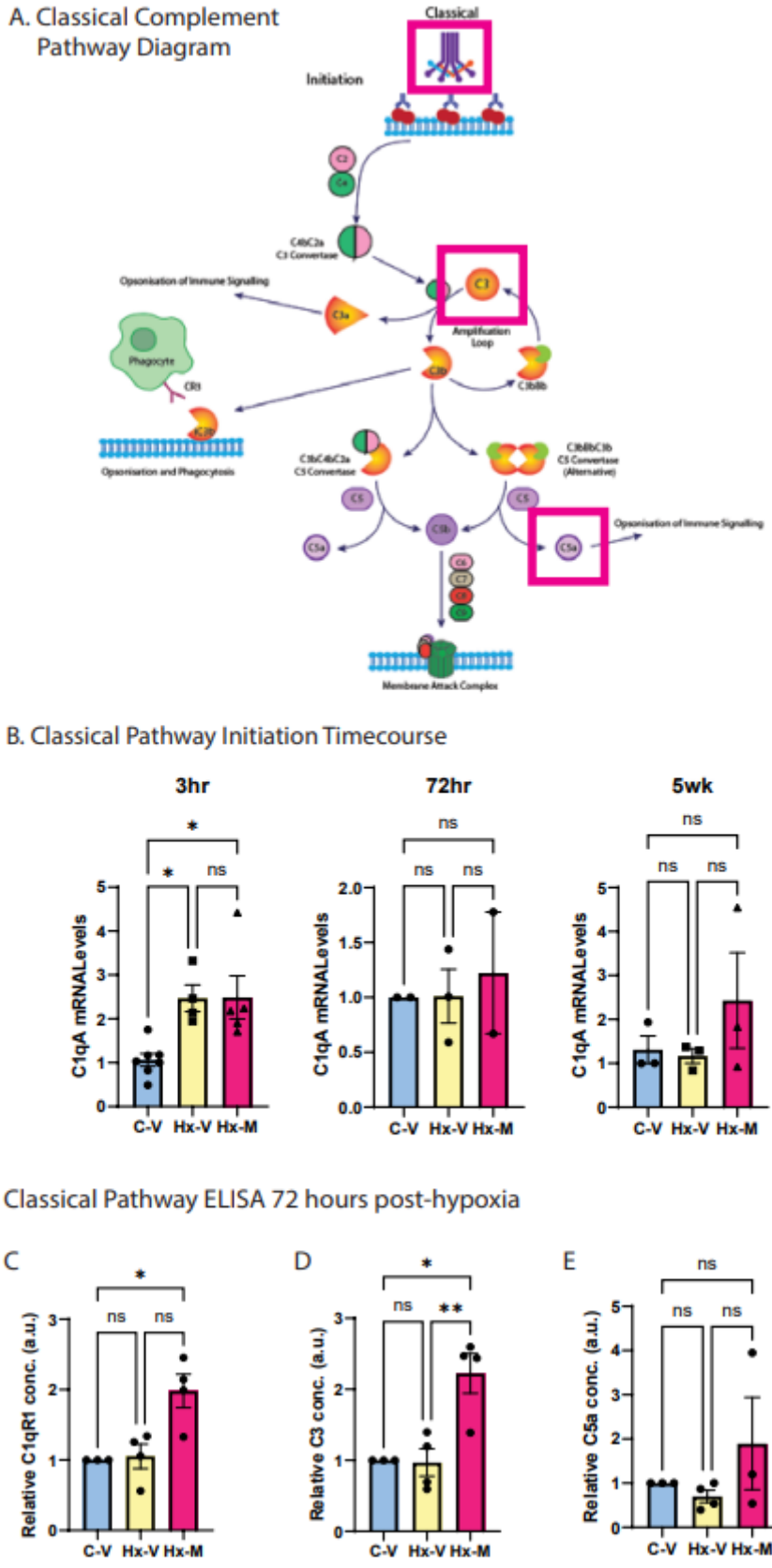


***Figure 4.16. Classical Complement Pathway Activation is slightly elevated by MCC950 post-hypoxia both acutely and chronically. Additionally, C1qR1, C3 and C5a are elevated at 72 hours post-hypoxia.*** ***(A)*** *Classical Complement Pathway Illustration, with the targets of this analysis marked in pink boxes.*

***(B)*** *Classical Pathway initiation time course, shown as mRNA fold change of C1qa at 3hrs, 72hrs and 5wks post-hx. At 3hrs post-hx, Hx-V and Hx-M expression are significantly higher than C-V. No trends are seen at 72hrs or 5 wks post-hx. 3hr C-V n=7, Hx-V n=4, Hx-M n=5. 3hr C-V v Hx-V p=0.0219, Hx-V v Hx-M p=0.9989, C-V v Hx-M p=0.0132. 72hr C-V n=2, Hx-V n=3, Hx-M n=2. 72hr C-V v Hx-V p=0.9996, Hx-V v Hx-M p=0.8885, C-V v Hx-M p=0.8962. 5wk n=3 per group. 5wk C-V v Hx-V p=0.9872, Hx-V v Hx-M p=0.4202, C-V v Hx-M p=0.4954. One-way ANOVA with Tukey's post-hoc, p < 0.05.* ***(C)*** *C1qR1 protein expression was normalised by litter and expressed as relative C1qR1 concentration. At 72hrs post-hx, Hx-MCC C1qR1 expression is higher than C-V and Hx-V littermates. C-V n=3, Hx-V n=4, Hx-M n=4. C1qR1 C-V v Hx-V p>0.9999, Hx-V v Hx-M p=0.2022, C-V v Hx-M p=0.0383.* ***(D)*** *C3 protein expression was normalised by litter and expressed as relative C3 concentration. Hx-M expression of C3 72hrs post-hx is significantly higher than C-V and Hx-V littermates. C-V n=3, Hx-V n=4, Hx-M n=4. C3 C-V v Hx-V p=0.9951, Hx-V v Hx-M p=0.0071, C-V v Hx-M p=0.0123.* ***(E)*** *C5a concentration at 72hrs post-hx was normalised by litter and expressed as relative C5a concentration. No significant differences emerge. C5a C-V n=3, Hx-V n=4, Hx-M n=3. C5a C-V v Hx-V p=0.9738, Hx-V v Hx-M p=0.3501, C-V v Hx-M p>0.9999. C-E Kruskal-Wallis test with Dunn's post-hoc, p < 0.05.*

## 4.4. Discussion

Previous results have shown that administration of a broad-spectrum anti-inflammatory drug CND provided neuroprotection after hypoxia (Quinlan et. al., 2019). Additional studies of P2X7R, an activator of the NLRP3 inflammasome, found that it is upregulated post-hypoxia, and that P2X7R antagonism or knockout was neuroprotective (Rodriguez-Alvarez et. al., 2017; Smith et. al., 2023). Given the relationship between P2X7R, the NLRP3 inflammasome and IL-1β release in microglia, the compound MCC950 was chosen to target NLRP3 inflammasome assembly. In this study, treatment with MCC950 immediately post-hypoxia provided attenuation in neonatal reflex development and a partial rescuing of neurobehavioural deficits post-hypoxia. When microglia and inflammatory markers were analysed at acute and chronic stages post-hypoxia, a partial rescuing of the inflammatory response is seen acutely post-hypoxia, although many of these differences are no longer detected 5 weeks post-hypoxia.

The neonatal reflex tests showed that MCC950 treatment post-hypoxia fully rescued deficits in forelimb grip strength, and almost fully attenuated vestibular and proprioceptive deficits seen post-hypoxia in the hypoxia-vehicle group of this study and in Results Chapter 1. MCC950 only partially attenuated ambulatory deficits, although hindlimb angles showed some slight postural improvements. While there is not an even attenuation of all reflexes, these results are still indicative of a neuroprotective effect. These results echo those produced by Luo and colleagues (2021), where treatment with an N-acetylserotonin derivative post-HIE inhibited the NLRP3 inflammasome and improved the negative geotaxis and the surface righting test. This is further supported by evidence that MCC950 treatment restores myelination in a model of developmental white matter injury (Holloway et. al., 2021). Other treatment studies in severe models of HIE have shown variability in the reflexes improved between therapeutic

modalities. For instance, therapeutic hypothermia (TH) treatment post-HIE improved performance in the negative geotaxis test, but not in the forelimb grip strength or the surface righting test (Diaz et. al., 2017). Meanwhile, treatment with melatonin (MT) improved ambulation, negative geotaxis, surface righting and forelimb grip strength in rodents (Wang et. al., 2013). This is further corroborated by improved Denver scores in human infants treated with MT and TH post-HIE (Aly et. al., 2015). This study strengthens current evidence that neonatal reflex development post-HIE is attenuated by anti-inflammatory intervention in both rodents and humans.

Neonatal reflex testing was followed by adult behavioural assessments at PND28 to PND35. MCC950 treatment recovered the spatial memory deficits and reduced the anxiety induced by hypoxia. These results support previous observations from the laboratory that anti-inflammatory treatment post-hypoxia rescues cognitive deficits (Quinlan et. al., 2019). Similarly, studies of severe HIE where the NLRP3 inflammasome was suppressed found the same rescuing effect on cognitive and behavioural deficits (Chen et. al., 2023; Tao et. al., 2024). Furthermore, MCC950 has been shown to ameliorate cognition and neurobehavioural outcomes in other neurological disease models, such as AD and TBI (Dempsey et. al., 2017; Ismael et. al., 2018; Xu et. al., 2018; McManus et. al., 2025). It is clear from these results and from the literature that neuroinflammation is at least partly responsible for the neurobehavioural deficits post-HIE, and administration of anti-inflammatory agents are protective. Furthermore, the inflammasome is potentially a key driver of these deficits, given the marked improvements shown after inhibiting this one pathway. This is not restricted to HIE but seen across the board in several neurological conditions where neuroinflammation is a pathological hallmark.

This thesis, in agreement with previous literature, identifies $CD68^{+}Iba1^{+}$ cells as proinflammatory or phagocytic microglia (Waller et. al., 2019), and $P2RY12^{+}Iba1^{+}$ cells as homeostatic, or anti-inflammatory (Sipe et. al., 2016). MCC950 treatment partially reduced the proportions of $CD68^{+}$ microglia present 72 hours post-hypoxia but had no effect on $CD68^{+}$ microglia at 5 weeks post-hypoxia, and did not change the proportions of $P2RY12^{+}$ microglia at either timepoint. Despite this apparent lack of changes, the neonatal reflex testing and adult behaviour tests show that MCC950 treatment is neuroprotective, therefore the microglial changes after MCC950 may be governed by alternative, neuroprotective pathways. The acute findings corroborate previous studies, as NLRP3 inflammasome inhibition reduced expression of CD68 and pro-inflammatory microglia acutely post-HIE (Lv et. al., 2020; Luo et. al., 2021), although none investigated how CD68 expression was affected in the longer term post-HIE. In models of AD where MCC950 treatment is administered, CD68 expression and enrichment of phagocytic pathways are increased (Dempsey et. al., 2017; McManus et. al., 2025), although $CD68^{+}$ cells also express Arg1, a classic marker for anti-inflammatory microglia (Cherry et. al., 2015; Dempsey et. al., 2017; He et. al., 2020). Therefore, this increased phagocytosis is potentially governed by alternative, anti-inflammatory pathways which promote the clearance of Aβ and contribute to the cognitive ameliorations (Dempsey et. al., 2017; He et. al., 2020; McManus et. al., 2025).

As seen previously in the literature, HIE negatively impacts on hippocampal function by altering neuronal morphology and inducing significant accumulations of microglia (Del Bigio & Becker., 1994; Quinlan et. al., 2019; Sheikh et. al., 2019; 2022; González Fuentes et. al., 2021). MCC950 increased phagocytosis which may be governed by neurodevelopmental pathways, and therefore may attenuate the altered neuronal pruning observed in this model (Quinlan et. al., 2019). Indeed, MCC950 rescued neuronal damage in the cortex of EAE mice

(Hou et. al., 2024), rescued structural plasticity of hippocampal dendrites in the dentate gyrus of socially isolated male mice (Li et. al., 2021b) and attenuated expression of synaptophysin and post-synaptic density protein 95 (PSD-95) in the hippocampi of mice after HIE (Yang et. al., 2023). A potential molecular determinant which may be responsible for these attenuations is the complement pathway, which was found to be acutely and chronically upregulated post-hypoxia in this study.

Gene and protein expression analysis found that MCC950 was most effective in dampening IL-1β and IL-18 expression 3 hours post-hypoxia, and this effect diminishes thereafter. These results corroborate the widely and consistently reported findings in the literature that MCC950 downregulates the expression and release of these two cytokines in numerous disease models (Coll et. al., 2015; Dempsey et. al., 2017; Chen et. al., 2018; Lv et. al., 2020). The other two markers related to the inflammasome in this study were TNF-α and IL-6, both of which were not affected by MCC950 treatment at any timepoint post-hypoxia. The elevated gene expression of TNF-α supports the elevated $CD68^{+}$ microglia and is supported by the literature, which found that MCC950 does not change TNF-α expression (Coll et. al., 2015; Ismael et. al., 2018; McManus et. al., 2025). A consensus has yet to be reached on the effects of MCC950 on IL-6 expression, with some studies finding expression to be unchanged (Dempsey et. al., 2017) and other finding IL-6 is downregulated after MCC950 (Coll et. al., 2015; Luo et. al., 2019).

In this study, MCC950 treatment significantly upregulated CXCR3 expression relative to both control and hypoxia-vehicle mice at 24 hours post-hypoxia, but at 5 weeks post-hypoxia CXCR3 expression in hypoxia-MCC mice was slightly lower than hypoxia-vehicle mice. It has also been shown that CXCL10/CXCR3 signalling is associated with impaired synaptogenesis and long-

term behavioural consequences in a rat model of neonatal hyperglycaemia (Satrom et. al., 2018). Therefore, the chronic downregulation of CXCR3 expression post-MCC950 treatment in this model is consistent with the improvements in adult behaviour also seen in this model, thus further corroborating the neuroprotection offered by MCC950.

The results of the microglia analysis indicate that, while the overall levels of phagocytic microglia are largely unchanged by MCC950 treatment, this is not reflective of the improvements in behavioural test performance or inflammatory markers described in this chapter. Therefore, the final part of the gene and protein expression analysis studied the complement pathway and classical complement pathway initiation. As discussed previously, complement is integral to shaping neuronal circuitry via synaptic pruning and elimination by microglia via complement-mediated phagocytosis, particularly during the neonatal phase (Schafer et. al., 2012; Weinhard et. al., 2018). Few studies have investigated how MCC950 treatment impacts on complement signalling, although, as discussed previously, MCC950 is associated with attenuations in neuronal and dendritic morphology in the hippocampus and the cortex in different disease models, including HIE (Li et. al., 2021b; Yang et. al., 2023; Hou et. al., 2024). A time course study of C1qA, representing classical complement pathway initiation, found that MCC950 had no bearing on expression of C1qA acutely post-hypoxia, and increased C1qA expression at 5 weeks post-hypoxia. Furthermore, protein expression studies at 72 hours post-hypoxia found that C1qR1 and C3 were significantly upregulated by MCC950. Previous work in this model found that global hypoxia at PND7 resulted in underpruned dendrites in the *stratum oriens* of the Ca1 chronically post-hypoxia, along with significantly poorer spatial memory test performance (Quinlan et. al., 2019). Therefore, the improved spatial memory test performance post-MCC950, coupled with elevated phagocytic microglia

and complement pathway marker expression, support the hypothesis that these phagocytic microglia are engaging in synaptic pruning, opening a door for future study.

This chapter has demonstrated the neuroprotective effects of a single dose of MCC950 administered immediately following moderate global hypoxia. This treatment dampened the acute inflammatory response, although this effect diminished with time. Despite this, MCC950 still rescued the cognitive and behavioural deficits associated with this model in the adolescent stage. An interesting finding of this study was the significant and chronic overexpression of the complement pathway induced by MCC950 treatment, which may explain how a neuroprotective effect has been found in behavioural studies despite the elevation in phagocytic microglia.

# Chapter 5: Results Chapter 3

## 5.1. Introduction

### 5.1.1. Chronic Inflammation After Neonatal Hypoxia.

The patterns of damage following HIE can be divided into phases; primary, secondary, and tertiary energy failures, each with its own physiological hallmarks (Introduction Chapter 1, Figure 1.1). The first two Results Chapters of this thesis have shown that, even in this moderate model of hypoxia, there is a chronically elevated proportion of pro-inflammatory microglia in the hippocampus many weeks after the original insult. This agrees with the literature, which has shown a chronic immune response, mainly mediated by pro-inflammatory microglia, in both humans and animal models of severe HIE (Bona et. al., 1999; Winerdal et. al., 2012; Zareen et. al., 2020; Zhou et. al., 2022). While microglia are responsible for some deleterious effects, they are still necessary for clearing debris and damage: when microglia are completely depleted in P10 mice following a model of HIE, the damage seen is far worse (Tsuji et al., 2020).

### 5.1.2. Potential Merits of Treatment During Chronic Stage Post-HIE

So far, most treatment strategies proposed for HIE are designed to be administered within the traditional therapeutic window of 0 to 6 hours post-insult, during the acute or latent phase. This is particularly challenging for clinicians who have an incredibly short window of opportunity to initiate appropriate treatment when the aetiology is not always clear (Aslam et. al., 2019; Pressler et, al., 2021; Molloy et. al., 2023). Research has begun to suggest the merits of neuroprotective or neurorestorative treatment during the tertiary energy failure phase (Fleiss & Gressens., 2012). In a review by Chakkarapani (et. al., 2021), erythropoietin and stem cell treatments were proposed as neurorestorative treatments for administration during the tertiary energy failure. Long-term studies in humans post-HIE have found that, even after TH treatment, circulating cytokines are elevated and may correlate with worse neurodevelopmental outcomes (Jenkins et. al., 2012; Bajnok et. al., 2017; Leifsdottir et. al.,

2018; Zareen et. al., 2020). Results Chapter 2 has shown the neuroprotection offered after treatment with MCC950 immediately post-hypoxia within the traditional therapeutic window, and previous work also found that a more latent treatment course was still neuroprotective. When mice were treated once daily with a P2X7R antagonist, JNJ-47965567, starting at 24 hours post-hypoxia for 7 days, this rescued later-life hyperexcitability otherwise induced by hypoxia (Smith et. al., 2023), and provided an anti-inflammatory alternative treatment strategy for neonatal seizures and subsequent hyperexcitability seen commonly in clinical cohorts (Zareen et. al., 2020; Akula et. al., 2023). These studies pose the question; can anti-inflammatory treatment later in life protect against these outcomes?

### 5.1.3. MCC950 Treatment in Models of Neurodegeneration; Hope for HIE?

MCC950, the NLRP3 inflammasome inhibitor administered in Results Chapter 2, has been used as a neuroprotective agent in other models of CNS disease or injury, although in models of injury such as TBI or ischaemia, MCC950 is administered before the insult and/or in the hours immediately after (Coll et. al., 2015; Ismael et. al., 2018; Ren et. al., 2018; Jiao et. al., 2020). Therefore, studies of MCC950 administered in neurodegenerative models may give a better insight into how a more delayed treatment strategy can be neuroprotective or neurorestorative. In mouse models of AD, MCC950 was administered at 12 months of age. Not only did MCC950 reduce neuroinflammation and NLRP3 inflammasome activation, but it also encouraged Aβ phagocytosis by microglia and had a positive impact on cognition (Dempsey et. al., 2017; McManus et. al., 2025). The increased phagocytosis corresponds with the findings of Results Chapter 2, where the complement pathway, involved in microglia-mediated phagocytosis, was upregulated in Hypoxia-MCC950 mice compared to both controls and hypoxia-vehicle mice. The findings by Dempsey (et. al., 2017) are corroborated by other studies where MCC950 treatment attenuated synaptic plasticity deficits (Qi et. al., 2018),

inhibited Aβ-induced microglial activation (Lučiūnaitė et. al., 2020) and protected against the development of memory impairment and other AD-related behavioural phenotypes (Heneka et. al., 2013). AD is not the only neurodegenerative disorder where the NLRP3 inflammasome has been implicated. In models of Parkinson's disease, MCC950 treatment in Atg5-deficient mice reduced neuroinflammation in the substantia nigra and protected against neuron loss (Cheng et. al., 2020).

### 5.1.4. Hypothesis and Aims

The results stated above have led to the hypothesis that treatment of HIE during the tertiary energy failure, 2 weeks post-hypoxia, will provide a neuroprotective effect. It is anticipated that the later timing of the MCC950 administration will be sufficient to reduce the chronic microglial activation seen in the previous chapter, which may or may not correspond with rescuing of the neurobehavioural deficits seen in this model post-hypoxia.

The aims of this study are:

1. To assess the effects of later term MCC950 treatment on anxiety and spatial memory.
2. To see how microglia 5 weeks post-hypoxia are affected by later MCC950 treatment using CD68 and P2RY12 as markers of phagocytic and homeostatic microglia, respectively.

## 5.2. Methods

Mice were prepared for hypoxia as described previously and sacrificed at the specified timepoints in the flowchart below in Figure 5.1. MCC950 was administered between PND21 – 25 as described in Methods Chapter 2 Section 2.3.2. Wellbeing scores presented in Table 5.2.

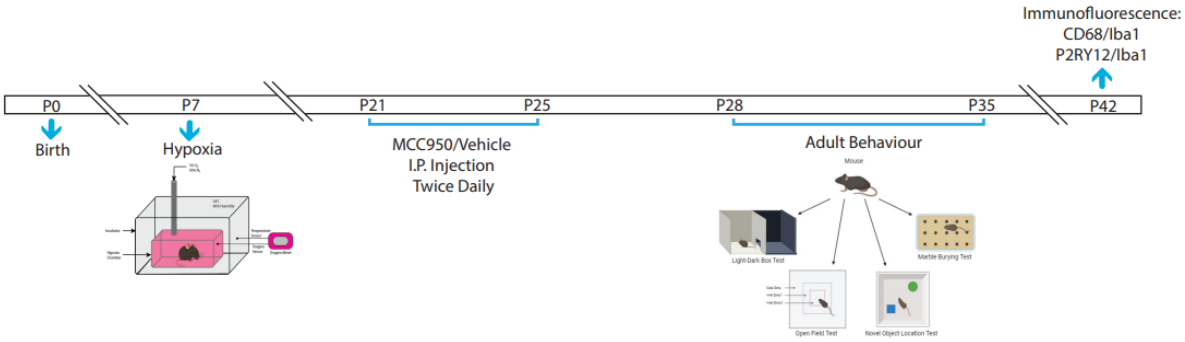


***Figure 5.1. Timeline of the molecular and behavioural studies conducted.***

### 5.2.1. Adult Behaviour

The Adult behaviour tests conducted were the Open Field test, the Light Dark Box test and the Novel Object Location test as detailed in the Methods Chapter 2, Section 2.5.

### 5.2.2. Immunofluorescence Staining and Imaging

Phagocytic microglia were visualised as described in Methods Section 2.6.3 (Guillot-Sestier et. al., 2021), incubated with Anti-CD68 (1:500) and Anti-Iba1 (1:500), followed by Alexafluor594 Donkey anti-Rat (1:500) and Alexafluor488 goat anti-rabbit (1:500). Homeostatic microglia were visualised as described in Methods Section 2.6.2, using Anti-P2RY12 (1:100), and Anti-Iba1 (1:500), followed by Alexafluor594 Donkey anti-Rat (1:500) and Alexafluor488 goat anti-rabbit (1:500). Z-stacks were imaged at 40x at 0.4µm Z-plain intervals using a Leica SP8 scanning confocal microscope (TBSI Imaging and Microscopy Centre).

| EXPERIMENT | TIME POST-HX | NO. C-VEH | NO. HX-VEH | NO. HX-MCC |
|---|---|---|---|---|
| **CD68/Iba1** | 5wks | 6 | 6 | 8 |
| **P2RY12/Iba1** | 5wks | 6 | 6 | 8 |

***Table 5.1. Experimental cohorts for immunofluorescence studies in Results Chapter 3.***

5.2.3. Cell Counting

Z-stack images were converted into a Z-projection in Image J for manual counting. Each image was counted twice, and the average was taken as the final count. The morphological analyses grouped cells by morphological features (Diz-Chaves et. al., 2012), as described in Methods Section 2.7.3, and the analysis of double-stained cells is described in Methods Section 2.7.

| PARAMETER | SCORING | P8 | | P9 | | P10 | |
|---|---|---|---|---|---|---|---|
| | | Control | Hypoxia | Control | Hypoxia | Control | Hypoxia |
| **WEIGHT GAIN** | 0-9% | 1 | 2 | 0 | 0 | 0 | 0 |
| | 10-14% | 7 | 19 | 0 | 2 | 0 | 1 |
| | 15-19% | 3 | 1 | 3 | 8 | 1 | 0 |
| | 20%+ | 0 | 1 | 8 | 13 | 10 | 22 |
| **DRINKING/ EATING** | Empty stomach | 0 | 0 | 0 | 0 | 0 | 1 |
| | Half-Full | 2 | 2 | 2 | 3 | 2 | 3 |
| | Full Stomach | 9 | 21 | 9 | 20 | 9 | 19 |
| **BREATHING** | Difficulty | 0 | 0 | 0 | 0 | 0 | 0 |
| | Fast | 0 | 0 | 0 | 0 | 0 | 0 |
| | Slow/calm | 11 | 23 | 11 | 23 | 11 | 23 |
| **GAIT/ POSTURE** | Markedly Abnormal | 0 | 0 | 0 | 0 | 0 | 0 |
| | Slightly Abnormal | 0 | 22 | 0 | 18 | 0 | 13 |
| | Normal | 11 | 1 | 11 | 5 | 11 | 10 |
| **NESTING/ MATERNAL CARE** | Nestlet 90% intact | 0 | 0 | 0 | 0 | 0 | 0 |
| | Partially torn mostly intact | 0 | 0 | 0 | 0 | 3 | 7 |
| | 50% torn but not nest | 3 | 7 | 3 | 7 | 0 | 0 |
| | Greater than body height | 8 | 16 | 8 | 16 | 8 | 16 |
| **TOTAL NO. MICE** | | 11 | 23 | 11 | 23 | 11 | 23 |

***Table 5.2. Breakdown of pups in the control and hypoxia groups of the Chapter 3 cohort to receive each score in their wellbeing sheets at PND8, PND9 and PND10. Hypoxia mice were not divided between vehicle and MCC for this table as they do not start treatment until PND21.***

## 5.3. Results

### 5.3.1. Adult Behaviour Shows that Later Treatment with MCC950 Partially Attenuates Neurobehavioural Deficits Post-Hypoxia.

Mice underwent the same battery of adult behaviour tests as in Results Chapter 2 to assess whether treatment with MCC950 two weeks post-hypoxia attenuated neurobehavioural assessment performance.

The Open Field (OF) Test, as in Chapters 1 and 2, assessed motor function to ensure that any differences seen in subsequent behaviour tests are due to changed behavioural rather than reduced mobility. The average speed and the number of line crossings were compared between groups, and no differences emerged between any groups, consistent with our Chapter 1 and 2 findings (Figure 5.2.B).

The Light Dark Box (LDB) Test is used to assess anxiety behaviours in mice. Previous work in this model has observed increased anxiety behaviour in the LDB (Rodriguez-Alvarez et. al., 2015; Quinlan et. al., 2018). LDB time was normalised by litter due to inter-litter variability. Consistent with Chapter 2 findings and previous literature, Hx-Veh mice take significantly longer to enter the dark box compared to Hx-MCC mice (Figure 5.2.D).

The Novel Object Location (NOL) test assesses spatial memory. The time spent by each mouse with the novel object location during the test period was standardised to account for object preferences. Hx-Veh mice performed poorer in this test than C-Veh mice and Hx-MCC mice trend towards an improvement in this test vs Hx-Veh mice (Figure 5.2.F).

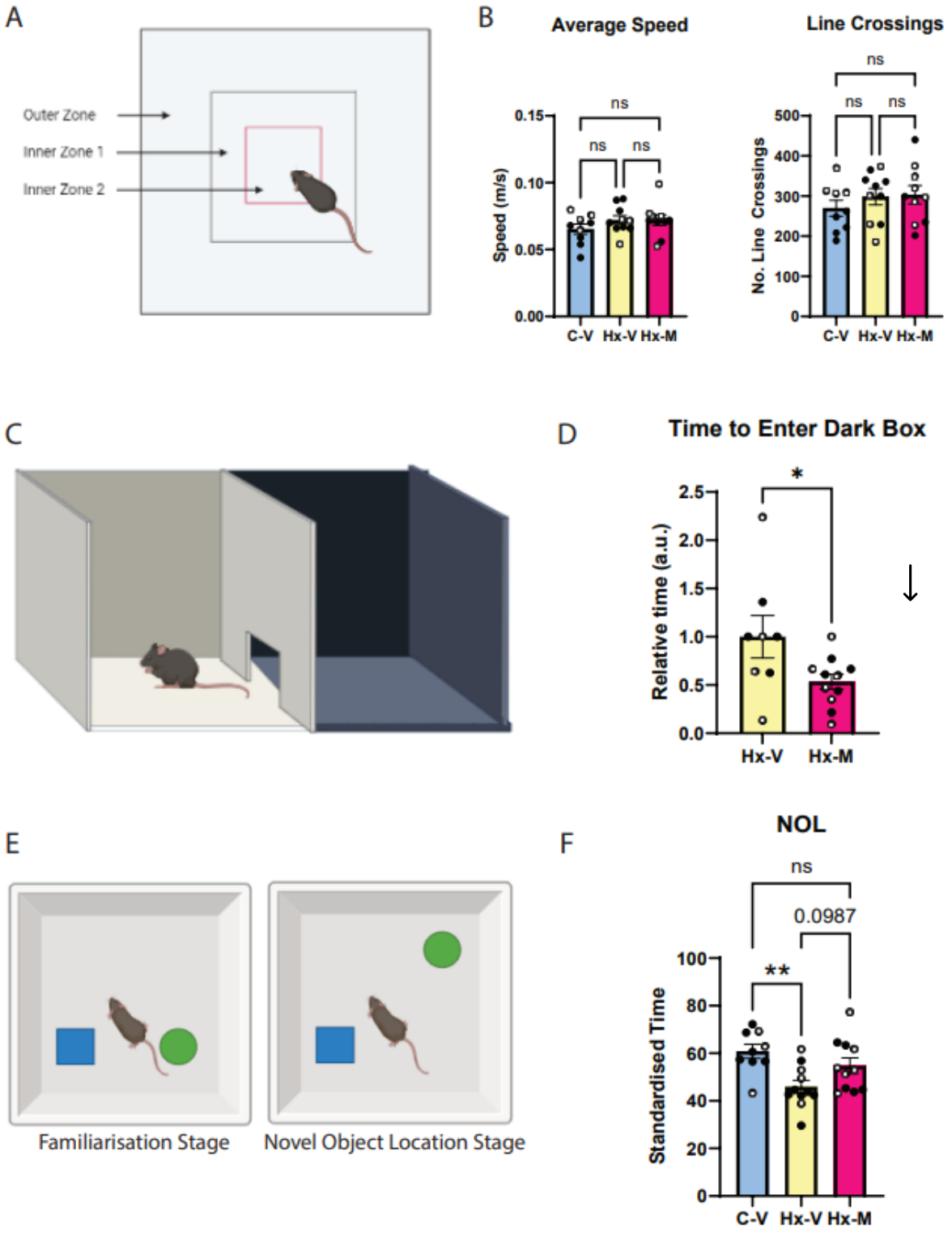


***Figure 5.2. MCC950 Treatment 2 weeks post-hypoxia causes some attenuations in adult behaviour compared to Hx-Veh littermates. (A)*** *Illustration of the OF test apparatus.* ***(B)*** *No differences were found in the average speed (L) or the number of line crossings (R) between groups. C-V n=9, Hx-V n=10 Hx-M n=10. Average Speed C-V v Hx-V p=0.411, Hx-V v Hx-M p=0.9998, C-V v Hx-M p=0.4215. Line Crossings C-V v Hx-V p=0.6123, Hx-V v Hx-M p=0.986, C-V v Hx-M p=0.5172. One-way ANOVA with*

*Tukey's post-hoc, p < 0.05.* ***(C)*** *Illustration of the LDB apparatus.* ***(D)*** *Time taken for each animal to enter the dark box after being placed in the light box, normalised by litter and expressed as relative time. Hx-Veh mice take significantly longer to enter the dark box than Hx-M littermates. Hx-V n=8, Hx-M n=11. Time to Enter Dark Box Hx-V v Hx-M p=0.0375. Unpaired, one-tailed t-test with arrow to indicate a-priori hypothesis, p < 0.05.* ***(E)*** *Illustration of the NOL apparatus. For the familiarisation stage (L), objects are in set positions, and for the NOL stage (R), one object is moved.* ***(F)*** *When the time spent with the moved object during the NOL stage is standardised, Hx-V mice spent less time with the moved object than C-V and Hx-M groups, indicating poorer memory in Hx-V mice. NOL C-V n=9, Hx-V n=11, Hx-M n=11. NOL C-V v Hx-V p=0.0.005, Hx-V v Hx-M p=0.0987, C-V v Hx-M p=0.3507. One-way ANOVA with Tukey's post-hoc, p < 0.05. In all graphs, female mice are white circles, male mice are black circles.*

### 5.3.2. Later Treatment with MCC950 Post-Hypoxia Reduces the Prevalence of Pro-Inflammatory Microglia.

CD68, the marker for phagocytic lysosomes, was used with Iba1 to identify, quantify, and morphologically assess phagocytic or pro-inflammatory microglia in the hippocampus (Diz-Chaves et. al., 2012). $CD68^{+}Iba1^{+}$ cells are expressed as a percentage of total $Iba1^{+}$ cells.

#### 5.3.2.1. MCC950 Reduces the Percentage of $CD68^{+}Iba1^{+}$ cells in the Hippocampus 5 weeks post-hypoxia.

Quantification of $CD68^{+}Iba1^{+}$ cells was conducted as previously described. At 5 weeks post-hypoxia, 17 days after cessation of treatment with MCC950, there is a marked decrease of $CD68^{+}Iba1^{+}$ cells compared to Hx-Veh mice in all regions of the hippocampus. This indicates that MCC950 treatment rescues the chronic inflammatory signature seen post-hypoxia.

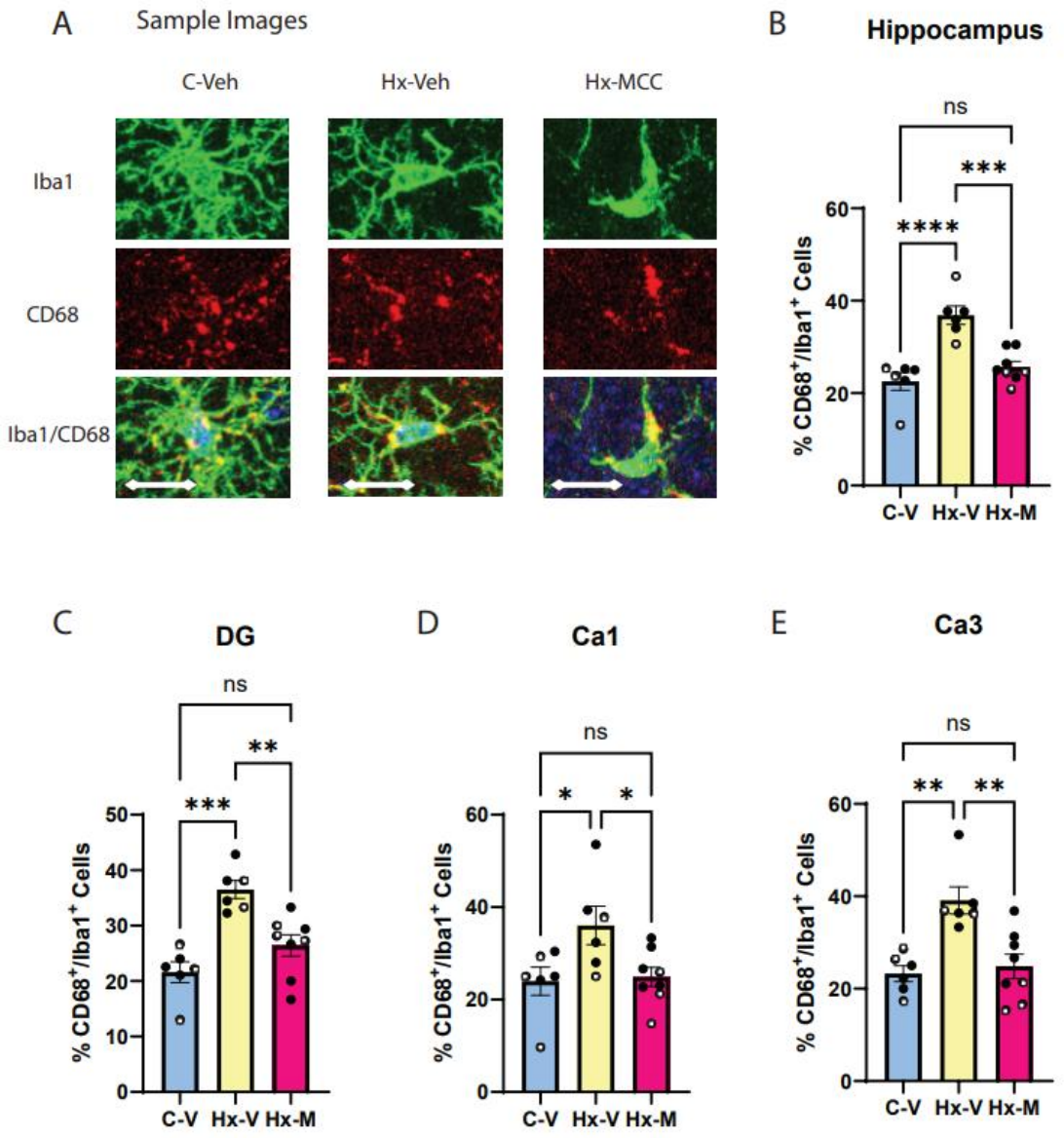


***Figure 5.3. MCC950 treatment post-weaning attenuates CD68⁺Iba1⁺ cell prevalence at 5 weeks post-hypoxia throughout the hippocampus. (A)*** *Sample Images of CD68/Iba1 double-labelled cells in C-V, Hx-V and Hx-M. Scale bar 10µm.* ***(B)*** *Hx-V mice have significantly higher CD68⁺Iba1⁺ cells versus C-V and Hx-M in the full hippocampus. C-V n=6, Hx-V n=6, Hx-M n=8. Hipp C-V v Hx-V p<0.0001, Hx-V v Hx-M p=0.0004, C-V v Hx-M p=0.3851.* ***(C)*** *Hx-V mice have significantly higher CD68⁺Iba1⁺ cells versus C-V and Hx-M in the dentate gyrus. C-V n=6, Hx-V n=6, Hx-M n=8. Hipp C-V v Hx-V p=0.001, Hx-V v Hx-M p=0.0033, C-V v Hx-M p=0.1798.* ***(D)*** *Hx-V mice have significantly higher CD68⁺Iba1⁺ cells versus C-V and Hx-M in the Ca1. C-V n=6, Hx-V n=6, Hx-M n=8. Hipp C-V v Hx-V p=0.0404, Hx-V v Hx-M p=0.0435, C-V v Hx-M p=0.9733.* ***(E)*** *Hx-V mice have significantly higher CD68⁺Iba1⁺ cells versus C-V and Hx-M in the Ca3. C-V n=6, Hx-V n=6, Hx-M n=8. Hipp C-V v Hx-V p=0.0017, Hx-V v Hx-M p=0.0024, C-V v Hx-M p=0.8963. One-way ANOVA with Tukey's post-hoc, $p < 0.05$. In all graphs, female mice are white circles, male mice are black circles.*

5.3.2.2. $CD68^+Iba1^+$ cells have pro-inflammatory phenotypes in all groups post-hypoxia, which are reduced to control levels after MCC950 treatment post-weaning.

$CD68^+Iba1^+$ cells were analysed for morphology as described previously (Diz-Chaves et. al., 2012). No $CD68^+Iba1^+$ cells were were morphologically consistent with Type I, II or III cells, therefore only Types IV and V are graphed. There were more $CD68^+Iba1^+$ cells post-hypoxia, particularly in the Type V group. Hx-MCC mice expressed similar levels of Type IV and Type V morphology cells to control mice (Figure 5.4.B).

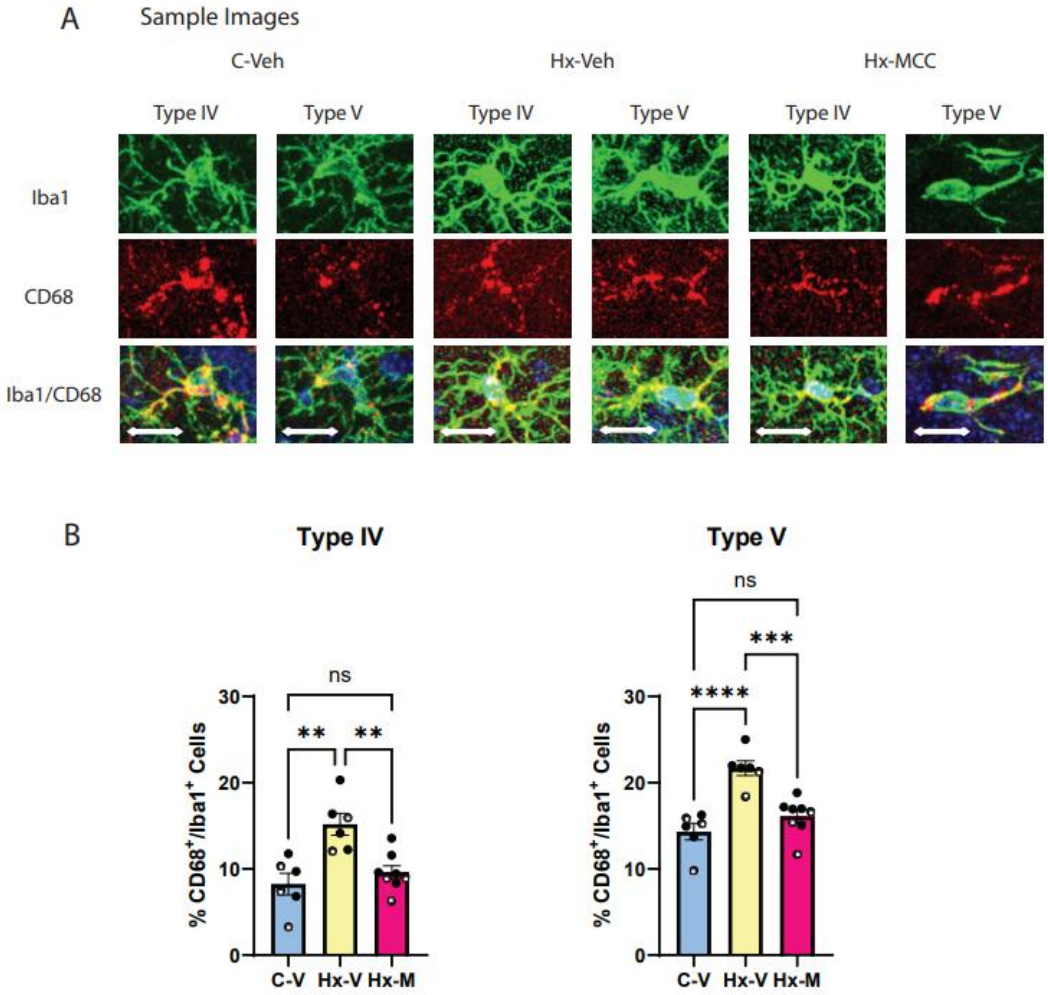


***Figure 5.4. MCC950 reduces percentages of Type IV and Type V pro-inflammatory morphologies. (A)*** *Samples Images of Type IV and Type V cells in C-V, Hx-V and Hx-M Images. Scale bar 10µm.* ***(B)*** *Hx-M and C-V have lower percentages of Type IV and Type V cells compared to Hx-V. C-V n=6, Hx-V n=6, Hx-M n=8. Type IV C-V v Hx-V p=0.0011, Hx-V v Hx-M p=0.004, C-V v Hx-M p=0.6327. Type V C-V v Hx-V*

*p<0.0001, Hx-V v Hx-M p=0.0005, C-V v Hx-M p=0.3174. One-way ANOVA with Tukey's post-hoc, p < 0.05. In all graphs, female mice are white circles, male mice are black circles.*

### 5.3.3. P2RY12 Iba1 Staining

P2RY12 was used as a marker for homeostatic microglia in the hippocampus for quantification (Sipe et. al., 2016) in a double staining with Iba1. P2RY12$^{+}$Iba1$^{+}$ cells were expressed as a percentage of total Iba1$^{+}$ cells present. At 5 weeks post-hypoxia, both Hx-Veh and Hx-MCC mice had fewer P2RY12$^{+}$Iba1$^{+}$ cells present than C-Veh mice in the hippocampus (Figure 5.5.B). This difference was significant in the Ca1 and was trending in the Ca3 (Figure 5.5.C-E).

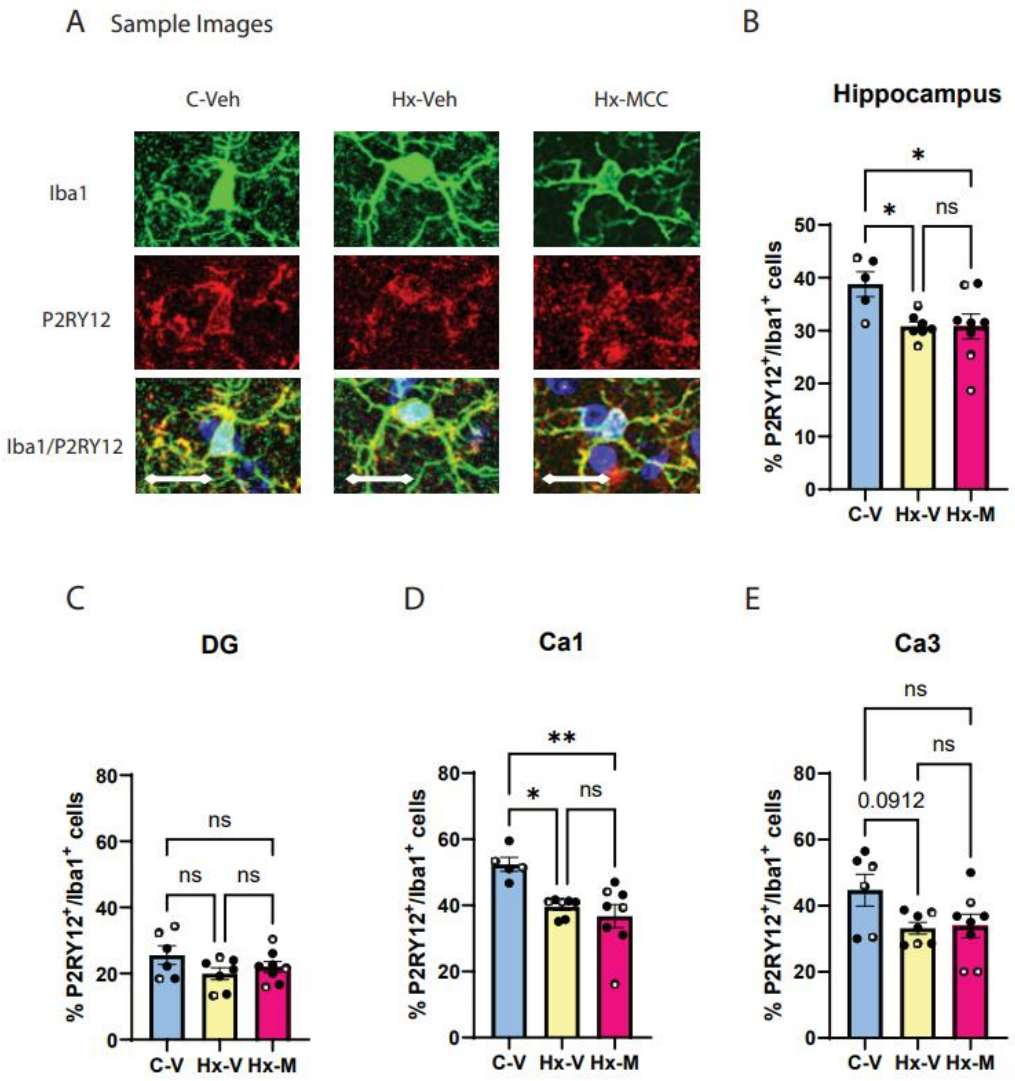


***Figure 5.5. P2RY12$^{+}$Iba1$^{+}$ cells are less abundant post-hypoxia relative to controls, with little differences found between Hx-Veh and Hx-MCC mice at either timepoint. (A)*** *Sample Images of P2RY12$^{+}$Iba1$^{+}$ cells. Scale bar 10µm.* ***(B)*** *C-V mice have higher percentages of P2RY12$^{+}$Iba1$^{+}$ cells in the*

*hippocampus relative to both Hx-V and Hx-M mice. C-V n=5, Hx-V n=7, Hx-M n=8. Hipp C-V vs Hx-V p=0.0419, Hx-V v Hx-M p>0.9999, C-V v Hx-M p=0.0358.* ***(C)*** *No significant differences emerge in the percentages of P2RY12$^{+}$Iba1$^{+}$ cells in the dentate gyrus. C-V n=5, Hx-V n=7, Hx-M n=8. Hipp C-V vs Hx-V p=0.1763, Hx-V v Hx-M p=0.7524, C-V v Hx-M p=0.4507.* ***(D)*** *C-V mice have higher percentages of P2RY12$^{+}$Iba1$^{+}$ cells present in the Ca1 relative to both Hx-V and Hx-M mice. C-V n=5, Hx-V n=7, Hx-M n=8. Hipp C-V vs Hx-V p=0.0151, Hx-V v Hx-M p=0.7135, C-V v Hx-M p=0.0028.* ***(E)*** *C-V mice trend towards higher percentages of P2RY12$^{+}$Iba1$^{+}$ cells present in the Ca3 relative to both Hx-V and Hx-M mice. C-V n=5, Hx-V n=7, Hx-M n=8. Hipp C-V vs Hx-V p=0.0912, Hx-V v Hx-M p=0.9885, C-V v Hx-M p=0.1041. One-way ANOVA with Tukey's post-hoc, $p < 0.05$. In all graphs, female mice are white circles, male mice are black circles.*

## 5.4. Discussion

This study examined the merits of using a neuroinflammatory therapeutic approach outside the traditional treatment window, and whether this provides any significant rescuing effect. As discussed in the introduction, the current methods for acute diagnosis of brain damage or seizures in neonates leave much to be desired. Optimal treatment strategies for treating HIE and neonatal seizures still come with significant risks, as they may exacerbate damage caused by HIE or cause unwanted side effects. In therapeutic hypothermia (TH), these risks are particularly associated with the rewarming period, a high-risk period for worsening encephalopathy (Kendall et. al., 2012). Anti-convulsant drugs such as PhB are only effective in 50% of neonates, with the rest experiencing either no change or a worsening of seizures. Furthermore, anticonvulsant treatment in the neonatal stage is associated with poorer neurodevelopmental outcomes later in life (Maitre et. al., 2013; Ghosh et. al., 2019; Liu et. al., 2020). By applying treatment in the weeks or months following injury, clinicians have time to definitively diagnose an infant with HIE retrospectively and treat as appropriate. The previous two chapters have shown that a chronic increase in pro-inflammatory microglia in the hippocampus is a defining characteristic of the tertiary phase post-hypoxia in this moderate injury model. This is supported by models of severe HIE which found elevated microglia populations and inflammatory markers expressed months after the hypoxic insult, and human studies which found chronically elevated cytokines (Bona et. al., 1999; Jenkins et. al., 2012).

The adult behaviour assessments were initiated 6 days after the last MCC950 injection. The open field reaffirmed that there were no motor deficits caused by hypoxia that could confound the other behavioural assessments. As in previous chapters, the NOL task measured spatial memory, as governed by the dorsal Ca1 region of the hippocampus (Geiller et. al., 2023) and

the LDB test measured anxiety, governed in part by the ventral hippocampus (Bannerman et. al., 2014). MCC950 treatment post-weaning partially recovered spatial memory in this task; hypoxia-vehicle mice perform significantly worse than control mice, and the hypoxia-MCC950 mice only perform slightly worse than the control mice. In the LDB test, MCC950-treated mice spent less time exploring the light before entering the dark box relative to hypoxia-vehicle mice, suggesting that this anxiety, manifesting as a longer time exploring the "danger zone" (light region) is rescued by MCC950 treatment. These results show that MCC950 administered later in life can still rescue the cognitive effects of chronic inflammation in the hippocampus after global hypoxia. As discussed previously, models of neurodegeneration found that treatment with MCC950 after the onset of neurodegeneration positively impacted on cognition and memory deficits (Heneka et. al., 2013; Dempsey et. al., 2017). These models further corroborate the potential merits of anti-inflammatory treatments against neurodegeneration with a strong neuroinflammatory component, such as AD or HIE.

The second part of this study was the microglia analysis. There was a significant reduction of $CD68^{+}Iba1^{+}$ phagocytic microglia in the hypoxia-MCC mice, which had similar proportions of pro-inflammatory microglia and phenotypes as controls. This was not reflected in the $P2RY12^{+}Iba1^{+}$ analysis, which saw no differences between hypoxia-vehicle and hypoxia-MCC mice, and both cohorts had significantly lower proportions of $P2RY12^{+}$ microglia than the control group. The proportions of $CD68^{+}$ microglia differ from those seen in Results Chapter 2, but the proportions of $P2RY12^{+}$ microglia echo those seen previously. The reduced expression of CD68 and pro-inflammatory microglia after MCC950 treatment contradicts what has been seen previously in models of AD (Dempsey et. al., 2017; McManus et. al., 2025), where upregulation of CD68 and pro-inflammatory microglia was seen alongside profound cognitive attenuations. Previous studies administered a P2X7R inhibitor from 24 hours post-

hypoxia for 1 week and rescued later-life hyperexcitability (Smith et. al., 2023). These studies provide a template for future studies to find an optimal therapeutic window for anti-inflammatory treatment and NLRP3 inflammasome inhibition.

# Chapter 6: Discussion

This study characterises the inflammatory response mediated by microglia in a moderate model of hypoxia. Neurological deficits were assessed using neonatal reflex tests at 1- and 3-days post-hypoxia, followed by behavioural testing 4 weeks post-hypoxia. Previous studies found a significant neuroinflammatory response acutely following global hypoxia (Rodriguez-Alvarez et. al., 2017; Quinlan et. al., 2019), and in animal and human studies of severe HIE, pro-inflammatory microglia and pro-inflammatory markers remain elevated for months (Bona et. al., 1999; Winerdal et. al., 2012; Jenkins et. al., 2012). Previous work noted that components of the NLRP3 inflammasome, caspase-1 and IL-1β were upregulated in the hippocampus acutely post-hypoxia (Rodriguez-Alvarez et. al., 2017) and that treatment with a broad-spectrum anti-inflammatory compound was neuroprotective (Quinlan et. al., 2019). Therefore, mice were treated with MCC950, an NLRP3 inhibitor, immediately post-hypoxia, and while it somewhat reduced the acute inflammatory response, it had little impact on microglial activation chronically, and attenuated neonatal reflexes, spatial memory, and anxiety. Expanding on these findings, a second approach was applied, whereby MCC950 was administered two weeks after hypoxia for 5 days to target the chronic immune response. There were attenuations in behaviour and pro-inflammatory microglia.

### 6.1. Characterising Changes in Neonatal Reflex Development

For the first time in this model, we performed a deep characterisation of microglia and behaviour studies acute and chronically. Hypoxia negatively impacted the general wellbeing of pups and the development of vestibular responses, proprioception, rostro-caudal gradient of limb movement and forelimb grip strength. These results are consistent with previous literature in models of severe HIE (Heyser et. al., 2003; Sun et. al., 2015; Feather-Schussler & Ferguson., 2016) and human studies, where mild HIE results in poorer developmental test performance (Halliglu et. al., 2001; Park et. al., 2023; Törn et. al., 2023). Studies of mild HIE in

humans have found that MRI abnormalities correlate with poorer performance in developmental testing in infancy (Chalak et. al., 2018; Reiss et. al., 2020), even after treatment with therapeutic hypothermia (TH) (Massaro et. al., 2015). Furthermore, murine studies found that neonatal inflammation contributes to developmental white matter injury (Favrais et. al., 2011; Holloway et. al., 2021). Therefore, our results support the translatability of this model in precipitating the same developmental deficits seen in humans with mild to moderate HIE.

Treatment with MCC950 immediately post-hypoxia provided improvements in overall reflex development; the main deficit which MCC950 failed to improve was the delayed transition from crawling to walking post-hypoxia, although some postural improvements were noted. While not all reflexes were attenuated, there was still an overall neuroprotective effect. NLRP3 inhibition with an N-acetylserotonin derivative post-HIE improved performance in the negative geotaxis and the surface righting tests (Luo et. al., 2021). Given the associations between HIE and poorer reflex development, the improvements found in this study and in the literature are supported by research showing that NLRP3 inhibition can rescue developmental outcomes in HIE. While previous studies focused on white matter injury and myelination deficits (Zhu et. al., 2021), our study further increases our knowledge of the pathophysiology of HIE by evaluating the role of microglia and neonatal inflammation (Holloway et. al., 2021). Other treatment studies have shown variability in neonatal reflex attenuations. TH treatment post-HIE improved negative geotaxis scores, but not forelimb grip strength or surface righting (Diaz et. al., 2017), whereas melatonin (MT) treatment improved all neonatal reflexes (Wang et al 2013), a finding supported by improved Denver scores in humans treated with MT and TH post-HIE (Aly et. al., 2015).

This thesis provides compelling evidence in support of neonatal reflex testing as an effective measure of neurodevelopmental deficits in a model of moderate global hypoxia. This work also supports previous findings that anti-inflammatory treatment, particularly NLRP3 inflammasome inhibition, post-hypoxia and post-HIE is neuroprotective, attenuating neonatal reflex development.

### 6.2. Understanding Long-term Effects on Hippocampal Behaviour at Adolescence

This study found that hypoxia caused increased anxiety and impaired spatial memory, as previously published (Rodriguez-Alvarez et. al., 2015; Quinlan et. al., 2018), and hypoxia males were particularly vulnerable to increased compulsivity or repetitive behaviours. Anxiety and spatial memory are governed by the dorsal and ventral regions of the hippocampus Ca1 respectively (Bannerman et. al., 2014; Geiller et. al., 2023), whereas repetitive behaviours are governed by the cortico-basal ganglia-thalamic pathway (Garnet et. al., 2004; Garner., 2005), connected to the hippocampus via the amygdala and the striatum, and there is evidence that hippocampal dysfunction can increase repetitive behaviours (Feduccia et. al., 2012; Ciocchi et. al., 2015). Neurodevelopmental deficits in adolescence and adulthood are widely reported in animal models ranging from mild to severe HIE, many of which have also found increased neuroinflammation (Bona et. al., 1999; Caputa et. al., 2005; Cardoso et. al., 2015; Min et. al., 2020; Yang et. al., 2023). Furthermore, long-term human studies have shown that even mild HIE causes long-lasting neurodevelopmental deficits (Shankaran et. al., 2012; Ahearne et. al., 2016; Conway et. al., 2018; Akula et. al., 2023). As discussed previously, the hippocampus is particularly vulnerable to hypoxia and inflammatory insults due to its higher density of immunoreactive receptors, thus the widely reported changes in these hippocampal-directed behaviours (Williamson & Bilbo., 2013).

MCC950 treatment immediately post-hypoxia improved both anxiety and spatial memory, corroborating previous findings that these hippocampal behaviours are improved by anti-inflammatory treatment post-hypoxia (Quinlan et. al., 2019). Studies of severe HIE have also found cognitive attenuations upon suppression of the NLRP3 inflammasome (Chen et. al., 2023; Tao et. al., 2024). MCC950 rescued deficits in spatial learning and memory in models of traumatic brain injury (Xu et. al., 2018), stroke (Li et. al., 2020), and anxiety in sepsis-associated encephalopathy (Fu et. al., 2019). When MCC950 was administered from PND21 to PND26, anxiety was significantly improved, but spatial memory was only partially attenuated. Therefore, targeting chronic inflammasome activation later in life post-hypoxia can still provide some benefits in rescuing hippocampal-directed behaviours. This aligns with previous findings, where MCC950 positively impacted on cognition and memory deficits in models of AD (Heneka et. al., 2013; Dempsey et. al., 2017; McManus et. al., 2025) and support the potential therapeutic benefits of later-term anti-inflammatory treatments against conditions with a strong neuroinflammatory pathophysiology, such as Alzheimer's Disease or HIE.

These results show that neuroinflammation contributes to the deficits in hippocampal-directed behaviours post-HIE, evidenced by the neuroprotective effects of anti-inflammatory agents, seen here and previously in this model (Quinlan et. al., 2019). Microglia, the glial cells studied in this thesis, are extremely important to the dynamic environment within the hippocampus throughout life, particularly during the neonatal period where they are responsible for supporting neurodevelopmental processes. Altered microglial activity caused by inflammatory or environmental stressors during the neonatal period has been linked to long-lasting alterations of developmental processes, including behaviour, which persist into adulthood (Smith et. al., 2014; Umekawa et. al., 2015; Delpech et. al., 2016). Furthermore,

the inflammasome is potentially a key driver of the microglial alterations which precipitate these deficits, given the extent of the attenuations provided by inhibiting this one pathway.

### 6.3. Microglia Density and Morphological Studies

Previous work showed that microglia were more abundant in the hippocampus 72 hours post-hypoxia (Quinlan et. al., 2019). In this study, microglia were more abundant at 72 hours post-hypoxia and remained so at 5 weeks post-hypoxia. This is corroborated by studies which have shown a significant accumulation of microglia in the brain regardless of HIE severity (Del Bigio & Becker., 1994; Liu & McCullough., 2013; Min et. al., 2020; Serdar et. al., 2019). When microglia were further characterized in phenotypic subtypes (Diz Chaves et al., 2012), microglia from hypoxia pups had swollen bodies and shorter, less complex dendrites; a phenotype related to pro-inflammatory microglia. These findings are supported by the chronic upregulation of pro-inflammatory markers in the brain post-HIE (Stridh et. al., 2011; Winerdal et. al., 2012; Lalancette-Hébert et. al., 2017).

### 6.4. Differences in Markers for Phagocytic and Homeostatic Microglia

As discussed previously, CD68 and P2RY12 were used to identify pro-inflammatory and homeostatic microglia respectively. $CD68^{+}$ microglia were more abundant at both 72 hours and 5 weeks post-hypoxia and had pro-inflammatory phenotypes, validating Type IV and Type V morphologies as indicative of pro-inflammatory microglia and showing that phagocytosis is inappropriately upregulated far beyond the injury stage. Similar upregulation of CD68 has been reported acutely post-HIE (Li et. al., 2017; Lv et. al., 2020; Han et. al., 2024), and enrichment of phagosome pathways by KEGG pathway analysis (Tao et. al., 2024). Fewer $P2RY12^{+}$ microglia were present in the hippocampus post-hypoxia acutely and chronically, as previously reported 72 hours post-hypoxia (Smith et. al., 2024). Downregulated P2RY12 is

associated with a functional shift towards more pro-inflammatory or phagocytic microglia (Koizumi et. al., 2013), as seen in models of neonatal stroke (Rayasam et. al., 2020) and neonatal inflammation (Dufour et. al., 2025). Previous work found that principal excitatory neurons had features consistent with under-pruning 5 weeks post-hypoxia in the *stratum oriens* of the Ca1 (Quinlan et. al., 2019. Similar features were recorded in subplate neurons of the auditory cortex 3 weeks post-HIE (Sheikh et. al., 2019; 2022). Postmortem studies of six neonates with HIE found somatostatin and neuropeptide Y expression, two markers for GABAergic hippocampal interneurons, were reduced in the *stratum oriens* and pyramidal cell layer of the Ca1, indicating impaired hippocampal function (González Fuentes et. al., 2021). There is compelling evidence to suggest that the chronic over-expression of CD68 and under-expression of P2RY12 induced by hypoxia hinders microglial engagement in development-associated functions, such as synaptic pruning (Schafer et. al., 2012), chemotaxis (Haynes et. al., 2006), maintenance of ramified morphology (Sipe et. al., 2016) and repair of a compromised blood brain barrier (Luo et. al., 2016), causing behavioural deficits characterised in this thesis, potentially due to altered neuronal morphology.

When MCC950 was administered immediately post-hypoxia, expression of both CD68 and P2RY12 was unchanged at acute and chronic timepoints, although at 72 hours post-hypoxia MCC950 treatment caused a significant downregulation of Type V ameboid $CD68^{+}$ microglia versus vehicle-treated hypoxia mice. Neonatal reflexes and adult behaviour assessments demonstrated the neuroprotective effects of MCC950: therefore, there may be alternative, non-inflammatory, mechanisms directing the microglial phagocytic lysosome expression post-HIE and MCC950 treatment. The unchanged expression of $CD68^{+}$ microglia acutely is in slight disagreement with the literature, where NLRP3 inflammasome inhibition reduced expression of CD68 and pro-inflammatory microglia in the days following HIE (Lv et. al., 2020; Luo et. al.,

2021), although none evaluated CD68 expression in the weeks post-hypoxia. Models of AD demonstrated increased expression of CD68 and microglia-mediated phagocytosis in the weeks and months post-MCC950 treatment (Dempsey et. al., 2017; He et. al., 2020), and chronic inhibition of NLRP3 increased expression of microglial metabolic and phagocytic pathways (McManus et. al., 2025). Furthermore, $CD68^{+}$ microglia in these studies also expressed Arg1, a classic marker for anti-inflammatory microglia (Cherry et. al., 2015; Dempsey et. al., 2017; He et. al., 2020). Therefore, increased phagocytosis in these AD models is potentially governed by alternative, anti-inflammatory pathways to promote the clearance of Aβ, contributing to the cognitive attenuations also recorded (Dempsey et. al., 2017; He et. al., 2020). Upon administration of MCC950 from PND21 to PND26, $CD68^{+}$ microglia were significantly reduced with no changes in $P2RY12^{+}$ microglia.

As demonstrated above, neonatal HIE has deleterious effects on neuronal morphology and hippocampal function, accompanied by significant accumulations of microglia (Del Bigio & Becker., 1994; Quinlan et. al., 2019; González Fuentes et. al., 2021; Sheikh et. al., 2019; 2022). Treatment with MCC950, while neuroprotective, still results in upregulated phagocytic microglia, leading to the hypothesis that neurodevelopmental phagocytosis is causing CD68 upregulation, the likes of which is seen in synaptic pruning and mediated by the complement pathway (Schafer et. al., 2012; Weinhard et. al., 2018). In Results Chapter 2, components of the classical complement pathway were significantly upregulated by MCC950 treatment at PND7 72 hours post-hypoxia. While this has not been studied with respect to the complement pathway, MCC950 treatment rescued neuronal and myelin damage in a model of experimental autoimmune encephalitis (EAE) (Hou et. al., 2024), ameliorated structural plasticity of dendrites in the hippocampal dentate gyrus of socially isolated male mice (Li et. al., 2021b) and rescued reduced expression of synaptophysin and PSD-95 in the hippocampus post-HIE in

mice (Yang et. al., 2023). Future studies could investigate how MCC950 post-hypoxia impacts on dendrite morphology in the Ca1 and compare the two treatment regimens to understand how the differing microglial responses between regimens is reflected in dendritic morphology. Future studies could also investigate alternative treatment courses using different time points or dosage regimens post-hypoxia to identify an optimal therapeutic strategy for MCC950 treatment.

### 6.5. Effects of MCC950 on Markers for Neuroinflammation

As discussed previously, pro-IL-1β and pro-IL-18 are cleaved by caspase 1 in the inflammasome to release their active forms which go on to participate in the inflammatory response. MCC950 was most effective in dampening IL-1β expression 3 hours post-hypoxia, although this effect diminished with time. The dampening of IL-1β expression is supported by the literature in models of HIE and other disorders such as AD and EAE (Coll et. al., 2015; Dempsey et. al., 2017; Chen et. al., 2018; Lv et. al., 2020).

At 3 hours and 5 weeks post-hypoxia, TNF-α mRNA expression was upregulated in vehicle and MCC950 hypoxia mice versus controls. Elevated expression of TNF-α supports the increased $CD68^{+}$ microglia in both groups at acute and chronic timepoints and is supported by the literature. MCC950 does not change TNF-α mRNA levels expressed by microglia after stimulation with LPS or Aβ-induced inflammasome activation (McManus et. al., 2025) and does not change TNF-α gene and protein expression in models of AD (Dempsey et. al., 2017), TBI (Ismael et. al., 2018) and EAE (Coll et. al., 2015). Similarly, IL-6 expression was unchanged by MCC950 treatment. A consensus has yet to be reached on the effects of MCC950 on IL-6 expression; in a model of AD, IL-6 expression was unaffected by MCC950 (Dempsey et. al., 2017), yet IL-6 expression was downregulated by MCC950 in models of intracerebral

haemorrhage (Ren et. al., 2018), EAE (Coll et. al., 2015) and early brain injury (Luo et. al., 2019).

CXCR3, the microglial chemokine receptor, was overexpressed 24 hours post-hypoxia and MCC950 treatment and slightly reduced at 5 weeks post-hypoxia. The chronic downregulation of CXCR3 is also supported by the literature, as CXCL10/CXCR3 signalling has been associated with impaired synaptogenesis and long-term behavioural deficits in a rat model of neonatal hyperglycaemia, a less common aetiology of NE (Satrom et. al., 2018).

As discussed, MCC950 treatment post-hypoxia is neuroprotective, leading to the hypothesis that the chronic upregulation of phagocytic $CD68^{+}$ microglia by MCC950 is homeostatic, as seen in models of AD (Dempsey et. al., 2017; He et. al., 2020; McManus et. al., 2025) and may be governed by the complement pathway. The complement pathway is widely expressed and important to the innate immune response, with complement-mediated phagocytosis and trogocytosis integral to synaptic pruning and elimination by microglia during the neonatal phase (Schafer et. al., 2012; Weinhard et. al., 2018). As hypothesised, MCC950 treatment chronically upregulated classical complement pathway initiation, and acutely upregulated classical complement pathway components C1qR1 and C3 at 72 hours post-hypoxia. So far there is a gap in the literature regarding the effects of NLRP3 inflammasome inhibition on complement-mediated phagocytosis during neurodevelopment. This thesis provides "circumstantial evidence" to support the role of complement in the neuroprotective effects of MCC950, as the complement pathway is the main mediator of homeostatic phagocytosis and opens the opportunity for future work to fully probe this relationship, and how this relates to the altered dendritic morphology seen chronically post-hypoxia (Quinlan et. al., 2019).

### 6.6. Limitations

No body of work is without its limitations, and this thesis is no exception. While the model presented has been carefully designed to offer a strong likeness to moderate HIE, it can only go so far in emulating the complex presentations observed in the human condition. This limitation is an unavoidable truth for all experiments which utilise rodent models to simulate a human condition. With this limitation in mind, previous work in this model has demonstrated key features which support its translatability to the human condition, such as a 56% positive response to phenobarbital (Quinlan et. al., 2018) and chronic hyperexcitability (Rodriguez-Alvarez et. al., 2015), which correspond with 50% response rate to phenobarbital and higher risks of developing epilepsy later in life for surviving infants.

The main body of molecular work in this model relied on immunofluorescence, staining for microglia and microglia-specific markers and using confocal microscope images to perform manual cell counting and morphological analyses. The first limitation was the lack of automation employed in these processes, opening the door to human error or subconscious subjectivity. Several programs, such as Analyse Skeleton (Image J) and 3D Morph (MATLAB, Young et. al., 2018) were trialled extensively to automate cell counting and morphological analyses, but these ultimately were unsuccessful. These automated methods would also have been unsuitable for analysing double-stained images as they were not designed to identify co-labelled cells. Ultimately, it was decided that manual counting was suitable for these experiments, but that it would be a future goal of the Jimenez laboratory to identify more suitable means for automating these analyses. Another limitation of the immunofluorescence study was the use of Iba1 as the marker for microglia. Iba1 is expressed abundantly on microglia and macrophages, so ultimately there were no means by which to discern microglia with active morphologies from infiltrating macrophages, nor could $CD68^{+}Iba1^{+}$ cells be truly

discerned from infiltrating phagocytic macrophages. Previous work in the laboratory has determined that, despite this limitation, Iba1 remains the superior marker for imaging microglia, as more specific markers such as TMEM119 are not expressed in the brain tissue of young mice to the levels required for accurate morphological analysis. CD68 also remains the superior marker for identifying phagocytic lysosomes in the brain and is widely used in the literature for similar characterisations of microglial-mediated phagocytosis.

The molecular studies in Results Chapter 2 gave a deeper insight into the inflammatory mechanisms post-hypoxia and how they are impacted by MCC950 treatment. Therefore, a limitation of the study presented in Results Chapter 3 was the lack of molecular studies investigating inflammatory markers and the complement pathway. These studies were omitted due to time constraints for the submission of this thesis. Despite the omission of these results, there are still significant changes recorded in Results Chapter 3 which make these molecular studies a worthwhile future direction for the Jimenez laboratory.

### 6.7. Conclusions

In conclusion, this thesis provides compelling evidence of an acute and chronic inflammatory response in the hippocampus after moderate global hypoxia, a significant driver of which is microglia. This supports previous findings in this model and others that there is a significant chronic immune response post-HIE (Bona et. al., 1999; Winerdal et. al., 2012), and that even moderate HIE leaves the brain more prone to hyperexcitability both acutely and chronically post-hypoxia (Rodriguez-Alvarez et. al., 2015; Quinlan et. al., 2018; 2019). These changes are reflected in the delayed consolidation of neonatal reflexes, which reflect the white matter damage already described in the literature (Izbudak & Grant., 2011; Machie et. al., 2021), and the persistent deficits in hippocampus-related behaviours such as spatial memory and anxiety.

Inhibition of the NLRP3 inflammasome immediately post-hypoxia causes distinct changes in hippocampal microglia and inflammatory marker expression. MCC950 partially attenuated neonatal reflexes and provided significant recovery to the post-hypoxia hippocampal-directed behavioural deficits, leading to the conclusion that MCC950 may provide limited protection against the white matter damage reflected in the neonatal reflexes, but has a more profound protective effect on the hippocampus, a region with the highest density of microglia, immunoreceptors and baseline IL-1β signalling in the brain. The results of Chapter 2 have opened a door to new research into the role of complement-mediated phagocytosis in the neuroprotective effects of NLRP3 inhibition. The neuroprotection provided by NLRP3 inhibition later in life, while less profound than the earlier treatment strategy, still proves that anti-inflammatory treatment long after the traditional therapeutic window can still have a positive impact. Current diagnostic and treatment strategies are restricted to an incredibly narrow therapeutic window of six hours post-injury, highlighting a significant unmet clinical need (Aslam et. al., 2018; Pressler et. al., 2021; Molloy et. al., 2023). Our findings are supported by the literature where the therapeutic potential of later term anti-inflammatory treatment has been demonstrated in models of HIE (Chakkarpani et. al., 2021; Smith et. al., 2023). This is also supported by studies in models of AD, where MCC950 administered long after disease onset still improves on hippocampal behaviours and cognitive deficits in models of neurodegeneration (Dempsey et. al., 2017; Lučiūnaitė et. al., 2019). The results of this thesis, combined with previous evidence in the literature, highlight the potential of NLRP3 inflammasome inhibition as promising therapeutic strategy for moderate hypoxia.

## 6.8. Future Directions

Future directions for this study can use several methods to validate the findings of this thesis and to more comprehensively understand the role of MCC950 in precipitating the positive effects characterised in this moderate model of hypoxia.

- To follow up on the findings of Results Chapter 1, researchers can investigate how to automate microglial counting and morphological analysis. While every effort was made to perform this analysis objectively, automation of this process may prove more robust and less time costly.
- By carrying out neuronal morphological studies of pyramidal neurons in the Ca1, one can elucidate whether the behavioural improvements observed in this thesis are due to a reversal of the long-lasting structural changes in neurons previously observed in this model. Expanding on this, future studies can also understand whether MCC950 can reduce long-lasting hyperexcitability as seen before following anti-inflammatory treatment (Quinlan et. al., 2019).
- Future studies can also perform more detailed analyses of complement marker expression with other methods such as immunofluorescence or Western Blot, investigating how these markers are affected by the later term treatment protocol employed in Results Chapter 3. Furthermore, immunofluorescence can be used to study the colocalization of microglial or neuronal markers and complement proteins to understand how MCC950 affects the distribution of these proteins in the brain acutely and chronically post-hypoxia.

# Bibliography

Addison CL, Daniel TO, Burdick MD, Liu H, Ehlert JE, Xue YY, Buechi L, Walz A, Richmond A, Strieter RM (2000) The CXC Chemokine Receptor 2, CXCR2, Is the Putative Receptor for ELR+ CXC Chemokine-Induced Angiogenic Activity. The Journal of Immunology 165:5269–5277.

Aderem A, Ulevitch RJ (2000) Toll-like receptors in the induction of the innate immune response. Nature 406:782–787.

Agostini L, Martinon F, Burns K, McDermott MF, Hawkins PN, Tschopp J (2004) NALP3 Forms an IL-1β-Processing Inflammasome with Increased Activity in Muckle-Wells Autoinflammatory Disorder. Immunity 20:319–325.

Ahearne CE, Boylan GB, Murray DM (2016) Short and long term prognosis in perinatal asphyxia: An update. World J Clin Pediatr 5:67–74.

Ahmad QM, Chishti AL, Waseem N (2018) Role of melatonin in management of hypoxic ischaemic encephalopathy in newborns: A randomized control trial. J Pak Med Assoc 68:1233–1237.

Ahmadpour-Kacho M, Zahedpasha Y, Hagshenas M, Akbarian Rad Z, Sadat Nasseri B, Bijani A (2015) Short Term Outcome of Neonates Born With Abnormal Umbilical Cord Arterial Blood Gases. Iran J Pediatr 25:e174.

Aker K, Støen R, Eikenes L, Martinez-Biarge M, Nakken I, Håberg AK, Gibikote S, Thomas N (2019) Therapeutic hypothermia for neonatal hypoxic-ischaemic encephalopathy in India (THIN study): a randomised controlled trial. Arch Dis Child Fetal Neonatal Ed:fetalneonatal-2019-317311.

Akula V-P, Sriram A, Xu S, Walsh E, Van Meurs K, Cranshaw M, Kuzniewicz MW (2023) Adverse short- and long-term outcomes among infants with mild neonatal encephalopathy. Pediatr Res 94:1003–1010.

Al Mamun A, Yu H, Romana S, Liu F (2018) Inflammatory Responses are Sex Specific in Chronic Hypoxic–Ischemic Encephalopathy. Cell Transplant 27:1328–1339.

Alonso-Alconada D, Alvarez A, Arteaga O, Martínez-Ibargüen A, Hilario E (2013) Neuroprotective effect of melatonin: a novel therapy against perinatal hypoxia-ischemia. Int J Mol Sci 14:9379–9395.

Alonso-Alconada D, Broad KD, Bainbridge A, Chandrasekaran M, Faulkner SD, Kerenyi Á,

Hassell J, Rocha-Ferreira E, Hristova M, Fleiss B, Bennett K, Kelen D, Cady E, Gressens P, Golay X, Robertson NJ (2015) Brain Cell Death Is Reduced With Cooling by 3.5°C to 5°C but Increased With Cooling by 8.5°C in a Piglet Asphyxia Model. Stroke 46:275–278.

Althaus HH, Klöppner S, Klopfleisch S, Schmitz M (2008) Oligodendroglial Cells and Neurotrophins: A Polyphonic Cantata in Major and Minor. J Mol Neurosci 35:65–79.

Aly H, Elmahdy H, El-Dib M, Rowisha M, Awny M, El-Gohary T, Elbatch M, Hamisa M, El-Mashad A-R (2015) Melatonin use for neuroprotection in perinatal asphyxia: a randomized controlled pilot study. J Perinatol 35:186–191.

Andjelkovic AV, Nikolic B, Pachter JS, Zecevic N (1998) Macrophages/microglial cells in human central nervous system during development: an immunohistochemical study. Brain Research 814:13–25.

Arrant AE, Schramm-Sapyta NL, Kuhn CM (2013) Use of the light/dark test for anxiety in adult and adolescent male rats. Behav Brain Res 256:119–127.

Aslam S, Strickland T, Molloy EJ (2019) Neonatal Encephalopathy: Need for Recognition of Multiple Etiologies for Optimal Management. Front Pediatr 7

Badawi N, Kurinczuk JJ, Keogh JM, Alessandri LM, O'Sullivan F, Burton PR, Pemberton PJ, Stanley FJ (1998) Antepartum risk factors for newborn encephalopathy: the Western Australian case-control study. BMJ 317:1549–1553.

Balasubramaniam J, Xue M, Buist RJ, Ivanco TL, Natuik S, Del Bigio MR (2006) Persistent motor deficit following infusion of autologous blood into the periventricular region of neonatal rats. Experimental Neurology 197:122–132.

Balschun D, Wetzel W, Del Rey A, Pitossi F, Schneider H, Zuschratter W, Besedovsky HO (2004) Interleukin-6: a cytokine to forget. FASEB J 18:1788–1790.

Bannerman DM, Sprengel R, Sanderson DJ, McHugh SB, Rawlins JNP, Monyer H, Seeburg PH (2014) Hippocampal synaptic plasticity, spatial memory and anxiety. Nat Rev Neurosci 15:181–192.

Bast T, Zhang WN, Feldon J (2001) Hippocampus and classical fear conditioning. Hippocampus 11:828–831.

Beamer E, O'Dea MI, Garvey AA, Smith J, Menéndez-Méndez A, Kelly L, Pavel A, Quinlan S, Alves M, Jimenez-Mateos EM, Tian F, Dempsey E, Dale N, Murray DM, Boylan GB, Molloy EJ, Engel T (2021) Novel Point-of-Care Diagnostic Method for Neonatal

Encephalopathy Using Purine Nucleosides. Front Mol Neurosci 14

Beattie EC, Stellwagen D, Morishita W, Bresnahan JC, Ha BK, Von Zastrow M, Beattie MS, Malenka RC (2002) Control of Synaptic Strength by Glial TNFα. Science 295:2282–2285.

Becker CE, O'Neill LAJ (2007) Inflammasomes in inflammatory disorders: the role of TLRs and their interactions with NLRs. Semin Immunopathol 29:239–248.

Bhattacharyya BJ, Banisadr G, Jung H, Ren D, Cronshaw DG, Zou Y, Miller RJ (2008) The Chemokine Stromal Cell-Derived Factor-1 Regulates GABAergic Inputs to Neural Progenitors in the Postnatal Dentate Gyrus. J Neurosci 28:6720–6730.

Bhatti A, Kumar P (2014) Systemic Effects of Perinatal Asphyxia. Indian J Pediatr 81:231–233.

Bilbo SD, Schwarz JM (2012) The immune system and developmental programming of brain and behavior. Frontiers in Neuroendocrinology 33:267–286.

Bittigau P, Sifringer M, Genz K, Reith E, Pospischil D, Govindarajalu S, Dzietko M, Pesditschek S, Mai I, Dikranian K, Olney JW, Ikonomidou C (2002) Antiepileptic drugs and apoptotic neurodegeneration in the developing brain. Proc Natl Acad Sci USA 99:15089–15094.

Black RE, Cousens S, Johnson HL, Lawn JE, Rudan I, Bassani DG, Jha P, Campbell H, Walker CF, Cibulskis R, Eisele T, Liu L, Mathers C, Child Health Epidemiology Reference Group of WHO and UNICEF (2010) Global, regional, and national causes of child mortality in 2008: a systematic analysis. Lancet 375:1969–1987.

Blevins HM, Xu Y, Biby S, Zhang S (2022) The NLRP3 Inflammasome Pathway: A Review of Mechanisms and Inhibitors for the Treatment of Inflammatory Diseases. Front Aging Neurosci 14

Boerger W, Mozun R, Frey B, Liamlahi R, Grass B, Brotschi B (2024) Blood Lactate Levels during Therapeutic Hypothermia and Neurodevelopmental Outcome or Death at 18–24 Months of Age in Neonates with Moderate and Severe Hypoxic-Ischemic Encephalopathy. Neonatology:1–10.

Bona E, Andersson AL, Blomgren K, Gilland E, Puka-Sundvall M, Gustafson K, Hagberg H (1999) Chemokine and inflammatory cell response to hypoxia-ischemia in immature rats. Pediatr Res 45:500–509.

Boss V, Sola A, Wen T-C, Decker MJ (2005) Mild Intermittent Hypoxia Does Not Induce Stress Responses in the Neonatal Rat Brain. Neonatology 88:313–320.

Boucher D, Monteleone M, Coll RC, Chen KW, Ross CM, Teo JL, Gomez GA, Holley CL,

Bierschenk D, Stacey KJ, Yap AS, Bezbradica JS, Schroder K (2018) Caspase-1 self-cleavage is an intrinsic mechanism to terminate inflammasome activity. Journal of Experimental Medicine 215:827–840.

Boutaybi N, Razenberg F, Smits-Wintjens VEHJ, van Zwet EW, Rijken M, Steggerda SJ, Lopriore E (2014) Neonatal Thrombocytopenia after Perinatal Asphyxia Treated with Hypothermia: A Retrospective Case Control Study. International Journal of Pediatrics 2014:e760654.

Boylan GB, Kharoshankaya L, Wusthoff CJ (2015) Seizures and hypothermia: Importance of electroencephalographic monitoring and considerations for treatment. Seminars in Fetal and Neonatal Medicine 20:103–108.

Briggs SW, Galanopoulou AS (2011) Altered GABA Signaling in Early Life Epilepsies. Neural Plasticity 2011:1–16.

Brines M, Cerami A (2013) Erythropoietin and Engineered Innate Repair Activators. In: Tissue-Protective Cytokines: Methods and Protocols (Ghezzi P, Cerami A, eds), pp 1–11. Totowa, NJ: Humana Press.

Calvo JR, González-Yanes C, Maldonado MD (2013) The role of melatonin in the cells of the innate immunity: a review. J Pineal Res 55:103–120.

Campanella GSV, Tager AM, El Khoury JK, Thomas SY, Abrazinski TA, Manice LA, Colvin RA, Luster AD (2008) Chemokine receptor CXCR3 and its ligands CXCL9 and CXCL10 are required for the development of murine cerebral malaria. Proc Natl Acad Sci U S A 105:4814–4819.

Cao P et al. (2021) Early-life inflammation promotes depressive symptoms in adolescence via microglial engulfment of dendritic spines. Neuron 109:2573-2589.e9.

Caputa M, Rogalska J, Wentowska K, Nowakowska A (2005) Perinatal asphyxia, hyperthermia and hyperferremia as factors inducing behavioural disturbances in adulthood: a rat model. Behav Brain Res 163:246–256.

Cardoso FL, Herz J, Fernandes A, Rocha J, Sepodes B, Brito MA, McGavern DB, Brites D (2015) Systemic inflammation in early neonatal mice induces transient and lasting neurodegenerative effects. J Neuroinflammation 12:82.

Carloni S, Perrone S, Buonocore G, Longini M, Proietti F, Balduini W (2008) Melatonin protects from the long-term consequences of a neonatal hypoxic-ischemic brain injury in rats. Journal of Pineal Research 44:157–164.

Castelhano-Carlos MJ, Sousa N, Ohl F, Baumans V (2010) Identification methods in newborn C57BL/6 mice: a developmental and behavioural evaluation. Lab Anim 44:88–103.

Castellano B, Bosch-Queralt M, Almolda B, Villacampa N, González B (2016) Purine Signaling and Microglial Wrapping. In: Glial Cells in Health and Disease of the CNS (von Bernhardi R, ed), pp 147–165. Cham: Springer International Publishing.

Chalak LF, Nguyen K-A, Prempunpong C, Heyne R, Thayyil S, Shankaran S, Laptook AR, Rollins N, Pappas A, Koclas L, Shah B, Montaldo P, Techasaensiri B, Sánchez PJ, Sant'Anna G (2018) Prospective research in infants with mild encephalopathy identified in the first six hours of life: neurodevelopmental outcomes at 18–22 months. Pediatr Res 84:861–868.

Chapman KE, Raol YH, Brooks-Kayal A (2012) Neonatal seizures: controversies and challenges in translating new therapies from the lab to the isolette. European Journal of Neuroscience 35:1857–1865.

Chechik G, Meilijson I, Ruppin E (1998) Synaptic Pruning in Development: A Computational Account. Neural Computation 10:1759–1777.

Chen A, Xu Y, Yuan J (2018) Ginkgolide B ameliorates NLRP3 inflammasome activation after hypoxic-ischemic brain injury in the neonatal male rat. International Journal of Developmental Neuroscience 69:106–111.

Chen J, Chen ZJ (2018) PtdIns4P on dispersed trans-Golgi network mediates NLRP3 inflammasome activation. Nature 564:71–76.

Chen L, Deng H, Cui H, Fang J, Zuo Z, Deng J, Li Y, Wang X, Zhao L (2017) Inflammatory responses and inflammation-associated diseases in organs. Oncotarget 9:7204–7218.

Chen Y, Li X, Xiong Q, Du Y, Luo M, Yi L, Pang Y, Shi X, Wang YT, Dong Z (2023) Inhibiting NLRP3 inflammasome signaling pathway promotes neurological recovery following hypoxic-ischemic brain damage by increasing p97-mediated surface GluA1-containing AMPA receptors. J Transl Med 21:567.

Cheng J, Liao Y, Dong Y, Hu H, Yang N, Kong X, Li S, Li X, Guo J, Qin L, Yu J, Ma C, Li J, Li M, Tang B, Yuan Z (2020) Microglial autophagy defect causes parkinson disease-like symptoms by accelerating inflammasome activation in mice. Autophagy 16:2193–2205.

Chevin M, Guiraut C, Sébire G (2018) Effect of hypothermia on interleukin-1 receptor antagonist pharmacodynamics in inflammatory-sensitized hypoxic-ischemic encephalopathy of term newborns. J Neuroinflammation 15:214.

Cho BP, Song DY, Sugama S, Shin DH, Shimizu Y, Kim SS, Kim YS, Joh TH (2006) Pathological dynamics of activated microglia following medial forebrain bundle transection. Glia 53:92–102.

Ciocchi S, Passecker J, Malagon-Vina H, Mikus N, Klausberger T (2015) Brain computation. Selective information routing by ventral hippocampal CA1 projection neurons. Science 348:560–563.

Clapp JF, Peress NS, Wesley M, Mann LI (1988) Brain damage after intermittent partial cord occlusion in the chronically instrumented fetal lamb. American Journal of Obstetrics and Gynecology 159:504–509.

Cleary RT, Sun H, Huynh T, Manning SM, Li Y, Rotenberg A, Talos DM, Kahle KT, Jackson M, Rakhade SN, Berry G, Jensen FE (2013) Bumetanide Enhances Phenobarbital Efficacy in a Rat Model of Hypoxic Neonatal Seizures Avoli M, ed. PLoS ONE 8:e57148.

Cohen P (2014) The TLR and IL-1 signalling network at a glance. Journal of Cell Science:jcs.149831.

Coll RC et al. (2015) A small molecule inhibitior of the NLRP3 inflammasome is a potential therapeutic for inflammatory diseases. Nature medicine 21:248.

Conway JM, Walsh BH, Boylan GB, Murray DM (2018) Mild hypoxic ischaemic encephalopathy and long term neurodevelopmental outcome - A systematic review. Early Human Development 120:80–87.

Cornet M-C, Kuzniewicz M, Scheffler A, Forquer H, Hamilton E, Newman TB, Wu YW (2023) Perinatal Hypoxic-Ischemic Encephalopathy: Incidence over Time Within a Modern US Birth Cohort. Pediatr Neurol 149:145–150.

Corps KN, Roth TL, McGavern DB (2015) Inflammation and neuroprotection in traumatic brain injury. JAMA Neurol 72:355–362.

Cowell RM, Plane JM, Silverstein FS (2003) Complement Activation Contributes to Hypoxic-Ischemic Brain Injury in Neonatal Rats. J Neurosci 23:9459–9468.

Cunningham CL, Martínez-Cerdeño V, Noctor SC (2013) Microglia Regulate the Number of Neural Precursor Cells in the Developing Cerebral Cortex. J Neurosci 33:4216–4233.

Cunningham ET, De Souza EB (1993) Interleukin 1 receptors in the brain and endocrine tissues. Immunol Today 14:171–176.

Dalitz P, Harding R, Rees SM, Cock ML (2003) Prolonged Reductions in Placental Blood Flow and Cerebral Oxygen Delivery in Preterm Fetal Sheep Exposed to Endotoxin: Possible

Factors in Whitge Matter Injury After Acute Infection. Journal of the Society for Gynecologic Investigation 10:283–290.

De Haan HH, Gunn AJ, Williams CE, Gluckman PD (1997) Brief Repeated Umbilical Cord Occlusions Cause Sustained Cytotoxic Cerebral Edema and Focal Infarcts in Near-Term Fetal Lambs. Pediatr Res 41:96–104.

Deacon RMJ (2006) Burrowing in rodents: a sensitive method for detecting behavioral dysfunction. Nat Protoc 1:118–121.

Del Bigio MR, Becker LE (1994) Microglial aggregation in the dentate gyrus: a marker of mild hypoxic-ischaemic brain insult in human infants. Neuropathol Appl Neurobiol 20:144–151.

del Rey A, Balschun D, Wetzel W, Randolf A, Besedovsky HO (2013) A cytokine network involving brain-borne IL-1β, IL-1ra, IL-18, IL-6, and TNFα operates during long-term potentiation and learning. Brain, Behavior, and Immunity 33:15–23.

Delpech J-C, Wei L, Hao J, Yu X, Madore C, Butovsky O, Kaffman A (2016) Early life stress perturbs the maturation of microglia in the developing hippocampus. Brain, Behavior, and Immunity 57:79–93.

Dempsey C, Rubio Araiz A, Bryson KJ, Finucane O, Larkin C, Mills EL, Robertson AAB, Cooper MA, O'Neill LAJ, Lynch MA (2017) Inhibiting the NLRP3 inflammasome with MCC950 promotes non-phlogistic clearance of amyloid-β and cognitive function in APP/PS1 mice. Brain, Behavior, and Immunity 61:306–316.

Di Virgilio F, Sarti AC, Coutinho-Silva R (2020) Purinergic signaling, DAMPs, and inflammation. American Journal of Physiology-Cell Physiology 318:C832–C835.

Diaz J, Schain RJ (1978) Phenobarbital: effects of long-term administration on behavior and brain of artificially reared rats. Science 199:90–91.

Dinarello C (1996) Biologic basis for interleukin-1 in disease. Blood 87:2095–2147.

Ding W, Guo H, Xu C, Wang B, Zhang M, Ding F (2016) Mitochondrial reactive oxygen species-mediated NLRP3 inflammasome activation contributes to aldosterone-induced renal tubular cells injury. Oncotarget 7:17479–17491.

Dixit PV, Sahu R, Mishra DK (2020) Marble-burying behavior test as a murine model of compulsive-like behavior. Journal of Pharmacological and Toxicological Methods 102:106676.

Diz-Chaves Y, Pernía O, Carrero P, Garcia-Segura LM (2012) Prenatal stress causes alterations

in the morphology of microglia and the inflammatory response of the hippocampus of adult female mice. J Neuroinflammation 9:71.

Dobbing J, Sands J (1979) Comparative aspects of the brain growth spurt. Early Human Development 3:79–83.

Donovan MD, Griffin BT, Kharoshankaya L, Cryan JF, Boylan GB (2016) Pharmacotherapy for Neonatal Seizures: Current Knowledge and Future Perspectives. Drugs 76:647–661.

Drobyshevsky A, Song S-K, Gamkrelidze G, Wyrwicz AM, Derrick M, Meng F, Li L, Ji X, Trommer B, Beardsley DJ, Luo NL, Back SA, Tan S (2005) Developmental Changes in Diffusion Anisotropy Coincide with Immature Oligodendrocyte Progression and Maturation of Compound Action Potential. J Neurosci 25:5988–5997.

Duncan JA, Bergstralh DT, Wang Y, Willingham SB, Ye Z, Zimmermann AG, Ting JP-Y (2007) Cryopyrin/NALP3 binds ATP/dATP, is an ATPase, and requires ATP binding to mediate inflammatory signaling. Proc Natl Acad Sci USA 104:8041–8046.

Dunn AJ, Swiergiel AH, Zhang H, Quan N (2006) Reduced Ingestion of Sweetened Milk Induced by Interleukin-1 and Lipopolysaccharide Is Associated with Induction of Cyclooxygenase-2 in Brain Endothelia. Neuroimmunomodulation 13:96–104.

Dupont-Thibodeau A, Barrington K, Taillefer C, Janvier A (2017) Changes in perinatal hospital deaths occurring outside the neonatal intensive care unit over a decade. Acta Paediatr 106:1456–1459.

Evavold CL, Ruan J, Tan Y, Xia S, Wu H, Kagan JC (2018) The Pore-Forming Protein Gasdermin D Regulates Interleukin-1 Secretion from Living Macrophages. Immunity 48:35-44.e6.

Executive Summary (2014) Executive Summary: Neonatal Encephalopathy and Neurologic Outcome, Second Edition. Obstetrics & Gynecology 123:896.

Fahn S, Davis JN, Rowland LP eds. (1979) Cerebral hypoxia and its consequences. New York: Raven Press.

Favrais G, van de Looij Y, Fleiss B, Ramanantsoa N, Bonnin P, Stoltenburg-Didinger G, Lacaud A, Saliba E, Dammann O, Gallego J, Sizonenko S, Hagberg H, Lelièvre V, Gressens P (2011) Systemic inflammation disrupts the developmental program of white matter. Ann Neurol 70:550–565.

Feather-Schussler DN, Ferguson TS (2016) A Battery of Motor Tests in a Neonatal Mouse Model of Cerebral Palsy. JoVE (Journal of Visualized Experiments):e53569.

Feduccia AA, Chatterjee S, Bartlett SE (2012) Neuronal nicotinic acetylcholine receptors:

neuroplastic changes underlying alcohol and nicotine addictions. Front Mol Neurosci 5

Ferrari D, Pizzirani C, Adinolfi E, Lemoli RM, Curti A, Idzko M, Panther E, Di Virgilio F (2006) The P2X7 Receptor: A Key Player in IL-1 Processing and Release. The Journal of Immunology 176:3877–3883.

Figee M, Pattij T, Willuhn I, Luigjes J, van den Brink W, Goudriaan A, Potenza MN, Robbins TW, Denys D (2016) Compulsivity in obsessive–compulsive disorder and addictions. European Neuropsychopharmacology 26:856–868.

Fleiss B, Gressens P (2012) Tertiary mechanisms of brain damage: a new hope for treatment of cerebral palsy? Lancet Neurol 11:556–566.

Forcelli PA, Janssen MJ, Vicini S, Gale K (2012) Neonatal exposure to antiepileptic drugs disrupts striatal synaptic development. Ann Neurol 72:363–372.

Forcelli PA, Kim J, Kondratyev A, Gale K (2011) Pattern of antiepileptic drug–induced cell death in limbic regions of the neonatal rat brain. Epilepsia 52:e207–e211.

Frost JL, Schafer DP (2016) Microglia: Architects of the Developing Nervous System. Trends in Cell Biology 26:587–597.

Garner JP (2005) Stereotypies and other abnormal repetitive behaviors: potential impact on validity, reliability, and replicability of scientific outcomes. ILAR J 46:106–117.

Garner JP, Weisker SM, Dufour B, Mench JA (2004) Barbering (Fur and Whisker Trimming) by Laboratory Mice as a Model of Human Trichotillomania and Obsessive-Compulsive Spectrum Disorders. Comparative Medicine 54:216–224.

Geiller T, Priestley JB, Losonczy A (2023) A local circuit-basis for spatial navigation and memory processes in hippocampal area CA1. Curr Opin Neurobiol 79:102701.

Ghosh S, Cabassa Miskimen AC, Brady J, Robinson MA, Zou B, Weiss M, Kang PB (2019) Neurodevelopmental outcomes at 9–14 months gestational age after treatment of neonatal seizures due to brain injury. Childs Nerv Syst 35:1571–1578.

Ginhoux F, Greter M, Leboeuf M, Nandi S, See P, Gokhan S, Mehler MF, Conway SJ, Ng LG, Stanley ER, Samokhvalov IM, Merad M (2010) Fate Mapping Analysis Reveals That Adult Microglia Derive from Primitive Macrophages. Science 330:841–845.

Giorgi FS, Galanopoulou AS, Moshé SL (2014) Sex dimorphism in seizure-controlling networks. Neurobiology of Disease 72:144–152.

Glass HC (2014) Neonatal Seizures. Clinics in Perinatology 41:177–190.

Glass HC, Kan J, Bonifacio SL, Ferriero DM (2012) Neonatal Seizures: Treatment Practices Among Term and Preterm Infants. Pediatric Neurology 46:111–115.

Glass HC, Shellhaas RA, Wusthoff CJ, Chang T, Abend NS, Chu CJ, Cilio MR, Glidden DV, Bonifacio SL, Massey S, Tsuchida TN, Silverstein FS, Soul JS, Bergin AM, Dlugos D, Ferriero DM, Staley K (2016) Contemporary Profile of Seizures in Neonates: A Prospective Cohort Study. The Journal of Pediatrics 174:98-103.e1.

Glausier JR, Lewis DA (2013) Dendritic spine pathology in schizophrenia. Neuroscience 251:90–107.

Gómez Morillas A, Besson VC, Lerouet D (2021) Microglia and Neuroinflammation: What Place for P2RY12? Int J Mol Sci 22:1636.

Gonzalez FF, Larpthaveesarp A, McQuillen P, Derugin N, Wendland M, Spadafora R, Ferriero DM (2013) Erythropoietin increases neurogenesis and oligodendrogliosis of subventricular zone precursor cells after neonatal stroke. Stroke 44:753–758.

Gonzalez-Ibarra FP, Varon J, Lopez-Meza EG (2011) Therapeutic Hypothermia: Critical Review of the Molecular Mechanisms of Action. Front Neurol 2

Green HF, Nolan YM (2014) Inflammation and the developing brain: Consequences for hippocampal neurogenesis and behavior. Neuroscience & Biobehavioral Reviews 40:20–34.

Grell M, Douni E, Wajant H, Löhden M, Clauss M, Maxeiner B, Georgopoulos S, Lesslauer W, Kollias G, Pfizenmaier K, Scheurich P (1995) The transmembrane form of tumor necrosis factor is the prime activating ligand of the 80 kDa tumor necrosis factor receptor. Cell 83:793–802.

Grell M, Wajant H, Zimmermann G, Scheurich P (1998) The type 1 receptor (CD120a) is the high-affinity receptor for soluble tumor necrosis factor. Proc Natl Acad Sci U S A 95:570–575.

Guillot-Sestier M-V, Araiz AR, Mela V, Gaban AS, O'Neill E, Joshi L, Chouchani ET, Mills EL, Lynch MA (2021) Microglial metabolism is a pivotal factor in sexual dimorphism in Alzheimer's disease. Commun Biol 4:1–13.

Gunn AJ, Gunn TR (1997) Changes in Risk Factors for Hypoxic-ischaemic Seizures in Term Infants. Aust NZ J Obst Gynaeco 37:36–39.

Gunn AJ, Parer JT, Mallard EC, Williams CE, Gluckman PD (1992) Cerebral Histologic and Electrocorticographic Changes after Asphyxia in Fetal Sheep. Pediatr Res 31:486–491.

Gustin A, Kirchmeyer M, Koncina E, Felten P, Losciuto S, Heurtaux T, Tardivel A, Heuschling P, Dostert C (2015) NLRP3 Inflammasome Is Expressed and Functional in Mouse Brain Microglia but Not in Astrocytes. PLOS ONE 10:e0130624.

Hagemeyer N, Hanft K-M, Akriditou M-A, Unger N, Park ES, Stanley ER, Staszewski O, Dimou L, Prinz M (2017) Microglia contribute to normal myelinogenesis and to oligodendrocyte progenitor maintenance during adulthood. Acta Neuropathol 134:441–458.

Hankins GDV, Koen S, Gei AF, Lopez SM, Van Hook JW, Anderson GD (2002) Neonatal organ system injury in acute birth asphyxia sufficient to result in neonatal encephalopathy. Obstetrics & Gynecology 99:688–691.

Hascoët M, Colombel M-C, Bourin M (1999) Influence of Age on Behavioural Response in the Light/Dark Paradigm. Physiology & Behavior 66:567–570.

Hassell KJ, Ezzati M, Alonso-Alconada D, Hausenloy DJ, Robertson NJ (2015) New horizons for newborn brain protection: enhancing endogenous neuroprotection. Archives of Disease in Childhood - Fetal and Neonatal Edition 100:F541–F552.

He M, Shi X, Yang M, Yang T, Li T, Chen J (2019) Mesenchymal stem cells-derived IL-6 activates AMPK/mTOR signaling to inhibit the proliferation of reactive astrocytes induced by hypoxic-ischemic brain damage. Exp Neurol 311:15–32.

Hellström Erkenstam N, Smith PLP, Fleiss B, Nair S, Svedin P, Wang W, Boström M, Gressens P, Hagberg H, Brown KL, Sävman K, Mallard C (2016) Temporal Characterization of Microglia/Macrophage Phenotypes in a Mouse Model of Neonatal Hypoxic-Ischemic Brain Injury. Front Cell Neurosci 10

Hendrickx DAE, van Eden CG, Schuurman KG, Hamann J, Huitinga I (2017) Staining of HLA-DR, Iba1 and CD68 in human microglia reveals partially overlapping expression depending on cellular morphology and pathology. Journal of Neuroimmunology 309:12–22.

Heneka MT, Kummer MP, Stutz A, Delekate A, Schwartz S, Vieira-Saecker A, Griep A, Axt D, Remus A, Tzeng T-C, Gelpi E, Halle A, Korte M, Latz E, Golenbock DT (2013) NLRP3 is activated in Alzheimer's disease and contributes to pathology in APP/PS1 mice. Nature 493:674–678.

Heyser CJ (2003) Assessment of Developmental Milestones in Rodents. Current Protocols in Neuroscience 25:8.18.1-8.18.15.

Hu Y, Wang Z, Liu Y, Pan S, Zhang H, Fang M, Jiang H, Yin J, Zou S, Li Z, Zhang H, Lin Z, Xiao J

(2017) Melatonin reduces hypoxic-ischaemic (HI) induced autophagy and apoptosis: An *in vivo* and *in vitro* investigation in experimental models of neonatal HI brain injury. Neuroscience Letters 653:105–112.

Imitola J, Raddassi K, Park KI, Mueller F-J, Nieto M, Teng YD, Frenkel D, Li J, Sidman RL, Walsh CA, Snyder EY, Khoury SJ (2004) Directed migration of neural stem cells to sites of CNS injury by the stromal cell-derived factor 1α/CXC chemokine receptor 4 pathway. Proc Natl Acad Sci USA 101:18117–18122.

Inder TE, Hunt RW, Morley CJ, Coleman L, Stewart M, Doyle LW, Jacobs SE (2004) Randomized trial of systemic hypothermia selectively protects the cortex on MRI in term hypoxic-ischemic encephalopathy. The Journal of Pediatrics 145:835–837.

Iribarren I, Hilario E, Álvarez A, Alonso-Alconada D (2022) Neonatal multiple organ failure after perinatal asphyxia. Anales de Pediatría (English Edition) 97:280.e1-280.e8.

Ismael S, Nasoohi S, Ishrat T (2018) MCC950, the Selective Inhibitor of Nucleotide Oligomerization Domain-Like Receptor Protein-3 Inflammasome, Protects Mice against Traumatic Brain Injury. Journal of Neurotrauma 35:1294–1303.

Izbudak I, Grant PE (2011) MR imaging of the term and preterm neonate with diffuse brain injury. Magn Reson Imaging Clin N Am 19:709–731; vii.

Jacobs SE, Berg M, Hunt R, Tarnow-Mordi WO, Inder TE, Davis PG (2013) Cooling for newborns with hypoxic ischaemic encephalopathy. Cochrane Database Syst Rev:CD003311.

Jaworska J, Ziemka-Nalecz M, Sypecka J, Zalewska T (2017) The potential neuroprotective role of a histone deacetylase inhibitor, sodium butyrate, after neonatal hypoxia-ischemia. J Neuroinflammation 14:34.

Jenkins DD, Rollins LG, Perkel JK, Wagner CL, Katikaneni LP, Bass WT, Kaufman DA, Horgan MJ, Languani S, Givelichian L, Sankaran K, Yager JY, Martin RH (2012) Serum Cytokines in a Clinical Trial of Hypothermia for Neonatal Hypoxic-Ischemic Encephalopathy. J Cereb Blood Flow Metab 32:1888–1896.

Jensen FE, Applegate CD, Holtzman D, Belin TR, Burchfiel JL (1991) Epileptogenic effect of hypoxia in the immature rodent brain. Ann Neurol 29:629–637.

Jensen FE, Blume H, Alvarado S, Firkusny I, Geary C (1995) NBQX Blocks Acute and Late Epileptogenic Effects of Perinatal Hypoxia. Epilepsia 36:966–972.

Jiao M, Li X, Chen L, Wang X, Yuan B, Liu T, Dong Q, Mei H, Yin H (2020) Neuroprotective effect of astrocyte-derived IL-33 in neonatal hypoxic-ischemic brain injury. Journal of

Neuroinflammation 17:251.

Jimenez-Mateos EM, Engel T, Merino-Serrais P, Fernaud-Espinosa I, Rodriguez-Alvarez N, Reynolds J, Reschke CR, Conroy RM, McKiernan RC, deFelipe J, Henshall DC (2015) Antagomirs targeting microRNA-134 increase hippocampal pyramidal neuron spine volume in vivo and protect against pilocarpine-induced status epilepticus. Brain Struct Funct 220:2387–2399.

Johnston MV (1998) Selective vulnerability in the neonatal brain. Annals of Neurology 44:155–156.

Juul S (2004) Recombinant erythropoietin as a neuroprotective treatment: in vitro and in vivo models. Clin Perinatol 31:129–142.

Juul SE, Comstock BA, Cornet M-C, Gonzalez FF, Mayock DE, Glass HC, Schreiber MD, Heagerty PJ, Wu YW (2023) Safety of High Dose Erythropoietin Used with Therapeutic Hypothermia as Treatment for Newborn Hypoxic-Ischemic Encephalopathy: Secondary Analysis of the HEAL Randomized Controlled Trial. The Journal of Pediatrics 258:113400.

Kahlenberg JM, Dubyak GR (2004) Mechanisms of caspase-1 activation by $P2X_7$ receptor-mediated $K^+$ release. American Journal of Physiology-Cell Physiology 286:C1100–C1108.

Karcioglu O, Topacoglu H, Dikme O, Dikme O (2018) A systematic review of safety and adverse effects in the practice of therapeutic hypothermia. Am J Emerg Med 36:1886–1894.

Katsarou A-M, Galanopoulou AS, Moshé SL (2018) Epileptogenesis in neonatal brain. Seminars in Fetal and Neonatal Medicine 23:159–167.

Kelley N, Jeltema D, Duan Y, He Y (2019) The NLRP3 Inflammasome: An Overview of Mechanisms of Activation and Regulation. Int J Mol Sci 20:3328.

Kendall GS, Mathieson S, Meek J, Rennie JM (2012) Recooling for Rebound Seizures After Rewarming in Neonatal Encephalopathy. Pediatrics 130:e451–e455.

Kerenyi A, Kelen D, Faulkner SD, Bainbridge A, Chandrasekaran M, Cady EB, Golay X, Robertson NJ (2012) Systemic effects of whole-body cooling to 35 °C, 33.5 °C, and 30 °C in a piglet model of perinatal asphyxia: implications for therapeutic hypothermia. Pediatr Res 71:573–582.

Keyel PA (2014) How is inflammation initiated? Individual influences of IL-1, IL-18 and HMGB1. Cytokine 69:136–145.

Kim S, Shah SB, Graney PL, Singh A (2019) Multiscale engineering of immune cells and lymphoid organs. Nat Rev Mater 4:355–378.

Kukka AJ, Waheddoost S, Brown N, Litorp H, Wrammert J, Kc A (2022) Incidence and outcomes of intrapartum-related neonatal encephalopathy in low-income and middle-income countries: a systematic review and meta-analysis. BMJ Global Health 7:e010294.

Kumar P, Hair P, Cunnion K, Krishna N, Bass T (2021) Classical complement pathway inhibition reduces brain damage in a hypoxic ischemic encephalopathy animal model. PLOS ONE 16:e0257960.

Kurinczuk JJ, White-Koning M, Badawi N (2010) Epidemiology of neonatal encephalopathy and hypoxic–ischaemic encephalopathy. Early Human Development 86:329–338.

Kutlu MG, Gould TJ (2016) Effects of drugs of abuse on hippocampal plasticity and hippocampus-dependent learning and memory: contributions to development and maintenance of addiction. Learn Mem 23:515–533.

Lalancette-Hébert M, Faustino J, Thammisetty SS, Chip S, Vexler ZS, Kriz J (2017) Live imaging of the innate immune response in neonates reveals differential TLR2 dependent activation patterns in sterile inflammation and infection. Brain, Behavior, and Immunity 65:312–327.

Lalancette-Hébert M, Gowing G, Simard A, Weng YC, Kriz J (2007) Selective Ablation of Proliferating Microglial Cells Exacerbates Ischemic Injury in the Brain. J Neurosci 27:2596–2605.

Lanser AJ, Rezende RM, Rubino S, Lorello PJ, Donnelly DJ, Xu H, Lau LA, Dulla CG, Caldarone BJ, Robson SC, Weiner HL (2017) Disruption of the ATP /adenosine balance in CD $39^{-/-}$ mice is associated with handling-induced seizures. Immunology 152:589–601.

Laptook AR et al. (2017) Effect of Therapeutic Hypothermia Initiated After 6 Hours of Age on Death or Disability Among Newborns With Hypoxic-Ischemic Encephalopathy: A Randomized Clinical Trial. JAMA 318:1550–1560.

Laroia N, McBride L, Baggs R, Guillet R (1997) Dextromethorphan ameliorates effects of neonatal hypoxia on brain morphology and seizure threshold in rats. Brain Res Dev Brain Res 100:29–34.

LaRosa DA, Ellery SJ, Walker DW, Dickinson H (2017) Understanding the Full Spectrum of Organ Injury Following Intrapartum Asphyxia. Front Pediatr 5

Lau SL, Lok ZLZ, Hui SYA, Fung GPG, Lam HS, Leung TY (2023) Neonatal outcome of infants

with umbilical cord arterial pH less than 7. Acta Obstet Gynecol Scand 102:174–180.

Lawson LJ, Perry VH, Dri P, Gordon S (1990) Heterogeneity in the distribution and morphology of microglia in the normal adult mouse brain. Neuroscience 39:151–170.

Lee HE, Yang G, Park YB, Kang HC, Cho Y-Y, Lee HS, Lee JY (2019) Epigallocatechin-3-Gallate Prevents Acute Gout by Suppressing NLRP3 Inflammasome Activation and Mitochondrial DNA Synthesis. Molecules 24:2138.

Leifsdottir K, Mehmet H, Eksborg S, Herlenius E (2018) Fas-ligand and interleukin-6 in the cerebrospinal fluid are early predictors of hypoxic-ischemic encephalopathy and long-term outcomes after birth asphyxia in term infants. Journal of Neuroinflammation 15:223.

Lemyre B, Chau V (2018) Hypothermia for newborns with hypoxic-ischemic encephalopathy. Paediatrics & Child Health 23:285–291.

Li B, Concepcion K, Meng X, Zhang L (2017) Brain-immune interactions in perinatal hypoxic-ischemic brain injury. Prog Neurobiol 159:50–68.

Li C-Y, Li X, Liu S-F, Qu W-S, Wang W, Tian D-S (2015) Inhibition of mTOR pathway restrains astrocyte proliferation, migration and production of inflammatory mediators after oxygen–glucose deprivation and reoxygenation. Neurochemistry International 83–84:9–18.

Li K, Koukoutselos K, Sakaguchi M, Ciocchi S (2024) Distinct ventral hippocampal inhibitory microcircuits regulating anxiety and fear behaviors. Nat Commun 15:8228.

Li N, Liu C, Wang C, Chen R, Li X, Wang Y, Wang C (2021a) Early changes of NLRP3 inflammasome activation after hypoxic-ischemic brain injury in neonatal rats. Int J Clin Exp Pathol 14:209–220.

Li W, Niu L, Liu Z, Xu X, Shi M, Zhang Y, Deng Y, He J, Xu Y, Wan W, Sun Q, Zhong X, Cao W (2021b) Inhibition of the NLRP3 inflammasome with MCC950 prevents chronic social isolation-induced depression-like behavior in male mice. Neuroscience Letters 765:136290.

Liddelow SA et al. (2017) Neurotoxic reactive astrocytes are induced by activated microglia. Nature 541:481–487.

Liesz A, Suri-Payer E, Veltkamp C, Doerr H, Sommer C, Rivest S, Giese T, Veltkamp R (2009) Regulatory T cells are key cerebroprotective immunomodulators in acute

experimental stroke. Nat Med 15:192–199.

Liesz A, Zhou W, Mracskó É, Karcher S, Bauer H, Schwarting S, Sun L, Bruder D, Stegemann S, Cerwenka A, Sommer C, Dalpke AH, Veltkamp R (2011) Inhibition of lymphocyte trafficking shields the brain against deleterious neuroinflammation after stroke. Brain 134:704–720.

Linker RA, Mäurer M, Gaupp S, Martini R, Holtmann B, Giess R, Rieckmann P, Lassmann H, Toyka KV, Sendtner M, Gold R (2002) CNTF is a major protective factor in demyelinating CNS disease: A neurotrophic cytokine as modulator in neuroinflammation. Nat Med 8:620–624.

Lintermans LL, Stegeman CA, Heeringa P, Abdulahad WH (2014) T Cells in Vascular Inflammatory Diseases. Front Immunol 5

Liu B-K, Jiang L, Li X-J, Hong S-Q, Chen W, Hu Y (2020) Efficacy and safety of levetiracetam in the off-label treatment of neonatal seizures. International Journal of Neuroscience 130:336–342.

Liu F, Mccullough LD (2013) Inflammatory responses in hypoxic ischemic encephalopathy. Acta Pharmacol Sin 34:1121–1130.

Liu XS, Chopp M, Pan WL, Wang XL, Fan BY, Zhang Y, Kassis H, Zhang RL, Zhang XM, Zhang ZG (2017) MicroRNA-146a Promotes Oligodendrogenesis in Stroke. Mol Neurobiol 54:227–237.

Liu Y, Silverstein FS, Skoff R, Barks JDE (2002) Hypoxic-Ischemic Oligodendroglial Injury in Neonatal Rat Brain. Pediatr Res 51:25–33.

Loetscher M, Loetscher P, Brass N, Meese E, Moser B (1998) Lymphocyte-specific chemokine receptor CXCR3: regulation, chemokine binding and gene localization. Eur J Immunol 28:3696–3705.

Logiacco F, Xia P, Georgiev SV, Franconi C, Chang Y-J, Ugursu B, Sporbert A, Kühn R, Kettenmann H, Semtner M (2021) Microglia sense neuronal activity via GABA in the early postnatal hippocampus. Cell Rep 37:110128.

Lou HC (1996) Etiology and pathogenesis of attention-deficit hyperactivity disorder (ADHD): significance of prematurity and perinatal hypoxic-haemodynamic encephalopathy. Acta Paediatr 85:1266–1271.

Low DA, Bailey TG, Timothy Cable N, Jones H (2016) Thermoregulatory responses to combined moderate heat stress and hypoxia. Microcirculation 23:487–494.

Low E, Boylan GB, Mathieson SR, Murray DM, Korotchikova I, Stevenson NJ, Livingstone V, Rennie JM (2012) Cooling and seizure burden in term neonates: an observational study. Archives of Disease in Childhood - Fetal and Neonatal Edition 97:F267–F272.

Lu A, Magupalli VG, Ruan J, Yin Q, Atianand MK, Vos MR, Schröder GF, Fitzgerald KA, Wu H, Egelman EH (2014) Unified Polymerization Mechanism for the Assembly of ASC-Dependent Inflammasomes. Cell 156:1193–1206.

Lučiūnaitė A, McManus RM, Jankunec M, Rácz I, Dansokho C, Dalgėdienė I, Schwartz S, Brosseron F, Heneka MT (2020) Soluble Aβ oligomers and protofibrils induce NLRP3 inflammasome activation in microglia. J Neurochem 155:650–661.

Luo Y, Lu J, Ruan W, Guo X, Chen S (2019) MCC950 attenuated early brain injury by suppressing NLRP3 inflammasome after experimental SAH in rats. Brain Research Bulletin 146:320–326.

Lv Y, Sun B, Lu X, Liu Y, Li M, Xu L-X, Feng C-X, Ding X, Feng X (2020) The role of microglia mediated pyroptosis in neonatal hypoxic-ischemic brain damage. Biochemical and Biophysical Research Communications 521:933–938.

Machie M, Weeke L, de Vries LS, Rollins N, Brown L, Chalak L (2021) MRI Score Ability to Detect Abnormalities in Mild Hypoxic-Ischemic Encephalopathy. Pediatric Neurology 116:32–38.

Maitre NL, Smolinsky C, Slaughter JC, Stark AR (2013) Adverse neurodevelopmental outcomes after exposure to phenobarbital and levetiracetam for the treatment of neonatal seizures. J Perinatol 33:841–846.

Malik A, Kanneganti T-D (2017) Inflammasome activation and assembly at a glance. Journal of Cell Science 130:3955–3963.

Malla RR, Asimi R, Teli MA, Shaheen F, Bhat MA (2017) Erythropoietin monotherapy in perinatal asphyxia with moderate to severe encephalopathy: a randomized placebo-controlled trial. J Perinatol 37:596–601.

Mallard C, Tremblay M-E, Vexler ZS (2019) Microglia and Neonatal Brain Injury. Neuroscience 405:68–76.

Martin LJ, Brambrink AM, Lehmann C, Portera-Cailliau C, Koehler R, Rothstein J, Traystman RJ (1997) Hypoxia—ischemia causes abnormalities in glutamate transporters and death of astroglia and neurons in newborn striatum. Annals of Neurology 42:335–348.

Martinon F, Burns K, Tschopp J (2002) The Inflammasome. Molecular Cell 10:417–426.

Matcovitch-Natan O et al. (2016) Microglia development follows a stepwise program to regulate brain homeostasis. Science 353:aad8670.

Mathew JL, Kaur N, Dsouza JM (2022) Therapeutic hypothermia in neonatal hypoxic encephalopathy: A systematic review and meta-analysis. J Glob Health 12:04030.

McIntyre S, Nelson KB, Mulkey SB, Lechpammer M, Molloy E, Badawi N (2021) Neonatal encephalopathy: Focus on epidemiology and underexplored aspects of etiology. Seminars in Fetal and Neonatal Medicine 26:101265.

McManus RM, Latz E (2024) NLRP3 inflammasome signalling in Alzheimer's disease. Neuropharmacology 252:109941.

McRae A, Gilland E, Bona E, Hagberg H (1995) Microglia activation after neonatal hypoxic-ischemia. Developmental Brain Research 84:245–252.

Meder U, Cseko AJ, Szakacs L, Balogh CD, Szakmar E, Andorka C, Kovacs K, Dobi M, Brandt FA, Szabo M, Szabo AJ, Jermendy A (2022) Longitudinal Analysis of Amplitude-Integrated Electroencephalography for Outcome Prediction in Hypoxic-Ischemic Encephalopathy. The Journal of Pediatrics 246:19-25.e5.

Michael BD, Griffiths MJ, Granerod J, Brown D, Keir G, Wnęk G, Cox DJ, Vidyasagar R, Borrow R, Parkes LM, Solomon T (2016) The Interleukin-1 Balance During Encephalitis Is Associated With Clinical Severity, Blood-Brain Barrier Permeability, Neuroimaging Changes, and Disease Outcome. J Infect Dis 213:1651–1660.

Michniewicz B, Szpecht D, Sowińska A, Sibiak R, Szymankiewicz M, Gadzinowski J (2020) Biomarkers in newborns with hypoxic-ischemic encephalopathy treated with therapeutic hypothermia. Childs Nerv Syst 36:2981–2988.

Mikati MA, Zeinieh MP, Kurdi RM, Harb SA, El Hokayem JA, Daderian RH, Shamseddine A, Obeid M, Bitar FF, El Sabban M (2005) Long-term effects of acute and of chronic hypoxia on behavior and on hippocampal histology in the developing brain. Developmental Brain Research 157:98–102.

Millar LJ, Shi L, Hoerder-Suabedissen A, Molnár Z (2017) Neonatal Hypoxia Ischaemia: Mechanisms, Models, and Therapeutic Challenges. Front Cell Neurosci 11 Available at: https://www.ncbi.nlm.nih.gov/pmc/articles/PMC5420571/ [Accessed January 27, 2020].

Miller SP, Ramaswamy V, Michelson D, Barkovich AJ, Holshouser B, Wycliffe N, Glidden DV, Deming D, Partridge JC, Wu YW, Ashwal S, Ferriero DM (2005) Patterns of brain injury

in term neonatal encephalopathy. J Pediatr 146:453–460.

Min Y, Yan L, Wang Q, Wang F, Hua H, Yuan Y, Jin H, Zhang M, Zhao Y, Yang J, Jiang X, Yang Y, Li F (2020) Distinct Residential and Infiltrated Macrophage Populations and Their Phagocytic Function in Mild and Severe Neonatal Hypoxic-Ischemic Brain Damage. Frontiers in Cellular Neuroscience 14

Miyamoto A, Wake H, Ishikawa AW, Eto K, Shibata K, Murakoshi H, Koizumi S, Moorhouse AJ, Yoshimura Y, Nabekura J (2016) Microglia contact induces synapse formation in developing somatosensory cortex. Nat Commun 7:12540.

Molloy EJ et al. (2023) Neonatal encephalopathy and hypoxic–ischemic encephalopathy: moving from controversy to consensus definitions and subclassification. Pediatr Res 94:1860–1863.

Molloy EJ, Bearer C (2018) Neonatal encephalopathy versus Hypoxic-Ischemic Encephalopathy. Pediatr Res 84:574–574.

Monif M, Reid CA, Powell KL, Drummond KJ, O'Brien TJ, Williams DA (2016) Interleukin-1β has trophic effects in microglia and its release is mediated by P2X7R pore. Journal of Neuroinflammation 13:173.

Morrison RS, Wenzel HJ, Kinoshita Y, Robbins CA, Donehower LA, Schwartzkroin PA (1996) Loss of the p53 tumor suppressor gene protects neurons from kainate-induced cell death. J Neurosci 16:1337–1345.

Mortola JP, Naso L (1998) Thermogenesis in newborn rats after prenatal or postnatal hypoxia. Journal of Applied Physiology 85:84–90.

Morton DB (2000) A Systematic Approach for Establishing Humane Endpoints. ILAR Journal 41:80–86.

Müller M, Carter SL, Hofer MJ, Manders P, Getts DR, Getts MT, Dreykluft A, Lu B, Gerard C, King NJC, Campbell IL (2007) CXCR3 signaling reduces the severity of experimental autoimmune encephalomyelitis by controlling the parenchymal distribution of effector and regulatory T cells in the central nervous system. J Immunol 179:2774–2786.

Nagarajan L, Ghosh S (2016) The role of the video EEG in neonates with seizures. In: Neonatal Seizures (Nagarajan L, ed), pp 12–29 International Review of Child Neurology. London: Mac Keith Press.

Neniskyte U, Gross CT (2017) Errant gardeners: glial-cell-dependent synaptic pruning and

neurodevelopmental disorders. Nat Rev Neurosci 18:658–670.

Ng A, Tam WW, Zhang MW, Ho CS, Husain SF, McIntyre RS, Ho RC (2018) IL-1β, IL-6, TNF- α and CRP in Elderly Patients with Depression or Alzheimer's disease: Systematic Review and Meta-Analysis. Sci Rep 8:12050.

Norden DM, Trojanowski PJ, Villanueva E, Navarro E, Godbout JP (2016) Sequential activation of microglia and astrocyte cytokine expression precedes increased iba-1 or GFAP immunoreactivity following systemic immune challenge. Glia 64:300–316.

Novak I et al. (2017) Early, Accurate Diagnosis and Early Intervention in Cerebral Palsy: Advances in Diagnosis and Treatment. JAMA Pediatrics 171:897–907.

Numis AL, Foster-Barber A, Deng X, Rogers EE, Barkovich AJ, Ferriero DM, Glass HC (2019) Early changes in pro-inflammatory cytokine levels in neonates with encephalopathy are associated with remote epilepsy. Pediatr Res 86:616–621.

Orrock JE, Panchapakesan K, Vezina G, Chang T, Harris K, Wang Y, Knoblach S, Massaro AN (2016) Association of Brain Injury and Neonatal Cytokine Response during Therapeutic Hypothermia (TH) in Newborns with Hypoxic-Ischemic Encephalopathy (HIE). Pediatr Res 79:742–747.

Osredkar D, Toet MC, van Rooij LGM, van Huffelen AC, Groenendaal F, de Vries LS (2005) Sleep-wake cycling on amplitude-integrated electroencephalography in term newborns with hypoxic-ischemic encephalopathy. Pediatrics 115:327–332.

Painter MJ, Scher MS, Stein AD, Armatti S, Wang Z, Gardiner JC, Paneth N, Minnigh B, Alvin J (1999) Phenobarbital compared with phenytoin for the treatment of neonatal seizures. N Engl J Med 341:485–489.

Pang R, Avdic-Belltheus A, Meehan C, Martinello K, Mutshiya T, Yang Q, Sokolska M, Torrealdea F, Hristova M, Bainbridge A, Golay X, Juul SE, Robertson NJ (2020) Melatonin and/or erythropoietin combined with hypothermia in a piglet model of perinatal asphyxia. Brain Commun 3:fcaa211.

Pang Y, Tien L-T, Zhu H, Shen J, Wright CF, Jones TK, Mamoon SA, Bhatt AJ, Cai Z, Fan L-W (2015) Interleukin-1 Receptor Antagonist Reduces Neonatal Lipopolysaccharide-Induced Long-Lasting Neurobehavioral Deficits and Dopaminergic Neuronal Injury in Adult Rats. International Journal of Molecular Sciences 16:8635–8654.

Paolicelli RC et al. (2022) Microglia states and nomenclature: A field at its crossroads. Neuron 110:3458–3483.

Paolicelli RC, Bolasco G, Pagani F, Maggi L, Scianni M, Panzanelli P, Giustetto M, Ferreira TA, Guiducci E, Dumas L, Ragozzino D, Gross CT (2011) Synaptic Pruning by Microglia Is Necessary for Normal Brain Development. Science 333:1456–1458.

Park J, Park SH, Kim C, Yoon SJ, Lim JH, Han JH, Shin JE, Eun HS, Park MS, Lee SM (2023) Growth and developmental outcomes of infants with hypoxic ischemic encephalopathy. Scientific Reports 13:23100.

Pavel AM et al. (2020) A machine-learning algorithm for neonatal seizure recognition: a multicentre, randomised, controlled trial. The Lancet Child & Adolescent Health 4:740–749.

Pavel AM et al. (2024) Temporal evolution of electrographic seizures in newborn infants with hypoxic-ischaemic encephalopathy requiring therapeutic hypothermia: a secondary analysis of the ANSeR studies. The Lancet Child & Adolescent Health 8:214–224.

Pellegrin S et al. (2019) Neonatal seizures: Case definition & guidelines for data collection, analysis, and presentation of immunization safety data. Vaccine 37:7596–7609.

Pembegul Yıldız E, Tatlı B, Ulak Ozkan M, Erarslan E, Aydınlı N, Çalışkan M, Özmen M (2020) Evaluation of the prognostic factors in school age children who experienced neonatal seizures. Epilepsy & Behavior 102:106673.

Pick CG, Yanai J (1985) Long term reduction in eight arm maze performance after early exposure to phenobarbital. Int J Dev Neurosci 3:223–227.

Pisani F, Facini C, Bianchi E, Giussani G, Piccolo B, Beghi E (2018) Incidence of neonatal seizures, perinatal risk factors for epilepsy and mortality after neonatal seizures in the province of Parma, Italy. Epilepsia 59:1764–1773.

Pisani F, Spagnoli C (2016) Monitoring of newborns at high risk for brain injury. Italian Journal of Pediatrics 42:48.

Pressler RM, Cilio MR, Mizrahi EM, Moshé SL, Nunes ML, Plouin P, Vanhatalo S, Yozawitz E, de Vries LS, Puthenveettil Vinayan K, Triki CC, Wilmshurst JM, Yamamoto H, Zuberi SM (2021) The ILAE classification of seizures and the epilepsies: Modification for seizures in the neonate. Position paper by the ILAE Task Force on Neonatal Seizures. Epilepsia 62:615–628.

Qi Y, Klyubin I, Cuello AC, Rowan MJ (2018) NLRP3-dependent synaptic plasticity deficit in an Alzheimer's disease amyloidosis model in vivo. Neurobiology of Disease 114:24–30.

Quinlan S, Merino-Serrais P, Di Grande A, Dussmann H, Prehn JHM, Ní Chonghaile T, Henshall

DC, Jimenez-Mateos EM (2019) The Anti-inflammatory Compound Candesartan Cilexetil Improves Neurological Outcomes in a Mouse Model of Neonatal Hypoxia. Front Immunol 10

Quinlan SMM, Rodriguez-Alvarez N, Molloy EJ, Madden SF, Boylan GB, Henshall DC, Jimenez-Mateos EM (2018) Complex spectrum of phenobarbital effects in a mouse model of neonatal hypoxia-induced seizures. Sci Rep 8:1–12.

Rakhade SN, Jensen FE (2009) Epileptogenesis in the immature brain: emerging mechanisms. Nat Rev Neurol 5:380–391.

Rakhade SN, Klein PM, Huynh T, Hilario-Gomez C, Kosaras B, Rotenberg A, Jensen FE (2011) Development of later life spontaneous seizures in a rodent model of hypoxia-induced neonatal seizures. Epilepsia 52:753–765.

Rappert A, Biber K, Nolte C, Lipp M, Schubel A, Lu B, Gerard NP, Gerard C, Boddeke HWGM, Kettenmann H (2002) Secondary Lymphoid Tissue Chemokine (CCL21) Activates CXCR3 to Trigger a Cl− Current and Chemotaxis in Murine Microglia. The Journal of Immunology 168:3221–3226.

Ren H, Kong Y, Liu Z, Zang D, Yang X, Wood K, Li M, Liu Q (2018) Selective NLRP3 (Pyrin Domain–Containing Protein 3) Inflammasome Inhibitor Reduces Brain Injury After Intracerebral Hemorrhage. Stroke 49:184–192.

Rice JE, Vannucci RC, Brierley JB (1981) The influence of immaturity on hypoxic-ischemic brain damage in the rat. Ann Neurol 9:131–141.

Richardson BS, Bocking AD (1998) Metabolic and Circulatory Adaptations to Chronic Hypoxia in the Fetus. Comparative Biochemistry and Physiology Part A: Molecular & Integrative Physiology 119:717–723.

Rio-Hortega P del (1919) El “tercer elemento” de los centros nerviosos. III. Naturaleza probable de la microglía. Bol Soc Esp Biol 8:108–115.

Robertson NJ, Faulkner S, Fleiss B, Bainbridge A, Andorka C, Price D, Powell E, Lecky-Thompson L, Thei L, Chandrasekaran M, Hristova M, Cady EB, Gressens P, Golay X, Raivich G (2013a) Melatonin augments hypothermic neuroprotection in a perinatal asphyxia model. Brain 136:90–105.

Robertson CS, Garcia R, Gaddam SSK, Grill RJ, Cerami Hand C, Tian TS, Hannay HJ (2013b) Treatment of Mild Traumatic Brain Injury with an Erythropoietin-Mimetic Peptide. Journal of Neurotrauma 30:765–774.

Rocha-Ferreira E, Hristova M (2016) Plasticity in the Neonatal Brain following Hypoxic-Ischaemic Injury. Neural Plast 2016:4901014.

Rodd C, Schwieger-Briel A, Hagmann C (2021) Subcutaneous fat necrosis associated with hypercalcemia in neonates with neonatal encephalopathy treated with therapeutic hypothermia. Seminars in Fetal and Neonatal Medicine 26:101269.

Rodríguez M, Valez V, Cimarra C, Blasina F, Radi R (2020) Hypoxic-Ischemic Encephalopathy and Mitochondrial Dysfunction: Facts, Unknowns, and Challenges. Antioxidants & Redox Signaling 33:247–262.

Rodriguez-Alvarez N, Jimenez-Mateos EM, Engel T, Quinlan S, Reschke CR, Conroy RM, Bhattacharya A, Boylan GB, Henshall DC (2017) Effects of P2X7 receptor antagonists on hypoxia-induced neonatal seizures in mice. Neuropharmacology 116:351–363.

Romeo DM, Brogna C, Sini F, Romeo MG, Cota F, Ricci D (2016) Early psychomotor development of low-risk preterm infants: Influence of gestational age and gender. Eur J Paediatr Neurol 20:518–523.

Ronen GM, Buckley D, Penney S, Streiner DL (2007) Long-term prognosis in children with neonatal seizures: A population-based study. Neurology 69:1816–1822.

Rothwell NJ, Hopkins SJ (1995) Cytokines and the nervous system II: actions and mechanisms of action. Trends in Neurosciences 18:130–136.

Rousset CI, Baburamani AA, Thornton C, Hagberg H (2012) Mitochondria and perinatal brain injury. The Journal of Maternal-Fetal & Neonatal Medicine 25:35–38.

Rupprecht TA, Koedel U, Muhlberger B, Wilske B, Fontana A, Pfister H-W (2005) CXCL11 is involved in leucocyte recruitment to the central nervous system in neuroborreliosis. J Neurol 252:820–823.

Salter MW, Beggs S (2014) Sublime Microglia: Expanding Roles for the Guardians of the CNS. Cell 158:15–24.

Schafer DP, Lehrman EK, Kautzman AG, Koyama R, Mardinly AR, Yamasaki R, Ransohoff RM, Greenberg ME, Barres BA, Stevens B (2012) Microglia Sculpt Postnatal Neural Circuits in an Activity and Complement-Dependent Manner. Neuron 74:691–705.

Schafer DP, Stevens B (2013) Phagocytic glial cells: sculpting synaptic circuits in the developing nervous system. Current Opinion in Neurobiology 23:1034–1040.

Schäfers M, Sommer C, Geis C, Hagenacker T, Vandenabeele P, Sorkin LS (2008) Selective stimulation of either tumor necrosis factor receptor differentially induces pain

behavior *in vivo* and ectopic activity in sensory neurons *in vitro*. Neuroscience 157:414–423.

Schmidt FI, Lu A, Chen JW, Ruan J, Tang C, Wu H, Ploegh HL (2016) A single domain antibody fragment that recognizes the adaptor ASC defines the role of ASC domains in inflammasome assembly. Journal of Experimental Medicine 213:771–790.

Sellgren CM, Gracias J, Watmuff B, Biag JD, Thanos JM, Whittredge PB, Fu T, Worringer K, Brown HE, Wang J, Kaykas A, Karmacharya R, Goold CP, Sheridan SD, Perlis RH (2019) Increased synapse elimination by microglia in schizophrenia patient-derived models of synaptic pruning. Nat Neurosci 22:374–385.

Semple BD, Blomgren K, Gimlin K, Ferriero DM, Noble-Haeusslein LJ (2013) Brain development in rodents and humans: Identifying benchmarks of maturation and vulnerability to injury across species. Progress in Neurobiology 106–107:1–16.

Serdar M, Kempe K, Rizazad M, Herz J, Bendix I, Felderhoff-Müser U, Sabir H (2019) Early Pro-inflammatory Microglia Activation After Inflammation-Sensitized Hypoxic-Ischemic Brain Injury in Neonatal Rats. Front Cell Neurosci 13

Shah P (2004) Multiorgan dysfunction in infants with post-asphyxial hypoxic-ischaemic encephalopathy. Archives of Disease in Childhood - Fetal and Neonatal Edition 89:152F – 155.

Shah TA, Pallera HK, Kaszowski CL, Bass WT, Lattanzio FA (2021) Therapeutic Hypothermia Inhibits the Classical Complement Pathway in a Rat Model of Neonatal Hypoxic-Ischemic Encephalopathy. Front Neurosci 15

Shaker T, Chattopadhyaya B, Amilhon B, Cristo GD, Weil AG (2021) Transduction of inflammation from peripheral immune cells to the hippocampus induces neuronal hyperexcitability mediated by Caspase-1 activation. Neurobiology of Disease 160:105535.

Shankaran S et al. (2012) Childhood Outcomes after Hypothermia for Neonatal Encephalopathy. N Engl J Med 366:2085–2092.

Shi C, Pamer EG (2011) Monocyte recruitment during infection and inflammation. Nature Reviews Immunology 11:762–774.

Shigemoto-Mogami Y, Hoshikawa K, Goldman JE, Sekino Y, Sato K (2014) Microglia Enhance Neurogenesis and Oligodendrogenesis in the Early Postnatal Subventricular Zone. J Neurosci 34:2231–2243.

Shimomura C, Ohta H (1988) Behavioral abnormalities and seizure susceptibility in rat after neonatal anoxia. Brain and Development 10:160–163.

Shingo T, Sorokan ST, Shimazaki T, Weiss S (2001) Erythropoietin Regulates the *In Vitro* and *In Vivo* Production of Neuronal Progenitors by Mammalian Forebrain Neural Stem Cells. J Neurosci 21:9733–9743.

Shipley L, Gale C, Sharkey D (2021) Trends in the incidence and management of hypoxic-ischaemic encephalopathy in the therapeutic hypothermia era: a national population study. Arch Dis Child Fetal Neonatal Ed 106:529–534.

Sierra A, Paolicelli RC, Kettenmann H (2019) Cien Años de Microglía: Milestones in a Century of Microglial Research. Trends in Neurosciences 42:778–792.

Sinha R, Venkatnarayan K, Negi V, Sodhi K, John B (2018) The effect of whole body cooling in asphyxiated neonates with resource limitation: Challenges and experience. J Clin Neonatol 7:7.

Sipe GO, Lowery, Tremblay M-È, Kelly EA, Lamantia CE, Majewska AK (2016) Microglial P2Y12 is necessary for synaptic plasticity in mouse visual cortex. Nat Commun 7:10905.

Slaughter LA, Patel AD, Slaughter JL (2013) Pharmacological Treatment of Neonatal Seizures: A Systematic Review. J Child Neurol 28:351–364.

Smith J, Menéndez Méndez A, Alves M, Parras A, Conte G, Bhattacharya A, Ceusters M, Nicke A, Henshall DC, Jimenez-Mateos EM, Engel T (2023) The P2X7 receptor contributes to seizures and inflammation-driven long-lasting brain hyperexcitability following hypoxia in neonatal mice. British J Pharmacology 180:1710–1729.

Spagnoli C, Seri S, Pavlidis E, Mazzotta S, Pelosi A, Pisani F (2016) Phenobarbital for Neonatal Seizures: Response Rate and Predictors of Refractoriness. Neuropediatrics 47:318–326.

Spandou E, Papoutsopoulou S, Soubasi V, Karkavelas G, Simeonidou C, Kremenopoulos G, Guiba-Tziampiri O (2004) Hypoxia–ischemia affects erythropoietin and erythropoietin receptor expression pattern in the neonatal rat brain. Brain Research 1021:167–172.

Spitzmiller RE, Phillips T, Meinzen-Derr J, Hoath SB (2007) Amplitude-Integrated EEG Is Useful in Predicting Neurodevelopmental Outcome in Full-Term Infants With Hypoxic-Ischemic Encephalopathy: A Meta-Analysis. J Child Neurol 22:1069–1078.

Statler PA, McPherson RJ, Bauer LA, Kellert BA, Juul SE (2007) Pharmacokinetics of high-dose recombinant erythropoietin in plasma and brain of neonatal rats. Pediatr Res 61:671–

675.

Stepanova A, Konrad C, Guerrero-Castillo S, Manfredi G, Vannucci S, Arnold S, Galkin A (2019) Deactivation of mitochondrial complex I after hypoxia–ischemia in the immature brain. J Cereb Blood Flow Metab 39:1790–1802.

Stremmel C et al. (2018) Yolk sac macrophage progenitors traffic to the embryo during defined stages of development. Nat Commun 9:75.

Stridh L, Smith PL, Naylor AS, Wang X, Mallard C (2011) Regulation of Toll-like receptor 1 and -2 in neonatal mice brains after hypoxia-ischemia. J Neuroinflammation 8:45.

Sun B, Feng X, Ding X, Bao L, Li Y, He J, Jin M (2012) Expression of Clock genes in the pineal glands of newborn rats with hypoxic-ischemic encephalopathy. Neural Regen Res 7:2221–2226.

Sun H, Juul HM, Jensen FE (2016) Models of hypoxia and ischemia-induced seizures. Journal of Neuroscience Methods 260:252–260.

Sun H-S, Xu B, Chen W, Xiao A, Turlova E, Alibraham A, Barszczyk A, Bae CYJ, Quan Y, Liu B, Pei L, Sun CLF, Deurloo M, Feng Z-P (2015) Neuronal KATP channels mediate hypoxic preconditioning and reduce subsequent neonatal hypoxic–ischemic brain injury. Experimental Neurology 263:161–171.

Tadic BV, Kravljanac R, Sretenovic V, Vukomanovic V (2018) Long-term outcome in children with neonatal seizures: A tertiary center experience in cohort of 168 patients. Epilepsy & Behavior 84:107–113.

Takemiya T, Fumizawa K, Yamagata K, Iwakura Y, Kawakami M (2017) Brain Interleukin-1 Facilitates Learning of a Water Maze Spatial Memory Task in Young Mice. Front Behav Neurosci 11

Talos DM, Sun H, Zhou X, Fitzgerald EC, Jackson MC, Klein PM, Lan VJ, Joseph A, Jensen FE (2012) The Interaction between Early Life Epilepsy and Autistic-Like Behavioral Consequences: A Role for the Mammalian Target of Rapamycin (mTOR) Pathway. PLOS ONE 7:e35885.

Tan E-K, Chao Y-X, West A, Chan L-L, Poewe W, Jankovic J (2020) Parkinson disease and the immune system — associations, mechanisms and therapeutics. Nat Rev Neurol 16:303–318.

Tan WKM, Williams CE, During MJ, Mallard CE, Gunning MI, Gunn AJ, Gluckman PD (1996) Accumulation of Cytotoxins During the Development of Seizures and Edema after

Hypoxic-Ischemic Injury in Late Gestation Fetal Sheep. Pediatr Res 39:791–797.

Tang G, Gudsnuk K, Kuo S-H, Cotrina ML, Rosoklija G, Sosunov A, Sonders MS, Kanter E, Castagna C, Yamamoto A, Yue Z, Arancio O, Peterson BS, Champagne F, Dwork AJ, Goldman J, Sulzer D (2014) Loss of mTOR-Dependent Macroautophagy Causes Autistic-like Synaptic Pruning Deficits. Neuron 83:1131–1143.

Ten VS, Bradley-Moore M, Gingrich JA, Stark RI, Pinsky DJ (2003) Brain injury and neurofunctional deficit in neonatal mice with hypoxic-ischemic encephalopathy. Behavioural Brain Research 145:209–219.

Teo EJ, Chand KK, Miller SM, Wixey JA, Colditz PB, Bjorkman ST (2023) Early evolution of glial morphology and inflammatory cytokines following hypoxic-ischemic injury in the newborn piglet brain. Sci Rep 13:282.

Teramo KA, Klemetti MM, Widness JA (2018) Robust increases in erythropoietin production by the hypoxic fetus is a response to protect the brain and other vital organs. Pediatr Res 84:807–812.

Thayyil S, Chandrasekaran M, Taylor A, Bainbridge A, Cady EB, Chong WKK, Murad S, Omar RZ, Robertson NJ (2010) Cerebral Magnetic Resonance Biomarkers in Neonatal Encephalopathy: A Meta-analysis. Pediatrics 125:e382–e395.

Thoresen M, Haaland K, Løberg EM, Whitelaw A, Apricena F, Hankø E, Steen PA (1996) A Piglet Survival Model of Posthypoxic Encephalopathy. Pediatr Res 40:738–748.

Thoresen M, Tooley J, Liu X, Jary S, Fleming P, Luyt K, Jain A, Cairns P, Harding D, Sabir H (2013) Time Is Brain: Starting Therapeutic Hypothermia within Three Hours after Birth Improves Motor Outcome in Asphyxiated Newborns. Neonatology 104:228–233.

Thornton P, Pinteaux E, Gibson RM, Allan SM, Rothwell NJ (2006) Interleukin-1-induced neurotoxicity is mediated by glia and requires caspase activation and free radical release. Journal of Neurochemistry 98:258–266.

Tian Q, Pan Y, Zhang Z, Li M, Xu L, Gong M, Miao P, Jiang X, Yang X, Feng C-X, Pan J, Yu Y, Sun B, Ding X (2021) Predictive value of early amplitude integrated electroencephalogram (aEEG) in sleep related problems in children with perinatal hypoxic-ischemia (HIE). BMC Pediatrics 21:410.

Törn AE, Hesselman S, Johansen K, Ågren J, Wikström A, Jonsson M (2023) Outcomes in children after mild neonatal hypoxic ischaemic encephalopathy: A population-based cohort study. BJOG 130:1602–1609.

Traudt CM, McPherson RJ, Bauer LA, Richards TL, Burbacher TM, McAdams RM, Juul SE (2013) Concurrent erythropoietin and hypothermia treatment improve outcomes in a term nonhuman primate model of perinatal asphyxia. Dev Neurosci 35:491–503.

Tremblay M-È, Majewska AK (2011) A role for microglia in synaptic plasticity? Communicative & Integrative Biology 4:220–222.

Triantafilou K, Hughes TR, Triantafilou M, Morgan BP (2013) The complement membrane attack complex triggers intracellular Ca2+ fluxes leading to NLRP3 inflammasome activation. Journal of Cell Science:jcs.124388.

Tsuda M (2017) P2 receptors, microglial cytokines and chemokines, and neuropathic pain. J of Neuroscience Research 95:1319–1329.

Tsuji S, Di Martino E, Mukai T, Tsuji S, Murakami T, Harris RA, Blomgren K, Åden U (2020) Aggravated brain injury after neonatal hypoxic ischemia in microglia-depleted mice. J Neuroinflammation 17:111.

Vainchtein ID, Chin G, Cho FS, Kelley KW, Miller JG, Chien EC, Liddelow SA, Nguyen PT, Nakao-Inoue H, Dorman LC, Akil O, Joshita S, Barres BA, Paz JT, Molofsky AB, Molofsky AV (2018) Astrocyte-derived interleukin-33 promotes microglial synapse engulfment and neural circuit development. Science 359:1269–1273.

van der Kooij MA, Groenendaal F, Kavelaars A, Heijnen CJ, van Bel F (2008) Neuroprotective properties and mechanisms of erythropoietin in in vitro and in vivo experimental models for hypoxia/ischemia. Brain Res Rev 59:22–33.

Van Laerhoven H, De Haan TR, Offringa M, Post B, Van Der Lee JH (2013) Prognostic Tests in Term Neonates With Hypoxic-Ischemic Encephalopathy: A Systematic Review. Pediatrics 131:88–98.

Vannucci RC, Christensen MA, Stein DT (1989) Regional Cerebral Glucose Utilization in the Immature Rat: Effect of Hypoxia-Ischemia. Pediatr Res 26:208–214.

Vannucci RC, Connor JR, Mauger DT, Palmer C, Smith MB, Towfighi J, Vannucci SJ (1999) Rat model of perinatal hypoxic-ischemic brain damage. J Neurosci Res 55:158–163.

Vannucci RC, Lyons DT, Vasta F (1988) Regional cerebral blood flow during hypoxia-ischemia in immature rats. Stroke 19:245–250.

Vezzani A, Baram TZ (2007) New Roles for Interleukin-1 Beta in the Mechanisms of Epilepsy. Epilepsy Curr 7:45–50.

Vezzani A, Viviani B (2015) Neuromodulatory properties of inflammatory cytokines and their

impact on neuronal excitability. Neuropharmacology 96:70–82.

Villa P, Bigini P, Mennini T, Agnello D, Laragione T, Cagnotto A, Viviani B, Marinovich M, Cerami A, Coleman TR, Brines M, Ghezzi P (2003) Erythropoietin Selectively Attenuates Cytokine Production and Inflammation in Cerebral Ischemia by Targeting Neuronal Apoptosis. The Journal of Experimental Medicine 198:971–975.

Viviani B, Bartesaghi S, Gardoni F, Vezzani A, Behrens MM, Bartfai T, Binaglia M, Corsini E, Luca MD, Galli CL, Marinovich M (2003) Interleukin-1β Enhances NMDA Receptor-Mediated Intracellular Calcium Increase through Activation of the Src Family of Kinases. J Neurosci 23:8692–8700.

Volpe JJ, Pasternak JF (1977) Parasagittal cerebral injury in neonatal hypoxic-ischemic encephalopathy: clinical and neuroradiologic features. J Pediatr 91:472–476.

Wake H, Moorhouse AJ, Jinno S, Kohsaka S, Nabekura J (2009) Resting Microglia Directly Monitor the Functional State of Synapses In Vivo and Determine the Fate of Ischemic Terminals. J Neurosci 29:3974–3980.

Wakselman S, Béchade C, Roumier A, Bernard D, Triller A, Bessis A (2008) Developmental Neuronal Death in Hippocampus Requires the Microglial CD11b Integrin and DAP12 Immunoreceptor. J Neurosci 28:8138–8143.

Wallisch JS, Simon DW, Bayır H, Bell MJ, Kochanek PM, Clark RSB (2017) Cerebrospinal Fluid NLRP3 is Increased After Severe Traumatic Brain Injury in Infants and Children. Neurocrit Care 27:44–50.

Wang D-S, Zurek AA, Lecker I, Yu J, Abramian AM, Avramescu S, Davies PA, Moss SJ, Lu W-Y, Orser BA (2012) Memory Deficits Induced by Inflammation Are Regulated by α5-Subunit-Containing GABAA Receptors. Cell Reports 2:488–496.

Wassink G, Davidson JO, Crisostomo A, Zhou KQ, Galinsky R, Dhillon SK, Lear CA, Bennet L, Gunn AJ (2021) Recombinant erythropoietin does not augment hypothermic white matter protection after global cerebral ischaemia in near-term fetal sheep. Brain Commun 3:fcab172.

Wassink G, Davidson JO, Fraser M, Yuill CA, Bennet L, Gunn AJ (2020) Non-additive effects of adjunct erythropoietin therapy with therapeutic hypothermia after global cerebral ischaemia in near-term fetal sheep. J Physiol 598:999–1015.

Weeke LC, Groenendaal F, Mudigonda K, Blennow M, Lequin MH, Meiners LC, van Haastert IC, Benders MJ, Hallberg B, de Vries LS (2018) A Novel Magnetic Resonance Imaging

Score Predicts Neurodevelopmental Outcome After Perinatal Asphyxia and Therapeutic Hypothermia. The Journal of Pediatrics 192:33-40.e2.

Weeke LC, Groenendaal F, Toet MC, Benders MJNL, Nievelstein RAJ, Rooij LGM van, Vries LS de (2015) The aetiology of neonatal seizures and the diagnostic contribution of neonatal cerebral magnetic resonance imaging. Developmental Medicine & Child Neurology 57:248–256.

Weinhard L, di Bartolomei G, Bolasco G, Machado P, Schieber NL, Neniskyte U, Exiga M, Vadisiute A, Raggioli A, Schertel A, Schwab Y, Gross CT (2018) Microglia remodel synapses by presynaptic trogocytosis and spine head filopodia induction. Nat Commun 9:1228.

Werner C, Engelhard K (2007) Pathophysiology of traumatic brain injury. British Journal of Anaesthesia 99:4–9.

White CRH, Doherty DA, Henderson JJ, Kohan R, Newnham JP, Pennell CE (2010) Benefits of introducing universal umbilical cord blood gas and lactate analysis into an obstetric unit. Aust NZ J Obst Gynaeco 50:318–328.

Williams CE, Gunn AJ, Mallard C, Gluckman PD (1992) Outcome after ischemia in the developing sheep brain: An electroencephalographic and histological study. Annals of Neurology 31:14–21.

Williams CE, Gunn AJ, Synek B, Gluckman PD (1990) Delayed Seizures Occurring with Hypoxic-Ischemic Encephalopathy in the Fetal Sheep. Pediatr Res 27:561–565.

Williams E, Scott JP (1954) THE DEVELOPMENT OF SOCIAL BEHAVIOR PATTERNS IN THE MOUSE, IN RELATION TO NATURAL PERIODS 1).

Williamson LL, Bilbo SD (2013) Chemokines and the hippocampus: A new perspective on hippocampal plasticity and vulnerability. Brain, Behavior, and Immunity 30:186–194.

Williamson LL, Sholar PW, Mistry RS, Smith SH, Bilbo SD (2011) Microglia and Memory: Modulation by Early-Life Infection. J Neurosci 31:15511–15521.

Wilton DK, Mastro K, Heller MD, Gergits FW, Willing CR, Fahey JB, Frouin A, Daggett A, Gu X, Kim YA, Faull RLM, Jayadev S, Yednock T, Yang XW, Stevens B (2023) Microglia and complement mediate early corticostriatal synapse loss and cognitive dysfunction in Huntington's disease. Nat Med 29:2866–2884.

Winerdal M, Winerdal ME, Kinn J, Urmaliya V, Winqvist O, Adén U (2012) Long lasting local and systemic inflammation after cerebral hypoxic ischemia in newborn mice. PLoS

ONE 7:e36422.

Wlodarczyk A, Benmamar-Badel A, Cédile O, Jensen KN, Kramer I, Elsborg NB, Owens T (2019) CSF1R Stimulation Promotes Increased Neuroprotection by CD11c+ Microglia in EAE. Front Cell Neurosci 12

Wu YW et al. (2022) Trial of Erythropoietin for Hypoxic-Ischemic Encephalopathy in Newborns. N Engl J Med 387:148–159.

Wu YW, Mathur AM, Chang T, McKinstry RC, Mulkey SB, Mayock DE, Van Meurs KP, Rogers EE, Gonzalez FF, Comstock BA, Juul SE, Msall ME, Bonifacio SL, Glass HC, Massaro AN, Dong L, Tan KW, Heagerty PJ, Ballard RA (2016) High-Dose Erythropoietin and Hypothermia for Hypoxic-Ischemic Encephalopathy: A Phase II Trial. Pediatrics 137:e20160191.

Xie CB, Qin L, Li G, Fang C, Kirkiles-Smith NC, Tellides G, Pober JS, Jane-wit D (2019) Complement Membrane Attack Complexes Assemble NLRP3 Inflammasomes Triggering IL-1 Activation of IFN-γ-Primed Human Endothelium. Circ Res 124:1747–1759.

Xu B, Xiao A-J, Chen W, Turlova E, Liu R, Barszczyk A, Sun CLF, Liu L, Tymianski M, Feng Z-P, Sun H-S (2016) Neuroprotective Effects of a PSD-95 Inhibitor in Neonatal Hypoxic-Ischemic Brain Injury. Mol Neurobiol 53:5962–5970.

Xu X, Yin D, Ren H, Gao W, Li F, Sun D, Wu Y, Zhou S, Lyu L, Yang M, Xiong J, Han L, Jiang R, Zhang J (2018) Selective NLRP3 inflammasome inhibitor reduces neuroinflammation and improves long-term neurological outcomes in a murine model of traumatic brain injury. Neurobiology of Disease 117:15–27.

Yager JY, Brucklacher RM, Vannucci RC (1991) Cerebral oxidative metabolism and redox state during hypoxia-ischemia and early recovery in immature rats. American Journal of Physiology-Heart and Circulatory Physiology 261:H1102–H1108.

Yanai J, Fares F, Gavish M, Greenfeld Z, Katz Y, Marcovici G, Pick CG, Rogel-Fuchs Y, Weizman A (1989) Neural and behavioral alterations after early exposure to phenobarbital. Neurotoxicology 10:543–554.

Yang J, Wise L, Fukuchi K (2020) TLR4 Cross-Talk With NLRP3 Inflammasome and Complement Signaling Pathways in Alzheimer's Disease. Front Immunol 11

Yang X-M, Downey JM, Cohen MV, Housley NA, Alvarez DF, Audia JP (2017) The Highly Selective Caspase-1 Inhibitor VX-765 Provides Additive Protection Against Myocardial

Infarction in Rat Hearts When Combined With a Platelet Inhibitor. J Cardiovasc Pharmacol Ther 22:574–578.

Yang Y, Wang H, Kouadir M, Song H, Shi F (2019) Recent advances in the mechanisms of NLRP3 inflammasome activation and its inhibitors. Cell Death Dis 10:128.

Yin J, Zhao F, Chojnacki JE, Fulp J, Klein WL, Zhang S, Zhu X (2018) NLRP3 Inflammasome Inhibitor Ameliorates Amyloid Pathology in a Mouse Model of Alzheimer's Disease. Mol Neurobiol 55:1977–1987.

Yıldız EP, Ekici B, Tatlı B (2017) Neonatal hypoxic ischemic encephalopathy: an update on disease pathogenesis and treatment. Expert Review of Neurotherapeutics 17:449–459.

Yıldız EP, Tatlı B, Ekici B, Eraslan E, Aydınlı N, Çalışkan M, Özmen M (2012) Evaluation of Etiologic and Prognostic Factors in Neonatal Convulsions. Pediatric Neurology 47:186–192.

Ystgaard MB, Scheffler K, Suganthan R, Bjørås M, Ranheim T, Sagen EL, Halvorsen B, Saugstad OD, Yndestad A (2019) Neuromodulatory Effect of NLRP3 and ASC in Neonatal Hypoxic Ischemic Encephalopathy. Neonatology 115:355–362.

Zareen Z, Strickland T, Eneaney VM, Kelly LA, McDonald D, Sweetman D, Molloy EJ (2020) Cytokine dysregulation persists in childhood post Neonatal Encephalopathy. BMC Neurology 20:115.

Zhang M-M, Guo M-X, Zhang Q-P, Chen X-Q, Li N-Z, Liu Q, Cheng J, Wang S-L, Xu G-H, Li C-F, Zhu J-X, Yi L-T (2022) IL-1R/C3aR signaling regulates synaptic pruning in the prefrontal cortex of depression. Cell & Bioscience 12:90.

Zhang X, Shen J, Man K, Chu ESH, Yau TO, Sung JCY, Go MYY, Deng J, Lu L, Wong VWS, Sung JJY, Farrell G, Yu J (2014) CXCL10 plays a key role as an inflammatory mediator and a non-invasive biomarker of non-alcoholic steatohepatitis. J Hepatol 61:1365–1375.

Zhao J, Chen Y, Xu Y, Pi G (2013) Effect of intrauterine infection on brain development and injury. International Journal of Developmental Neuroscience 31:543–549.

Zhou KQ, Bennet L, Wassink G, McDouall A, Curtis MA, Highet B, Stevenson TJ, Gunn AJ, Davidson JO (2022) Persistent cortical and white matter inflammation after therapeutic hypothermia for ischemia in near-term fetal sheep. Journal of Neuroinflammation 19:139.

Zhou Z, Xu M-J, Gao B (2016) Hepatocytes: a key cell type for innate immunity. Cell Mol

Immunol 13:301–315.

Zhu C, Kang W, Xu F, Cheng X, Zhang Z, Jia L, Ji L, Guo X, Xiong H, Simbruner G, Blomgren K, Wang X (2009) Erythropoietin improved neurologic outcomes in newborns with hypoxic-ischemic encephalopathy. Pediatrics 124:e218-226.